

University of Louisville

ThinkIR: The University of Louisville's Institutional Repository

Electronic Theses and Dissertations

12-2021

Pyridine nucleotide redox potential in coronary smooth muscle couples myocardial blood flow to cardiac metabolism.

Marc Matthew Dwenger
University of Louisville

Follow this and additional works at: <https://ir.library.louisville.edu/etd>



Part of the [Cellular and Molecular Physiology Commons](#)

Recommended Citation

Dwenger, Marc Matthew, "Pyridine nucleotide redox potential in coronary smooth muscle couples myocardial blood flow to cardiac metabolism." (2021). *Electronic Theses and Dissertations*. Paper 3700. <https://doi.org/10.18297/etd/3700>

This Doctoral Dissertation is brought to you for free and open access by ThinkIR: The University of Louisville's Institutional Repository. It has been accepted for inclusion in Electronic Theses and Dissertations by an authorized administrator of ThinkIR: The University of Louisville's Institutional Repository. This title appears here courtesy of the author, who has retained all other copyrights. For more information, please contact thinkir@louisville.edu.

PYRIDINE NUCLEOTIDE REDOX POTENTIAL IN CORONARY SMOOTH MUSCLE
COUPLES MYOCARDIAL BLOOD FLOW TO CARDIAC METABOLISM

By

Marc Matthew Dwenger

B.A., Simpson College, 2013

M.S., University of Louisville, 2018

A Dissertation

Submitted to the Faculty of the
School of Medicine of the University of Louisville
In Partial Fulfillment of the Requirements
for the Degree of

Doctor of Philosophy

in Pharmacology and Toxicology

Department of Pharmacology and Toxicology

University of Louisville

Louisville, Kentucky

August 2021

PYRIDINE NUCLEOTIDE REDOX POTENTIAL IN CORONARY SMOOTH MUSCLE
COUPLES MYOCARDIAL BLOOD FLOW TO CARDIAC METABOLISM

By

Marc M. Dwenger

B.A., Simpson College, 2013

M.S., University of Louisville, 2018

A Dissertation Approved on

July 15, 2021

by the following Dissertation Committee:

Dissertation Director
Matthew Nystoriak, Ph.D.

Aruni Bhatnagar, Ph.D.

Steven P. Jones, Ph.D.

Bradford G. Hill, Ph.D.

Brian P. Ceresa, Ph.D.

DEDICATION

This dissertation is dedicated to my friends and family, especially my beloved wife Unnu.

ACKNOWLEDGEMENTS

I would like to thank everyone in my lab for their tremendous support through these years working on my dissertation project. Foremost, I am grateful for the mentorship of my committee members. I am especially grateful to my mentor, Dr. Nystoriak, who has helped me to grow intellectually and as a bench scientist. He has been an outstanding collaborator and has always been receptive to my questions and encouraging me through the recurring struggles that arose during this project. I am also grateful for the friendship and collaboration of both current and former members of the lab. I would like to thank Zachary Wohl who helped me to learn the difficult procedure of patch clamping isolated coronary vascular smooth muscle cells. Furthermore, I would like to thank Sean Raph for providing his expertise regarding pressure myography and always being open to discussion concerning this project. I would also like to thank Dr. Deqing (John) Zhang who guided me at the outset of this project and taught me many techniques regarding cell culture and molecular biology. I would also like to thank Xuemei Hu and Li Luo for providing their expertise with various molecular biology techniques that support the findings of this study and assisting with the maintenance of our mouse colony. Also, I would like to thank everyone in Diabetes and Obesity Center for their support and friendship. Lastly, I would like to thank our collaborators: Dr. Vahagn Ohanyan at Northeast Ohio Medical University and Dr. Michelle Reyzer and Lisa Manier at Vanderbilt University.

ABSTRACT

PYRIDINE NUCLEOTIDE REDOX POTENTIAL IN CORONARY SMOOTH MUSCLE COUPLES MYOCARDIAL BLOOD FLOW TO CARDIAC METABOLISM

Marc M. Dwenger

July 15, 2021

The maintenance of myocardial oxygen supply during stress is essential for sustaining cardiac health. Enhancement of coronary blood flow upon increases in myocardial oxygen demand (i.e., hyperemia) relies on regulation of voltage-gated K^+ (Kv) channels by their intracellular β subunits (i.e., $Kv\beta$ proteins). Considering that, $Kv\beta$ proteins are Aldo-Keto Reductases (AKRs) and regulate Kv channel gating, we tested the hypothesis that elevation of myocardial oxygen demand modifies intracellular NAD(H) in arterial myocytes. Furthermore, we tested whether the resultant change in the redox state of the pyridine nucleotide pool directly regulates coronary Kv1 channel activity. High-resolution imaging mass spectrometry and live-cell fluorescent imaging revealed that augmented cardiac workload significantly increases the cytosolic NADH:NAD⁺ ratio in intramyocardial arterial myocytes. Intracellular pyridine nucleotide redox ratios reflecting elevated oxygen demand potentiated whole-cell I_{Kv} density and stimulated native Kv1 channel activity in a $Kv\beta 2$ -dependent manner. Mutations in the $Kv\beta 2$ catalytic site prevented NADH-induced increases in Kv1 activity, abolished vasodilation in response to elevated L-lactate, and suppressed the relationship between myocardial blood flow and cardiac workload. These results indicate that the AKR activity and pyridine nucleotide sensitivity of $Kv\beta$ proteins regulate coronary vasoreactivity and blood flow to the heart during metabolic stress.

TABLE OF CONTENTS

	PAGE
DEDICATION.....	iii
ACKNOWLEDGEMENTS.....	iv
ABSTRACT.....	v
LIST OF FIGURES.....	ix
LIST OF TABLES.....	xii
CHAPTER	
I. Introduction	
a. Background.....	1
b. Coronary vascular physiology.....	3
c. Foundational laws of blood flow.....	5
d. Myogenic control and autoregulation of vascular tone.....	6
e. Regulation of vascular membrane potential and contractility.....	7
f. Major potassium channels involved in metabolic hyperemia	
i. Large-conductance Ca^{2+} -activated K^+ channels.....	10
ii. Inwardly rectifying K^+ channels.....	11
iii. K_{ATP} channels.....	13
iv. Voltage-gated K^+ channels.....	14
g. The role for K^+ channels in metabolic hyperemia.....	15
h. Potential vasoactive signals involved in metabolic hyperemia	
i. Sympathetic and parasympathetic innervation.....	16

ii.	Nitric oxide.....	19
iii.	Eicosanoids.....	21
iv.	Endothelial derived hyperpolarizing factors.....	24
v.	Arterial oxygen tension.....	26
vi.	Adenosine.....	28
vii.	Erythrocyte-derived adenylate nucleotides.....	29
viii.	Myocardial potassium release.....	32
ix.	Myocardial-derived hydrogen peroxide.....	32
x.	Lactate.....	35
i.	NAD(P)H/NAD(P) ⁺ ratio and metabolic demand.....	36
j.	Historical perspective and Kv1 channel structure.....	38
k.	Enzymatic properties and regulatory roles of the Kvβ proteins.....	41
l.	The role of Kvβ subunits in the cardiovascular system.....	46
m.	Hypothesis & Specific Aims.....	48
II.	Materials and Methods	
a.	Animals and animal euthanasia.....	61
b.	Human Tissue.....	61
c.	Isolation of coronary arterial smooth muscle cells.....	62
d.	Imaging mass spectrometry.....	62
e.	Smooth muscle and hiPSC-CM co-culture preparation and live-cell fluorescence imaging.....	63
f.	Patch clamp electrophysiology.....	65
g.	Echocardiography.....	67
h.	Ex vivo arterial diameter measurements.....	68
i.	In situ proximity ligation.....	69
j.	Western blot.....	70

k. Statistics.....	71
III. In vivo cardiac workload and in vitro cardiomyocyte stimulation increases vascular NADH/NAD ⁺ ratio	
a. Introduction.....	72
b. Results.....	73
c. Discussion.....	76
d. Significance, limitations, future directions.....	79
IV. Redox control of coronary arterial blood flow via the AKR activity of Kvβ2 subunits	
a. Introduction.....	88
b. Results.....	90
c. Discussion.....	95
d. Significance, limitations, future directions.....	99
V. Summary & Conclusions.....	112
REFERENCES.....	117
APPENDIX A.....	146
APPENDIX B.....	184
CURRICULUM VITAE.....	200

LIST OF FIGURES

FIGURE	PAGE
1.1 Model of the Kv1 channel structure.....	52
1.2 Mechanism of Kv voltage-dependent gating.....	53
1.3 N-type and C-type inactivation.....	54
1.4 Kv β 1 imparts N-type inactivation upon delayed rectifier Kv1 channels.....	55
1.5 Catalytic mechanism of the Kv β 2 subunit.....	56
1.6 Oxidized pyridine nucleotides decrease inactivation of the Kv1.5/ Kv β 1.3 channel complex	57
1.7 Regulation of Kv1.5 α /Kv β 2 channel complexes by pyridine nucleotides.....	58
1.8 Kv β 2 AKR catalytic activity decreases Kv1 channel inactivation.....	59
1.9 Hypothetical mechanism of the Kv β 2 auxiliary complex in metabolic hyperemia.....	60
3.1 Increased myocardial workload promotes local elevation of lactate:pyruvate ratio in the coronary arterial wall.....	82
3.2 Measurement of cytosolic NADH:NAD ⁺ in arterial smooth muscle cells.....	83
3.3 Relationship between sensor expression and cytosolic NADH/NAD ⁺ readout.....	84
3.4 Arterial myocyte NADH:NAD ⁺ is sensitive to changes in proximal cardiomyocyte beating frequency.....	85
3.5 Reduction in O ₂ levels increases NADH:NAD ⁺ in arterial smooth muscle cells.....	86
3.6 NADH:NAD ⁺ ratio is not elevated by direct β -adrenergic stimulation.....	87

4.1 Representative isolated coronary arterial myocyte and patch pipette tip utilized for whole cell recordings.....	103
4.2 Impact of Kvβ2 ablation on whole cell I_K in coronary arterial smooth muscle.....	104
4.3 Modulation of coronary arterial myocyte I_{Kv} upon changes in intracellular pyridine nucleotide redox potential.....	105
4.4 Potentiation of native coronary Kv1 activity by NADH requires Kvβ2.....	108
4.5 Native Kv1 channels in human coronary arterial myocytes associate with Kvβ proteins.....	109
4.6 The Y90F mutation in Kvβ2 does not alter the abundance of vascular Kvβ2.....	110
4.7 Loss of Kvβ2 catalytic function prevents redox-mediated increases in Kv1 activity and vasodilation, and suppresses MBF.....	111
5.1.....	116

APPENDIX A

FIGURE	PAGE
1 Loss of Kvβ2 impairs cardiac pump function during stress.....	169
2 Relationship between myocardial blood flow and cardiac workload in Kvβ-null mice.....	170
3 Ablation of Kvβ2 attenuates coronary vasodilation in response to hypoxia.....	171
4 L-lactate enhances I_{Kv} in coronary arterial myocytes and promotes coronary vasodilation via Kvβ2.....	172
5 Kvβ2 controls redox-dependent vasoreactivity in resistance mesenteric arteries.....	173

6 Increasing the ratio of Kv β 1.1:Kv β 2 subunits in smooth muscle inhibits L-lactate-induced vasodilation and suppresses myocardial blood flow.....	174
7 Heart rate and mean arterial pressure in wild type and Kv β -null mice during catecholamine-induced stress.....	175
8 Hypoxia-induced vasodilation of isolated coronary arteries is attenuated in the presence of psora-4.....	176
9 Loss of Kv β subunits does not impact vasoconstriction in response to increases in intravascular pressure, membrane depolarization, or thromboxane A ₂ receptor activation.....	177
10 Vasodilation in response to L-lactate is independent of endothelial function and requires changes in membrane potential.....	178
11 L-lactate-induced vasodilation is not altered in arteries from Kv β 1.1 ^{-/-} mice.....	179
12 Ablation of Kv β proteins does not impact vasodilation in response to adenosine.....	180
13 Heart rate and mean arterial pressure in double transgenic SM22 α -rtTA:TRE- β 1 and single transgenic control SM22 α -rtTA mice in the absence and presence of catecholamine-induced stress.....	181

APPENDIX B

FIGURE	PAGE
1 Kv β -dependent regulation of Kv1 activity by pyridine nucleotide cofactors.....	197
2 Hypothetical model of coronary blood flow regulation by pyridine nucleotide-mediated activation of Kv1 channels.....	198
3 Coronary smooth muscle Kv1 channel modulation by cellular redox.....	199

LIST OF TABLES

TABLE	PAGE
1. Pyridine nucleotide concentrations and redox ratios for whole cell I_{Kv} recordings protocol.....	106
2. Voltage-sensitivity of Kv activation and inactivation	107
3. Body weight and cardiac structural parameters for wild type and Kv β -null mice.....	182
4. Echocardiographic parameters in wild type and Kv β -null mice.....	183

CHAPTER 1

BACKGROUND

The maintenance of life under the duress of an ever-changing external environment depends upon homeostatic mechanisms to balance energy supply and demand. In multicellular systems, this balance relies upon the delivery of oxygen and energetic substrates through intricate transport systems. Vertebrates utilize a closed vascular system to establish homeostasis between various organs and tissues. Tissue metabolism fluctuates with exposure to dynamic external conditions. Thus, the vascular tone of a closed circulatory system must be exquisitely regulated to ensure proper blood flow and homeostatic maintenance.

The regulation of blood flow is particularly important when considering perfusion of the myocardium. Circulation of blood through the chambers of the heart does not appreciably provide oxygen to the surrounding myocardium. Thus, an intricate network of vessels (i.e., the coronary vasculature) pervades the heart, providing the required nutrients and oxygen. The regulation of coronary vascular tone is particularly vital because the heart consumes a substantial amount of oxygen even at rest ($\sim 60 \mu\text{l}\cdot\text{min}^{-1}\cdot\text{g}^{-1}$, MVO_2 of the left ventricle, 75% O_2 extraction) ^{1, 2}. Therefore, increased myocardial oxygen consumption (MVO_2) is principally met with robust vasodilation in the coronary vascular bed to increase oxygen delivery to the myocardial tissue ^{2, 3}. This process is termed 'functional' or 'metabolic' hyperemia and is regulated by several pathways that are intrinsic and extrinsic to the myocardial tissue. Yet, despite decades of research, a single overarching mechanism to explain the rapid coronary vasodilation in response to increased MVO_2 has not been elucidated. While much of this research has focused on

identifying metabolic mediators involved in this mechanism, recently, more attention has been placed upon the involvement of potassium channels expressed at the coronary vascular smooth muscle cell membrane. Efflux of K^+ ions through potassium channels ultimately determines membrane potential and the extent of vasodilation. Thus, potassium channel activity is highly integrated with the physiological process of metabolic hyperemia.

Several recent publications have demonstrated that voltage-gated Kv1 potassium channels can sense metabolic demand and promote coronary vasodilation in the context of increased cardiac work, noted by significant disruption in the relationship between coronary blood flow and MVO_2 upon Kv1 channel inhibition⁴⁻⁶. This metabolic sensing capacity of the Kv α pore complex may derive from cytosolic auxiliary Kv β subunits of the Kv pore complex. In heterologous expression systems, Kv β subunits are functional aldo-keto reductase (AKR) enzymes that regulate Kv1 channel activity by promoting hydride transfer from pyridine nucleotide cofactors to carbonyl substrates⁷⁻¹⁰. The pyridine nucleotides NAD(H) and NADP(H) are extensively integrated with several metabolic pathways. Therefore, Kv β subunits in the coronary vasculature could possess the capacity to adjust Kv channel activity and, ultimately, coronary vascular tone to metabolic demand. This intriguing capacity could play an essential role in metabolic hyperemia in the myocardium.

This literature review will be separated into three distinct sections to establish a foundation of knowledge that supports this potential role of Kv β subunits in the vasculature. The first section will give an overview of the regulatory processes that control coronary vascular tone and membrane potential. First, this section will focus on the basic physiology of coronary blood flow and membrane potential regulation. This section will be followed by structural and functional details concerning the fundamental properties of various potassium channels potentially involved in metabolic hyperemia in the myocardium. The second section will provide information concerning the various

purported metabolic vasodilators of metabolic hyperemia and their known actions upon these potassium channels. Finally, the third section will provide a historical overview of the literature concerning Kv channels, the pyridine nucleotide sensitivity of the Kv β subunits, and the enzymatic properties of the auxiliary complex. This section will conclude with an overview of recent literature depicting the critical role of Kv β subunits in the cardiovascular system. Collectively, this literature review will provide rationale for the hypothesis and specific aims of this dissertation.

Coronary vascular physiology

In humans, the cardiovascular system consists of two separate but sequential circulatory systems: the systemic and pulmonary circulation. The systemic vasculature consists of arteries, veins, arterioles, venules, and capillary beds that run in parallel such that each organ system receives an oxygen rich supply of blood. As blood is pumped away from the left ventricle, blood flows first through arteries, then the arterioles and capillary beds, with each vessel subtype becoming progressively smaller in diameter. For example, the typical human aorta is 25 millimeters in diameter; whereas, the typical human capillary is 8 micrometers in diameter ¹¹. Each of these subtypes possesses a unique vascular anatomy and dynamic diameter range to serve certain critical physiological functions appropriate to their location in the vascular tree. For example, larger arteries need to withstand high blood pressures from the beating myocardium during systolic contraction and act as pressure reservoirs to move blood continually through the body during diastole. To execute this function, these vessels possess a refined ratio of elastic and fibrous connective tissue, providing them with the appropriate compliance to serve both these purposes. On the contrary, the capillary beds consist of only a basement membrane and a lining of endothelial cells to exchange oxygen and substrates to systemic tissues. Immediately preceding the capillaries, the arterioles are the site of the highest resistance,

meaning the greatest pressure drop occurs over these vessels ¹². This high resistance is partially due to a relatively thick vascular smooth muscle layer in these vessels. Because of this muscular layer, the diameter of these vessels can be finely regulated to control flow. Therefore, arterial and arteriolar beds serve as the primary point of blood flow control to capillary beds. Control of vascular resistance in the coronary arterial vascular bed is of particular importance because the constant pumping action of the heart induces a continuous demand for oxygen and energetic substrates in the myocardium. Therefore, multiple intrinsic and extrinsic control mechanisms tightly regulate coronary vascular resistance with MVO_2 to maintain oxygen delivery to the dynamic cardiac tissue.

Due to the vital role of the coronary arteries, an extensive network of arteries, arterioles, and capillary beds pervades the entire myocardium from epicardium to endocardium. In the human heart, the coronary vascular tree begins at the sinus of Valsalva which gives rise to the right and left coronary artery ¹³. The right coronary artery extends from the anterior surface of the aorta and tracks closely along the atrioventricular groove ¹³. Numerous branches extend from the right coronary artery to supply the right ventricle, right auricle, interventricular septum, and the conduction system of the heart ¹³. The right coronary artery terminates in the posterior left ventricle after passing across the acute margin of the heart to reach the posterior surface of the myocardium ¹³. The left coronary artery extends from the sinus of Valsalva from the posterior surface of the aorta, almost immediately dividing into the left anterior descending artery and the circumflex branch ¹³. The left anterior descending artery follows the interventricular groove and branches of this artery supply blood to the interventricular septum and apex ¹³. The circumflex branch of the left coronary artery courses in the atrioventricular groove towards the left side of the heart, supplying blood to the left ventricular wall ¹³. Arteriolar branches of these main vessels course across the epicardial surface and, at a diameter of 1,500 microns, begin to penetrate the endocardium ¹⁴. Ultimately, these arteriolar branches feed

into numerous myocardial capillary beds (in humans, 5734 capillaries/mm² in the left ventricle, 5679 capillaries/mm² in the right ventricle) ¹⁵. In mammalian capillary beds, each myocyte receives oxygen from one capillary ¹⁶. Arteriolar branches also regulate flow into the capillary beds to sustain oxygen exchange to myocardial tissue. In fact, arteries less than 75-130 μm in diameter contribute substantially to this regulation, as these vessels contribute 50% percent of the total vascular resistance ¹⁷.

Foundational laws of blood flow

Before proceeding into a discussion concerning blood flow regulation in the coronary vasculature, the basic laws of physics that govern blood flow deserves consideration. Blood flow can be described simply by a derivation of Darcy's law which states:

$$\text{Equation 1: } Q = \frac{\Delta P}{R}$$

This mathematical relationship means the systemic blood flow, Q , is determined primarily by two factors the resistance of the vasculature, R , and the pressure gradient, ΔP , across the systemic vasculature which equates to the difference between mean arterial pressure and central venous pressure established by the heart. The pressure gradient is directly proportional to blood flow such that increases in mean arterial pressure enhance flow; whereas, resistance is inversely proportional to flow.

$$\text{Equation 2: } R = \frac{8L\eta}{\pi r^4}$$

As shown in equation 2, resistance is determined by vessel length, blood viscosity, and the radius of the blood vessel. Equations 1 and 2 can be combined to form Poiseuille's law which gives an approximation of blood flow through the vasculature.

$$\text{Equation 3: } Q = \frac{\Delta P \pi R^4}{8\eta L}$$

In this equation, vessel length is represented by L , blood viscosity by η , and blood vessel radius by R . As in equation 1, flow is represented by Q . This law demonstrates that blood flow is directly proportional to the pressure gradient across the vasculature and the radius of the vessel. On the contrary, blood flow is inversely proportional to vessel length and blood viscosity. However, vessel length and blood viscosity are constant; thus these variables do not contribute substantially to blood flow. This equation demonstrates that blood flow is influenced by the resistance of the vasculature. For example, if a vessel with a cross-section of 1 cm^2 decreases to a cross-section of 0.8 cm^2 , flow decreases by over 50%, assuming that all other variables are constant.

However, this equation is a simplification and does not accurately describe blood flow through the coronary vasculature. The pressure gradient, the difference between mean arterial pressure and central venous pressure, is not the difference in pressure that determines flow to the myocardial tissue. The coronary vasculature endures significant compressive forces due to the beating myocardium, such that certain segments of the coronary vasculature undergo periods of retrograde flow¹⁸. In fact, compressive forces in the left ventricular myocardium are so intense that during systole left ventricular coronary flow is significantly interrupted (75% reduction in flow during systole)¹⁹. Thus, a majority of flow into the coronary vascular bed of the left ventricular myocardium occurs during diastole¹⁹. Therefore, blood flow in the coronary vasculature is better described by taking into account the compressive forces of the myocardium as the beating cardiac tissue increases the perfusion pressure required to increase coronary blood flow²⁰. The pressure gradient that determines flow in Equation 1 is more adequately described by the difference between myocardial tissue pressure and arterial pressure.

Myogenic control and autoregulation of vascular tone

In the context of these compressive forces, the coronary arterial tone must be maintained to ensure adequate blood flow. The most essential phenomenon to maintain flow is the vasculature's myogenic response to changes in intravascular pressure. This myogenic response was first identified in 1902 when William Bayliss discovered that blood volume in the systemic vasculature is proportional to blood pressure²¹. In both felines and canines, a decrease in blood volume is met with a rapid decrease in blood pressure in enervated limbs²¹. On the contrary, an increase in blood volume is met with a rapid increase in intravascular pressure in enervated limbs²¹. Thus, he concluded that vascular tone is maintained in the absence of external neural feedback, and the vasculature itself can maintain proper tone in the context of fluctuating intravascular pressures²¹. A critical consequence of the myogenic response is pressure-flow autoregulation. This myogenic response maintains coronary blood flow at physiological intravascular pressures (60-120 mmHg)²²; however, outside this range of physiological intravascular pressures, blood flow is completely dependent upon perfusion pressure²². Thus, at physiological intravascular pressures, pressure-flow autoregulatory processes establish a basal tone. From this basal tone, several intrinsic and extrinsic control mechanisms can modulate vascular diameter in the coronary vascular bed²³.

Regulation of vascular membrane potential and contractility

Similar to other vascular beds, physiological control mechanisms of coronary arterial and arteriolar diameter ultimately influence vascular smooth muscle membrane potential. At physiological perfusion pressures, the resting membrane potential of the vascular smooth muscle is steady between -40 mV and -60 mV, and small changes in membrane potential cause dramatic shifts in vascular diameter²⁴. For example, in pressurized cerebral arteries, held at 75 mmHg, a 12 mV depolarization in membrane potential causes a dramatic vasoconstriction that decreases the vessel diameter by

approximately ~50%²⁴. The contractile response to membrane depolarization is primarily determined by the intracellular calcium concentration. Membrane potential depolarization of the vascular membrane causes a dramatic increase in arterial wall calcium that is mediated through voltage-dependent Ca^{2+} channels which concomitantly decreases arterial wall diameter²⁵. The relationship between vascular smooth muscle membrane potential and intracellular Ca^{2+} is very sensitive such that small changes in membrane potential dramatically increase Ca^{2+} influx and vascular tone. For example, in the resistance vasculature, a 1 mV depolarization in membrane potential generates a 7.5 nM increase in intracellular Ca^{2+} concentration²⁵. This relationship between membrane potential and Ca^{2+} concentration translates to a 7.5 μm change in diameter per 1 mV shift in membrane potential²⁵. Therefore, only small changes in membrane potential and, subsequently, intracellular calcium concentration are required to regulate vascular tone in the resistance vasculature, including in the coronary vasculature. A 35 mV change in membrane potential and a shift in intracellular Ca^{2+} concentration from approximately 125 nM to 350 nM comprises the full range of arterial diameters observed in the resistance vasculature²⁵.

Intracellular Ca^{2+} regulates arterial diameter and smooth muscle contraction by interacting with several regulatory proteins. In a fully dilated artery of the resistance vasculature, intracellular Ca^{2+} concentration is low (between 100-150 nM in arteries exposed to an L-type calcium channel blocker or unpressurized vessels)²⁶. Upon depolarization of a vascular smooth muscle cell, the electrochemical gradient favors calcium influx through voltage-dependent Ca^{2+} channels²⁵. In addition, circulating ligands can activate G-protein coupled receptors linked to the phospholipase C-inositol triphosphate-diacylglycerol pathway, causing the release of Ca^{2+} from intracellular stores in the sarcoplasmic reticulum²⁷. Once in the cytoplasm, calcium is quickly bound to Ca^{2+} binding proteins, including calmodulin (CaM)²⁸. Ca^{2+} -sensing N-terminal EF loop proteins

on CaM chelate intracellular calcium²⁸. The binding of four Ca²⁺ ions to CaM induces a conformational change, which allows for activation of myosin light chain kinase^{27, 28}. The CaM-kinase complex phosphorylates the regulatory light chain of myosin at Ser-19, which increases actomyosin ATPase activity, contraction, and cross-bridge cycling^{27, 29}. To reverse contraction, smooth muscle relaxation involves independent processes of calcium reuptake and the removal of the phosphorylated group on Ser-19 by myosin light chain phosphatase^{30, 31}. Upon dephosphorylation at Ser-19, cross-bridge cycling and detachment between actin and myosin heads slow³¹. Concomitantly, calcium is extruded from the cytoplasm primarily by three different transport mechanisms. Plasma membrane Ca²⁺-ATPase (PMCA) transporters and Na⁺/Ca²⁺ exchangers move calcium from the cytoplasm into the extracellular space; sarcoplasmic reticulum Ca²⁺-ATPase (SERCA) restores intracellular calcium stores³². Both SERCA and PMCA use phosphorylation mediated by ATP and counter proton transport to remove calcium from the cytosol against the concentration gradient for calcium³². On the contrary, Na⁺/Ca²⁺ exchangers move calcium into the extracellular space by utilizing the intracellularly directed concentration gradient of sodium³². Because this exchanger utilizes the gradient of sodium, these exchangers are coupled with Na⁺/K⁺ ATPase which establishes the sodium/potassium concentration gradient of the cell³².

Calcium extrusion, membrane potential hyperpolarization, and vascular relaxation are ultimately determined by potassium efflux across the vascular smooth muscle cell membrane. Membrane depolarization and subsequent calcium influx can activate potassium channels in the smooth muscle membrane, leading to hyperpolarization and relaxation of the vasculature³³. When the vascular smooth muscle becomes depolarized, the membrane potential moves away from the equilibrium potential of potassium, E_K (about -85 mV)³³. Because the influx of positive charge during membrane depolarization shifts the membrane potential away from E_K, an electrical driving force directs potassium

out of the cell. In addition, a large concentration gradient of potassium ions between the cytoplasm and the extracellular space ($[K^+]_i \approx 140 \text{ mM}$, $[K^+]_o \approx 3 \text{ mM}$) also favors potassium out of the cell. The membrane has high resistance potassium, allowing small changes in potassium efflux to substantially influence membrane potential³³. Therefore, during vascular relaxation, the electrochemical driving force can effectively move potassium out of the cell, returning the membrane potential closer to E_K . During this hyperpolarization mediated by potassium efflux, SERCA, PMCA transporters, and Na/Ca²⁺ exchangers extrude calcium from the cytosol to promote vascular relaxation. This repolarization and relaxation are mediated by the activation of several types of potassium channels at the smooth muscle membrane such as voltage-dependent K_v channels, Ca²⁺-activated potassium channels, K_{ATP} potassium channels, and inwardly rectifying K_{ir} channels³³. The next part of this section will give an overview of the structural and functional characteristics of these potassium channels expressed in coronary vascular smooth muscle cells.

Major potassium channels involved in coronary vascular tone regulation

Large-conductance Ca²⁺-activated K⁺ channels

Large-conductance Ca²⁺-activated K⁺ channels (BK_{Ca}) mediate large outward currents upon increased intracellular calcium and membrane potential depolarization³⁴. Due to the importance of calcium signaling in the regulation of vascular tone, large-conductance Ca²⁺-activated K⁺ channels (BK_{Ca}) are critical to modulating smooth muscle membrane potential. At a concentration of 100 μM of intracellular calcium, the channel persists in the open state 90% of the time³⁴. Because of this calcium-sensing property, localized release of calcium ions from the sarcoplasmic reticulum, termed Ca²⁺ sparks, can promote vascular relaxation by activating BK_{Ca} channels at the membrane³⁵. Furthermore, these channels possess a voltage-sensitive component that is independent of calcium-binding³⁶.

These properties are due to the unique composition of the channel. The BK_{Ca} channel is a tetrameric structure consisting of four individual polypeptides with each peptide chain consisting of 10 unique segments (S0-S10)^{37, 38}. The S0 confers a cytoplasmic facing N-terminus and, both the transmembrane segment and the N-terminus are important for regulation by a two-transmembrane auxiliary β subunit^{37, 39}. The S1-S6 region shares a similar topology to other voltage-gated ion channels^{37, 39}. Like other voltage-dependent potassium channels, the S1-S4 region is a voltage sensor that modulates ion flux through the channel pore in the S5-S6 region⁴⁰. The final S7-S10 segments are cytoplasmic and possess two Ca²⁺-sensing domains (RCK1 and RCK2), providing both calcium and voltage sensitivity to the channel^{41, 42}.

In the coronary vasculature, inhibition of BK_{Ca} channels decreases basal tone and the BK_{Ca} mediated efflux during stretch-induced myogenic tone responses^{43, 44}. Similar to other vascular beds, in the coronary arterial smooth muscle cells, BK_{Ca} channels are activated by Ca²⁺ sparks, transient releases of Ca²⁺ from the sarcoplasmic reticulum⁴⁵. This response to Ca²⁺ sparks is important as a negative feedback mechanism to vascular tone development during membrane potential depolarization⁴⁶. As such, BK_{Ca} channels have an important role in maintaining basal tone from which metabolic hyperemia is initiated.

Inwardly Rectifying K⁺ channels

Inwardly rectifying, K_{ir}, channels display a characteristic inward rectification that depends specifically upon the electrochemical gradient of potassium ions⁴⁷. Therefore, K_{ir} channels display a large depolarizing current at V_m negative to E_K, and a hyperpolarizing current at membrane potentials positive to E_K⁴⁷; however, this hyperpolarizing current quickly degrades as membrane potential proceeds to more positive potentials⁴⁷. A reduction in outward K⁺ efflux through inwardly rectifying K⁺

channels at membrane potentials positive to E_K is due to a voltage-dependent block by magnesium and intracellular polyamines such as spermine ⁴⁸.

This unique property of inward rectification is related to specific aspects of the channel structure. The primary amino acid sequence ROMK1 (renal outer medullary potassium channel) and IRK1 (Inward rectifier K^+ channel), two inwardly rectifying potassium channels isolated from mammalian macrophages and kidneys, indicated that the channel structure consists of two membrane-spanning segments (M1 and M2) and an H5-like pore region, which is similar to other voltage-gated ion channels ^{49,50}. Visualization of the channel structure by X-ray crystallography demonstrated that the channel consists of four monomers, each with two transmembrane segments, that coalesce to form a tetrameric structure ⁵¹. In the ion-conducting pathway, negatively charged residues in the C-terminal vestibule are precisely spaced for intracellular block by polyamines ⁵¹. Interestingly, the addition of external potassium can inhibit the rectification induced by polyamines ⁵²; however, the mechanism of this relief from polyamine-induced rectification remains unclear. For example, K^+ ions may relieve inward rectification by interacting with negative surface charges on the extracellular face of the channel ⁵³. In contrast, recent evidence suggests outward potassium current persists even in an extracellular solution with 0 K^+ ⁵⁴. Thus, this effect of extracellular K^+ may be due to shifts in the voltage-dependence of polyamine block and E_K rather than the interaction of potassium with the channel.

These unique characteristics of inwardly rectifying channels endow these channels with crucial roles in the coronary vasculature. The resting membrane potential of coronary vascular cells (-40 to -60 mV) is positive relative to E_K (-85 mV). Therefore, relief of rectification by modest increases (~15 mM) in external K^+ leads to potassium efflux, membrane potential hyperpolarization, and dilation in the coronary vascular smooth muscle cells ⁵⁵. Furthermore, release of external K^+ is an important signal to promote

outward efflux through inward rectifying channels and the initiation of vasodilatory processes ⁵⁶. For example, recent data demonstrates that, during conditions of increased metabolic demand, endothelial K_{ir} channels in capillaries may activate in response to K^+ release by proximal ventricular myocytes to induce coronary vasodilation and restore oxygen delivery to the myocardium ⁵⁷.

K_{ATP} channels

K_{ATP} channels are multimeric structures that are sensitive to metabolism through binding adenosine 5'-triphosphate. ATP binding inhibits conductance through single K_{ATP} channels in excised membrane patches ⁵⁸. The ion-conducting component of the channel consists of two transmembrane, inwardly rectifying, $K_{ir6.X}$ subunits that have sequence homology with the channel pores of other voltage-gated ion channels ⁵⁰; however, when reconstituted in heterologous expression systems, the pore itself does not elicit expected electrophysiological properties. Alone, the pore complex elicits an unexpectedly high conductance value and lacks ATP sensitivity ⁵⁹. This incongruous conductance suggests the presence of another subunit in the channel.

In pancreatic β islet cells, sulfonylurea receptors appear to colocalize with the K_{ATP} channel ⁶⁰⁻⁶². Only when the pore complex was co-expressed with an ATP-binding cassette protein, a sulphonylurea receptor, did the channel elicit an expected conductance value, inhibition by sulfonylureas, and inhibition by ATP ⁵⁹. The channel was found to consist of several subtypes of both the pore $K_{ir6.x}$ subunits ($K_{ir6.1}$ and $K_{ir6.2}$) and the sulfonylurea receptors ($SUR1$, $SUR2A$, and $SUR2B$) ⁶³⁻⁶⁵. Additionally, when these subunits were expressed in different heteromeric conformations, they reconstituted the electrophysiological properties of K_{ATP} channels in cardiac, skeletal, and smooth muscle tissue ⁶³⁻⁶⁵. Each two-transmembrane $K_{ir6.x}$ subunits are in complex with a 17-transmembrane sulfonylurea receptor which combine to form either an octameric or tetra-

dimeric complex^{66,67}. This ATP-binding cassette protein imparts sensitivity of the channel to several sulfonylurea compounds (e.g., glibenclamide) which are widely used to interrogate the role of K_{ATP} channels in the regulation of coronary vascular tone⁶⁸⁻⁷⁰.

In the coronary vasculature, glibenclamide-induced inhibition of K_{ATP} channels blunts the vasodilatory response to several vasoactive substrates and conditions. These substrates and conditions include prostacyclin, hypoxia, adenosine, and hydrogen peroxide⁷⁰⁻⁷². Collectively, these experiments concerning coronary blood flow suggest a critical role for K_{ATP} channels in the control of basal vascular tone and vasodilatory responses to ischemia^{70, 73-75}; however, although inhibition of K_{ATP} channels disrupts several processes related to vascular tone, in the absence of functional K_{ATP} channels, autoregulation is conserved, suggesting that basal tone does not completely depend upon the function of these potassium channels⁷⁶.

Voltage-gated K^+ channels

Voltage-gated K^+ channels belonging to the Kv family are widely expressed among excitable cells and participate in the control of membrane excitability in neurons, cardiomyocytes, and vascular smooth muscle, as well as others. This control of membrane excitability is due to the voltage-sensing capacity of these channels. Upon membrane potential depolarization, these channels open and inhibit calcium influx and vascular smooth muscle contraction⁷⁷. Unlike other voltage-gated ion channels (e.g., Na_v , Ca_v), the Kv pore-forming complex is comprised of four distinct subunits (i.e., $Kv\alpha$) that consist of a selectivity filter, gating apparatus, and voltage-sensing domains^{78,79}. These Kv pore proteins associate with several classes of cytoplasmic auxiliary complexes that regulate subcellular localization and gating kinetics^{79,80}. The $Kv\beta$ proteins, which predominantly associate with the Kv1 and Kv4 families, are functional AKRs that catalyze the NAD(P)H-dependent reduction of carbonyl substrates to primary and secondary alcohols⁸⁰.

Intriguingly, Kv β AKR activity has been shown to regulate cellular trafficking as well as channel activation and inactivation^{10, 81}. Thus, the enzymatic properties of these auxiliary proteins are thought to function as a molecular switch that may couple membrane excitability to cell metabolism, or *vice versa*. That is, Kv β may adjust membrane potential to the metabolic state of the cell, or could couple ionic current to local pyridine nucleotide redox potential, thus providing a means for membrane excitability to regulate metabolism and long-term remodeling processes⁷⁹. The structure and function of these channels will be expanded upon in the third section of this literature review.

The role for K⁺ channels in metabolic hyperemia

Because K⁺ efflux largely determines membrane potential, the potassium channels outlined above may respond to several metabolic signals that initiate metabolic hyperemia in the coronary vasculature; however, the potential influence of each potassium channel subtype upon the physiological process of metabolic hyperemia varies. For example, inhibition of both K_{ATP} channels and BK_{Ca} channels does not significantly disrupt myocardial oxygen saturation with enhanced metabolic demand^{82, 83}. Furthermore, the role of K_{ir} channels in metabolic hyperemia in the coronary vasculature is less well understood. However, these channels partially mediate metabolic and reactive hyperemia in skeletal muscle^{84, 85}. Therefore, the possibility exists that K_{ir} channels could influence metabolic hyperemia in the heart. In contrast to these other potassium channels, promising results indicate that proper functioning of voltage-gated K⁺ channels in the coronary vasculature is essential to metabolic hyperemia. For example, dysfunction of Kv1 channel activity significantly disrupts the relationship between coronary blood flow and MVO₂^{4, 6}. Regardless of their overall influence upon metabolic hyperemia, a common theme amongst these ion channels is that they influence signaling pathways potentially

related to this physiological phenomenon. The next section will overview these mediators, each mediator's influence on metabolic hyperemia, and their interaction with potassium channels on the smooth muscle membrane.

Potential vasoactive signals involved in metabolic hyperemia

Sympathetic and parasympathetic neural-innervation

While the myocardial tissue possesses the intrinsic ability to produce electrical potentials to stimulate contraction, the heart is also extensively innervated and regulated by both sympathetic and parasympathetic branches of the autonomic nervous system. Over the past century, our knowledge concerning autonomic regulation of the coronary vasculature has dramatically expanded from early anatomical descriptions to how neural control integrates with myocardial metabolism in the regulation of coronary blood flow. In the 1920s, Herbert Woollard provided an extensive description of the heart's neural anatomy, demonstrating that numerous parasympathetic and sympathetic nerves innervate the coronary vasculature⁸⁶. This neural anatomy of the myocardial vessels follows the architecture of the vasculature. The nerves that innervate these vessels become finer in thickness and more numerous as the coronary vasculature divides and spreads throughout the myocardium⁸⁷. These early anatomical descriptions laid the foundation for future work concerning the regulation of blood flow by the autonomic nervous system.

Due to this extensive neural innervation, blood flow in the resistance vasculature is highly regulated by the autonomic nervous system, particularly by the sympathetic branch. While parasympathetic innervation is evident, this branch of the nervous system does not substantially regulate coronary vascular tone both at rest and during exercise⁸⁸.⁸⁹ Despite this lack of general influence upon the coronary vasculature, parasympathetic stimulation does promote endothelial-mediated vasodilation in the coronary vasculature in

several different species^{90,91}. A seminal study by Feigl demonstrated that in the absence of the effects of vagal stimulation on cardiac heart rate and contractility, parasympathetic activity promotes vasodilation and enhances coronary blood flow⁹². While the effect of parasympathetic innervation is insubstantial, this branch of the autonomic nervous system could contribute to the regulation of transmural blood flow as intracoronary infusion of acetylcholine shunts blood flow from the epicardial to the subendocardial surface⁹³. In contrast to this limited role of parasympathetic innervation, the sympathetic nervous system possesses a more substantial influence over coronary blood flow both at rest and during increased metabolic demand.

The α and β adrenergic branches of sympathetic innervation in the coronary vasculature oppositely influence coronary vascular tone. In general, activation of α adrenergic receptors promote coronary vasoconstriction, whereas activation of β adrenergic receptors induce coronary vasodilation. Because of these opposing influences, the arterioles that compose the coronary resistance vasculature differentially express these receptors. For example, coronary arterioles highly express β_2 -adrenergic receptors in comparison to β_1 -adrenergic receptors with the ratio of β_2/β_1 receptor expression in small coronary arterioles being 93% β_2 receptors and 7% β_1 receptors, respectively⁹⁴. Considering the α -adrenergic branch of sympathetic innervation, pharmacological inhibition of α_1 and α_2 receptor indicates that the resistance coronary arterioles possess more α_2 receptors in comparison to α_1 receptors⁹⁵. The activation of each of these receptors induces different responses in the coronary vasculature. For example, when both β_1 and β_2 receptors are activated by pharmacological agonists, such as isoproterenol, coronary blood flow increases independent of myocardial contractility or metabolism^{96,97}. In contrast, pharmacological activation of α -adrenergic receptors increases vasoconstriction and decreases coronary blood flow primarily through α_2 receptor activation⁹⁸. This polarization between α and β adrenergic receptor activation on coronary

vascular flow is also apparent during direct electrical stimulation of the stellate ganglion in the vertebral column ⁹⁹. Stimulation of this sympathetic collection of nerves induces a robust increase in coronary blood flow that is blunted by β -adrenergic inhibition due to the polarizing activation of α adrenergic receptors ⁹⁹.

Due to these significant effects on vascular tone, stimulation of sympathetic receptors on the smooth muscle membrane induces K^+ efflux through potassium ion channels expressed on the coronary vascular smooth muscle cell membrane. For example, isoproterenol-induced dilation of pressurized porcine subepicardial and subendocardial vessels involves the activation of K_{ATP} in porcine subepicardial and subendocardial vessels ¹⁰⁰. Likewise, isoproterenol can increase the open channel probability of calcium-activated channels both through direct G-protein activation and cyclic adenosine monophosphate (cAMP)-dependent protein kinase A (PKA) phosphorylation ¹⁰¹. As such, this regulation of vascular potassium channels by sympathetic stimulation substantially influences the response of the coronary vasculature to metabolic demand.

Autonomic stimulation acts as a feed-forward regulatory mechanism of metabolic hyperemia in the cardiovascular system. A feed-forward regulatory mechanism means sympathetic and parasympathetic stimulation can regulate vascular tone independent of the myocardium's response to stimulation. A seminal study by Miyashiro and Feigl clearly described this mode of regulation. In this study, they showed that norepinephrine increased coronary blood flow in the absence of myocardial contraction, suggesting that β -mediated coronary vasodilation does not rely on feedback from myocardial metabolism ¹⁰². Another aspect of this feed-forward mechanism is that the myocardium is also innervated by the sympathetic nervous system ¹⁰³. Thus, these two feed-forward mechanisms work in tandem to control blood flow in the context of metabolic hyperemia ¹⁰³. As sympathetic stimulation to the myocardium increases contractility and heart rate,

α -adrenergic and β -adrenergic activation in the coronary vasculature regulates coronary vascular tone ¹⁰³. The importance of this feedforward regulation of coronary vascular tone is emphasized by the fact that, in exercising dogs, α -adrenoreceptor blockade enhances vasodilation with increasing exercise intensity; whereas, combined α and β adrenoreceptor blockade decreases vasodilation in the context of increasing exercise intensity ¹⁰⁴. Although this feed-forward sympathetic regulation has considerable influence over coronary vascular tone during metabolic hyperemia, mathematical modeling suggests interstitial norepinephrine reaches 12.2 nM during intense exercise which would only increase coronary blood flow by 67% ¹⁰⁵. Considering blood flow increases by 260% during intense exercise, sympathetic stimulation can account for only 25% of the coronary vasodilation during metabolic demand ¹⁰⁵. This result suggests that several other factors influence coronary blood flow in the context of metabolic demand, including both metabolic dilators and factors released by the endothelium.

Nitric oxide

The endothelium is a lining of cells in the vascular lumen that secretes several diffusible factors that modulate vascular tone. Nitric oxide is the most prominent factor secreted by the endothelium that mediates endothelial-derived vasodilation in the coronary vascular bed. A serendipitous observation by Furchgott and Zawadski led to the discovery of this signaling molecule when they determined that unintentional disruption of the endothelial cell layer inhibited acetylcholine-induced vasodilation ¹⁰⁶. This vasoactive substance secreted by the endothelium was aptly named “endothelial-derived relaxing factor” until studies by Ignarro, Palmer, and Moncada concluded that this relaxing factor was indeed nitric oxide ¹⁰⁷⁻¹⁰⁹. The factor’s identity was confirmed by demonstrating that vasodilation induced by endothelial-derived relaxing factor was not significantly different from vasodilation induced by nitric oxide ¹⁰⁹.

Several factors, such as acetylcholine, bradykinin, and shear stress act upon the endothelial cell layer, leading to the activation of nitric oxide synthase (NOS) and the production of nitric oxide ^{106, 110}. Endothelial nitric oxide synthase (eNOS) is activated by these factors both through calcium-dependent and calcium-independent pathways. A common regulator between these pathways is the interaction between scaffolding protein caveolin-1 and eNOS. Upon calcium influx, calcium/calmodulin form a complex that disrupts the interaction between caveolin and eNOS, leading to enzyme activation ¹¹¹. eNOS can also be stimulated independently of calcium by pathways such as albumin-induced gp60 activation and caveolae internalization ¹¹². After activation, eNOS converts L-arginine to L-citrulline generating diffusible nitric oxide that interacts with vascular soluble guanylyl cyclase to produce cGMP (cyclic guanosine monophosphate) which activates protein kinase G (PKG) to promote relaxation ^{110, 113-115}. In bovine coronary arteries, NO-induced production of cGMP can activate K_{Ca} channels, possibly through PKG activation, which contributes to the dilation of the coronary vascular smooth muscle ^{113, 116}. In addition to K_{Ca} channels, NO-induced relaxation may also involve the activation of other K^+ currents such as voltage-gated potassium channels ¹¹⁷. In human coronary arteries, tetraethylammonium, an inhibitor of Kv channels more robustly disrupts relaxation to a NO donor than block of K_{Ca} channels by iberiotoxin, suggesting activation of voltage-gated potassium channels could be involved in NO-induced vasodilation ¹¹⁷. On the contrary, K_{ATP} channels do not appear to be a major end effector in the NO-cGMP pathway ^{117, 118}. In both the porcine and human coronary vasculature, glibenclamide fails to inhibit both sodium nitroprusside-induced increases in current density and coronary vascular dilation ^{117, 118}.

While these observations demonstrate that nitric oxide can profoundly affect coronary vascular tone through certain potassium channels known to be involved in metabolic hyperemia, the role of this endothelial-derived signaling molecule in coronary

vasodilation during increased metabolic demand is not substantial. For example, in canines, nitric oxide-induced coronary vasodilation is not influential to functional hyperemia. During exercise, LNA-induced inhibition of NOS does not disrupt the linear relationship between coronary blood flow and MVO_2 ; rather, NOS inhibition shifts the relationship between coronary venous oxygen tension and MVO_2 in a downward parallel fashion ¹¹⁹. While these results indicate that nitric oxide is not essential to metabolic hyperemia, this signaling molecule may possess a more critical role in mediating dilations in coronary arteries to shear stress. For example, nitric oxide suppresses shear stress in small arteries (>160 μm in diameter) during adenosine-induced increases in blood flow by promoting vasodilation ¹²⁰; however, this regulation of shear stress by nitric oxide is absent in arterioles (<160 μm in diameter) as adenosine receptor activation in the coronary vasculature causes a robust rise in shear stress in vessels of this caliber ¹²⁰. As result of this response to adenosine, upon inhibition of nitric oxide synthase with LNMA, shear stress increases to a greater extent both in small arteries and arterioles ¹²⁰. Therefore, NO release in the coronary vascular bed may be critical in regulating shear stress in arteriolar beds ¹²⁰.

Eicosanoids

Another major family of endothelial derived signaling molecules, eicosanoids, consists of many different molecules produced by several different enzymatic pathways in the endothelium. This family of vasoactive molecules was first discovered by Goldblatt and Von Euler who observed that prostate gland and seminal vesicle secretions affect smooth muscle contractility and blood pressure regulation ^{121, 122}. For example, both the small intestine of rabbit and the rectus abdominis muscle of frog robustly contract upon exposure to human seminal fluid ¹²¹. Euler coined the term “prostaglandin” to describe these unique vasoactive substances derived from the male reproductive system ¹²².

Decades later, work by Bergstrom and Samuelsson identified several of these prostaglandins, including those in human seminal fluid ¹²³. Several other eicosanoids besides prostaglandins exist such as prostanoids, leukotrienes, lipoxins, hydroxyeicosatetraenoic acid (HETES), and epoxyeicosatrienoic acids (EETs) ¹²⁴.

Eicosanoids are similar in that these vasoactive signaling molecules are formed from the same precursor molecule, arachidonic acid. When phospholipase A₂ releases arachidonic acid from the phospholipid bilayer of endothelial cells, this fatty acid is metabolized by several different enzymatic pathways (e.g., cyclooxygenase (COX), lipoxygenase, and epoxygenase) into a variety of eicosanoid signaling molecules ¹²⁴. The most notable vasodilatory compounds produced by this pathway are prostacyclin and arachidonic acid metabolites of epoxygenase called epoxyeicosatrienoic acids (EETs).

In the coronary vasculature, prostacyclin activates K_{ATP} channels at the smooth muscle membrane to induce vasodilation and increase blood flow. For example, glibenclamide inhibits both prostacyclin-induced vasodilation and blood flow in the rabbit coronary vasculature ⁷¹. This signaling molecule stimulates adenylyl cyclase and the production of cAMP through binding to G-protein coupled receptors; accumulation of cAMP may lead to the activation of several potassium channels at the membrane ^{124, 125}. Thus, the opening of K_{ATP} channels, upon prostacyclin stimulation, may occur through a cAMP-dependent mechanism, but the possibility still exists that prostacyclin could directly activate the channel ⁷¹.

EETs relax smooth muscle through two different mechanisms. Indirectly, EETs can induce calcium influx through TRPV4 channels, generating Ca²⁺ sparks from the sarcoplasmic reticulum and subsequent activation of BK_{Ca} at the smooth muscle membrane ¹²⁶. Alternatively, EETs can bind to EET receptors on the smooth muscle membrane that activates BK_{Ca} channels through a G-protein mediated mechanism ^{127, 128}. These mechanisms demonstrate that eicosanoids represent a diverse family of signaling

molecules that can regulate vascular tone through many mechanisms; however, their role in the regulation of metabolic hyperemia is unclear.

Several studies have demonstrated that inhibition of COX and cytochrome P450 (CYP) epoxygenases do not impair metabolic hyperemia, suggesting that prostaglandins and EETs do not have a substantial role in this phenomenon. For example, while the infusion of arachidonate into the coronary circulation of canines causes a robust increase in coronary flow, inhibition of COX does not disrupt the linear relationship between coronary blood flow and MVO_2 during exercise¹²⁹. Furthermore, similar results have been observed in human subjects; while ibuprofen effectively antagonizes the production of prostacyclin metabolites in humans, the inhibition of COX does not disrupt the decrease in coronary vascular resistance noted during exercise¹³⁰. While prostaglandins most likely do not significantly influence metabolic hyperemia, studies in swine suggest that cyclooxygenase-derived vasodilating factors have a more critical role in maintaining coronary vascular tone at rest rather than mediating metabolic hyperemia¹³¹.

Concerning the relationship between EETs and metabolic hyperemia, the impact of cytochrome P450-derived epoxygenase metabolites on the hyperemic response differs depending upon the muscular tissue under examination. For example, in human skeletal muscle tissue, the combination of NOS and CYP 2C9 inhibition substantially reduces blood flow to the quadriceps during knee extensor exercise¹³². This result suggests that, under NOS inhibition, EETs could have a critical role in mediating metabolic hyperemia in skeletal muscle¹³²; however, in the myocardium, EETs have a rather unexpected effect on metabolic hyperemia. In swine, CYP2C9 inhibition generates a vasodilatory response in the coronary vasculature during exercise¹³³. This increase in vasodilation may be due to the removal of vasoconstrictive reactive oxygen species also produced by CYP enzymes¹³³. In summary, arachidonic acid metabolites have several effects on coronary

blood flow regulation; however, the role of these signaling molecules in metabolic hyperemia is not substantial.

Endothelial derived hyperpolarizing factors

In addition to these rather unambiguous endothelial pathways related to vasodilation, the endothelium also possesses another vasodilatory mechanism that has no distinct mediator or factors. The collective term for these obscure mediators is endothelial-derived hyperpolarizing factors or EDHFs. The discovery of these factors began with early investigations using various pharmacological agents to probe for pathways of endothelial-induced relaxations in canine femoral arteries ¹³⁴. These pharmacological studies identified three endothelial signaling pathways of vascular smooth muscle relaxation ^{134, 135}. Two of these pathways were observed to depend upon arachidonic acid metabolism, while the other was noted to be independent of signaling by this fatty acid ^{134, 135}. The mediators of two of these pathways, nitric oxide and prostacyclin, are well known ^{134, 135}; however, the signaling molecule or molecules responsible for one of the arachidonic acid-dependent pathway has yet to be determined ^{134, 135}. Subsequently, these unidentified mediators of this pathway eventually became known as EDHFs ¹³⁵. Regardless of the identity of EDHFs, these factors are known to regulate smooth muscle tone in several vascular beds, including in coronary arteries and arterioles. For example, in the large arterioles of the canine coronary vasculature, inhibition of both NOS and COX does not abolish acetylcholine-induced vasodilation, providing substantial evidence for EDHF-mediated vasodilation in the coronary vascular bed ¹³⁶.

While the mechanism of EDHF-induced vasodilation is unclear, a common theme exists amongst these endothelial-derived factors. These mediators (e.g., S-nitrosothiols, K⁺ ions, H₂O₂, EETs) transmit a hyperpolarizing signal from endothelial cells to the vascular smooth muscle layer to induce vasodilation ^{133, 137-139}. In coronary arteries,

inhibition of small conductance and intermediate conductance K_{Ca} (SK_{Ca} & IK_{Ca}) channels in the endothelial cell layer decreases EDHF-induced vasodilation, providing evidence for the transmission of a hyperpolarizing signal during EDHF-induced vasodilation that could be propagated by several factors¹³⁷⁻¹³⁹. Furthermore, the hyperpolarizing signal appears to be mediated by these specific subtypes of calcium-activated channels as inhibition of large-conductance K_{Ca} (BK_{Ca}) channels does not disrupt the transmission of the endothelial-derived hyperpolarizing signal^{137, 138}. The EDHFs could potentially communicate this signal to the vascular smooth muscle cell membrane through many mechanisms. These pathways include the direct activation of vascular K_{Ca} channels, the indirect activation of vascular K_{ir} channels by promoting the accumulation of potassium ions in the myoendothelial space, or the activation of vascular soluble guanylyl cyclase by alternative sources of nitric oxide besides NOS¹³⁷⁻¹³⁹. Alternatively, this hyperpolarizing signal may propagate by means other than a diffusible factor. The hyperpolarizing signal could transmit through gap junctions between the endothelial and vascular smooth muscle cell layers¹⁴⁰. Collectively, these studies indicate several potential factors and mechanisms that could potentially mediate EDHF-mediated vasodilation.

Due to the rather obscure nature of EDHF-induced vasodilation, much less is known regarding its role in metabolic hyperemia in the cardiovascular system. At present, the evidence for EDHF signaling in this physiological phenomenon is lacking.

However, EDHF-signaling is potentially involved in the functional hyperemic response of skeletal tissue and regulatory processes of coronary vascular tone unrelated to metabolic hyperemia. As mentioned in the section concerning EET signaling, the combination of NOS and CYP 2C9 inhibition substantially inhibits metabolic hyperemia in skeletal muscle¹³². EETs are also a potential mediator of endothelial-derived hyperpolarization; therefore, functional hyperemia in this muscle tissue could involve EDHF signaling¹³². Yet, the involvement of this EDHF signal in cardiovascular metabolic hyperemia may be

insubstantial. As mentioned in the section concerning EET signaling, the inhibition of EET production generates a vasodilatory response in the coronary vasculature during exercise: therefore, this potential EDHF signal, at least, does not substantially influence metabolic hyperemia in the heart ¹³³. Furthermore, IK_{Ca} channel inhibition does not affect reactive hyperemia, suggesting that EDHF signaling may not possess a significant role in other hyperemic responses ¹⁴¹. Another study more specific to the collective EDHF signaling pathway suggests that EDHF signaling may be more critical to autoregulatory processes of the coronary vasculature. For example, inhibition of IK_{Ca} channels with TRAM-34 inhibits the ability of the coronary vasculature to regulate flow at physiological perfusion pressures ¹⁴¹.

Arterial oxygen tension

Due to oxygen's critical role in oxidative phosphorylation as the final electron acceptor in the electron transport chain, the most obvious potential mediator of local metabolic coronary vasodilation is a change in oxygen tension in the cardiovascular system. Since the early twentieth century, studies utilizing a working canine lung and heart apparatus demonstrated that nitrogen ventilation promotes anoxemia and causes marked coronary vasodilation ^{142, 143}. These findings have been recapitulated in isolated vessels from pigs and humans using pressure myography. Both in the context of flow and stagnant conditions, hypoxia induces vasodilation in porcine coronary arterioles ¹⁴⁴. Likewise, in human coronary arterioles, hypoxia hyperpolarizes the smooth muscle membrane generating a rapid vasodilatory response ¹⁴⁵.

The mechanism concerning hypoxic vasodilation is unclear; however, evidence suggests that the mechanism is complex involving multiple signaling pathways. For example, under conditions of no flow, NOS inhibition blunts hypoxic vasodilation of isolated porcine coronary resistance arterioles substantially more than COX inhibition ¹⁴⁴.

Whereas under conditions of flow, COX inhibition more extensively reduces hypoxic vasodilation as compared to NOS inhibition ¹⁴⁴. During hypoxia, indomethacin, an inhibitor of COX, significantly decreases hypoxia-induced vasodilation in the canine coronary vasculature *in vivo*, further supporting the involvement of COX-derived circulating factors ¹⁴⁶. Hypoxia appears to mediate vasodilation through several potassium channels expressed on the smooth muscle membrane. Most notably, hypoxia activates K_{ATP} channels on the smooth muscle membrane as ATP:ADP ratio is closely tied with oxygen supply to the cell ⁷². For example, hypoxia-induced dilation of resistance arteries dissected from branches of porcine left anterior descending arteries (50-150 μm) is significantly inhibited by glibenclamide ¹⁴⁷. Both at the single-channel and whole-cell level hypoxia induces K_{ATP} channel activation in porcine coronary smooth muscle cells that is inhibited by glibenclamide which further supports this mechanism ¹⁴⁸. The response to hypoxia may also involve activation of other potassium channels such as inwardly rectifying K_{ir} channels and voltage-gated K_v channels. For example, hypoxia significantly increases inwardly rectifying current of small coronary arterial myocytes derived from left anterior descending arterial tissue dissected from rabbits ¹⁴⁹. Furthermore, Ba^{2+} , an inhibitor of inwardly rectifying potassium channels, significantly inhibits the increase in coronary blood flow observed in the presence of hypoxia ¹⁴⁹. In addition to these data, in porcine left anterior descending artery segments, low oxygen tension increases K_v7 -mediated outward current, which relieves arterial tension ¹⁵⁰. These data demonstrate that hypoxia can mediate the opening of several potassium channels, indicating its potential importance in regulating blood flow to the myocardium.

Although changes in oxygen tension can significantly affect vascular tone, several valid criticisms exist against the argument that oxygen is the main mediator of coronary vasodilation in the context of increased metabolic demand. Most prominently, myocardial oxygen delivery does not decrease during exercise. For example, even at strenuous levels

of exercise, coronary venous PO₂ levels do not substantially diminish, indicating that myocardial tissue oxygen supply remains steady even upon increased oxygen consumption ¹⁵¹. Furthermore, concomitantly with hypoxia, various other vasoactive metabolites are released into the circulation that can affect vascular tone, such as lactate and adenosine ¹⁵². Thus, the role of oxygen in the context of other circulating vasoactive substances during metabolic hyperemia is difficult to determine.

Adenosine

As alluded to above, a derivative of the hypothesis that decreased oxygen tension mediates metabolic hyperemia is the myocardial release of adenosine into the interstitial space and the circulation. Over half a century ago, Berne demonstrated that, during hypoxia-induced vasodilation, a substantial amount of the breakdown products of adenosine, hypoxanthine, and inosine, is released by the myocardium into the circulation ¹⁵³. Furthermore, intracoronary infusion of adenosine increases coronary blood flow ¹⁵³. These results support the hypothesis that myocardial release of adenosine can promote coronary vasodilation, potentially influencing coronary vasodilation in the context of increased metabolic demand.

Adenosine mediates its vasodilatory properties through two main pathways: an endothelial-mediated pathway and by direct activation of potassium channels on the vascular smooth muscle membrane. In the resistance coronary vascular smooth muscle, adenosine binds to A_{2A} receptors on endothelial cells and smooth muscle cells ¹⁵⁴. When adenosine binds to A_{2A} receptors on endothelial cells, pertussis toxin-sensitive G-protein stimulation activates endothelial K_{ATP} channels and, subsequently, NOS ¹¹⁸. Release of NO by endothelial cells mediates vascular smooth muscle relaxation through activation of soluble guanylate cyclase and cGMP accumulation ¹¹⁸. Adenosine can also directly activate K_{ATP} channels on the smooth muscle membrane to promote vasodilation ¹¹⁸. This

metabolite is not specific for K_{ATP} channels and can also mediate its effects through other potassium channels such as Kv1 channels, calcium-activated potassium channels, and inwardly-rectifying potassium channels. For example, a Kv1 channel inhibitor, 4-aminopyridine (4-AP), significantly inhibits the increase in coronary blood flow observed during adenosine treatment ¹⁵⁵. *In vitro*, this same inhibitor significantly reduces adenosine-induced vasodilation in isolated canine coronary arterioles and decreases the sensitivity of swine coronary arterioles to adenosine-induced vasodilation ^{155, 156}. Adenosine can also mediate its effects by promoting potassium efflux through BK_{Ca} channels. For example, iberiotoxin, a BK_{Ca} channel inhibitor, inhibits adenosine-induced relaxation of porcine and canine arterioles and arteries ^{157, 158}. Furthermore, this response to adenosine may activate inwardly-rectifying potassium channels. In rabbit small coronary arterial smooth muscle cells, adenosine increases Ba^{2+} -sensitive K_{ir} currents through adenylate-cyclase and PKA activation which mediates an increase in blood flow through the coronary vasculature ¹⁵⁹.

While adenosine imparts significant effects on many potassium channels, adenosine's role in metabolic hyperemia is minimal. Initial studies demonstrated a positive correlation between enhanced coronary blood flow, pericardial adenosine concentration, and coronary sinus adenosine concentrations in exercising dogs ^{160, 161}; however, further experiments demonstrated that pharmacological degradation or blockage of adenosine does not inhibit metabolic hyperemia, suggesting adenosine does not possess a critical role in this phenomenon ¹⁶². Adenosine appears to be more closely related to coronary blood flow in the context of hypoxia rather than states of physiological myocardial consumption. For example, this same study demonstrated that inhibition of adenosine activity significantly blunts reactive hyperemia that occurs during coronary occlusion ¹⁶².

Erythrocyte-derived adenylate nucleotides

The precursors to adenosine (i.e., ATP, ADP, and AMP) can also influence vascular tone in the context of increased metabolic demand. Adenylate signaling can occur in context of decreased oxygen saturation. Erythrocytes, when exposed to low O₂ tension, release ATP into the circulation, which can act as a vasoactive signal ^{163, 164}. Circulating ATP can bind to purinergic receptors on endothelial cells, initiating a signaling cascade, involving NO and prostaglandins, which generates vascular smooth muscle cell relaxation ¹⁶⁴. This metabolic signaling may be significant during increased metabolic demand, in which oxygen tension decreases in the coronary capillary bed ¹⁶⁵. During increased metabolic demand, ATP release from erythrocytes in these capillary beds may act as a retrograde signal to produce vasodilation in upstream arterioles ^{163, 165}.

Several studies support this retrograde signaling mechanism. For example, coronary venous and arterial ATP increases with MVO₂ in the canine vasculature ¹⁶⁶. This accumulation of ATP correlates with a decrease in coronary venous hemoglobin saturation and an increase in coronary blood flow ¹⁶⁶. Furthermore, other investigations demonstrated that intracoronary injection of exogenous ATP into closed-chested dogs increases coronary flow ¹⁶⁵. Antagonists for the purinergic receptors (e.g., 8-phenyltheophylline, MRS-2500) and nitric oxide synthesis (e.g., L-nitroarginine) blunt the increase in coronary blood flow to injection of ATP, suggesting the direct activation of endothelial purinergic receptors ¹⁶⁵. Furthermore, upon increased MVO₂, these inhibitors decrease coronary venous hemoglobin saturation, suggesting that this mechanism is necessary to maintain oxygen delivery to the myocardium ¹⁶⁵; however, the absolute increase in coronary blood flow is not inhibited, suggesting that other receptors and signaling pathways respond to ATP ¹⁶⁵.

This mechanism may also involve signaling by the breakdown products of ATP, such as ADP and adenosine, which could contribute to the collective control of ion channel flux on the endothelial cell membrane by adenylate nucleotides. For example, ADP can

increase both coronary blood flow and dilate coronary arterioles pre-constricted with endothelin-1 through purinergic (P2Y1) activation ¹⁶⁷. Furthermore, adenosine may also contribute to adenine nucleotide-induced vasodilation. For example, adenosine deaminase and inhibition of the adenosine receptor, P1, by 8-PST blunts ATP and ADP induced vasodilation of human atrial coronary arteries ¹⁶⁸. This result suggests that ATP released by erythrocytes can be converted to adenosine, which can then promote coronary vasodilation. These adenine nucleotides may propagate hyperpolarizing signals to vascular smooth muscle cells by modulating ion channel function in endothelial cells both directly and indirectly. The signaling cascades initiated by ATP binding to purinergic receptors may stimulate intracellular calcium release, which activates chloride and BK_{Ca} channels at the membrane ¹⁶⁹. Extracellular ATP may also directly inactivate chloride channels on the endothelial cell membrane ¹⁷⁰. Therefore, signaling by ATP from erythrocytes may potentially involve several ATP breakdown products and ion channels expressed at the endothelial cell membrane.

Collectively, these results suggest a powerful mechanism to propagate vasodilatory signals upstream from local sites of hypoxia; however, several observations argue against a critical role for ATP release from erythrocytes as a major mechanism in metabolic hyperemia. Foremost, as stated previously, strenuous levels of exercise do not decrease myocardial tissue oxygenation ¹⁵¹. Thus, whether erythrocytes receive a sufficient 'hypoxic' signal during increased metabolic demand is uncertain. Furthermore, purinergic receptor and NOS inhibition disrupts the relationship between coronary blood flow and hemoglobin saturation such that more hemoglobin desaturation is required to initiate vasodilation ¹⁶⁵. Yet, these antagonists do not decrease the maximal coronary blood flow response in the context of metabolic demand ¹⁶⁵, suggesting that this mechanism is not the sole mediator of metabolic hyperemia.

Myocardial Potassium Release

As mentioned in the section concerning inward rectifier channels, relief of inward rectification through K_{ir} channels by external K^+ leads to potassium efflux, membrane potential hyperpolarization, and dilation in coronary smooth muscle cells^{55,56}. Therefore, increased external K^+ release by the contracting myocardium could act as a vasodilator by activating K_{ir} channels on the smooth muscle membrane. K_{ir} channels can propagate local vasodilatory signals generated by vasoactive compounds (e.g, bradykinin, adenosine) to remote sites in isolated porcine coronary arterioles, suggesting that signaling through these channels is an influential mechanism to promote an increase in global coronary blood flow¹⁷¹; however, while increased heart rate is associated with K^+ release and vasodilation, this effect is transient and not sustained⁵⁶. In general, upon an increase in heart rate, coronary sinus K^+ concentration reaches a plateau after 30 seconds and then decreases rapidly⁵⁶. This result indicates that this mechanism could initiate vasodilation in the context of increased metabolic demand; however, other vasoactive signals must act to sustain decreased vascular resistance during metabolic hyperemia⁵⁶.

Myocardial-derived Hydrogen Peroxide

Recently, several different studies have indicated the potential role of hydrogen peroxide (H_2O_2) as a vasoactive signal that mediates metabolic hyperemia. Most notably, upon pacing and norepinephrine infusion, hydrogen peroxide accumulates in the canine myocardial tissue and mediates a substantial increase in coronary blood flow¹⁷². Catalase, an enzymatic inhibitor of H_2O_2 , significantly reduces the vasodilation induced by tachypacing of the canine myocardium, suggesting that the accumulation of H_2O_2 is the primary mediator of this increase in blood flow¹⁷³. In vitro experiments indicate that cardiomyocytes could be a source of this ROS as buffer collected from electrically paced myocytes dilates isolated rat coronary arterioles, with the extent of vasorelaxation

dependent upon stimulation frequency ¹⁷². Similar to *in vivo* experiments, the addition of catalase inhibited this vasodilation, supporting the idea that cardiomyocytes are the source of ROS in H₂O₂ mediated dilation *in vivo* ¹⁷². Collectively, these experiments support an integral role of the local myocardial release of H₂O₂ in the dilation of the coronary vasculature during increased metabolic demand.

Hydrogen peroxide most likely mediates these effects upon vascular smooth muscle cells by oxidizing intracellular redox-sensitive residues involved in the modulation of voltage-gated Kv channels activity ^{174, 175}. The involvement of Kv channels is evident because, both *in vivo* and *in vitro*, 4-AP treatment inhibits the vasodilatory effects of hydrogen peroxide. This antagonist inhibits coronary blood flow upon increased metabolic demand and blunts the vasodilation induced by buffer from paced myocytes, suggesting that H₂O₂ accumulation during increased cardiac work activates 4-AP sensitive channels at the vascular smooth muscle cell membrane ¹⁷². Hydrogen peroxide appears to modulate voltage-gated Kv channel activity by reacting with intracellular redox-sensitive residues. For example, dithiothreitol (DTT), a thiol reductant, reverses H₂O₂-induced relaxation of canine arterial rings and dilation of rat coronary arterioles ¹⁷⁵. Patch-clamp experiments reinforce this mechanism of action concerning hydrogen peroxide as DTT blunts H₂O₂-mediated activation of 4-AP sensitive channels ¹⁷⁴. While the exact mechanism of hydrogen peroxide in the activation of 4-AP sensitive Kv channels is unknown, mechanistic experiments revealed that SB-203580, a p38 MAP kinase inhibitor, reduces vasodilation to conditioned buffer and hydrogen peroxide, suggesting that intracellular redox-sensitive kinases could potentially mediate Kv channel opening to reactive oxygen species ¹⁷⁶. Collectively, these results suggest that hydrogen peroxide could activate Kv channels by reacting with intracellular redox-sensitive residues either in the channel itself or in associated regulators of the channel. While these studies strongly support the involvement of Kv channels in H₂O₂-mediated vascular tone regulation other ion channels,

such as BK_{Ca} channels, may also be involved in H₂O₂ signaling during metabolic hyperemia. Several studies, utilizing porcine models and human subjects, demonstrate that exogenous H₂O₂ activates BK_{Ca} channels in vascular smooth muscle cells¹⁷⁷⁻¹⁷⁹. Furthermore, *in vivo* experiments demonstrate that both catalase and TEA, a non-specific antagonist of Kv and BK_{Ca} channels, significantly blunt coronary vasodilation in response to cardiac pacing¹⁷³; however, the role of BK_{Ca} channels in H₂O₂-induced vasodilation during metabolic hyperemia is uncertain. At present, no study utilizing a specific inhibitor of BK_{Ca} channels has demonstrated a disruption of the relationship between enhanced MVO₂ and increased coronary flow, suggesting that endogenous accumulation of H₂O₂ during increased cardiac work does not activate BK_{Ca} channels. Therefore, in the context of metabolic hyperemia, the literature indicates that hydrogen peroxide release mediates vasodilation by primarily activating voltage gated Kv channels in vascular smooth muscle cells.

While this evidence indicates that myocardial release of reactive oxygen species, such as hydrogen peroxide, may be vital for metabolic hyperemia, further studies are needed to directly confirm the association between endogenous hydrogen peroxide release and metabolic hyperemia. For example, *in vivo* experiments suggesting the importance of this phenomenon are correlative rather than causative. While an increase in MVO₂ is associated with an accumulation of H₂O₂ and increased coronary flow, whether the fate *in vivo* of myocardial-derived hydrogen peroxide is to mediate coronary vascular relaxation by way of voltage-gated Kv channel activation is unclear. H₂O₂ is a highly unstable molecule; which could react with several different substrates before being able to react with targets in the vascular smooth muscle cell layer. Thus, *in vivo* studies that track whether H₂O₂ released by the myocardium definitively acts upon coronary vasculature are needed.

Lactate

While the literature does not demonstrate a direct causal relationship between lactate and metabolic hyperemia in the heart, several investigations suggest that lactate enhances vascular smooth muscle cell NADH/NAD⁺ ratio to increase blood flow and oxygen delivery. Modulation of lactate/pyruvate ratio is in close equilibrium with cytosolic NADH/NAD⁺ ratio through the lactate dehydrogenase reaction; thus, this metabolite pair partially exerts its effects through manipulating the cytosolic pyridine nucleotide redox state^{180, 181}. For example, increased lactate/pyruvate ratio augments blood flow to skeletal muscle during contraction and the central nervous system during neuronal stimulation¹⁸²⁻¹⁸⁴. Furthermore, pronounced lactate levels in contracting skeletal muscle tissue suggest that metabolic demand can induce diffusion of this metabolite to adjacent vascular smooth muscle cells to promote vasodilation through modulating pyridine nucleotide redox state¹⁸³. Plasma lactate secreted into the blood by active skeletal tissue may also increase blood flow through modulating cytosolic NADH/NAD⁺ ratio in distant tissues as moderate exercise correlates with enhanced cerebral blood flow and an accumulation of arterial lactate¹⁸⁵.

Lactate release into the plasma could potentially increase coronary arterial NADH/NAD⁺ to enhance coronary blood flow. Whether lactate acts as a circulating vasoactive factor to increase myocardial blood flow is uncertain. Lactate accumulates in the blood during increased metabolic demand; however, the myocardium readily oxidizes this circulating energy source^{186, 187}. Therefore, the effect of circulating lactate, on coronary vascular pyridine nucleotide redox state and coronary flow during increased metabolic demand is difficult to ascertain. The myocardium readily uptakes lactate, noted by an enhanced myocardial NADH/NAD⁺ redox state¹⁸⁸. Likewise, during atrial pacing of human subjects, lactate uptake by the myocardium significantly increases above baseline; therefore, the determination of the direct effect of circulating lactate upon coronary flow is

unclear due to the confounding influence of lactate on myocardial metabolism¹⁸⁹. Concomitantly upon atrial pacing, the release of lactate by the myocardium also substantially increases; therefore, the effect of local myocardial release of lactate upon pyridine nucleotide redox state in the coronary vascular wall may contribute to metabolic hyperemia¹⁸⁹.

NAD(P)H/NAD(P)⁺ ratio and metabolic demand

Regardless of whether lactate is a mediator of metabolic hyperemia, these studies demonstrate a potential association between cytosolic NADH/NAD⁺ ratio, metabolic demand, and the regulation of vascular tone that could potentially involve pyridine-nucleotide sensitive Kv1 channel activity. While the connection between physiological MVO₂ and vascular cytosolic pyridine nucleotide redox state is unclear, several experiments indicate a relationship between these two variables. For example, a recent study demonstrates that the NADH/NAD⁺ ratio of the myocardium rapidly increases in many conditions of simulated metabolic demand, such as electrical pacing, gradual hypoxia, and ischemia¹⁹⁰. Electrical pacing, at a 170-ms interval, of the myocardium in a working heart apparatus generates a ~40% increase in NADH¹⁹⁰. Whereas in the context of gradual hypoxia, biventricular working heart NADH content increases significantly, reaching 50% of the overall increase in NADH at an oxygen concentration of $67.8 \pm 13.7\%$ ¹⁹⁰. Furthermore, NADH rises rapidly in working hearts in the context of global ischemia¹⁹⁰. in the absence of aortic pressure, after 17.3 ± 10.3 seconds, NADH reaches 66% of its maximum value¹⁹⁰.

Vascular pyridine nucleotide redox state has also interrelates with metabolism, oxygen consumption, and contractility. Upon increased oxygen consumption induced by extracellular KCl-mediated contraction, the ratio of redox couples, lactate/pyruvate, and glycerol 3-phosphate/dihydroxyacetone phosphate (G3P/DHAP) that represent

NADH/NAD⁺ ratio increase in isolated porcine carotid arteries ¹⁹¹. Alternatively, varying the extracellular concentration of lactate or pyruvate modulates the contractile response to extracellular potassium. While a hyperpolarizing concentration of extracellular KCl (10 mM) induces relaxation in porcine carotid arteries incubated with 10 mM pyruvate, a pronounced constriction occurs to this extracellular potassium concentration in the presence of 10 mM lactate ¹⁹². In addition to these experiments that establish a relationship between oxygen consumption and pyridine nucleotide redox state, direct inhibition of metabolism also alters cytosolic NADH reducing equivalents in vascular smooth muscle. For example, antagonism of the malate-aspartate shuttle that transports NADH-reducing equivalents into the mitochondria significantly increases cytosolic NADH/NAD⁺ as measured by lactate/pyruvate and G3P/DHAP ratio ^{193, 194}. These studies demonstrate that cytosolic pyridine nucleotide redox state in the vasculature can be regulated by many factors. Due to the proximity between cytosolic pyridine nucleotides and the vascular smooth muscle membrane, these studies suggest that changes in cytosolic NADH/NAD⁺ ratio during enhanced MVO₂ could regulate Kv channel activity by binding to Kv-associated Kvβ auxiliary complexes.

As stated in the beginning of this introduction, Kvβ proteins, auxiliary subunits of Kv1 channels, have an innate capacity to sense pyridine nucleotide redox state through their homology to aldo-keto reductase enzymes ^{7, 9, 10, 80}. In heterologous expression systems, Kvβ subunits associated with Kv1 channels can sense changes in pyridine nucleotide redox state and adjust Kv channel efflux to NADH/NAD⁺ ratio ^{9, 195}. Collectively, these results demonstrate that cytosolic pyridine nucleotide redox potential can regulate Kv1 channel activity and Kv1-mediated vasodilation. Furthermore, these results suggest that vascular Kvβ subunits could be oxygen sensors in the coronary vasculature.

Therefore, Kv β subunits in the vasculature could potentially cause vasodilation to match demand in the context of metabolic hyperemia.

The following section will further detail the literature related to Kv channels that supports this potential role of Kv β subunits in the vasculature. Many of these past studies revealed the regulatory functions of Kv β proteins via the expression of cloned channels in heterologously expressing cells. Nonetheless, recent research has expanded on foundational views and is beginning to assign physiological roles to native proteins *in vivo*¹⁹⁶⁻¹⁹⁸. In the next section, we discuss historical literature related to the discovery and structural characterization of Kv1 channels and Kv β proteins. This overview will provide current knowledge on the role of Kv β proteins in regulating Kv currents. In the last section, we will detail the function of Kv β proteins in the cardiovascular system.

Historical perspective and Kv1 channel structure

Investigation of Kv channels was first sparked by early serendipitous observations of a shaking leg phenotype in mutant *Drosophila melanogaster* that were associated with aberrant K⁺ conductance and synaptic transmission¹⁹⁹⁻²⁰¹. The so-called “*Shaker*” locus was later shown to encode “A-type” outward K⁺ currents^{202, 203} mediated by a diverse array of N and C terminal splice variants²⁰⁴⁻²⁰⁷. The *Shaker* variants were identified as one of several subfamilies of K⁺ channels that also consists of the *Shab*, *Shaw*, and *Shal* proteins,²⁰⁸⁻²¹⁰ which correspond to the Kv1, Kv2, Kv3, and Kv4 vertebrate homologues, respectively²¹¹⁻²¹⁵. Crude structural models of Kv multi-protein complexes were predicted via electrophysiological studies using various toxins. Dendrotoxin, a protein in the venom of the eastern green mamba that induces convulsant effects via inhibition of A-type channels²¹⁶ bound to channels consisting of two discrete proteins with molecular masses of ~65 and 37 kDa^{216, 217}. Consequently, sedimentation and electrophysiological analysis

of toxin-bound proteins suggested a $\alpha_4\beta_4$ octameric assembly^{218, 219} which was later confirmed by x-ray crystallography (Figure 1.1)⁷⁹. Each α subunit consists of six transmembrane spanning α -helices with the first four segments comprising the voltage sensor⁷⁹. Within the fourth membrane segment (S4), four positively charged arginine residues account for the gating charge^{79, 220}. An S4-S5 linker connects the voltage sensor domain to the outer and inner helices (S5 and S6, respectively) that form the pore^{79, 220}. These S4-S5 linkers of each α subunit are in close proximity with the inner helix bundle, a structural motif consisting of S6 helices from each of the four α subunits^{79, 220}. The S6 inner helices, by way of a Pro-Val-Pro sequence, curve towards the membrane, bringing the S6 near to the S4-S5 linker^{79, 220}. Because of this proximity, movement of S4 towards the inner membrane compresses the S4-S5 linker and the inner helix bundle activation gate upon membrane hyperpolarization, thus closing the channel (Figure 1.2)²²⁰. Upon depolarization, the channel transitions to the open-state and intervening sequences between S5 and S6 from each α subunit form a selectivity filter that permits selective K^+ conductance (Figure 1.2)^{79, 221}. As channel activation proceeds, the selectivity filter slowly changes conformation, returning the channel to an inactivated state, a process termed C-type inactivation (Figure 1.3)^{222, 223}. In contrast, with some Kv subtypes, rapid channel inactivation through an N-terminal “ball and chain” mechanism also occurs, in which, an N-terminal peptide, from either an α or β subunit, rapidly plugs the channel pore upon activation (Figure 1.3)^{224, 225}.

While the N-terminal segments of α subunits can promote rapid channel inactivation, these sequences also create a docking platform for complex formation with the β tetramer. Segments near the N-termini of each α subunit merge to form the T1 domain: a hanging gondola-like structure that protrudes slightly into the cytoplasm and acts as a docking platform for the β complex (Figure 1.1)^{79, 226-228}. Each of four β subunits

bind to N-terminal loops on the cytoplasmic face of the T1 tetramer (Figure 1.1) ²²⁶. Only members of Kv1 and Kv4 subfamilies possess these loops and accordingly, Kv β subunits have only been shown to associate with these channels ²²⁶. The hanging gondola structure obstructs the direct flow of ions into the pore, shunting ions and N-terminal “ball-and-chain” peptides to maneuver around the T1/ β complex to access the pore ^{79, 226, 227}. Similar to the α complex, the tetrameric β assembly has four-fold symmetry, with each β subunit interacting with another in a side-to-end conformation ²²⁹. This arrangement creates a β_4 structure with a flat surface facing the membrane, promoting stable interaction with the T1 domain ^{226, 229}. Each β subunit consists of a triose-phosphate isomerase (TIM) barrel composed of eight parallel β strands with intervening α helical sequences surrounding the perimeter ²²⁹. Three mammalian genes encode Kv β proteins (i.e., Kv β 1-3) with highly conserved C-terminal regions and variable N-termini ^{225, 230}. The β 1 and β 3 proteins have longer N-termini that form “a ball-and-chain” inactivation peptides, whereas the β 2 lacks this structural motif ^{225, 231}. Thus, the Kv β gene products feature variable N-termini lengths that diversify the regulatory effects of these proteins on channel gating ⁸⁰.

In heterologous expression systems, co-expression of β subunits with the α pore complexes significantly modulates channel activity. Generally, co-expression of β 1 and β 2 variants with Kv1 channels increase Kv current density; whereas β 3 induces no significant change upon current density ⁸⁰. Furthermore, association of certain Kv1 and Kv4 family members with the three β splice variants results in shifts in the voltage-sensitivity of the pore complex. Several α/β complexes cause a hyperpolarizing shift in the voltage-sensitivity of activation (10-15 mV) ⁸⁰. Likewise, formation of certain heteromeric complexes can induce rapid N-type inactivation to otherwise noninactivating pore complexes or increase N-type inactivation (Figure 1.4) ⁸⁰. As such, this phenomenon can occur both through the N-terminal peptides of the β complex or the α pore region.

Interestingly, despite the lack of an N-terminal ball-and-chain motif, association with the $\beta 2$ subunit increases N-type inactivation of Kv1.4⁸⁰.

While these co-expression studies indicate the potential for a vast array of $Kv\alpha/\beta$ mosaic structures, heteromerization is not entirely stochastic among all Kv subunits, as only α and β splice variants of a specific subfamily (e.g., Kv1) can bind together^{210, 232-235}; however, an exception to this rule of subfamily specificity is the observation that “electrically silent” subfamilies (Kv5, Kv6, Kv8, Kv9) require heteromerization with Kv2 family members for functional expression.²³⁶ Structural determinants, such as the N-terminal docking site for the β subunit complex, restrict interactions between subunit subtypes^{235, 237-241}. This molecular diversity among heteromeric complexes may be critical for precise control of membrane excitability in a manner that accommodates the needs and enables proper function of different excitable cells. As the needs of a particular organ change, the subunit composition of Kv channels may change to meet these needs. Spatially, the variety among heteromeric complexes could allow for the fine control of membrane excitability in a manner that is tailored to specific cell phenotypes within tissues.

Enzymatic properties and regulatory roles of the $Kv\beta$ proteins

Nearly two decades ago, β -subunits were found to have significant sequence homology with the AKR superfamily of enzymes²⁴². This finding led to speculation that cellular redox state and membrane potential regulation are integrated as these enzymes metabolize numerous carbonyl substrates through hydride transfer from a bound nicotinamide adenine dinucleotide (i.e., NAD(P)H)²⁴³. Subsequent structural information demonstrated that, like other AKR enzymes, $Kv\beta$ subunits possess an active catalytic site and a pyridine nucleotide cofactor binding pocket near its C-terminal end²²⁹. The NADP⁺

cofactor found bound to the β complex strongly adheres to the active site, and, even after extensive washing of the purified protein, the pyridine nucleotide is still bound to the catalytic site ²²⁹. The nicotinamide cofactor is held in place by hydrogen bonding with a basic arginine and non-covalent interactions with an aromatic ring ⁷. This orientation promotes ternary complex formation between the active site protein, the pyridine nucleotide cofactor, and the carbonyl substrate (Figure 1.5) ²⁴⁴. In such positioning, the active site catalytic tyrosine can form a hydrogen bond with a substrate carbonyl group, promoting hydride transfer from the pyridine nucleotide cofactor to the carbonyl carbon (Figure 1.5) ²⁴⁴. The reverse reaction can also occur in which an alcohol is oxidized to an aldehyde compound by reduction of the bound pyridine nucleotide cofactor (Figure 1.5) ^{10, 244}. However, the catalytic rate of Kv β subunits regarding carbonyl reduction (0.06 to 0.4 min⁻¹ for Kv β 2) is slower than for other AKR enzymes; slow turnover is due to rate-limiting hydride transfer (0.3–0.8 min⁻¹, Kv β 2-mediated reduction of 4-nitrobenzaldehyde) and nucleotide cofactor release (0.9 min⁻¹, Kv β 2-mediated release of NADP⁺) ^{10, 244, 245}. The active site can bind both pyridine nucleotides with and without a phosphate group; thus, in vivo, substrate reduction may be achieved using NADH or NADPH ⁷. The pyridine nucleotide predominantly used for catalysis in vivo is unclear, although NADPH may predominate due to higher binding affinity ($K_d = 0.12 \pm 0.004 \mu\text{M}$) ⁷. However, the greater total intracellular pool of NAD/NADH⁺ as compared to NADP⁺/NADPH could overcome differences due to disparate binding affinities (NADH, $K_d = 1.23 \pm 0.16 \mu\text{M}$, NAD⁺ $K_d = 3.61 \pm 0.4 \mu\text{M}$) ^{7, 181, 246}.

Similar to cofactor preference, the identity of physiological substrates for the Kv β and their impact of channel function are unknown. However, several in vitro studies demonstrate that Kv β 2 reduces a range of endogenous and exogenous aldehydes and ketones. Purified Kv β 2 enzyme appears to possess an apparent preference for aldehydes

over ketones^{244, 247}. For example, reduction of the aldehyde group of 4-oxo-2-nonenal occurs rather than the ketone group, leading to the production of 4-oxo-nonenol²⁴⁴. Furthermore, this study demonstrated that the enzymatic capacity of the β subunits rely upon an essential catalytic tyrosine residue, shared amongst other AKR donors, at the 90th position of the amino acid chain in the active site of the protein²⁴⁴. Mutation of this tyrosine to phenylalanine nearly abolishes catalytic turnover of the substrates such as 4-nitrobenzaldehyde (specific activity, WT=0.118 \pm .2 min⁻¹, Y90F=0.009 \pm .002 min⁻¹) and 4-nitroacetophenone (specific activity, WT=0.050 \pm 0.008 min⁻¹, Y90F=0.006 \pm 0.003)²⁴⁴. Along with these C-nitro compounds, The Kv β 2 protein also readily reduced phenanthrenequinone (0.19 \pm 0.7 min⁻¹), and the glycolytic byproduct methylglyoxal (0.32 \pm 0.04 min⁻¹), oxidized phospholipids 1-palmitoyl-2-oxovaleroyl phosphatidylcholine (POVPC) (0.078 \pm 0.16 min⁻¹), 1-palmitoyl-2-arachidonoyl-sn-glycero-3-phosphocholine (PAPC)^{244, 247}. The finding that β 2 can catalyze oxidative products of PAPC indicates that Kv β AKR activity may respond to membrane stress occurring in disease states (e.g., atherosclerosis)²⁴⁷.

Although speculation of physiological substrates and cofactors continues, several classic studies demonstrate that both Kv β -mediated AKR activity and pyridine nucleotide-binding differentially influence Kv function. For example, in COS-7 cells, internal perfusion of 0.1 mM NADPH decreased Kv1.5/ Kv β 1.3 steady-state current, increased Kv β -mediated inactivation, and shifted $V_{1/2}$ of activation to more hyperpolarized potentials relative to internal application of 0.5 mM NADP⁺ (V_h of activation for 0.1 mM NADPH, -18.5 \pm .6 mV, V_h of activation for 0.5 mM NADP⁺, -0.1 \pm 0.3 mV) (Figure 1.6)⁹. Perfusion with 1 mM NAD⁺ or 0.1 mM NADH impacted these parameters similar to NADP⁺ and NADPH, respectively⁹. The effects of pyridine nucleotides on Kv1 currents are also observed in channels associated with Kv β 2 and Kv β 3 proteins. The internal application of

250 μM NADPH reduced the steady-state current mediated by Kv1.5 α /Kv β 3 complexes and increased inactivation relative to 1 mM NADP⁺ ¹⁹⁵. However, unlike with β 1, NADPH did not substantially shift the $V_{1/2}$ of activation of these Kv α / β complexes relative to internal perfusion of NADP⁺ ¹⁹⁵. In contrast, internal perfusion of 250 μM NADPH significantly shifted the $V_{1/2}$ of activation of Kv1.5 α / β 2 complexes to hyperpolarized potentials relative to 1 mM NADP⁺ (V_h of activation for 250 μM NADPH, -17.2 ± 1.8 mV, V_h of activation for 1 mM NADP⁺, -10 ± 0.7 mV) (Figure 1.7) ¹⁹⁵. Kv β 2 does not possess an N-terminal “ball and chain peptide”; therefore, this hyperpolarizing shift occurred without a concomitant increase in inactivation ^{195, 225, 231}. Moreover, C-terminal truncation of Kv1.5 (ΔC56 Kv1.5) eliminated pyridine nucleotide sensitivity imparted by Kv β 2 ¹⁹⁵. These results suggest that interactions between Kv α C-termini and Kv β pyridine nucleotide-binding pockets are critical for functional modulation by pyridine nucleotide redox state. As a general summary, Figure 1, in Appendix B, illustrates a simplified scheme of pyridine nucleotide regulation of various Kv α / β complexes.

In addition to differential regulation of channel activity upon binding pyridine nucleotides, the catalytic activity of Kv β may also impact channel function. Several experiments demonstrate that the Kv β active site can react with carbonyl substrates and oxidizing agents to modulate channel activity. 4-cyanobenzaldehyde (4-CY), at a 5 mM concentration, or 10 mM H₂O₂ treatment significantly increased steady-state current density of *Xenopus* oocytes expressing Kv1.1/Kv β 1 complexes, (0.50 ± 0.04 , ΔI_{ss} for 4-CY, 0.40 ± 0.06 , ΔI_{ss} for H₂O₂) ²⁴⁸. Concomitantly, time constants of current decay robustly increased upon 4-CY and H₂O₂ treatment ²⁴⁸. 4-CY increased τ_{fast} from 3.3 ± 0.1 to 11.2 ± 0.5 ms and increased τ_{slow} from 35.1 ± 2.2 to 103.3 ± 3.3 ms ²⁴⁸. Similarly, H₂O₂ increased τ_{fast} from 3.2 ± 0.1 to 8.3 ± 0.9 ms and increased τ_{slow} from 33.7 ± 3.0 to 81.8 ± 10.4 ms ²⁴⁸. The substantial increase in steady-state current upon AKR activity occurs due to

oxidant-induced exposure of two glutamate residues (E349 and E265) on the $\beta 1$ subunit, which bind to two arginine residues (R48 and R37) on the $\beta 1$ N-terminal motif, restraining the inactivation peptide from blocking the channel pore⁸. A chimeric Kv1.1 ion channel, with no AKR sequence, supports this model as this mutant has a blunted response to H₂O₂ and 4-CY²⁴⁸. Furthermore, $\beta 1.1$ subunits, with AKR point mutations (D119A, Y152F, K152A), have reduced β -mediated inactivation (10 ± 1 % WT I_s/I_{peak} vs. 81 ± 3 % D119A I_s/I_{peak}), suggesting that AKR activity regulates N-terminal inactivation²⁴⁹. Similar to $\beta 1$ subunits, the $\beta 2$ AKR catalytic site also substantially affects the (in)activation properties of the alpha pore complex. For example, Kv1.4/Kv $\beta 2$ complexes respond to the perfusion of 4-CY with increased steady-state current and decreased channel inactivation rate (81 ± 1.9 sec⁻¹ to 46 ± 1.4 sec⁻¹) (Figure 1.8)¹⁰. Like Kv $\beta 1$ complexes, mutations at the catalytic site (D85N and K118M) abolished these effects on current density and inactivation¹⁰. However, whether these effects are primarily due to blunted turnover is uncertain as the Kv β AKR catalytic can also affect Kv complex expression.

Mutations in both the cofactor binding pocket and AKR catalytic site of Kv $\beta 1$ and Kv $\beta 2$ have varied effects upon expression of the channel. For example, a single amino acid substitution (R316E) in the cofactor binding pocket of Kv $\beta 1.3$ significantly increased the K_D value for NADPH by disrupting cofactor binding²⁵⁰. This mutation elicited a diffuse pattern of Kv1.5/Kv $\beta 1.3$ expression across the membrane and the cytosol of Cos-7 cells, indicating that cofactor binding pocket mutations affect channel trafficking and expression²⁵⁰. Likewise, a mutation in the cofactor binding site of Kv $\beta 1.1$, W277V, significantly depleted the trafficking of Kv1.2 α complexes to the membrane in both Cos-1 cells and hippocampal neurons⁸¹. In contrast, Kv $\beta 2$ catalytic mutants (Y90F, Y90A) retained axonal localization of Kv1.2 channels to a much greater extent than the Kv $\beta 1.1$ W277V mutant⁸¹. This result is not consistent amongst all Kv1 complexes as mutations in both the binding

pocket (S188A, R189L) and catalytic site (D85A, Y90F) of Kv β 2 abolished the ability of the auxiliary complex to increase Kv1.4 expression in *Xenopus oocytes*²⁵¹. Thus, cofactor binding pocket and catalytic site mutations could induce various effects depending on the Kv α/β composition.

The broad physiological properties of Kv β subunits, including effects upon membrane trafficking and channel activity, indicate that they may possess many diverse functions in several organ systems. As discussed in the next section, recent studies, concerning the *in vivo* roles of Kv complexes in the cardiovascular system, display this multifunctional nature of the complex. These recently discovered physiological roles will give a basis for the hypotheses in this dissertation.

The role of Kv β subunits in the cardiovascular system

These recent studies in cardiovascular system demonstrate that modulating the cytosolic NADH/NAD⁺ ratio imparts significant effects upon the cardiac action potential. In isolated cardiomyocytes, lactate concentrations of 10 mM and 20 mM, increased the action potential duration at 20% and 50%^{196, 252}. Similarly, lactate, at a concentration of 20 mM, significantly increased monophasic action potentials of wild-type mouse hearts at 20%, 50, 70%, and 90% of the action potential duration^{196, 252}. On the contrary, pyruvate, at concentrations of 1 mM and 20 mM, reversed the lactate-induced prolongation of monophasic action potential duration^{196, 252}. Measurement of whole heart NADH levels demonstrated an accumulation of reduced pyridine nucleotides after lactate treatment, suggesting lactate directly causes the generation of a reduced pyridine nucleotide redox state to affect action potential morphology^{196, 252}. To simulate a situation of metabolic demand rather than utilize lactate treatment, isoproterenol was perfused into *ex-vivo* heart preps and changes in pyridine nucleotide redox state and action potential morphology were measured²⁵². Similar to lactate, β -adrenergic signaling increased action potential

duration at 20%, 50%, and 70% ²⁵². Furthermore, this agonist caused a robust increase in NADH in the myocardium ²⁵². To test a more direct effect upon pyridine nucleotide redox state, I_{Kv} currents of isolated cardiomyocytes were recorded in the presence of a “hypoxic” intracellular mixture of pyridine nucleotides (high NADH/NAD⁺) and a “normoxic” intracellular solution of pyridine nucleotides (low NADH/NAD⁺) ¹⁹⁶. In agreement with the indirect lactate measurements, the hypoxic mixture substantially increased the rate of inactivation compared to the normoxic solution, indicating action potential prolongation ¹⁹⁶. In addition to these experiments in wild-type mice, knockout of either the $\beta 1.1$ or $\beta 2$ subunit disrupted the action potential prolongation induced by both lactate and reduced pyridine nucleotides ^{196, 252}. Collectively, these results suggest that cardiac $Kv\beta$ complexes can modulate action potential morphology in the context of metabolic demand by sensing shifts in pyridine nucleotide redox state.

In addition to these investigations focusing on the myocardium, recent studies suggest that these $Kv\alpha/\beta$ complexes sense cardiac workload and promote vasodilation to increase systemic blood flow. For example, Kv channel inhibition significantly dysregulates the vasodilatory response in the context of increased metabolic demand. A $Kv1$ channel blocker, 4-AP, decreased the coronary venous PO_2 of swine in the context of increasing MVO_2 , compared to swine not given a $Kv1$ antagonist ²⁵³. Similarly, infusion of correolide, a specific $Kv1$ channel blocker, into the circulation of anesthetized pigs disrupted the linear relationship between MVO_2 and coronary blood flow ⁴. Other studies demonstrate that knockout of specific $Kv\alpha$ subunits inhibit the coronary flow response to increased metabolic demand, reinforcing that $Kv1$ channels are metabolic sensors in the vasculature. For example, knockout of $Kv1.5$ ion channels in mice significantly disrupted the linear relationship between cardiac work and myocardial blood flow ⁶. However, doxycycline-induced reconstitution of $Kv1.5$ channels re-established this association

between metabolic demand and vasodilation ⁶. This relationship appears to involve signaling by oxidizing agents through the redox-sensing capacity of Kv α / β complexes as hydrogen peroxide is unable to produce a robust vasodilatory response in Kv1.5 knockout coronary microvessels ⁶. Like the Kv1.5 α subunit, Kv1.3 knockout mice also exhibit similar disruptions in hydrogen peroxide-induced vasodilation and cardiac work-induced enhancements in myocardial blood flow ⁵.

Hypothesis & specific aims

This previous literature indicates that in heterologous expression systems, auxiliary intracellular Kv β subunits regulate Kv opening by binding to pyridine nucleotides ^{9, 195, 244}. Since established literature also suggests Kv1 channels are integral in metabolic hyperemia and that pyridine nucleotide reflect metabolic changes in the myocardium, Kv β subunits may be a key factor in sustaining coronary blood flow in the context of increased metabolic demand ^{4-6, 190, 191, 194}. However, whether the AKR activity of the Kv β subunits directly influence metabolic hyperemia is unknown. Based on the established literature concerning Kv β function, the Kv β 2 subunit may possess an influential role regarding metabolic hyperemia in the heart. In heterologous expression systems, Kv β 2 subunits promote Kv1 channel activation in the presence of reduced pyridine nucleotides without a concomitant increase in channel inactivation ¹⁹⁵. Therefore, during metabolic hyperemia, Kv β 2 subunits could potentiate Kv1 activity by sensing an accumulation of reduced pyridine nucleotides in the coronary vasculature. Since NADH accumulates in the myocardium upon increased metabolic demand, reduced pyridine nucleotides could accumulate in the coronary vasculature during metabolic hyperemia ¹⁹⁰. Therefore, we hypothesized coronary arteries dilate in response to high demand via the pyridine nucleotide sensing capacity of Kv1-associated β 2 subunit complexes. A schematic of this

overall hypothesis is represented in Figure 1.9. To test this hypothesis, we established three aims.

Aim 1: Quantify the relationship between myocardial metabolic demand and PN redox state.

The first component of our hypothetical mechanism proposes that, upon increased myocardial demand, NADH/NAD⁺ ratio increases in the coronary vascular wall. To investigate this concept, we isolated aortic vascular smooth muscle cells from wild-type mice, and we tracked cytosolic NADH/NAD⁺ ratio in these cells utilizing a Peredox-NADH biosensor. We recorded cytosolic NADH/NAD⁺ ratio of Peredox-expressing aortic vascular smooth muscle cells under different conditions of metabolic demand (e.g., hypoxia, β -adrenergic receptor activation, electrical stimulation). Most notably, we co-cultured Peredox-expressing aortic vascular smooth muscle cells with human induced pluripotent stem-cell derived cardiomyocytes, and we recorded cytosolic NADH/NAD⁺ ratio in the Peredox-expressing aortic vascular smooth muscle cells while stimulating the co-culture with increasing electrical pacing frequencies. We found that electrical stimulation of the co-culture significantly increased cytosolic NADH/NAD⁺ ratio in the Peredox-expressing aortic vascular smooth muscle cells. However, electrical stimulation of Peredox-expressing aortic vascular smooth muscle cells alone did not increase cytosolic NADH/NAD⁺ ratio. We supported these in vitro results by demonstrating that, upon dobutamine-challenge of wild-type mice, lactate/pyruvate ratio increases significantly in the coronary wall. Since lactate/pyruvate is in close equilibrium with NADH/NAD⁺ ratio, this result indicates that NADH/NAD⁺ ratio increases in the coronary wall upon increased cardiac workload^{180, 181}. These in vitro and in vivo experiments both support that hypothesis that upon enhanced cardiac workload NADH/NAD⁺ ratio increases in the coronary vascular wall.

Aim 2: Establish that the influence of PNs on Kv1 channel gating depends upon the associated β subunit complexes in CVSM cells.

Aim 1 was designed to demonstrate that cytosolic pyridine nucleotide redox state in the coronary vasculature reflects myocardial demand. The experiments in this aim were designed to test whether coronary vascular Kv1 channels can respond to myocardial metabolic demand by sensing pyridine nucleotide redox state. We utilized patch clamp electrophysiology, and recorded Kv1-mediated currents from coronary vascular smooth muscle (CVSM) cells. We recorded both single Kv1 channel and whole Kv1-mediated currents in the context of variable pyridine nucleotide redox state. We found that, while a reduced pyridine nucleotide redox state, increased Kv1 channel activity in wild-type coronary vascular cells, Kv β 2 knockout ablated the increase in Kv1 activity mediated by reduced pyridine nucleotides. To further elucidate the mechanism of Kv β 2, we investigated how the AKR catalytic activity of Kv β 2 influences the increase in Kv1 channel activity in response to NADH. Our results indicate that the Kv1 channels in the coronary vasculature are responsive to pyridine nucleotide redox state. Furthermore, the data demonstrate that the Kv β 2 subunit is essential in mediating the increase in coronary vascular Kv1 activity observed upon an increase cytosolic NADH/NAD⁺ ratio. Lastly, mutation of the Kv β 2 AKR catalytic site inhibited the increase in Kv1 channel activity that occurs in response to NADH. Collectively, these results suggest Kv β 2 AKR enzyme could be critical in sensing the accumulation of reduced cytosolic pyridine nucleotides in the coronary vasculature that could potentially occur during metabolic hyperemia.

Aim 3: Delineate the influence of Kv β 2 expression on the relationship between CVSM metabolic status, Kv1 channel activity, and coronary vascular tone.

Aims 1 and 2 establish experiments to demonstrate that pyridine nucleotide sensitive Kv β 2 subunits can regulate outward Kv1-mediated currents to changes in

myocardial demand. In this aim, we investigated whether this pyridine nucleotide sensing capacity can function to manifest appropriate changes in vascular tone in the context of metabolic hyperemia. Furthermore, we investigated whether the regulation of vascular tone and coronary blood flow during metabolic hyperemia depends on the expression of functional Kv β 2 subunits. In this regard, we assessed lactate-induced vasodilation of isolated murine vessels derived from Kv β 2 knockout and mice possessing a mutant Kv β 2 AKR catalytic site. Also, utilizing echocardiography, we determined whether ablation of Kv β 2 subunits or mutation of the Kv β 2 AKR catalytic site blunts the linear relationship between myocardial blood flow and increased myocardial demand. We found that both ablation of the Kv β 2 functionality inhibits lactate-induced dilation and metabolic hyperemia. Cumulatively, these experiments demonstrate that Kv β 2 AKR catalytic activity is critical to metabolic hyperemia in the coronary vasculature.

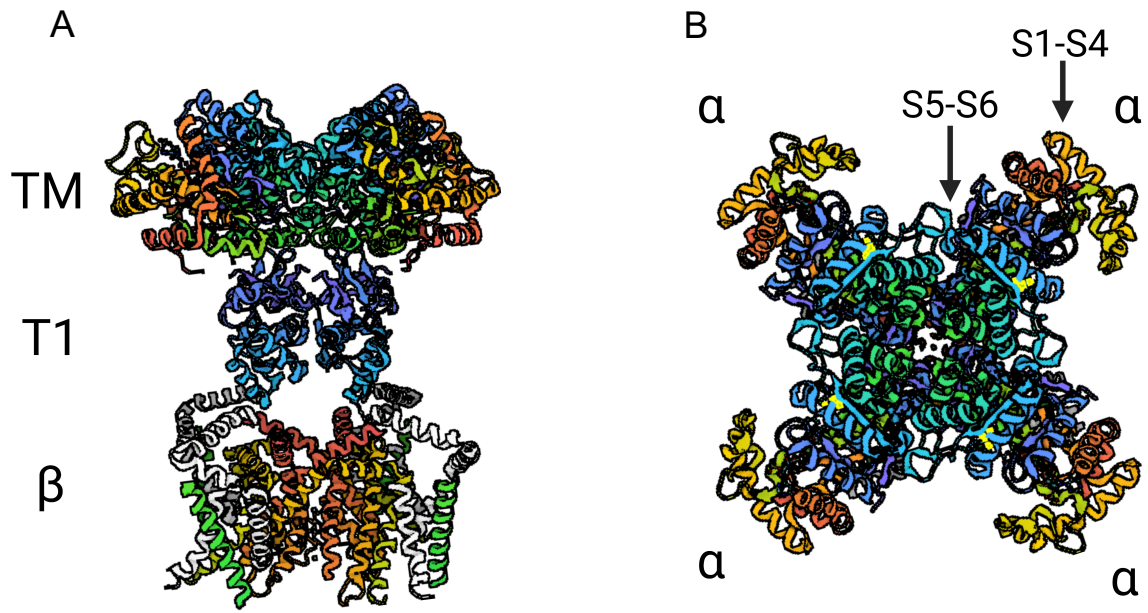


Fig. 1.1. Model of the Kv1 channel structure. A) This structural model shows the octameric structure of the Kv1 channel. The transmembrane α pore domain is labelled TM. The TM domain is composed of four α subunits with the N-terminal segments of each α subunit coalescing together to form the T1 domain shown below the α pore complex. The tetrameric β complex, labelled with the symbol β , docks upon the T1 domain. B) This structural model displays a top-down view of each of the four α subunits that compose the pore. The inner helices closer to the pore center are the S5-S6 helices that comprise the pore. The S1-S4 helices surround the pore helices around the outer edge of the channel. Created with Biorender.com. Adapted from Long, S.B., Campbell, E.B., Mackinnon, R. (2005) Kv1.2- β 2 subunit complex. doi: 10.1126/pdb2A79/pdb, 10.1126/science.111629

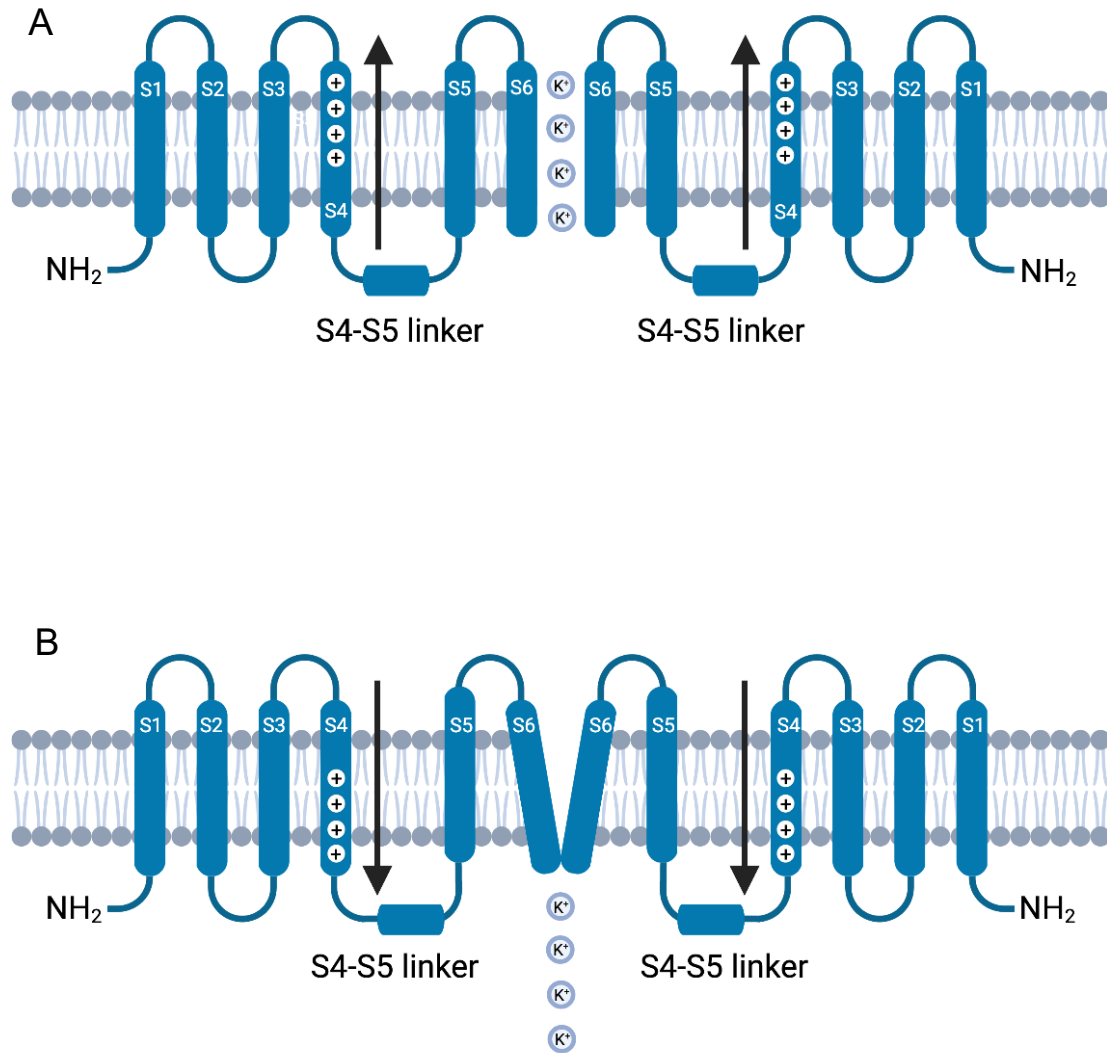


Fig. 1.2. Mechanism of Kv voltage-dependent gating. This schematic displays a 2-dimensional model showing the transition between the open and closed state of the Kv channel. A) Membrane potential depolarization shifts positively charged residues in S4 of the voltage sensor towards the extracellular space which shifts the pore into an open state by relieving compression of the inner helix bundle imparted by the S4-S5 linkers B) Upon hyperpolarization, the change in potential shifts the S4 gating charges towards the cytosolic space such that the S4-S5 linkers compress the inner helix bundle, closing the pore. This simplified model only shows two α subunits. In vivo, closure of the channel is mediated by four α subunits that comprise the pore. Created with Biorender.com.

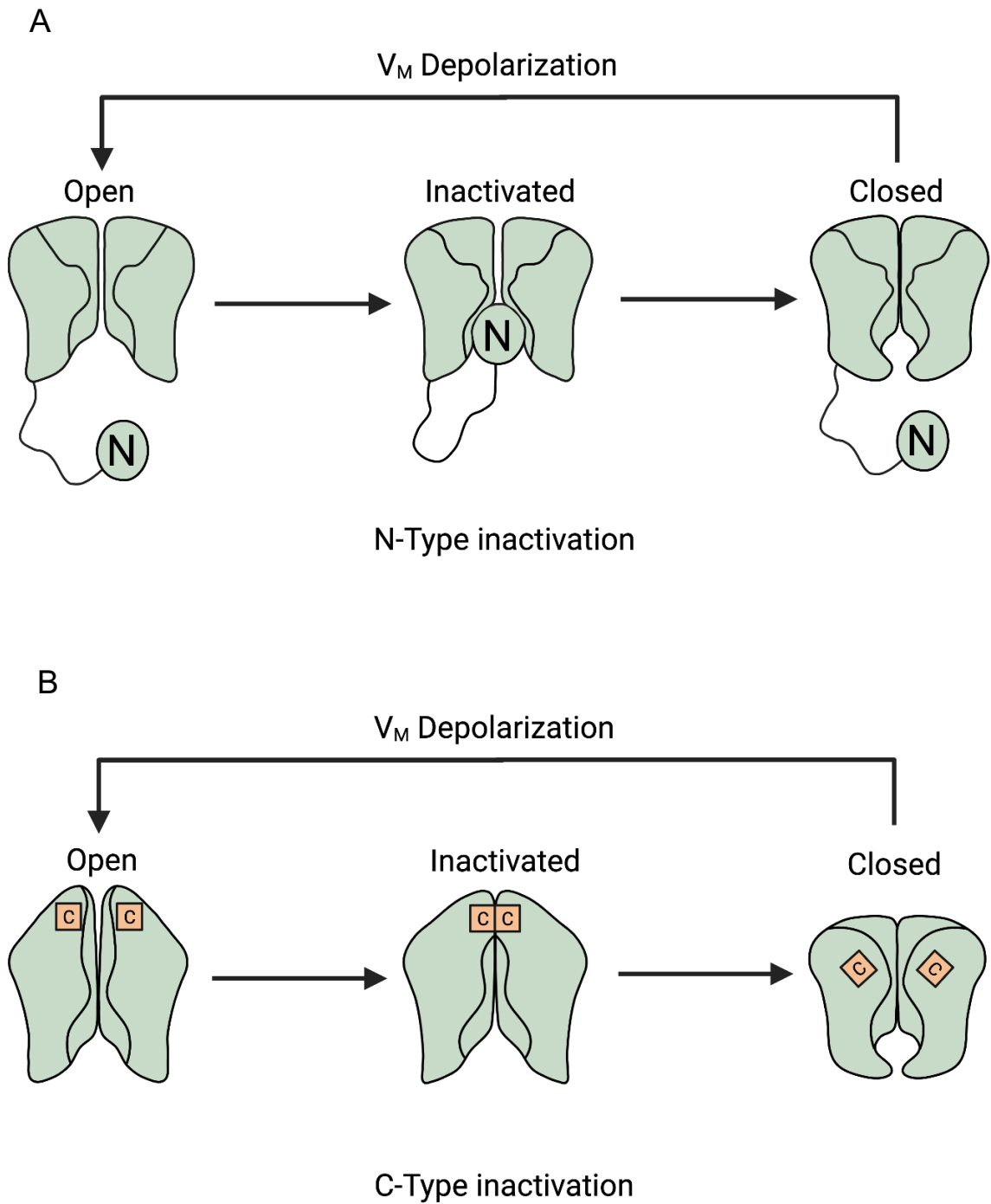


Fig. 1.3. N-type and C-type inactivation. A) N-type inactivation occurs when an N-terminal ball-and-chain domain rapidly obstructs the pore following channel activation B). C-type inactivation occurs when the extracellular mouth of the pore closes following activation of the channel. Created with Biorender.com. Adapted from Rasmusson RL et al. *Circ Res.* 1998 Apr 20;82(7):739-50

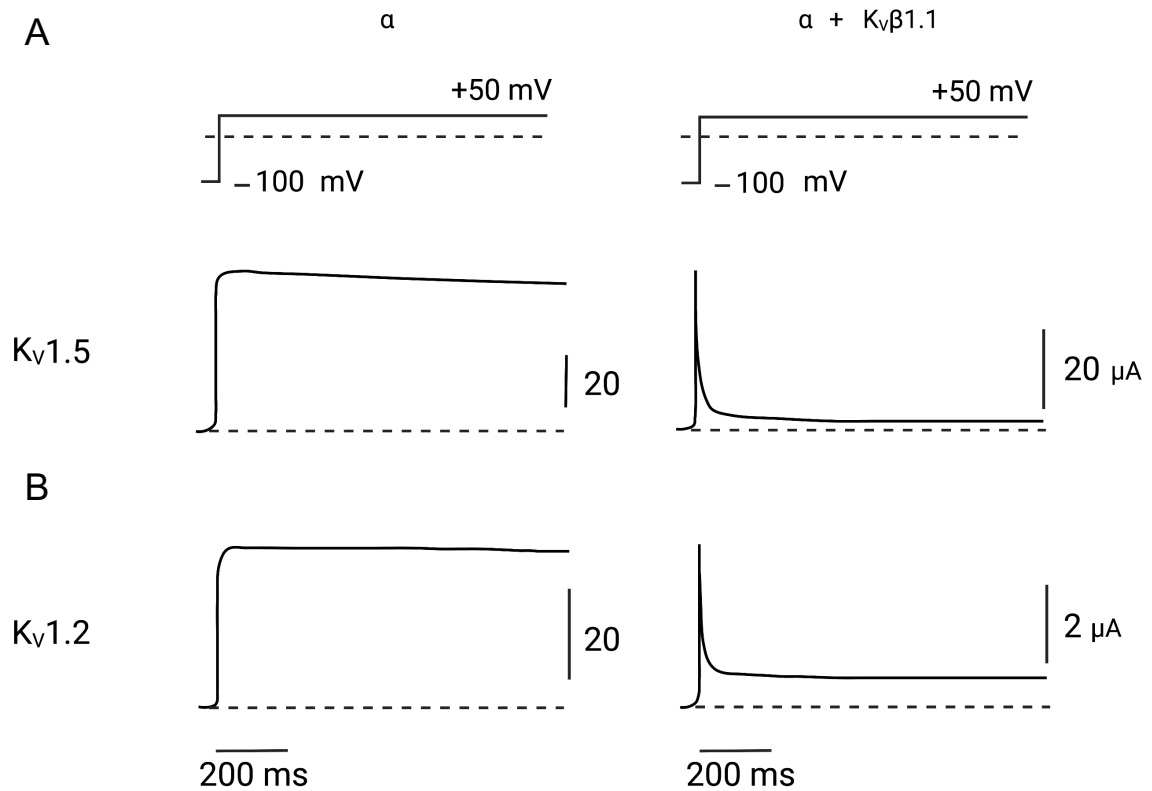


Fig. 1.4. $Kv\beta 1$ imparts N-type inactivation upon delayed rectifier $Kv1$ channels. A) When expressed alone the α subunits, $Kv1.5$ and $Kv1.2$, elicit delayed rectifier currents upon depolarization to +50 mV B) Upon co-expression of $Kv1.2$ and $Kv1.5$ with $Kv\beta 1.1$, these α subunits elicit rapidly inactivating currents when depolarized to +50 mV. $Kv\beta 1.1$ imparts rapid N-type inactivation upon these pore complexes. Created with Biorender.com. Adapted from Heinemann SH et al. J Physiol. 1996 Jun 15;493 (Pt 3)(Pt 3):625-33

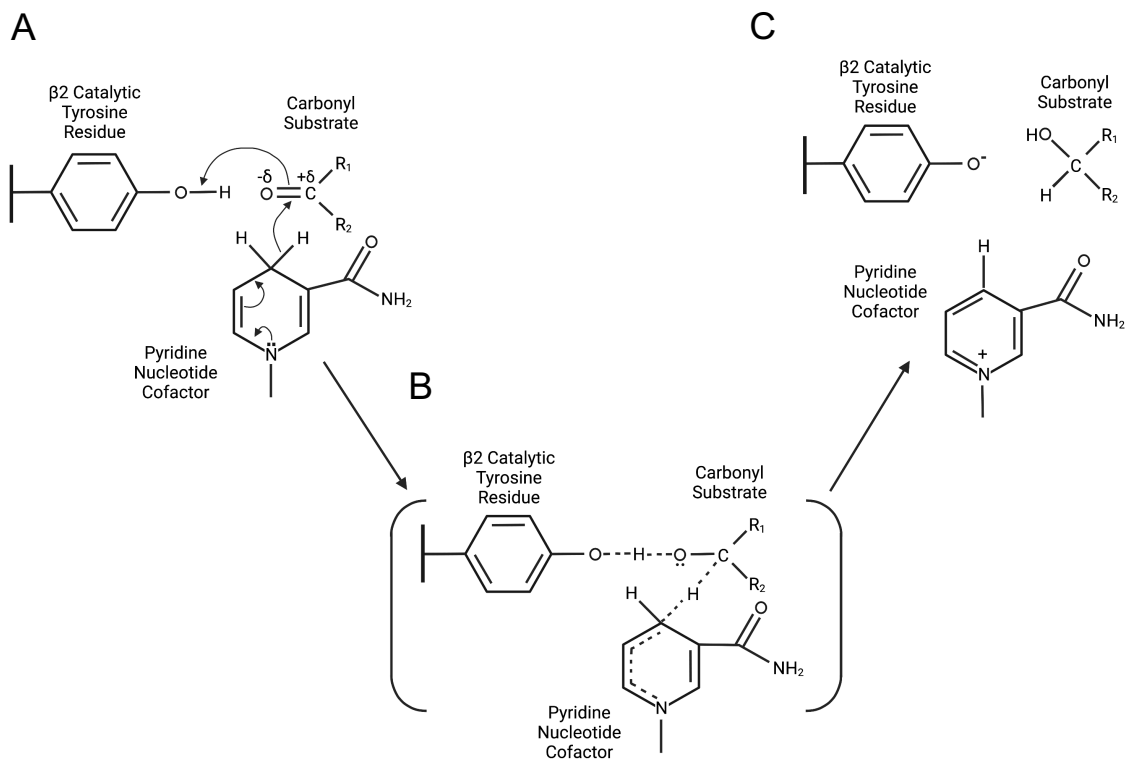


Fig. 1.5. Catalytic mechanism of the Kv $\beta 2$ subunit. This model demonstrates how the AKR catalytic site of the Kv $\beta 2$ subunit utilizes NAD(P)H to reduce carbonyl substrates. (A, B) The tyrosine-90 in the AKR catalytic site forms a hydrogen bond with the carbonyl substrate to form the transition state shown in B. The hydrogen bond promotes hydride transfer between the pyridine nucleotide co-factor and the carbonyl carbon of the substrate. (C) The carbonyl substrate is then released from the binding pocket as an alcohol. In addition to the formation of alcohols, the reverse reaction can occur in which an alcohol is converted into an aldehyde. Created with Biorender.com. Adapted from Tipparaju SM et al. *Biochemistry*. 2008 Aug 26;47(34):8840-54

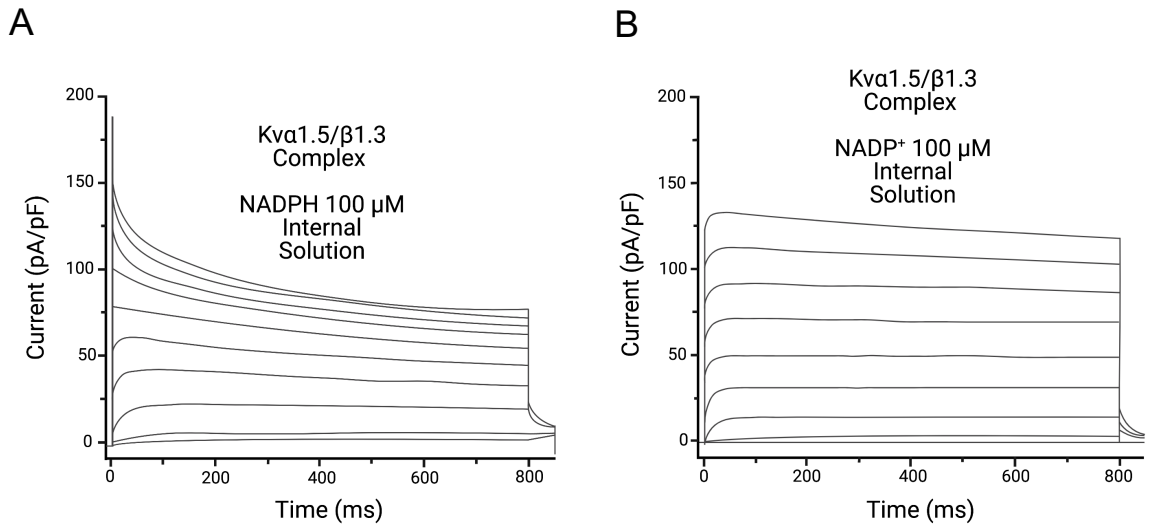


Fig. 1.6. Oxidized pyridine nucleotides decrease inactivation of the Kv1.5/ Kv β 1.3 channel complex. A) Intracellular exposure to NADPH (100 μ M) promotes inactivation of Kv1.5 α /Kv β 1.3 channel complexes expressed in Cos-7 cells. B) Intracellular exposure to NADP⁺ increases current density and relieves inactivation of Kv1.5 α / Kv β 1.3 complexes expressed in Cos-7 cells. Created with Biorender.com. Adapted from Tipparaju SM et al. Am J Physiol Cell Physiol. 2005 Feb;288(2):C366-76

A

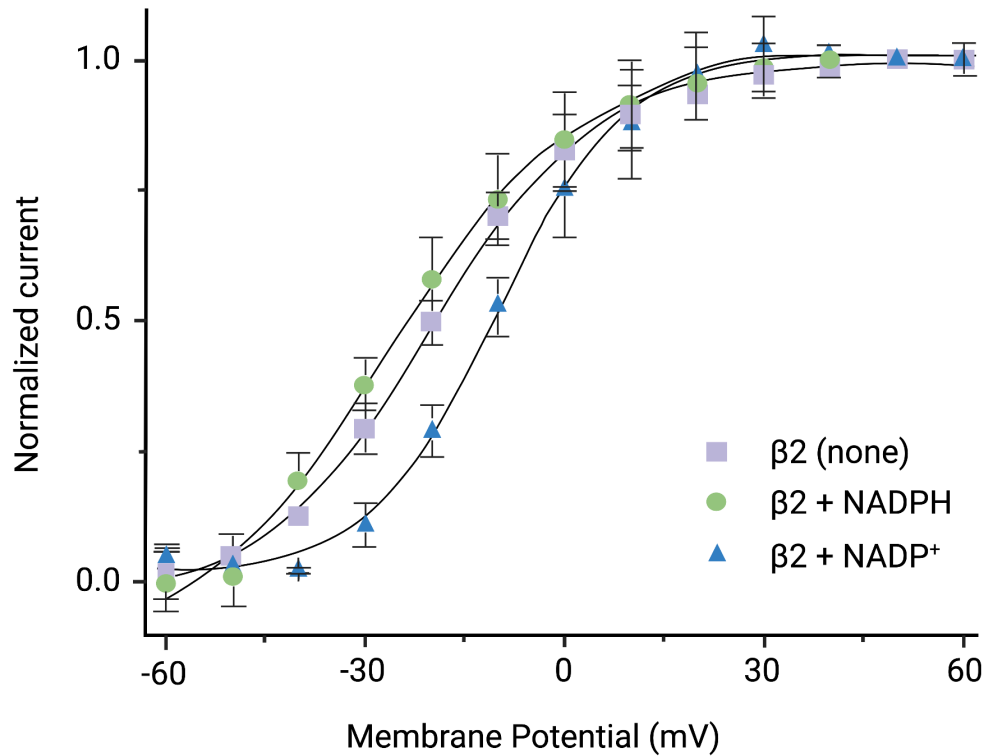


Fig. 1.7. Regulation of Kv1.5 α /Kv β 2 channel complexes by pyridine nucleotides. A) COS-7 cells expressing Kv1.5 α /Kv β 2 were exposed intracellularly to 250 μM NADPH or 1 mM NADP $^+$. NADPH shifted V_h of activation to hyperpolarized potentials in comparison to NADP $^+$. (V_h of activation for 250 μM NADPH, -17.2 ± 1.8 mV, V_h of activation for 1 mM NADP $^+$, -10 ± 0.7 mV) Created with Biorender.com. Adapted from Tipparaju SM et al. Pflugers Arch. 2012 Jun;463(6):799-818

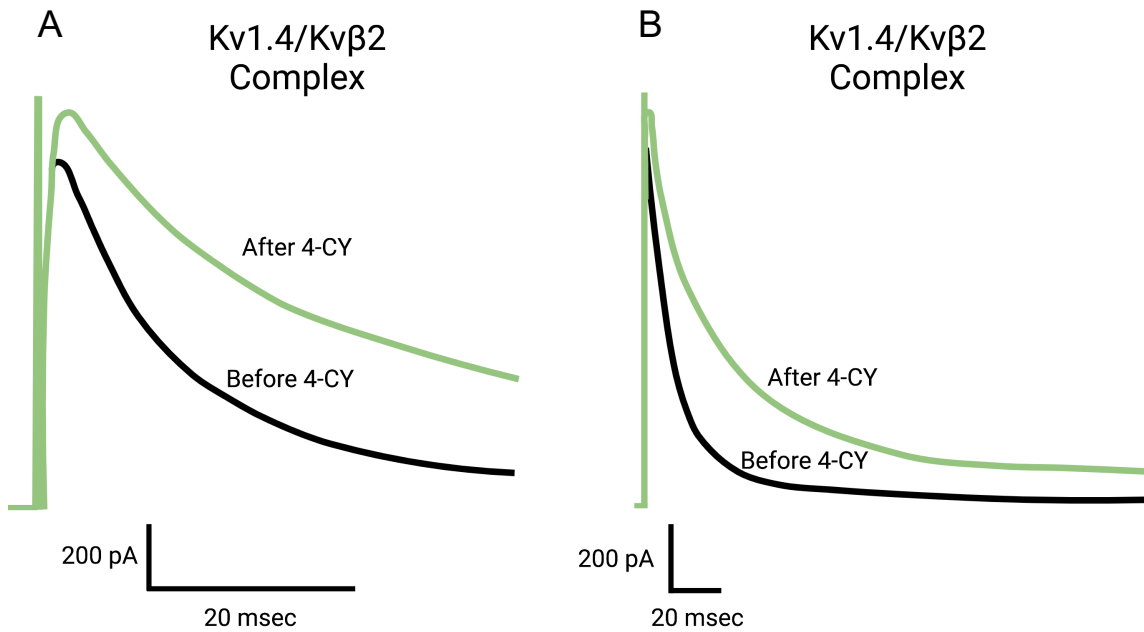


Fig. 1.8. Kvβ2 AKR catalytic activity decreases Kv1 channel inactivation. Current traces were recorded from *Xenopus* oocytes expressing Kv1.4 α /Kvβ2 complexes. Currents were recorded before (black trace) and after (red trace) exposure to 5 mM 4-carboxybenzaldehyde (4-CY). A and B show two different time scales of the traces. Catalytic turnover of 4-CY decreases channel inactivation rate. Created with Biorender.com. Adapted from Weng J et al. *J Biol Chem.* 2006 Jun 2;281(22):15194-20

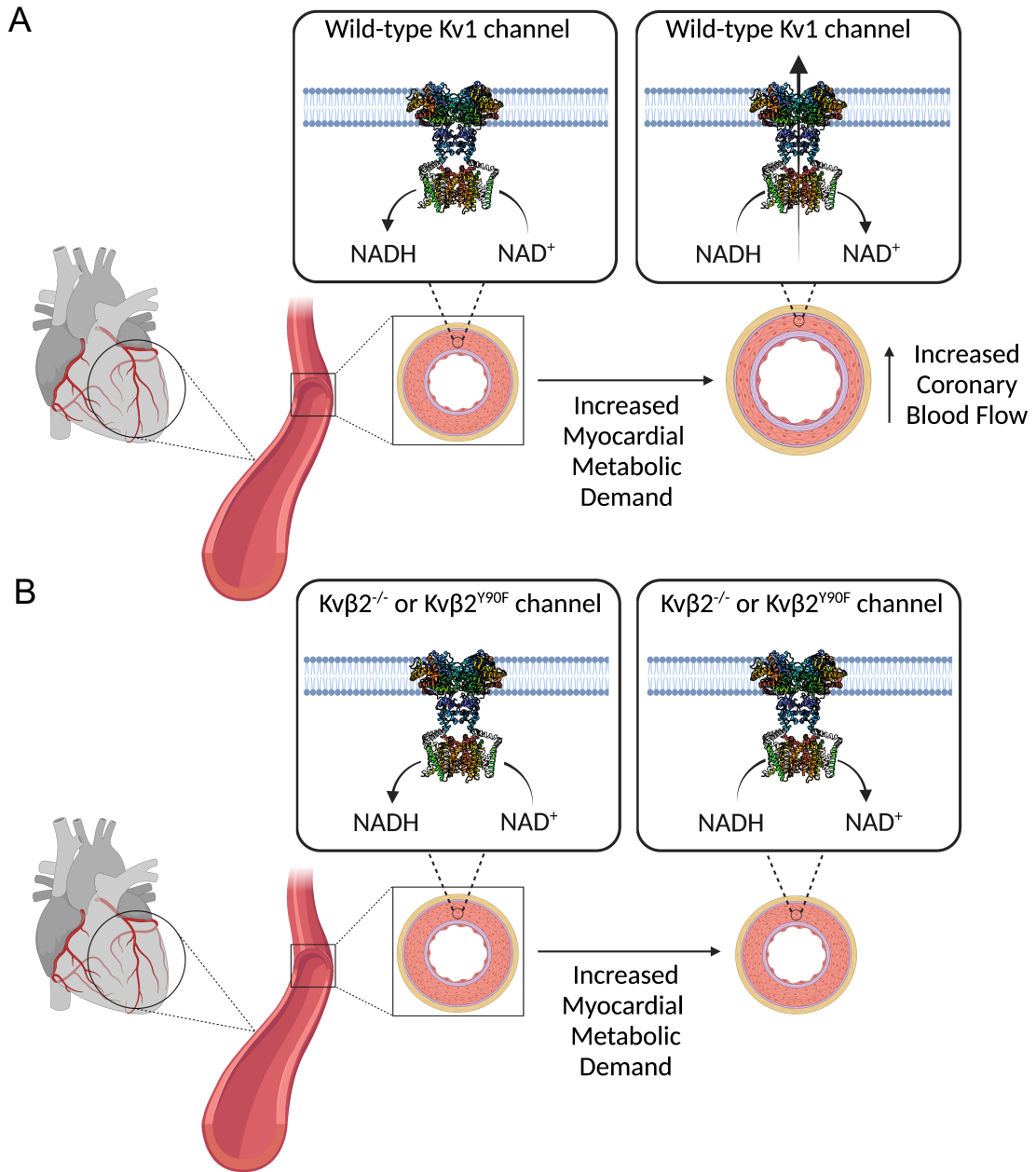


Fig. 1.9. Hypothetical mechanism of the Kvβ2 auxiliary complex in metabolic hyperemia. A) Under resting conditions, NADH/NAD⁺ ratio remains low in the cytosolic compartment of coronary vascular smooth muscle cells, and Kv1 channel activity is not substantial enough to promote vasodilation. However, upon increasing myocardial metabolic demand, cytosolic NADH/NAD⁺ ratio increases, which induces Kvβ2-mediated potassium efflux through Kv1 channels, initiating vasodilation and increasing blood flow. B) Knockout of the Kvβ2 subunit or mutation of the Kvβ2 AKR catalytic site inhibits Kvβ2-mediated potassium efflux through Kv1 channels and, subsequently, the increase in coronary blood flow that occurs upon increased metabolic demand. Created with Biorender.com. Protein structure retrieved from Long, S.B., Campbell, E.B., Mackinnon, R. (2005) Kv1.2-β2 subunit complex. doi: 10.1126/pdb2A79/pdb, 10.1126/science.111629

CHAPTER II

MATERIALS AND METHODS

Animals and animal euthanasia

All animal procedures were performed as approved by the Institutional Animal Care and Use Committees at the University of Louisville and Northeast Ohio Medical University. Genetically engineered mouse strains in which *Kcnab1* or *Kcnab2* genes were ablated (i.e., $Kv\beta 1.1^{-/-}$, $Kv\beta 2^{-/-}$, respectively)^{254, 255} or in which tyrosine 90 of $Kv\beta 2$ was mutated to phenylalanine ($Kv\beta 2^{Y90F}$)²⁵⁵ were used for this study. Strain-matched wild type mice (WT; C57BL6N for $Kv\beta 1.1^{-/-}$, 129SvEv for $Kv\beta 2^{-/-}$) were used as controls (indicated in figure legends). Due to the potential for confounding effects of estrogen on the functional expression of vascular K^+ channels,²⁵⁶⁻²⁵⁸ only male mice (aged-3-6 months) were used. All mice were bred in house and fed normal chow ad libitum. Mice were euthanized by sodium pentobarbital (150 mg/kg; i.p.) and thoracotomy and tissues were excised immediately for *ex vivo* assessments as described below.

Human tissue

Deidentified fresh human tissues, obtained through the Midwest Transplant Network, were kindly provided for this study by Dr. Tamer Mohamed (Division of Cardiovascular Medicine, University of Louisville). Branches of superficial and subepicardial left anterior descending coronary arteries were dissected from an excised heart (male, 52 yrs old) in ice-cold Ca^{2+} -free physiological saline solution consisting of (in

mM): 140 NaCl, 5 KCl, 2 MgCl₂, 10 HEPES, 10 glucose, pH 7.4. Arteries were enzymatically digested to isolate individual arterial myocytes as described below.

Isolation of coronary arterial smooth muscle cells

Hearts were excised and immediately transferred to ice-cold physiological saline solution containing (in mM): 134 NaCl, 6 KCl, 1 MgCl₂, 2 CaCl₂, 10 HEPES, and 7 glucose, pH 7.4. First and second-order branches of the left anterior descending coronary artery were manually dissected and smooth muscle cells were isolated as previously described²⁵⁹. Briefly, arterial segments were incubated at 37°C in Ca²⁺-free physiological saline (composition described above), containing papain (1 mg/ml) and dithiothreitol (1 mg/ml) for 5 min with gentle agitation. Then, the solution was replaced with buffer containing trypsin inhibitor (1 mg/ml) and collagenase (type H, 1 mg/ml) and incubated at 37°C for an additional 5 min with gentle agitation. For human tissues, arterial myocytes were digested in collagenase (type H, 3 mg/mL; Sigma Aldrich), elastase (1 mg/mL; Sigma Aldrich), and bovine serum albumin (10 mg/mL; Sigma Aldrich) at 37°C for 30 min with gentle agitation. Digested tissues were washed three times with ice-cold enzyme-free buffer. Cells were liberated by gentle trituration with a flame-polished glass pipette and kept on ice until use.

Imaging Mass Spectrometry

Hearts from anesthetized (sodium pentobarbital, 50 mg/kg, i.p.) mice that were acutely treated with dobutamine (10 mg/kg, i.p.) or vehicle (phosphate buffered saline;) were rapidly frozen with liquid N₂ and immediately excised and stored at -80°C. Thin sections (12 μm) of fresh frozen mouse hearts were obtained from a cryostat (Leica CM 1900) and thaw-mounted onto gold-coated stainless steel MALDI target plates. Serial sections were obtained for H&E staining on standard glass microscope slides. Four serial sections were obtained for each heart and used for imaging mass spectrometry (IMS). An

automated sprayer (TM Sprayer, HTX Technologies) was used to apply the MALDI matrix to the tissues. 9-Aminoacridine (9AA, hydrochloride salt, Sigma-Aldrich A38401) was prepared at 5 mg/ml in 90% methanol and sprayed at 0.12 ml/min, 85°C, and 700 mm/min stage velocity. Eight passes were deposited at 3 mm track spacing, alternating horizontal and vertical positions between passes. Metabolite images were acquired on a 9.4T FT-ICR mass spectrometer (Bruker Solarix, Bruker Daltonics) in negative ionization mode at 20 µm spatial resolution. Data were acquired in CASI mode, with Q1 isolating m/z 86 with a 6 amu window with a detected mass range of 72-350 amu. Images were visualized with FlexImaging software (Bruker). Regions of interest were selected to encompass the coronary wall and the surrounding tissue. Spectra were averaged for each region of interest, and the intensities for signals corresponding to lactate (m/z 89.0244) and pyruvate (m/z 87.0088) were exported.

Smooth muscle and hiPSC-CM co-culture preparation and live-cell fluorescence imaging

Vascular smooth muscle cells were isolated using previously described methods shown to yield highly pure CD31/CD45/lineage marker-negative and α -smooth muscle actin-positive cells.²⁶⁰ Thoracic and abdominal aortae were excised and placed in ice-cold Dulbecco's Modified Eagle Media (DMEM) containing Fungizone™ (1:1000; Thermo Fisher Scientific). Vessels were cleaned of connective tissue, minced into 1 mm segments, and transferred to a sterile 15 ml tube and washed (3x) with cold Tyrode's solution containing (in mM): 126 NaCl, 44 KCl, 17 mM NaHCO₃, 1 MgCl₂, 10 Glucose, and 4 mM HEPES, pH 7.4. After washing, the solution was replaced with 1 ml of Tyrode's solution containing 1 mg/ml Collagenase (Type 2, Worthington) and 20 µM CaCl₂. The tissue was incubated with intermittent agitation (4-5 hrs, 37 °C, 5% CO₂), centrifuged at 300 xg, and resuspended in DMEM containing 10% fetal bovine serum and 1% penicillin streptomycin.

The cells were plated in 35 mM Primaria™ plates (Corning) for 5 days prior to use (P0-2) in imaging experiments.

Human induced pluripotent stem cells (iPSCs; line #SCVI15; Joseph Wu Laboratory, Stanford University) were reprinted from cryogenic storage and plated on Matrigel (Corning)-coated tissue culture grade dishes. The iPSCs were subsequently propagated in a feeder-free environment using StemFlex Medium (Thermo Fisher Scientific), replaced every two days, and maintained under standard incubation conditions (37 °C with 5% atmospheric CO₂). When approaching 85% confluency, iPSCs underwent clump cell passaging using Versene dissociation agent (Thermo Fisher Scientific). Cells were then differentiated using the iPSC Cardiomyocyte Differentiation Kit (Thermo Fisher) following the manufacturer's instructions. Briefly, at ~75-80% confluency, cells were stimulated to differentiate by the addition of pre-warmed Cardiomyocyte Differentiation Medium A (day 1). On differentiation day 3, medium was replaced with pre-warmed Cardiomyocyte Differentiation Medium B. At differentiation day 5, medium was replaced with pre-warmed Cardiomyocyte Maintenance Medium and replenished every other day until differentiation day 10. At this time, differentiated cells were subjected to metabolic selection using cardiomyocyte enrichment medium (48.1 mL of glucose-free RPMI 1640 Medium, 1.7 mL of Bovine Albumin Fraction V 7.5% w/v, 0.4 mL of 1M sodium lactate, and 0.13 mL of 250x ascorbic acid solution). This solution was then replaced every other day for 5 days, after which, cultures were replenished with kit-supplied Cardiomyocyte Maintenance Medium with replacement every other day until use.

Plasmids for peredox-mCherry were obtained via Addgene (pcDNA3.1-Peredox-mCherry, #32383) and Ad-peredox-mCherry adenovirus was generated by insertion to an adenoviral backbone (Type 5, dE1/E3; Vector Biolabs). After reaching 50-80% confluency, smooth muscle cells were treated with Ad-peredox-mCherry (6.4x10⁷ PFUs, 50-100 MOI; 4 h at 37°C). During infection and thereafter, cells were maintained in antibiotic-free DMEM

supplemented with 2% FBS. For smooth muscle-iPSC-CM co-cultures, Ad-peredox-mCherry-treated (24 h) smooth muscle cells were seeded onto iPSC-CM monolayers, and the co-culture was maintained in DMEM supplemented with 5% FBS for 48 h prior to imaging.

Calibration of peredox-mCherry fluorescence for quantification of cytosolic NADH:NAD⁺ was performed as previously described.²⁶¹ Briefly, cells were perfused with a baseline extracellular solution consisting of (in mM) 121.5 NaCl, 2 KCl, 25 NaHCO₃, 1.25 NaH₂PO₄, 1 MgCl₂, and 2 CaCl₂ (pH 7.4, maintained by aeration with 5% CO₂). Bath temperature was monitored throughout all experiments with a thermistor probe and maintained at 36.5-37.5°C. Green (ex 405, em 525) and red (ex 560, em 630) fluorescence was monitored during sequential application (10-15 min each) of lactate:pyruvate at ratios of 500, 160, 50, 20, and 6. At the end of each experiment, maximum and minimum green:red fluorescence was recorded in the presence of 10 mM lactate and 10 mM pyruvate, respectively. For experiments testing the effects of hypoxia and electrical stimulation of co-cultures, cells were bathed in DMEM/2% FBS in an enclosed stage-top incubation system (Warner Harvard Apparatus) to allow equilibration of the bath solution to controlled O₂ levels (1-5%). Co-cultures and smooth muscle cells alone (i.e., in the absence of iPSC-CMs) were electrically paced from 1-3 Hz using platinum electrodes connected to a MyoPacer field stimulator (IonOptix). Fluorescence images were acquired using a Keyence BZ-X800 epifluorescence imaging system in time-lapse mode with a 4X objective lens. Images were captured every 20 seconds in brightfield, green (T-sapphire), and red (mCherry) channels. Image series were converted to .avi files and analyzed using FIJI software (NIH).

Patch Clamp Electrophysiology

Coronary arterial myocytes were isolated from mice as described above. Outward K^+ currents were recorded using the conventional whole-cell configuration of the patch clamp technique in voltage clamp mode of an Axopatch 200B amplifier (Axon Instruments). Borosilicate glass pipettes were pulled using a P-87 micropipette puller (Sutter Instruments) to a resistance of 5-7 M Ω and filled with a pipette solution containing (in mM): 87 K^+ -aspartate, 20 KCl, 1 MgCl₂, 5 Mg-ATP, 10 EGTA, 10 HEPES, pH 7.2. In some experiments, pyridine nucleotides were added into the internal solution (see Table 1 for concentrations). Cells were allowed to adhere to a glass coverslip in a 0.25 ml recording chamber (Warner Instruments) and were bathed in a solution containing (in mM) 134 NaCl, 6 KCl, 1 MgCl₂, 0.1 CaCl₂, 10 Glucose, 10 HEPES. Series resistance was electronically compensated at $\geq 80\%$. Outward K^+ currents recorded during a series of 500 msec step-wise depolarizations in 10 mV increments (-70 – +50 mV) from a holding potential of -70 mV. The voltage-dependence of activation was determined from tail currents elicited from repolarization to -40 mV. Voltage-dependence of inactivation was separately determined from a standard two-pulse voltage protocol in which cells were subjected to step-wise depolarizations (-100 – 50 mV) for 8 sec followed by 200 msec pulse to 50 mV.

Single Kv channel activity was recorded using the inside-out configuration of the patch clamp technique with symmetrical bath/pipette K^+ conditions. Glass pipettes (8-10 M Ω) were filled with a solution containing (in mM) 140 KCl, 1 HEDTA, 10 HEPES, and 0.0001 iberiotoxin (pH 7.3 with KOH). The bath solution consisted of (in mM) 140 KCl, 1 HEDTA, 10 HEPES, and 0.001 glibenclamide. Excised membrane patches were held at a constant potential and stochastic channel activity was recorded in gap-free mode at a sampling frequency of 10 kHz. All electrophysiological data were analyzed using Clampfit 10 software (Axon Instruments). Whole cell current densities are expressed as the peak currents at each 500 msec depolarizing voltage step normalized to cell capacitance (pA/pF). $V_{0.5,act}$ and $V_{0.5,inact}$ are the voltages at half-maximum normalized current (I/I_{max})

determined from fitting data with Boltzmann function. For single channel analysis, open probabilities (nPo) were determined from recordings that had stable channel activity for at least two minutes. Values of nPo and amplitude were determined using the Single-Channel Search function in Clampfit 10 software.

Echocardiography

In vivo measurements of myocardial blood flow and cardiac function were performed as previously described^{6, 262}. Briefly, mice were anesthetized with isoflurane (3% induction, 1-2% maintenance; supplemental O₂ delivered at 1 L/min) and placed on a controlled heating platform in the supine position. A small incision was made on the right side of the neck for placement of a jugular venous catheter (sterile PE-50 tubing, prefilled with heparinized saline; 50 units/ml) to deliver contrast agent and drugs. For continuous monitoring of arterial blood pressure, a small incision was made on the hind limb and the femoral artery was isolated and cannulated with a 1.2 F pressure catheter (Transonic Systems), which was then advanced ~10 mm into the abdominal aorta. Ultrasound gel was applied to the chest and cardiac function was measured by M-mode transthoracic imaging in the parasternal short axis view, mid-papillary level using a Vevo 2100 high resolution echocardiography imaging system (FujiFilm Visual Sonics). For myocardial contrast echocardiography (MCE), lipid-shelled microbubbles were prepared by sonication of decafluorobutane gas-saturated aqueous suspension of distearoylphosphatidylcholine (2 mg/mL) and polyoxyethylene-40-stearate (1 mg/mL), and intravenously infused at ~5 x 10⁵ microbubbles/min. Imaging was performed using a Sequoia Acuson C512 imaging system (Siemens) with a high frequency linear array probe (15L8). A multi-pulse contrast specific pulse sequence was used to detect non-linear contrast signal at low mechanical index (MI = 0.18 – 0.25) and data were acquired during (i.e., destruction) and following (replenishment phase) a short 1.9 MI pulse sequence to destruct microbubbles within the

acoustic field. Measurements were performed at baseline, after administration of the autonomic ganglionic blocker hexamethonium (5 mg/kg, i.v.), and subsequently after consecutive infusions of norepinephrine (0.5 – 5.0 µg/kg/min; 3 min each followed by 5 min washout). Mice that did not complete all norepinephrine infusions were excluded from the study. All data analyses and calculations of cardiac functional data and myocardial perfusion were conducted offline. Lab Chart 8 software (AD Instruments) was used for pressure and heart rate measurements. Left ventricular chamber dimensions were measured and averaged from 3-5 cardiac cycles as previously described²⁶².

For MCE, gain was adjusted to obtain images without myocardial signal in the absence of contrast agent infusion. Long axis images were acquired at a penetration depth of 2-2.5 cm. Images were analyzed to determine MBF by fitting intensity data from anterolateral regions of interest with an exponential function: $y = A(1 - e^{-\beta t})$ where y is the signal intensity at time t , A is the signal intensity at plateau during the replenishment phase (reflects microvascular cross sectional volume) and β is the initial slope corresponding to the volume exchange frequency²⁶³. Myocardial blood flow was estimated from 3-5 images per condition as the product of β x relative blood volume (RBV; myocardial to cavity signal intensity)^{263, 264}. MCE analyses were conducted in a genotype/treatment-blinded fashion.

Ex vivo arterial diameter measurements

Third and fourth order branches of the mesenteric arteries were dissected and kept in ice-cold isolation buffer consisting of (in mM) 134 NaCl, 6 KCl, 1 MgCl₂, 2 CaCl₂, 10 HEPES, 7 D-glucose, pH adjusted to 7.4 with NaOH. Arteries were cleaned of connective tissue and used for diameter measurements within 8 h of isolation. Vessels were cannulated in cold isolation buffer on flame polished glass micropipettes mounted in a linear alignment single vessel myograph chamber (Living Systems Instrumentation). After cannulation, the myography chamber was placed on an inverted microscope and

arteries were equilibrated to temperature (37°C) and static intraluminal pressure (80 mmHg), maintained with a pressure servo control unit (Living Systems Instrumentation) under continuous superfusion (3-5 mL/min) of physiological saline solution (PSS) consisting of (in mM): 119 NaCl, 4.7 KCl, 1.2 KH₂PO₄, 1.2 MgCl₂, 7 D-glucose, 24 NaHCO₃, and 2 CaCl₂, maintained at pH 7.35-7.45 via aeration with 5% CO₂, 20% O₂ (N₂ balanced).

Following equilibrium (45-60 min), intraluminal diameter was continuously monitored and recorded with a charge coupled device (CCD) camera and edge detection software (IonOptix). Experiments were performed to examine the effects of increases of L-lactate (Sigma Aldrich) (5-20 mM) in arteries precontracted with the synthetic thromboxane A₂ analogue U46619 (100 nM; Tocris Bioscience). At the end of each experiment, the maximum passive diameter was measured in the presence of Ca²⁺-free PSS containing the L-type Ca²⁺ channel inhibitor nifedipine (1µM) and adenylyl cyclase activator forskolin (0.5 µM) as described previously^{265, 266}. Changes in diameter in response to L-lactate are expressed as the change from baseline (i.e., in the presence of 100 nM U46619) normalized to the difference between baseline and maximum passive diameters measured for each vessel.

In situ proximity ligation

Coronary arteries were enzymatically digested to isolate individual arterial myocytes, as described above, and allowed to adhere to glass microscope slides. After fixation with 4% paraformaldehyde (10 min, room temperature), cells were permeabilized with 0.1% triton-X100 and in situ proximity ligation was performed following manufacturer's instructions. Briefly, non-specific antibody binding sites were blocked with the supplied blocking reagent and cells were labelled with primary antibodies against Kv1.5 (Neuromab, 75-011, 1:50), Kvβ1 (Abcam, Ab174508, 1:100), and Kvβ2 (Aviva Systems Biology, ARP37678-t100, 1:100) overnight at 4°C. Cells were then treated with secondary

oligonucleotide-conjugated probes, followed by ligation and rolling amplification by incubation with manufacturer-supplied ligase and polymerase, respectively. Sites of close proximity were labelled with fluorophore (ex 554 nm, em 579 nm) and slides were mounted and sealed with coverslips. Brightfield and fluorescent images were captured using a 20x objective on a Keyence BZ-X800 All-in-One imaging system and fluorescent punctate sites and cell footprint area was quantified using FIJI software (NIH).

Western blot

Tissue lysates were obtained from mesenteric arteries (6-8 pooled segments of 3rd and 4th order branches) and homogenized in lysis buffer containing 150 mM NaCl, 50 mM Tris-HCl, 0.25% deoxycholic acid, 1% NP-40, 1 EDTA, with Complete Mini protease inhibitor cocktail (Roche; per manufacturer's instructions), pH 7.4. Tissue homogenates were sonicated on ice and centrifuged (10,000 xg, 10 min, 4°C). Supernatants were transferred to another tube and boiled with Laemmli sample buffer (10 min) and run on a Stain-free Mini-PROTEAN 4-20% polyacrylamide gel (Bio-Rad). Total protein was assessed prior to transfer using a myECL Imager (Thermo Fisher Scientific). Following transfer of proteins to polyvinylidene fluoride (PVDF), membranes were blocked for non-specific binding with 5% milk (wt/vol) in tris-buffered saline (TBS) and incubated (overnight, 4°C) in primary antibodies against Kvβ2 (Neuromab, 75-021, 1:400) or α-tubulin (Sigma Aldrich, T5168, 1:4000) in TBS containing 0.1% Tween-20 (TBSt). After washing with TBSt (5x, room temperature), membranes were incubated with horseradish peroxidase (HRP)-conjugated secondary antibodies (anti-mouse IgG, Cell Signaling, 7076S, 1:3000). HRP was then detected with Pierce ECL Plus Western Blotting Substrate (Thermo Fisher Scientific) and a myECL imager (Thermo Fisher Scientific). Densitometry was performed for immunoreactive bands using FIJI software (NIH).

Statistics

Group data are presented as mean \pm SEM, unless otherwise indicated. All data were analyzed with Prism 9 software (GraphPad Software). Normality was determined for datasets by Shapiro-Wilk tests. For normal datasets, unpaired or paired *t* tests were used to compare two groups and one-way ANOVA and appropriate post-hoc tests were used for multiple comparisons of three or more groups. Two way repeated measures ANOVA was used to test for interaction in time and genotype or treatment. For non-normal datasets, nonparametric tests were used. Specific tests used to compare experimental groups are provided in figure legends. $P < 0.05$ was considered statistically significant.

Supplementary Methods & Results

Refer to Appendix A for description of methods and results that also contributed to this work. My personal contributions to this work were the perforated patch clamp data. Also, I dissected and isolated the coronary arteries for the pressure myography experiments. The other data were collected by other lab members and our collaborators at Northeast Ohio Medical University.

CHAPTER III
IN VIVO CARDIAC WORKLOAD AND IN VITRO CARDIOMYOCYTE STIMULATION
INCREASES VASCULAR NADH/NAD⁺ RATIO

Introduction

A component of our hypothetical mechanism proposes that enhanced cardiac workload increases cytosolic NADH/NAD⁺ ratio in the vascular wall (Figure 1.9). In turn, this change in pyridine nucleotide redox state regulates Kv1 channel activity by altering Kvβ2-mediated regulation of the channel pore to promote an increase in myocardial blood flow. However, whether physiological changes in MVO₂ modulate NADH/NAD⁺ ratio specifically in vascular cytosolic compartment is unknown. This investigation is critical because, if pyridine nucleotide regulation of Kvβ subunits is essential to metabolic hyperemia, upon physiological increases in MVO₂, the vascular cytosolic pyridine nucleotide redox state must reflect changes in metabolic demand. As alluded to in the background and introduction, previous investigations suggest that metabolic demand is related to both the pyridine nucleotide redox state in the myocardium and the vasculature.

Epicardial fluorescence imaging of NADH in isolated working hearts demonstrates that several conditions of metabolic demand generate an accumulation of NADH in the myocardium. For example, NADH rapidly increases in the myocardium during electrical pacing, gradual hypoxia, and global ischemia¹⁹⁰. Similar to the myocardium, changes in vascular cell oxygen consumption and contractility modulate cytosolic NADH/NAD⁺ ratio. For example, KCl-induced contraction of isolated porcine carotid arteries generates increased oxygen consumption¹⁹¹. During this contraction, increased

MVO₂ elevates lactate/pyruvate and G3P/DHAP, metabolite ratios reflective of cytosolic NADH/NAD⁺ ratio ¹⁹¹. Inhibition of vascular cell metabolism, by inhibiting the malate/aspartate shuttle, also demonstrates a direct connection between mitochondrial energy metabolism and cytosolic NADH/NAD⁺ ratio in vascular smooth muscle cells modulates ¹⁹⁴. Malate-aspartate shuttle inhibition increases lactate/pyruvate ratio and G3P/DHAP ratio in isolated porcine carotid arteries. Therefore, these results demonstrate that MVO₂ and metabolism integrate both with pyridine nucleotide redox state of the heart and vasculature, suggesting that, upon increased myocardial workload, reduced pyridine nucleotides could accumulate in the coronary vascular wall.

Therefore, the overall aim of this section of the dissertation was to answer the question whether cytosolic NADH/NAD⁺ ratio increases in the vascular wall upon physiological increases in MVO₂. To investigate this question, we performed both MALDI-MS and live-cell imaging experiments to determine whether *in vivo* contractility and/or *in vitro* stimulation of cardiomyocytes can increase the cytosolic NADH/NAD⁺ ratio of proximal vascular smooth muscle cells. Collectively, the results support that NADH/NAD⁺ ratio increases in the cytosolic compartment of vascular smooth muscle cells. This increase in cytosolic NADH/NAD⁺ occurs upon both enhanced cardiac workload and electrical stimulation of proximal myocytes in co-culture.

Results

Cardiac workload-dependent changes in vascular pyridine nucleotide redox potential

To test whether acute changes in cardiac workload and metabolic demand impact the redox state of the myocardium and coronary arterial wall *in vivo*, we used high spatial resolution imaging mass spectrometry (IMS) to visualize and compare relative levels of lactate and pyruvate in hearts of mice subjected to short-term (i.e., ~5 min) elevation of

cardiac workload (high workload) with those from low workload control mice (see Figure 3.1 A) ¹⁸¹. The intracellular lactate:pyruvate ratio is a sensitive surrogate indicator of redox state of the pyridine nucleotide pair - NADH:NAD⁺ ; both ratios are highly sensitive to oxygen levels in tissues and rise dramatically during ischemia ²⁶⁷. Hence, we tested whether transient changes of myocardial O₂ consumption caused by elevated workload modulate lactate:pyruvate in the heart and coronary vasculature. For this, we subjected mice to elevated heart rate via administration of the β -adrenoceptor agonist dobutamine (10 mg/kg, i.p.) and hearts were frozen immediately (Figure 3.1 B). Branches of the left anterior descending coronary arteries were identified in H&E-stained sections as regions of interest for IMS measurements. Exemplary IMS images for lactate (m/z 89.024), pyruvate (m/z 87.009), and merged lactate:pyruvate, in hearts from low and high workload mice are shown in Figure 3.1 C. Comparison of signal intensities revealed significantly higher lactate:pyruvate in hearts from high workload mice relative to those in low workload mice both in the perivascular region and the coronary wall (Figure 3.1 C, D). These data suggest that an acute increase in cardiac workload elevates the lactate:pyruvate ratio in the intramyocardial vasculature, consistent with a rise in intracellular levels of NADH relative to NAD⁺.

Myocardial contractility dependent changes in vascular cytosolic pyridine nucleotide redox ratio in vitro

To determine directly whether the NADH:NAD⁺ ratio in arterial smooth muscle cells is sensitive to local cardiomyocyte contractile function, we monitored the cytosolic NADH:NAD⁺ ratio using the genetically-encoded fluorescent biosensor peredox-mCherry (see Figure 3.2 A) ^{261, 268}. Consistent with previous reports, we observed a reduction in peredox-mCherry green:red fluorescence in the presence of decreasing external lactate:pyruvate in arterial myocytes (Figure 3.2). Figure 3.3 illustrates the range of the

sensor for different expression levels of the sensor across numerous cells. At baseline the cytosolic NADH:NAD⁺ ratio estimated by this technique was 0.0027 ± 0.0001 , which is consistent with previous estimates made in vascular smooth muscle of porcine carotid strips,¹⁹³ and indicated that most of the nucleotide is in its oxidized form (NAD⁺). To examine whether the NADH:NAD⁺ ratio in arterial myocytes is affected by the metabolic activity of cardiomyocytes, we seeded isolated arterial myocytes expressing peredox-mCherry on two-dimensional monolayers of induced pluripotent stem cell-derived cardiomyocytes (iPSC-CMs; Figure 3.4 A). After incorporation of peredox-mCherry-positive arterial myocytes into iPSC-CM monolayers (Figure 3.4 B), we monitored NADH:NAD⁺ in arterial myocytes during step-wise increases in the frequency of electrical stimulation (1–3 Hz). Consistent with the redox modifications resulting from changes in cardiac workload seen *in vivo* (Figure 3.1), we observed a significant increase in arterial myocyte cytosolic NADH:NAD⁺ as the pacing frequency was increased (Figure 3.4 C, D). In contrast, no significant frequency-dependent changes in NADH:NAD⁺ were observed in stimulated arterial myocytes alone (i.e., in the absence of iPSC-CMs). Electrical pacing of co-cultures increased cytosolic NADH:NAD⁺ in the arterial myocytes to a similar degree as a reduction in chamber O₂ levels from 5 to 1% (Figure 3.5). Moreover, to rule out the possibility that the changes in pyridine nucleotide ratios seen *in vivo* after β -adrenergic stimulation (Figure 3.1) were due to direct agonist effects in arterial myocytes, we tested whether activation of β -adrenoceptors on arterial myocytes alters cytosolic the NADH:NAD⁺ ratio. However, application of the synthetic catecholamine – isoproterenol modestly reduced (e.g., 0.0018 ± 0.0010 at 1 μ M; 0.0022 ± 0.0001 at baseline), rather than enhanced, the NADH:NAD⁺ ratio (Figure 3.6). Taken together, these data suggest that inotropic and chronotropic stimulation of cardiomyocytes elevates NADH:NAD⁺ in adjacent arterial myocytes.

Discussion

Recent work indicates that Kv1 channels are essential for metabolic hyperemia mediated by the coronary vasculature⁴⁻⁶. This result suggests that Kv β subunit complexes could potentially regulate coronary vascular tone by sensing changes in vascular pyridine nucleotide redox state that occur upon increased metabolic demand. However, whether the cytosolic NADH/NAD⁺ ratio increases upon enhanced MVO₂ in the physiological range is unclear. The results in this section of the dissertation demonstrate that enhanced cardiac contractility increases the NADH/NAD⁺ ratio of proximal arterial myocytes. In our dobutamine challenge experiments, we showed that lactate/pyruvate ratio increases in the coronary wall. Since this metabolite pair is in equilibrium with the cytosolic NADH/NAD⁺ ratio, through the lactate dehydrogenase reaction, this result demonstrates that increased cardiac workload generates an accumulation of reduced pyridine nucleotides in the coronary vascular wall^{180,181}. We supported these results in vitro results by demonstrating, upon electrical stimulation of a cardiomyocyte and vascular smooth muscle cell co-culture, the cytosolic NADH/NAD⁺ ratio increased in isolated vascular cells.

The results of these experiments could potentially involve several hypothetical mechanisms. For example, while myocardial tissue supply does not substantially decrease upon enhanced MVO₂, changes in oxygen tension could partially mediate this increase in NADH/NAD⁺ ratio in the vascular wall¹⁵¹. A steady coronary venous PO₂ suggests that myocardial tissue oxygen supply remains stable upon increased MVO₂. However, this is not a direct measurement of oxygen supply in the coronary vasculature. The left ventricular myocardium undergoes significant compressive forces during systole which significantly interrupts left ventricular coronary blood flow¹⁹. Also, during increased metabolic demand, oxygen tension decreases in the coronary capillary bed¹⁶⁵. Therefore, during increased metabolic demand, hypoxic regions localized to the coronary vasculature could manifest. These hypoxic regions could contribute to coronary vasodilation through lactate

accumulation in the coronary wall, as demonstrated in isolated porcine coronary arteries²⁶⁹. Lactate accumulation in the coronary vascular wall during hypoxia could mediate vasodilation through modulation of the cytosolic pyridine nucleotide redox state and, subsequent, Kv1 channel regulation by pyridine nucleotide sensitive auxiliary Kv β proteins. Our data support this mechanism as the cytosolic NADH/NAD⁺ ratio increases in the context of limited oxygen saturation, and coronary Kv β 2 subunits are essential regulators of hypoxia-induced vasodilation (Figure 3.5, Appendix A, Figure 3)²⁶². However, the generation of hypoxic regions may not be necessary for Kv β -mediated coronary vasodilation. In the absence of localized regions of hypoxia, the release of lactate may still occur from several sources upon physiological increases in metabolic demand. This mechanism may be more relevant in the context of metabolic hyperemia.

As stated above, both the myocardium and skeletal muscle can release lactate into the circulation and interstitial space upon increased metabolic demand, which could underly the accumulation of this metabolite in the coronary vascular wall. For example, skeletal muscle releases lactate into the circulation upon increased contractile activity¹⁸⁵. However, the fate of circulating lactate is uncertain as the myocardium may use this lactate as an energy source upon increased metabolic demand^{186, 187}. A possibly more likely source for arterial lactate accumulation and arterial cytosolic NADH/NAD⁺ ratio in the context of increased metabolic demand could be the local release of lactate by stimulated cardiomyocytes. Depolarization of the atria induces lactate release from the myocardium; thus, the arterial wall could accumulate lactate released by the myocardium upon increased cardiac workload¹⁸⁹. Our co-culture experiments support this potential mechanism; these results suggest electrical stimulation could induce efflux of lactate from cardiomyocytes that can functionally modulate the cytosolic pyridine nucleotide redox state of proximal arterial myocytes. The unique metabolic properties of human-induced pluripotent stem cell-derived cardiomyocytes (hiPSC-CMs) lend support to lactate as a

mediator in these experiments. hiPSC-CMs rely on aerobic glycolysis under standard culture conditions ²⁷⁰. Therefore, under the co-culture conditions present in this study, hiPSC-CMs produce lactate through dependence upon this anaerobic pathway of ATP production. Likewise, since atrial pacing increases lactate release by the myocardium, this response to stimulation suggests that isolated hiPSC-CMs, in co-culture with vascular smooth muscle cells, may release increasing amounts of lactate into the media upon enhanced electrical pacing frequency ¹⁸⁹. This lactate released into the co-culture medium may diffuse to the proximal arterial myocytes, increasing the vascular cell cytosolic NADH/NAD⁺ ratio. Likewise, a similar mechanism of lactate release by the myocardium during increased metabolic demand following dobutamine challenge may also occur.

However, the possibility exists that neurons that directly innervate the coronary vasculature could also release lactate to increase cytosolic NADH/NAD⁺ ratio in the vessel wall. Recently, stimulation of the central nervous system was demonstrated to transiently increase cytosolic NADH/NAD⁺ in neurons, indicating an enhancement of aerobic glycolysis ²⁷¹. Furthermore, these data also suggest that the transient increase in aerobic glycolysis may partially depend on export of lactate from the cell ²⁷¹. Therefore, lactate may be released from neurons that innervate the coronary vasculature upon neuronal stimulation which could potentially contribute to the increase in cytosolic NADH/NAD⁺ ratio in the coronary wall upon increased metabolic demand. Previous studies indicate that neural innervation is a vital feed-forward mechanism to regulate coronary vascular tone during metabolic hyperemia ¹⁰²⁻¹⁰⁵. Therefore, lactate release by these neurons could be another contributing factor to this feed-forward control. However, lactate may not be the only mediator of this physiological phenomenon. Other metabolic mediators released by cardiomyocytes could influence cytosolic pyridine nucleotide redox state in arterial myocytes. One of the most prominent signaling molecules in recent literature is hydrogen peroxide.

Several studies collectively demonstrate hydrogen peroxide accumulates in the myocardium during enhanced metabolic demand and generates Kv1-mediated vasodilation, supporting this potential mechanism ¹⁷²⁻¹⁷⁶. While the relationship between hydrogen peroxide and cytosolic NADH/NAD⁺ ratio is not direct, a connection between hydrogen peroxide, enhanced glucose uptake, and increased cytosolic NADH/NAD⁺ ratio can be formed from the established literature. This work demonstrates an inhibitor of p38 MAP kinase, SB203580, substantially inhibits coronary vasodilation induced by conditioned buffer from paced myocytes and hydrogen peroxide ¹⁷⁶. Furthermore, a p38 MAP kinase inhibitor substantially decreases glucose uptake into skeletal muscle induced by hydrogen peroxide ²⁷². Thus, in the coronary vasculature, hydrogen peroxide could increase glucose uptake via p38 MAP kinase activation. This enhanced glucose uptake could increase the cytosolic NADH/NAD⁺ ratio of vascular cells to promote Kv1-mediated vasodilation. From our own observation, the cytosolic NADH/NAD⁺ ratio increases in Perox-expressing vascular smooth muscle cells upon exposure to glucose, suggesting that glucose uptake readily modulates cytosolic NADH/NAD⁺ ratio. Thus, if hydrogen peroxide stimulates glucose uptake in coronary vascular smooth muscle cells, as observed in skeletal muscle, the possibility exists that Kv β -mediated coronary vasodilation could occur due to H₂O₂ exposure.

Significance, Limitations, and Future Directions

The data presented relate to the relationship between metabolic demand and vascular pyridine nucleotide redox state demonstrate significant findings to the field of cardiovascular biology particularly in the study of metabolic hyperemia. This work establishes that physiological increases in cardiac metabolic demand both in vivo and in vitro modulate the pyridine nucleotide redox state in coronary arteries and in isolated coronary arterial myocytes. To our knowledge, these data are the first demonstration that

coronary arterial NADH/NAD⁺ ratio increases in the physiological range of MVO₂. While this finding implicates that metabolic demand in the physiological range can regulate arterial Kv1 channels through pyridine nucleotide regulation of Kvβ subunits, this relationship could also regulate other signaling pathways in the cell. For example, pyridine nucleotides are cofactors of many enzymes involved in oxidative phosphorylation. Therefore, this relationship could have many effects on vascular cell metabolism that deserve investigation. Furthermore, NADH could potentially regulate other potassium channels at the smooth muscle membrane. Recently, a study demonstrated that endothelial calcium-activated K⁺ channels are regulated by intracellular pyridine nucleotides, suggesting that coronary vascular calcium-activated K⁺ channels could also be modulated by pyridine nucleotide redox state ²⁷³.

While the implications of these results are significant, this portion of our study is not without limitations. For example, while our MALDI-MS imaging data showed an accumulation lactate in the arterial wall, we cannot exclude the effect of hypoxia as the heart was removed from the animal. Thus, the measure of lactate/pyruvate ratio measured could possibly be altered by these hypoxic effects. Furthermore, while lactate/pyruvate ratio correlates with cytosolic NADH/NAD⁺ ratio, this is not a direct measurement of NADH/NAD⁺ ratio. A future experiment could be designed to measure NADH/NAD⁺ ratio directly in the arterial vasculature. Possibly, a mouse model, expressing Peredox, specifically in the coronary vasculature could be utilized for these potential experiments. Pressure myography experiments could be performed upon isolated coronary vessels from this Peredox-expressing murine model. These vessels could be exposed to conditioned buffer from electrically stimulated myocytes, and the change in cytosolic NADH/NAD⁺ ratio could monitored during vasodilation.

Our in vitro experiments also had limitations regarding experimental design. For example, our co-culture system does not exactly reflect the normal cellular anatomy of the

human heart. For example, our co-culture system utilized cell types from two different species: murine vascular cells and human iPSC-derived cardiomyocytes. Furthermore, the culture system utilized in this study only contained cardiomyocytes and arterial vascular smooth muscle cells; however, the cardiac system is a diverse environment of endothelial cells, fibroblasts, pericytes, cardiomyocytes, and vascular smooth muscle cells. Furthermore, this system is only a 2-dimensional monolayer which omits the effect of compressive forces upon the smooth muscle cells. Also, this 2-dimensional system does not reflect the circulatory system of the in vivo tissue as there was no aspect to induce perfusion in this system. Finally, the stimulation of myocytes in this co-culture system does not reflect normal action potential propagation in the heart. In the myocardium, the cardiac contractile cells are not normally depolarized by electric field stimulation, rather action potentials are propagated from the cardiac conduction system to the contractile cardiomyocytes. The limitations of this system could possibly be improved by incorporating Peredox-expressing human coronary vascular cells into an engineered cardiac tissue system. This engineered cardiac tissue system could be designed to replicate perfusion and physiological conduction of cardiac action potentials. To replicate physiological cardiac conduction, possibly a subset of cardiomyocytes could be infected to express an optogenetic sensor so that action potential propagation could be initiated from focused point in the tissue.

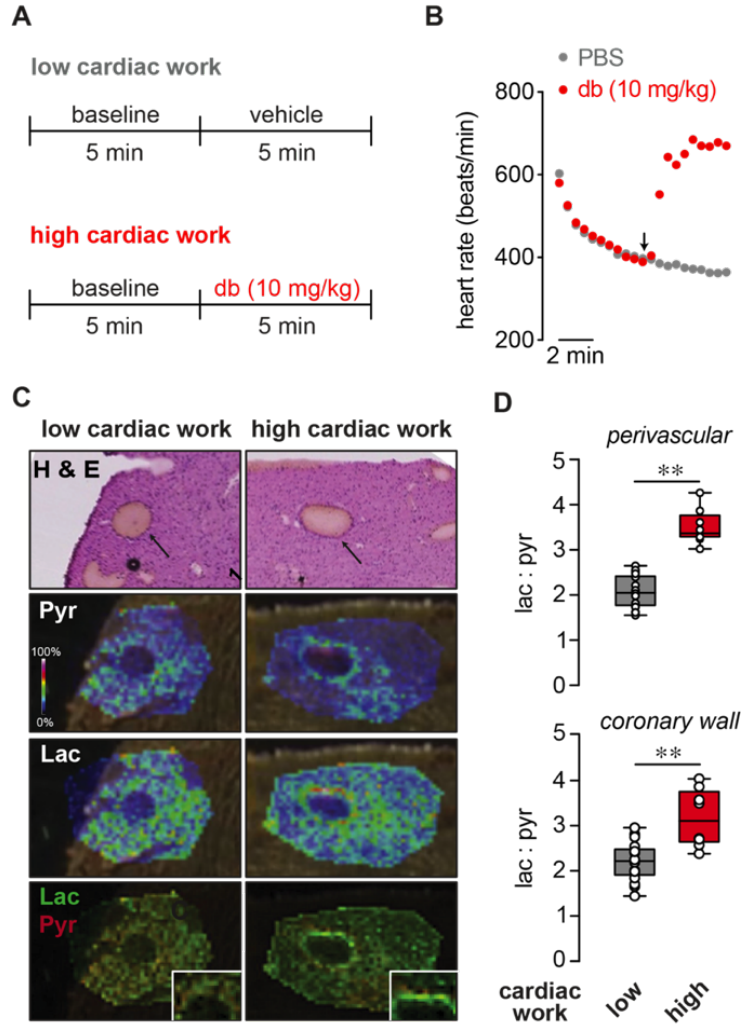


Figure 3.1: Increased myocardial workload promotes local elevation of lactate:pyruvate ratio in the coronary arterial wall. (A) Schematic showing protocol for induction of acute cardiac stress prior to collection of tissues for MALDI-MS imaging. To induce high cardiac work, anesthetized mice with stable heart rates of 400–450 bpm were treated with dobutamine (db; 10 mg/kg, i.p.). Heart rate was continuously monitored, and hearts were rapidly cryopreserved in the thoracic cavity and excised after 2–3 minutes of stabilized heart rate responses to either db or PBS (vehicle). (B) Symbol plot showing exemplary heart rates recorded every 30 seconds before (i.e., during induction and stabilization of anesthesia) and after administration of either db (10 mg/kg; i.p.) or PBS. (C) Images of left ventricular intramyocardial coronary arteries in H & E-stained heart sections and corresponding intensity-coded MALDI-MS images showing lactate and pyruvate (relative to background signals) in hearts from low and high cardiac work mice. x-y resolution: ~20 μ m. Insets show magnified region of interest at coronary arterial wall. (D) Box and whiskers plots showing lactate:pyruvate ratios in perivascular myocardium (top) and coronary wall (bottom) in hearts of low and high cardiac work mice. (low cardiac work: n = 16 technical replicates, 4 mice, high cardiac work group: n = 8 technical replicates, 2 mice), perivascular, p < 0.0001, coronary, p = 0.0003 (unpaired t test). These experiments were performed by our collaborators, Dr. Michelle Reyzer and Lisa Manier, at Vanderbilt University.

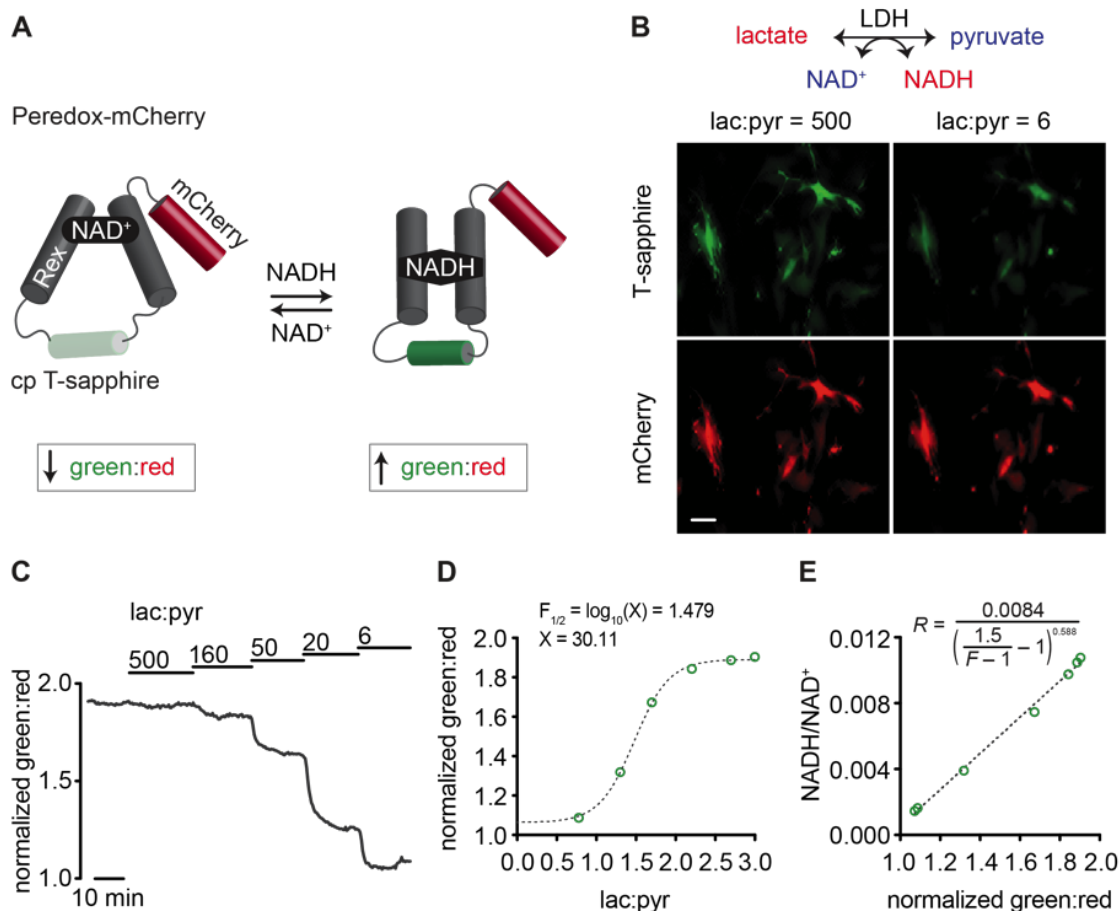


Figure 3.2: Measurement of cytosolic NADH:NAD⁺ in arterial smooth muscle cells. (A) Schematic representation of peredox-mCherry NADH:NAD⁺-sensitive fluorescent biosensor. Peredox-mCherry is a modified bacterial redox-sensitive transcriptional repressor (i.e., Rex) that consists of circularly permuted T-sapphire and mCherry (see ref ²⁶⁸). Upon binding of NADH, T-sapphire fluorescence is enhanced. No change in fluorescence is observed with mCherry, enabling normalization to biosensor expression via red fluorescence. (B) Representative fluorescence images showing T-sapphire and mCherry fluorescence in aortic vascular smooth muscle cells expressing peredox-mCherry in the presence of external lactate:pyruvate (lac:pyr) of 500 or 6. Scale bar represents 50 μm . (C-E) Green:red fluorescence intensities (normalized to minimum ratio obtained in 10 mM pyruvate) in the presence of lac:pyr of 500-6 (C), mean green:red over the tested range of lac:pyr ratios (log scale), and mean cytosolic NADH:NAD⁺ vs. green:red fluorescence, estimated using the protocol described in ²⁶¹. Inset in E shows equation used to calculate cytosolic NADH:NAD⁺. n = 87 cells, 3 independent experiments.

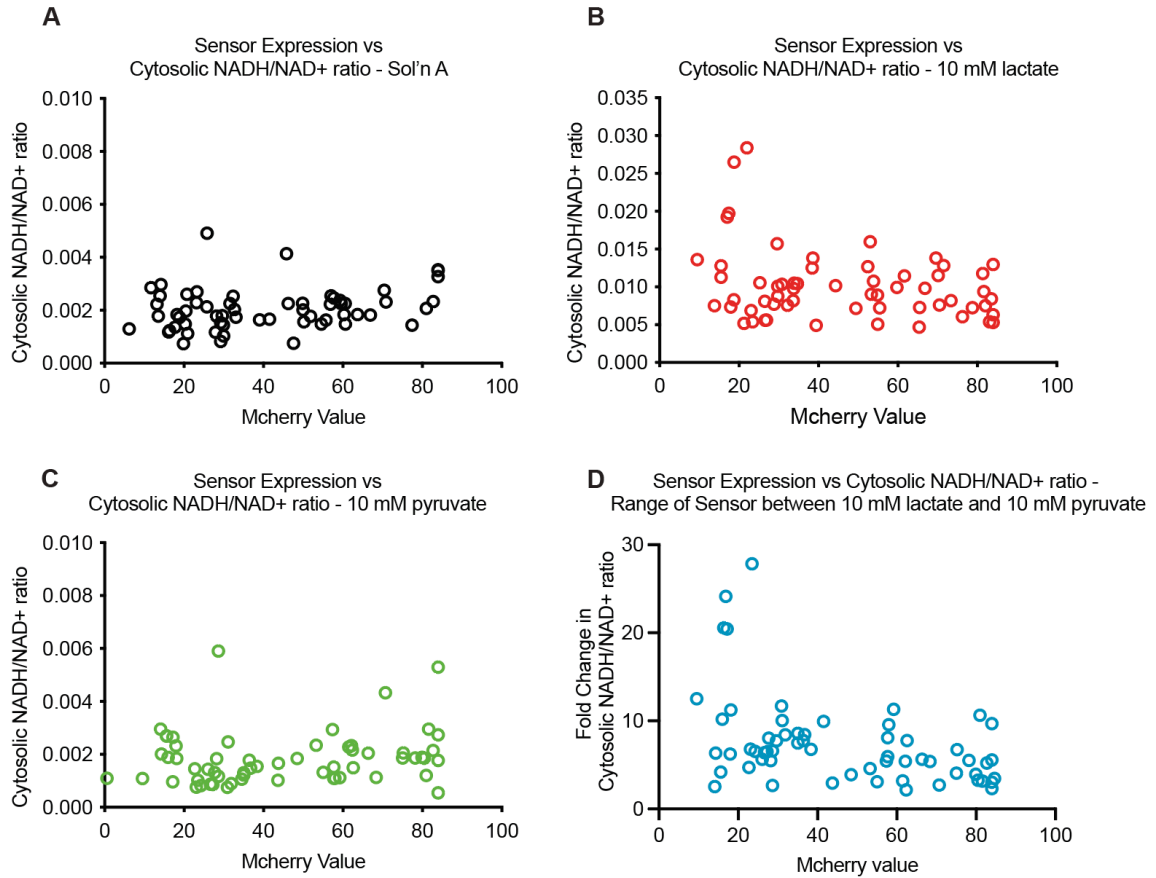


Figure 3.3: Relationship between sensor expression and cytosolic NADH/NAD⁺ readout. (A) Relationship between the sensor expression (estimated by the Mcherry value of the sensor) and the cytosolic NADH/NAD⁺ in individual cells (each scatter plot point represents one individual cell) perfused with baseline extracellular solution. (B) Relationship between the sensor expression and the average cytosolic NADH/NAD⁺ in individual cells perfused with baseline extracellular solution containing 10 mM lactate. (C) Relationship between the sensor expression and the cytosolic NADH/NAD⁺ in individual cells perfused with baseline extracellular solution containing 10 mM pyruvate. (D) Fold change in cytosolic NADH/NAD⁺ ratio between the 10 mM pyruvate treatment and 10 mM lactate treatment for each individual cell. n = 60 cells from 3 independent experiments.

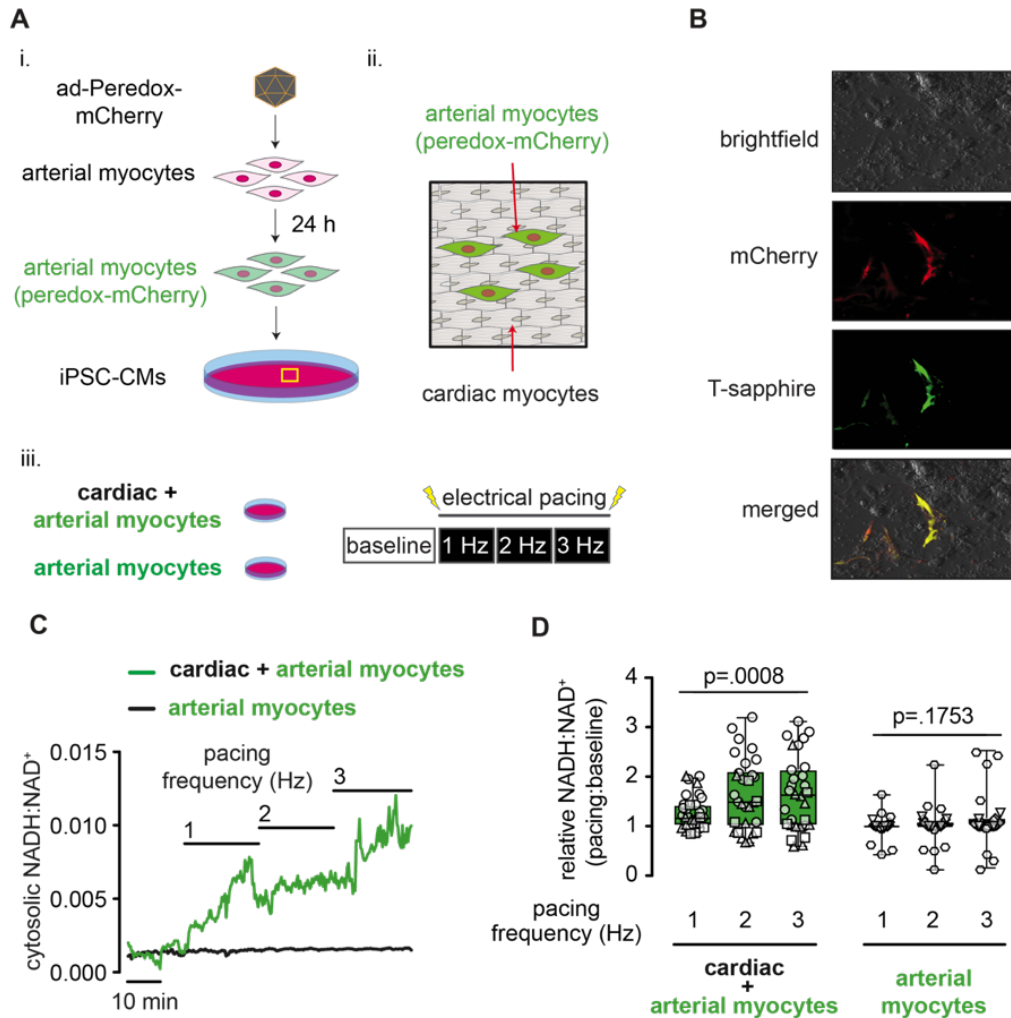


Figure 3.4: Arterial myocyte NADH:NAD⁺ is sensitive to changes in proximal cardiomyocyte beating frequency. (A) Schematic illustration depicting the preparation of arterial myocyte/induced pluripotent stem cell-derived cardiomyocyte (iPSC-CM) co-culture. Primary aortic vascular smooth muscle cells (passage 0-2) were treated with adenovirus to express the NADH:NAD⁺-sensitive fluorescent biosensor peredox-mCherry (i.). Arterial myocytes were then seeded and allowed to integrate (48 hr) onto a two-dimensional monolayer of iPSC-CMs (ii.). Imaging was performed on either arterial/cardiac co-cultured myocytes or arterial myocytes alone during electrical stimulation (1–3 Hz; iii.) while monitoring peredox-mCherry green:red fluorescence. (B) Exemplary brightfield and fluorescence images showing red (mCherry) and green (T-sapphire) in the presence of non-fluorescent cardiac myocytes in arterial + cardiac myocyte co-culture. (C) Exemplary time series of NADH:NAD⁺ in arterial myocytes in either an arterial/cardiac myocyte co-culture (green trace) or arterial myocytes alone (– cardiac myocytes; black trace) at baseline (0 Hz) and during electrical stimulation (1–3 Hz). (D) Box and whiskers plots summarizing fold-change in NADH:NAD⁺ in arterial myocytes in arterial/cardiac myocyte co-cultures or arterial myocytes alone. Arterial/cardiac, n = 30 cells from 3 independent experiments, 1 vs 2 Hz, p=.0018; 1 vs. 3 Hz, p=.0065; Arterial only, n = 30 cells from 3 independent experiments, 1 vs 2 Hz, p = 0.6527; 1 vs. 3 Hz, p = 0.2636 (two-way repeated measures ANOVA with Dunnett’s multiple comparisons test).

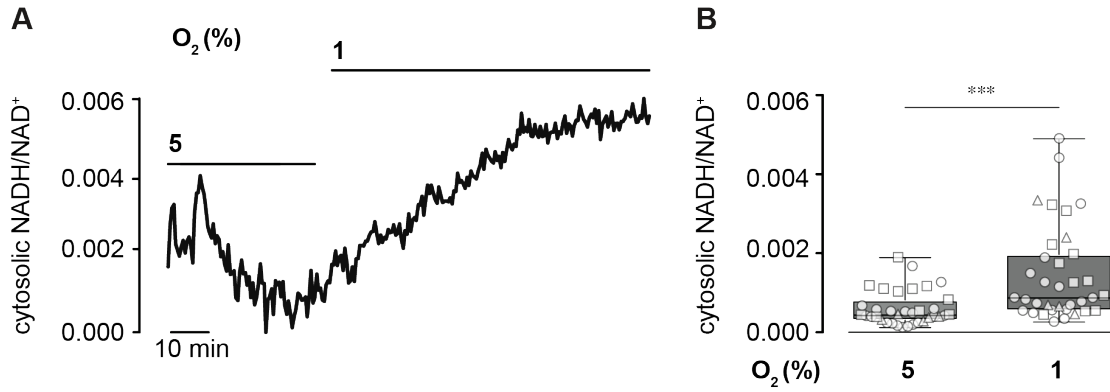


Figure 3.5: Reduction in O₂ levels increases NADH:NAD⁺ in arterial smooth muscle cells. (A) Representative recording of cytosolic NADH:NAD⁺ in a smooth muscle in the presence of 5% and 1% O₂. NADH:NAD⁺ measured at the end of the experiment in the presence of 10 mM lactate and 10 mM pyruvate were 0.0043 and 0.0015, respectively. (B) Box and whiskers plot showing summarized NADH:NAD⁺ in smooth muscle cells in the presence of 5% and 1% O₂. n = 35 cells, 3 independent experiments (denoted by symbols). ***P<0.001 (Wilcoxon matched pairs signed rank test).

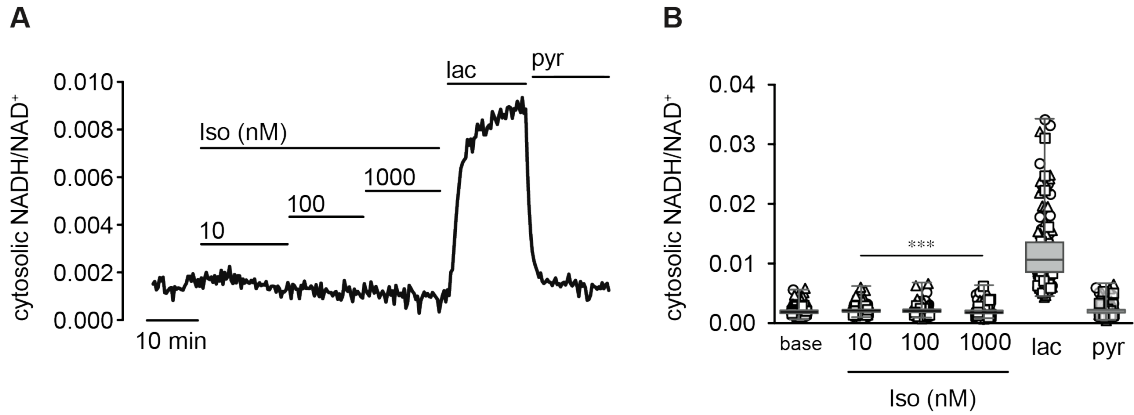


Figure 3.6: NADH:NAD⁺ is not elevated by direct β -adrenergic stimulation. (A) Representative recordings of cytosolic NADH:NAD⁺ in smooth muscle before and after application of isoproterenol (iso; 10-1000 nM), prior to application of 10 mM lactate and 10 mM pyruvate at the end of the experiment. **(B)** Box and whiskers plot summarizing NADH:NAD⁺ at baseline (base) and in the presence of iso at concentrations indicated, or in the presence of 10 mM lactate or pyruvate. N = 136 cells, 3 independent experiments (denoted by symbols). ***P<0.001 vs. base (one-way repeated measures ANOVA).

CHAPTER IV

REDOX CONTROL OF CORONARY ARTERIAL Kv1 ACTIVITY, VASODILATION, AND MYOCARDIAL BLOOD FLOW VIA THE AKR ACTIVITY OF KV β 2 SUBUNITS

Introduction

Our overarching mechanism suggests that, upon increased myocardial demand, cytosolic NADH/NAD⁺ ratio increases in the coronary vasculature. Upon this increase in cytosolic NADH/NAD⁺ ratio, Kv β complexes associated with Kv1 channel pores sense cytosolic pyridine nucleotide redox state to adjust vascular smooth muscle tone to the metabolic needs of the myocardium. In chapter III, we demonstrated that the NADH/NAD⁺ ratio of arterial vascular smooth muscle cells increases upon physiological enhancements in myocardial demand. However, whether Kv β -associated auxiliary complexes of arterial Kv1 channels can directly sense these changes in pyridine nucleotide redox state to adjust Kv1 channel activity and vascular tone to metabolic demand is unknown. This investigation is critical to ensuring that coronary vascular Kv β proteins can communicate metabolically induced changes in NADH/NAD⁺ ratio to regulate coronary vascular tone.

In heterologous expression systems, Kv β subunits are known to significantly influence Kv channel activity. After the initial identification of Kv β subunits in rat brain membranes by affinity chromatography utilizing a dendrotoxin-1 column, Rettig and Pongs cloned and functionally characterized the Kv β 1 protein in a heterologous expression system^{225, 274}. In this seminal study, co-expression of Kv β 1 with Kv1.1 was shown to impart N-terminal inactivation upon this noninactivating current²²⁵. Furthermore, they demonstrated that co-expression of Kv β 1 with Kv1.4 increases N-type inactivation of the

pore complex²²⁵. Interestingly, Kv β 1 restored N-type inactivation to a mutated Kv1.4 channel with a truncated N-terminal domain²²⁵. This result demonstrates the Kv β 1 protein possesses a functional “ball and chain” mechanism that can modulate Kv pore inactivation kinetics. Subsequently, further studies demonstrated that co-expression of many other various α and β heteromeric complexes generate a vast array of Kv1 channels with variable gating and kinetic properties⁸⁰. β complexes induce or increase N-type inactivation, but, also, these complexes affect the current density and the voltage sensitivity of the channel. For example, co-expression of Kv1.5, a major α splice variant expressed in smooth muscle cells, with Kv β 1.3 shifts the $V_{1/2}$ of activation of the channel to hyperpolarized potentials (V_h of activation for Kv1.5 alone, -3.4 ± 2 mV, V_h of activation for Kv1.5/ Kv β 1.3, -18.8 ± 2 mV)^{6, 9, 262, 275}. A similar hyperpolarizing shift in the $V_{1/2}$ of activation occurs when Kv1.5 is co-expressed with Kv β 2 potentials (V_h of activation for Kv1.5 alone, -25.7 ± 2.2 mV, V_h of activation for Kv1.5/ Kv β 2, -34.5 ± 3.0 mV)²⁷⁶.

In addition to these effects of Kv β proteins on Kv1 channel activity, Kv β proteins are functional aldo-keto reductase enzymes that interact with pyridine nucleotide cofactors and carbonyl substrates to regulate Kv1 channel gating. In general, heterologous cells expressing Kv1 channels with Kv β 1 or Kv β 3, respond to internal perfusion of reduced pyridine nucleotides with increased inactivation relative to perfusion with oxidized nucleotides^{9, 195} (Appendix B, Figure 1 A). In contrast, heterologous cells expressing Kv β 2 respond to internal perfusion of reduced pyridine nucleotides with a hyperpolarizing shift in the $V_{1/2}$ of activation relative to oxidized pyridine nucleotides¹⁹⁵ (Appendix B, Figure 1 B). Because Kv β 2 subunits do not possess an N-terminal “ball and chain” for N-terminal inactivation, the hyperpolarizing shift in the $V_{1/2}$ of activation induced by reduced pyridine nucleotides is unopposed by an increase in N-terminal inactivation in cells co-expressing Kv1 with Kv β 2^{225, 231}. Therefore, this shift in $V_{1/2}$ of activation induced by reduced pyridine

nucleotides most likely increases current density of these Kv1 channels relative to oxidized pyridine nucleotides. Interestingly, Kv β subunits also regulate potassium efflux through its AKR catalytic activity. For example, both 4-cyanobenzaldehyde and H₂O₂ treatment significantly increased steady-state current density of *Xenopus* oocytes expressing Kv1.1/Kv β 1 complexes²⁴⁸. Similar to Kv β 1, Kv1.4/Kv β 2 complexes respond to the perfusion of 4-CY with increased steady-state current and decreased channel inactivation rate¹⁰. Collectively, these results in heterologous expression systems suggest that in vivo Kv β subunits could influence several physiological processes through its pyridine nucleotide binding capacity and AKR enzymatic activity. Recently, several experiments demonstrated that these characteristics of the Kv β complex influence the conduction of action potentials in the cardiovascular system^{196, 252}. Thus, the Kv β complex could also be critical regulating other cardiovascular processes such as metabolic hyperemia that is mediated by the coronary vasculature.

Therefore, the overall aim of this section of the dissertation was to determine the potential functional regulation of vascular Kv1 channels via the AKR enzymatic activity of Kv β subunits. To investigate this question, we performed patch clamp electrophysiology, myography, and echocardiography experiments. Primarily, we investigated how Kv β subunit knockout or mutation of the Kv β 2 AKR catalytic site affected pyridine nucleotide regulation of coronary vascular Kv1 channels. Also, we determined the effect of Kv β 2 AKR catalytic site mutation upon vascular reactivity to a reduced pyridine nucleotide redox state. Lastly, we investigated the influence of a Kv β 2 AKR catalytic site mutation on the relationship between coronary blood flow and MVO₂.

Results

Intracellular pyridine nucleotide redox states reflecting augmented O₂ demand increase coronary Kv1 activity

Coronary arterial myocyte Kv1 channels are essential for proper metabolic hyperemia^{4-6, 175, 262}. Under native conditions, these channels are associated with ancillary Kv β proteins, which bind pyridine nucleotides with high affinity^{259, 277}. Based on results presented in Figures 3.1 and 3.3, we tested whether covaried pyridine nucleotide levels in smooth muscle that simulate altered myocardial O₂ demand could influence Kv1 activity. For this, using the conventional whole-cell configuration of the patch clamp technique, we recorded voltage-dependent outward K⁺ currents after internal dialysis of cells with altered NAD(P)H:NAD(P)⁺ ratios, referred to hereafter as either “oxidized” or “reduced” nucleotide compositions (see Table 1 for concentrations and ratios)^{278, 279}. Figure 4.1 shows a representative cell and pipette tip utilized for these recordings. Under the applied patch conditions, the Kv1-selective inhibitor psora-4 (500 nM) inhibited ~60% of the total outward K⁺ current recorded from isolated coronary arterial myocytes (Figure 4.3). As shown in Figure 4.3 A, the magnitude of I_K recorded from coronary arterial myocytes perfused with reduced nucleotides was significantly higher than the current recorded from myocytes perfused with oxidized nucleotides (Figure 4.3 A, B – i.). No significant differences in I_K density were observed between groups when the recordings were performed in the presence of 500 nM psora-4 (Figure 4.3 A, B – ii.). Exemplary psora-4-sensitive I_K and summarized current densities in the presence of either oxidized or reduced nucleotide ratios are shown in Figure 4.3 A, B – iii. Reduced nucleotide conditions also promoted hyperpolarizing shifts in the voltage-sensitivity of activation and inactivation ($V_{0.5,act}$ and $V_{0.5,inact}$, respectively; Figure 4.3 C and Table 2). These data support the notion that the intracellular redox ratio of pyridine nucleotides is a critical regulator of Kv1 activity, and

that pyridine nucleotides at levels expected under conditions of high O₂ demand augment Kv1 current density.

In its native state, Kv1 associates with intracellular Kvβ, which is a key regulator of Kv1 gating. The data supplementary to this work demonstrates that, in the coronary vasculature, loss of the Kvβ2 subunit hampers coronary vasodilatory function and suppresses myocardial blood flow (Appendix A, Figure 2 D)²⁶². In arterial myocytes, loss of Kvβ2 does not significantly impact basal I_K density, but results in modest shifts in V_{0.5,act} and V_{0.5,inact} (Figure 4.2). However, deletion of Kvβ2 completely abolished the pyridine nucleotide sensitivity of Kv current. In contrast to effects observed in coronary arterial myocytes from wild type mice, no differences in I_K density were observed between oxidized and reduced nucleotide conditions in cells from Kvβ2^{-/-} mice (Figure 4.3 D). In addition, the loss of Kvβ2 proteins markedly altered voltage-sensitivity responses to reduced nucleotides; whereas robust hyperpolarizing shifts in V_{0.5,act} and V_{0.5,inact} were observed in cells from wild type mice (Figure 4.3 C), depolarizing shifts were observed in V_{0.5,act} and V_{0.5,inact} in arterial myocytes from Kvβ2^{-/-} mice (Figure 4.3 E and Table 2). Collectively, these data indicate that in coronary arterial myocytes, Kvβ2 imparts sensitivity of native Kv1 channels to pyridine nucleotide redox state.

Direct potentiation of native coronary Kv1 channel activity by NADH.

We next tested whether an elevation of NADH in the cytosolic compartment would affect the activity of native coronary Kv1 channels. To test this, we measured the open probability of single Kv channels using the inside-out patch configuration. Unitary current amplitudes recorded over a range of voltage in the presence of K_{ATP} and BK_{Ca} channel inhibitors (i.e., glibenclamide and iberiotoxin, respectively) showed similar conductance values between patches from freshly isolated coronary arterial myocytes and Cos-7 cells expressing Kv1.5 (Figure 4.4 A, B). Moreover, single channel events with amplitudes

similar to that reported for Kv1 channels (+40 mV)⁹ were abolished by application of 500 nM psora-4 in the bath solution (Figure 4.4 C, D), further supporting that channel activity under the applied conditions is mediated by Kv1 channels. At a holding potential of -40 mV, application of 1 mM NADH in the bath resulted in an immediate increase in Kv1 open probability (nP_o , Figure 4.4 E, F). In contrast, no change in nP_o was observed in the presence of NAD⁺, suggesting that nucleotide-induced changes in Kv1 activity are dependent on redox state. Similar responses in channel activity in response to 1 mM NADH were observed in excised membrane patches from human coronary arterial myocytes (Figure 4.4 G). Note that using in situ proximity ligation to assess Kv1 subunit interactions as previously described, we found that freshly isolated human coronary arterial myocytes, like murine cells, express Kv1 pore-forming subunits that interact with Kv β 1.1 and Kv β 2 proteins (Figure 4.5, Appendix A, Figure 5 A, B)^{196, 262, 280}. Whereas the NADH-induced increase in open probability was unaffected by ablation of Kv β 1.1, this effect was abolished in coronary arterial myocyte membrane patches from mice lacking Kv β 2 (Figure 4.4 H, I). Together, these results indicate that NADH directly increases the activity of native coronary Kv1 channels and that the regulation of Kv1 by NADH is attributed to the Kv β 2 subunit.

Redox control of Kv1 activity, vasodilation, and myocardial blood flow require intact enzymatic function of Kv β 2.

Considering that myocardial metabolism modifies coronary arterial myocyte pyridine nucleotide redox state and that this regulates Kv1 activity via the Kv β 2 subunit, we next tested whether this mode of regulation involves Kv β 2 mediated catalysis. Previous work has shown that the Kv β 2 protein possesses weak aldehyde reductase activity that depends on a tyrosine residue at position 90 (Y90) for hydride transfer during the reductive catalytic cycle^{7, 244}. Therefore, to examine the role of Kv β 2-catalysis, we isolated arterial

myocytes from mice in which the catalytic site tyrosine (Y90) of Kv β 2 is mutated to phenylalanine (Kv β 2^{Y90F}). Western blot analysis revealed no significant difference in Kv β 2 abundance in arteries from Kv β 2^{Y90F} mice compared with those from wild type mice (Figure 4.6). We found that in contrast to the NADH-induced increases in single Kv1 channel activity in coronary arterial myocytes from wild type mice (Figure 4.4 E, F), no significant change in nP_o was observed upon application of NADH in coronary arterial myocytes from Kv β 2^{Y90F} mice (Figure 4.7 A, B). These observations suggest that catalytic turnover is essential for the redox regulation of Kv1 currents by Kv β 2. Next, we examined whether catalytic turnover is also required for redox-dependent vasoreactivity and regulation of myocardial blood flow in vivo. The data supplementary to this investigation demonstrates that ablation of the Kv β 2 subunit suppresses redox-dependent vasodilation induced by elevated external L-lactate (Appendix A, Figure 4 I) ²⁶². In agreement with these observations, we found that elevation of L-lactate caused vasodilation in arteries isolated from wild type mice; however, this effect was abolished in arteries from Kv β 2^{Y90F} mice (Figure 4.7 C, D), indicating that Kv1-mediated vasodilation in response to changes in intracellular pyridine nucleotides depends entirely upon the catalytic activity of Kv β 2.

Next, to investigate whether Kv1-mediated regulation of myocardial blood flow depends similarly on the Kv β 2-catalysis, we examined blood flow at different cardiac workloads, as described previously ^{6, 262}. Intravenous infusion of norepinephrine led to similar increases in mean arterial pressure and heart rate in wild type and Kv β 2^{Y90F} mice (Figure 4.7 E). In wild type mice, increases in cardiac workload (double product of mean arterial pressure x heart rate) was accompanied by a proportional increase in myocardial blood flow (Figure 4.7 F). Nonetheless, myocardial blood flow across the range of observed cardiac workloads was significantly suppressed in Kv β 2^{Y90F} mice. These data

indicate that a catalytically-active Kv β 2 protein is essential for the regulation of myocardial blood flow by cardiac workload.

Discussion

Our data that supplements this work demonstrates that Kv β 2 subunits are essential to the linear relationship between coronary blood flow and MVO₂ (Appendix A, Figure 2 D)²⁶². In addition, we found that lactate, a metabolite that enhances cytosolic NADH/NAD⁺ ratio, increases both coronary Kv1 channel activity and vasodilation (Appendix A, Figure 4)²⁶². Furthermore, we observed that this vasodilation was dependent upon Kv β 2 subunit expression (Appendix A, Figure 4 H, I)²⁶². These results suggest that Kv β 2 subunits could increase Kv1 channel activity and vasodilation in the coronary vasculature upon enhanced cytosolic NADH/NAD⁺ ratio. In Chapter III, we demonstrated that lactate accumulates in the coronary vasculature upon increased myocardial demand. Thus, Kv β 2 subunits could sense this change in cytosolic NADH/NAD⁺ ratio to promote Kv1 channel activation and coronary vasodilation to increase coronary blood flow upon enhanced metabolic demand. However, whether pyridine nucleotides regulate Kv1 channels in coronary vascular smooth muscle cells is unknown.

Therefore, in this section of the dissertation, we investigated whether coronary vascular Kv1 channels can be directly regulated by pyridine nucleotides and how β subunit expression influences this pyridine nucleotide sensitivity. Finally, because AKR catalytic activity is critical in the regulation of Kv1 channel activity in heterologous expression systems, we investigated whether mutation of the Kv β 2 catalytic site could inhibit pyridine nucleotide sensitivity of the channel and disrupt the linear relationship between coronary blood flow and MVO₂^{8, 10}. The results, presented in this section, demonstrate that Kv β 2 subunits have a significant influence upon vascular Kv1 channel pyridine nucleotide sensitivity, regulation of vascular tone, and the relationship between coronary blood flow

and MVO_2 . Our patch clamp electrophysiology data demonstrates that $Kv\beta 2$ subunits are critical in mediating the increase in $Kv1$ -channel activation observed in the context of an elevated $NADH/NAD^+$ ratio. Both the single channel data and the whole cell data support this conclusion. Furthermore, the single channel data indicates that pyridine nucleotides interact directly with $Kv\beta$ subunits to modulate $Kv1$ channel activity in the coronary vasculature. The inhibition of $Kv1$ channel activity due to $Kv\beta 2$ knockout, in the context of an elevated $NADH/NAD^+$ ratio, appears to rely upon the AKR catalytic activity of the auxiliary complex as p-open probability of $Kv\beta 2^{Y90F}$ did not increase upon exposure to $NADH$. Furthermore, this catalytic site of the $Kv\beta 2$ subunit possesses an integral role in mediating vasodilation to lactate and in maintaining myocardial blood flow in the context of increased metabolic demand. Collectively, these results suggest that the pyridine nucleotide sensing capacity and AKR catalytic activity of $Kv\beta 2$ subunits could significantly influence metabolic hyperemia mediated by the coronary vasculature.

These findings regarding $Kv\beta 2$ subunits derived from the coronary vasculature correlate well with previous experiments in heterologous expression systems. In the presence of an internal solution containing a reduced nucleotide composition, $V_{1/2}$ of activation shifted by approximately 15 mV in wild-type mice in comparison to the oxidized nucleotide composition (V_h of activation for reduced mix, -17.5 ± 3.1 mV, V_h of activation for oxidized mix, -2.5 ± 3.8 mV) (Figure 4.3 C, Table 2). In comparison, internal perfusion of $NADPH$ significantly shifted the $V_{1/2}$ of activation of $Kv1.5\alpha/\beta 2$ complexes to hyperpolarized potentials relative to 1 mM $NADP^+$ (Figure 1.7)¹⁹⁵. This result supports the concept that $Kv\beta 2$ subunits, in the coronary vasculature, increase $Kv1$ channel activity in response to reduced pyridine nucleotides to promote hyperpolarization and coronary vasodilation. However, when $Kv\beta 1$ is co-expressed with $Kv1$ channels in heterologous expression systems, $NADH$ increases inactivation of the channel pore which decreases overall channel activity in comparison to treatment with NAD^+ ⁹.

Since wild-type coronary vascular cells are expected to express as heteromeric channels, with both variable α and β subunit expression, how Kv β 2 overcomes competing fast inactivation of the Kv1 channel by Kv β 1 of Kv α subunits during metabolic hyperemia is unclear. Although these competing influences may exist in the coronary vasculature, previous research in heterologous expression systems indicates potential mechanisms for Kv β 2-mediated channel activation in the presence of Kv β 1 expression. Most notably, in heterologous expression systems, Kv β 2 by merely co-expressing with Kv β 1 could possibly alleviate the fast inactivation imparted by this subunit²⁸¹. In Cos cells, Kv β 2 subunits can relieve the inactivation imparted by Kv β 1 subunits upon an α -pore complex²⁸¹. This relief of inactivation is most likely due to the ability of Kv β 2 to prevent Kv β 1 subunits from interacting with the pore complex²⁸¹. This characteristic of Kv β 2 subunits may be due to the ability of these subunits to form oligomeric complexes; whereas, Kv β 1 subunits do not possess this ability to oligomerize efficiently²⁸². Since oligomers are multivalent and have more potential sites of contact, Kv β 2 can more efficiently bind to the α pore complex and suppress the effect of β 1-mediated inactivation²⁸². Therefore, in vivo in the coronary vasculature, the stoichiometry of the Kv β complex may favor expression of Kv β 2 because of the formation of these oligomers, leading to enhanced hyperpolarization and coronary vasodilation during metabolic hyperemia even in the presence of Kv β 1 subunit expression.

However, rather than Kv β 2 inherently inhibiting Kv β 1-mediated inactivation, other signaling pathways could disrupt Kv β 1-mediated inactivation. These pathways could include signaling through Ca²⁺, lipids, and protein kinases²⁸³⁻²⁸⁷. For example, formation of Ca²⁺/calmodulin complexes can restrain the inactivation domain of β 1 subunits^{286, 287}. This signaling pathway might be particularly important in the coronary smooth muscle as Ca²⁺/calmodulin regulates vascular tone. Other signaling pathways that involve oxidation/reduction reactions upon the channel complex may also regulate β -mediated inactivation. In heterologous expression systems, aldehyde substrates or hydrogen

peroxide can oxidize reduced pyridine nucleotides bound to Kv β 1 subunits, inhibiting the N-terminal inactivation imparted by this auxiliary subunit^{8, 248}. As mentioned previously, hydrogen peroxide is released by the myocardium during increased cardiac workload^{172, 173}. H₂O₂ could potentially diffuse to the coronary vascular wall and oxidize the reduced pyridine nucleotides bound to Kv β 1 subunits, restraining N-terminal inactivation, and increasing outward current through the channels pore. Alternatively, an unidentified endogenous substrate could increase upon enhanced cardiac workload that could mediate the same effects upon Kv β 1-mediated inactivation. Potential endogenous substrates include lipid-derived aldehydes that form from lipid peroxidation^{244, 247}. Since myocardial hydrogen peroxide could also induce the production of lipid peroxidation products by reacting with the cell membrane, H₂O₂ could also inhibit N-terminal inactivation by producing aldehyde substrates for the Kv β 1 AKR catalytic site²⁸⁸. These aldehyde substrates and hydrogen peroxide could also potentially increase Kv channel current by acting through Kv β 2 subunits. In heterologous expression systems, 4-carboxybenzaldehyde substantially increases current through Kv1.4/Kv β 2 complexes and concomitantly decreases channel inactivation (Figure 1.8)¹⁰. Thus, multiple signaling pathways could potentially converge upon the AKR activity of the Kv β complex to increase outward K⁺ current through heteromeric Kv1 channel complexes during metabolic hyperemia. In particular, the data in this study support an influential role of β -mediated catalytic activity in metabolic hyperemia, indicating that these signaling pathways could be highly active during increased cardiac workload.

Our results demonstrate that inhibition of Kv β 2 catalytic turnover significantly disrupts the pyridine nucleotide sensitivity of Kv1 channels, vasodilation, and regulation of coronary blood flow. However, the overarching mechanism of how Kv β 2 AKR activity regulates these physiological processes during catalytic turnover is unclear. The mechanisms mentioned above could potentially be involved in this regulation, but the

extent of activation of each of these pathways is not evident from this current data. Interestingly, our single channel data suggest that mutation of the catalytic site at Kv β 2 inhibits the increase in Kv1 channel p-open probability in response to NADH treatment. Therefore, this result indicates that, in our wild-type membrane patches, Kv1 channel open-probability may depend solely upon catalytic turnover at Kv β 2 subunits independent of paracrine or intracellular signaling pathways. Nevertheless, this result does not completely eliminate the potential influence of the signaling pathways mentioned above. While these signaling pathways may not be a dominant influence, they could still substantially have an additive effect upon the increase in Kv1-mediated current, vasodilation, and coronary blood flow that occurs during metabolic hyperemia.

Significance, Limitations, and Future Directions

The work presented here related to the relationship between coronary Kv β subunits and metabolic hyperemia contributes several significant findings to the field of cardiovascular biology. In this study, we provided evidence that coronary vascular smooth muscle Kv1 channels are regulated by intracellular pyridine nucleotide redox state. We demonstrated this regulatory mechanism of Kv1 channels in several different contexts, utilizing several different techniques: patch clamp electrophysiology, pressure myography, and echocardiography. Furthermore, we showed that coronary vascular Kv1 channels are regulated by pyridine nucleotides both at the whole cell and single channel level. Our data also show that pyridine nucleotide regulation of coronary vascular Kv1 channels depends upon Kv β subunit expression. In particular, we demonstrated that knockout of the Kv β 2 subunit disrupts the increase in Kv1 channel activity to a reduced pyridine nucleotide redox state. Furthermore, knockout of this subunit significantly disrupted the relationship between MVO₂ and coronary flow. Lastly, we demonstrated that pyridine nucleotide regulation of vascular Kv1 channels and metabolic hyperemia in the myocardium depends

upon the catalytic function of the Kv β 2 subunit. Kv β 2^{Y90F}, AKR catalytic mutants, displayed significant dysfunction in regulating Kv1 channel activity in response to NADH and coronary flow in response to increased metabolic demand. Collectively, our data demonstrate that Kv β 2 subunits are essential to regulating metabolic hyperemia, possibly through their pyridine nucleotide sensing and AKR enzymatic capacity. Furthermore, this data suggest that Kv β 2 subunits could sense the shift to pyridine nucleotide redox state that occurs during increased metabolic demand to promote Kv1 channel hyperpolarization and metabolic hyperemia. These findings represent a novel mechanism, by which, the coronary vasculature can sense metabolic demand to match coronary blood flow with MVO₂. While other studies have demonstrated pyridine nucleotide regulation of Kv channels in other cells, this study is the first to demonstrate that pyridine nucleotide regulation of Kv channels can function to regulate coronary blood flow to the myocardium during increased metabolic demand^{196, 273}. This mechanism could represent a previously overlooked regulatory pathway critical to the function of the myocardium in the context of increased metabolic demand. However, this study does have several limitations that need to be addressed in future studies.

Foremost, the genetic knockout models utilized in this study were not specific to the vasculature. Therefore, we cannot disregard the effects these knockout models have on cardiomyocyte metabolism apart from their effect on the coronary vasculature. Also, our Kv β 1.1 knockout model does not account for the other Kv β 1 splice variants. Therefore, expression of other Kv β 1 splice variants could upregulate to compensate for the deletion of Kv β 1.1 splice variant. In future studies, we should follow these studies with experiments involving mouse models that have Kv β subunits specifically deleted in the coronary vasculature. Furthermore, we should develop a mouse model that has all splice variants of Kv β 1 deleted to further elucidate the influence of this Kv β subtype on metabolic hyperemia in the coronary vasculature.

Also, with regard to specific experiments, our patch experiments can be improved in future studies. In our whole cell experiments, while we utilized pyridine nucleotide mixes reflective of low and high metabolic demand, these ratios do not equate to the pyridine nucleotide ratios measured in the context of our co-culture system or in-vivo dobutamine challenge experiments^{278, 279}. Future whole cell experiments should utilize pyridine nucleotide ratios that are more reflective of physiological increases in MVO_2 . Furthermore, our single channel experiments did not investigate regulation by all pyridine nucleotides. While we focused on regulation of the coronary vascular Kv1 channels by NAD(H), future studies should incorporate how NADP(H) directly regulates these channels. Also, while we attempted to isolate the recording of Kv channels through our recording conditions by blocking other major potassium channels, we were unable to robustly support the presence of Kv channels in the membrane patches by treatment with a Kv channel inhibitor. Future studies should be performed which use a Kv channel inhibitor during these single channel traces. Lastly, while we identified a substantial influence of Kv β 2 enzymatic turnover in this process, the role of how this AKR activity mediates this mechanism is unclear. In follow-up investigations, more mechanistic investigations regarding elucidating the role Kv β 2 enzymatic turnover should be completed. For example, single channel experiments that involve exposing membrane patches of wild-type and Kv β 2^{Y90F} to hydrogen peroxide could be planned to demonstrate if this myocardial-derived oxidant can cause turnover at the AKR site to increase Kv1 channel activity. Also, another potential mechanism of action of hydrogen peroxide could be the production of lipid peroxidation products that could act as substrates for the AKR catalytic site^{244, 247}. Therefore, this experiment could potentially be utilized to identify substrates of the Kv β subunit.

Another significant hindrance to the experimental design of these studies is that the results observed only demonstrate evidence for regulation of Kv1 channels directly by pyridine nucleotides rather than under conditions that more effectively replicate metabolic

hyperemia. An interesting future experiment could be to collect buffer from electrically paced myocytes and determine if this buffer could increase Kv1-mediate outward current both at the single channel and whole cell level. Furthermore, at the whole heart level, this buffer could be perfused through a working heart system, to determine if metabolites in paced buffer could induce coronary vasodilation.



Figure 4.1: Representative isolated coronary arterial myocyte and patch pipette tip utilized for whole recordings. $R_{\text{pipette}}=6-8 \text{ M}\Omega$

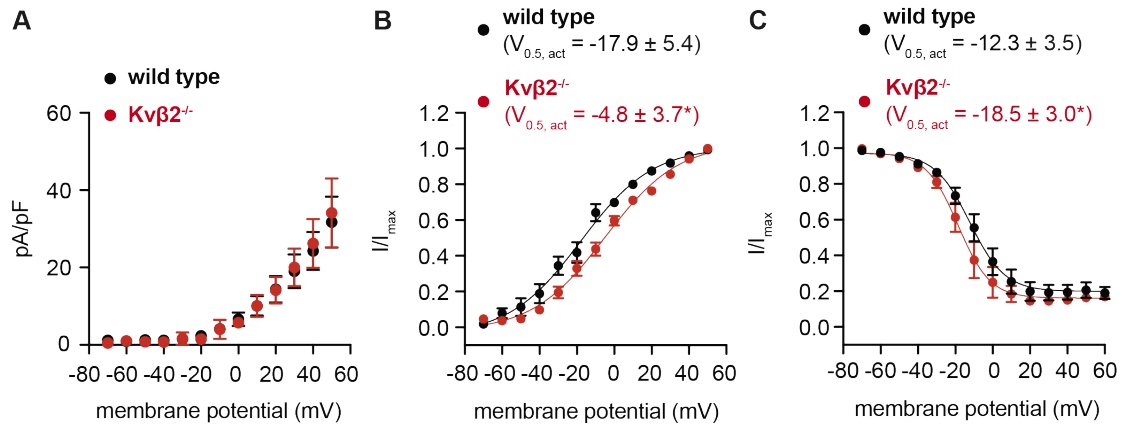


Figure 4.2: Impact of $Kv\beta 2$ ablation on whole cell I_K in coronary arterial smooth muscle. (A) Summary of total outward I_K density in freshly isolated coronary arterial myocytes from wild type (129SvEv) and $Kv\beta 2^{-/-}$ mice. $n = 7-8$ cells, 4-5 mice for each. (B, C) Plots showing summarized I/I_{max} across range of membrane potentials from activation and inactivation two-pulse voltage protocols in wild type and $Kv\beta 2^{-/-}$ mice. Data are fit with Boltzmann function. $n = 8-12$ cells, 4-5 mice for each. * $P < 0.05$, $V_{0.5, act/inact}$, $Kv\beta 2^{-/-}$ vs. wild type (extra sum-of-squares F test).

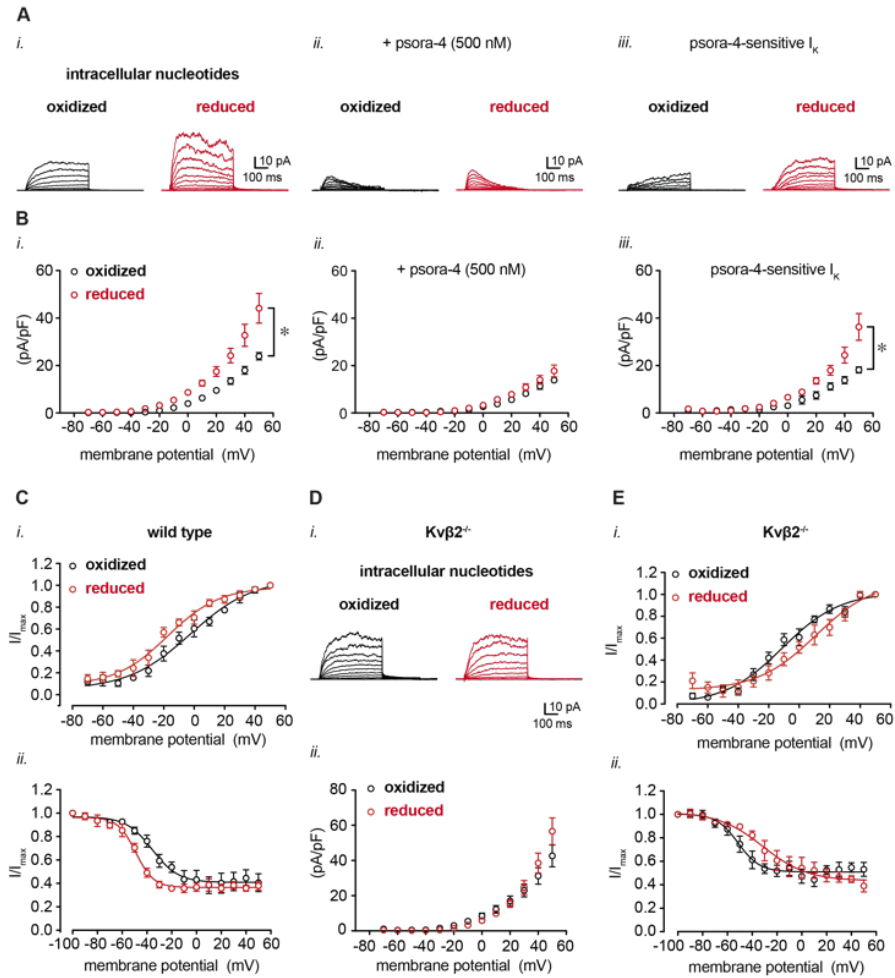


Figure 4.3: Modulation of coronary arterial myocyte I_{Kv} upon changes in intracellular pyridine nucleotide redox potential. Isolated coronary arterial myocytes were dialyzed with pyridine nucleotides at concentrations as indicated in **Table 1** for voltage-clamp recordings in the conventional whole cell configuration. **(A-B)** Representative outward K^+ currents (**A**) and I_K densities (pA/pF; **B**) recorded in coronary arterial myocytes from wild type mice (129SvEv) in the presence of either oxidized or reduced pyridine nucleotide redox ratios. Recordings were performed in the absence (*i.*) and presence (*ii.*) of the $Kv1$ channel inhibitor psora-4 (500 nM). Representative psora-4-sensitive currents (i.e., total outward I_K – psora-insensitive I_K) and summarized densities are shown in *iii.* panels. $n = 5-6$ cells, 4-5 mice for each. $*P < 0.001$, oxidized vs. reduced (mixed effects analysis) **(C)** Summarized I/I_{max} from two-pulse activation voltage protocol (*i.*) and inactivation protocol (*ii.*) for coronary arterial myocytes from wild type mice in the presence of oxidized or reduced pyridine nucleotide ratios. Curves were fit with Boltzmann function; $V_{0.5, act}$ and $V_{0.5, inact}$ are provided in **Table 2**. $n = 5-6$ cells, 4-5 mice for each. **(D)** Representative total outward I_K and summarized I_K density, as in **A**, recorded in coronary arterial myocytes from $Kv\beta 2^{-/-}$ mice in the presence of either oxidized or reduced pyridine nucleotide ratios. $n = 8-9$ cells, 5 mice for each. **(E)** Plots showing summarized I/I_{max} with Boltzmann fittings, as in **D**, recorded from coronary arterial myocytes from $Kv\beta 2^{-/-}$ mice. $V_{0.5, act}$ and $V_{0.5, inact}$ for each condition are provided in **Table 2**. $n = 5-7$ cells, 4-5 mice for each.

Table 1: Pyridine nucleotide concentrations and redox ratios for whole cell I_{Kv} recordings.

	Oxidized	Reduced
NAD⁺ (μM)	1000	200
NADH (μM)	50	1000
NADH:NAD⁺	0.05	5
NADP⁺ (μM)	30	50
NADPH (μM)	100	100
NADPH:NADP⁺	3.33	2

Table 2: Voltage-sensitivity of Kv activation and inactivation.

	Wild type		Kv β 2 ^{-/-}	
	Oxidized	Reduced	Oxidized	Reduced
V _{0.5, act} (mV)	-2.5 ± 3.8	-17.5 ± 3.1*	-11.2 ± 3.0	10.9 ± 6.3*
V _{0.5, inact} (mV)	-35.7 ± 3.1	-49.0 ± 1.4*	-51.4 ± 2.9	-31.4 ± 4.9*

V_{0.5, act/inact}: voltage at 50% of maximum I/I_{max}, n = 5-7 cells, 4-5 mice for each, *P<0.05, reduced vs. oxidized (extra sum-of-squares F test).

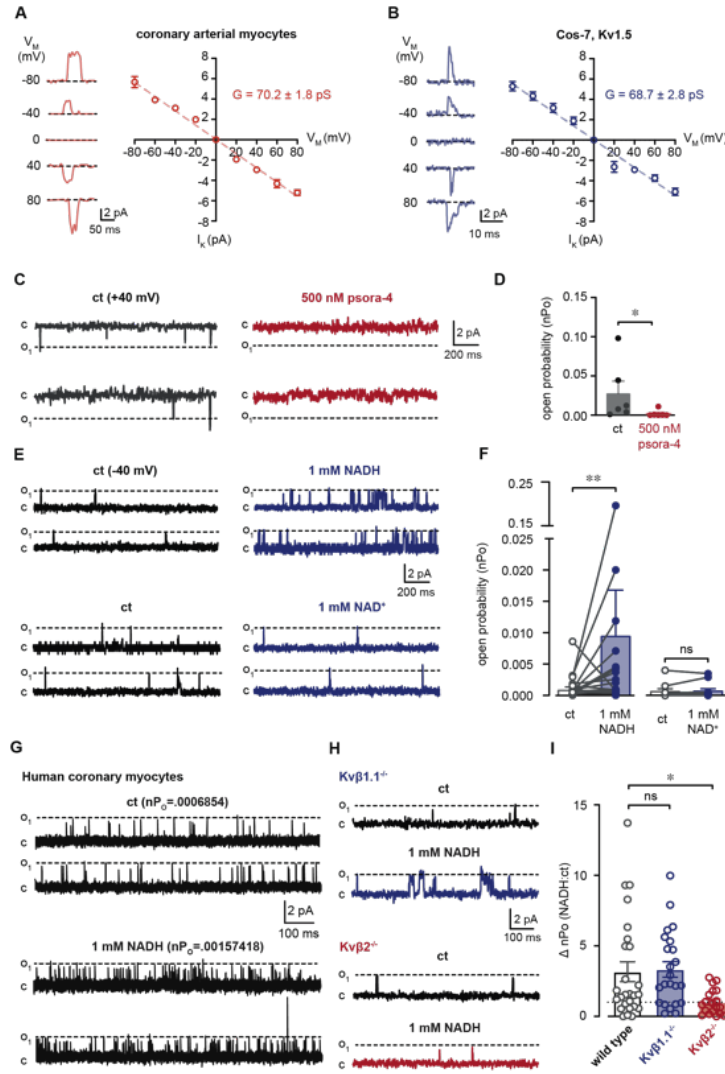


Figure 4.4: Potentiation of native coronary Kv1 activity by NADH requires Kvβ2. (A-B) Unitary K⁺ channel currents (-80-80 mV as indicated, *left*) and summarized I-V relationships (*right*) from inside-out patch recordings from isolated coronary arterial myocytes (wild type 129SvEv, A) or Cos-7 cells transiently expressing Kv1.5 (B). A, n = 9 cells; B, n = 4 cells (D) Single K⁺ channel activity in patches from coronary arterial myocytes at a holding potential of +40 mV in the absence and presence of psora-4 (500 nM). (D) Summary of K⁺ channel open probabilities (nPo) recorded in the absence and presence of 500 nM psora-4. n = 6 cells, *P<0.05 (paired t-test). (E) Representative single Kv current recordings (holding potential = -40 mV) in the absence (ct) and presence of 1 mM NADH (*top*) or 1 mM NAD⁺ (*bottom*). (F) Summary of Kv channel nPo recorded before (ct) and after bath application of 1 mM NADH or NAD⁺. **P<0.01 (paired t-test). (G) Single Kv channel currents recorded from freshly isolated human coronary arterial myocytes membrane patches before and after application of 1 mM NADH. nPo values for each condition are provided above each set of example traces. Data are representative of 4 independent experiments (one donor). (H) Inside-out patch recordings in coronary arterial myocyte membrane patches from Kvβ1.1^{-/-} or Kvβ2^{-/-} mice before and after application of 1 mM NADH. (I) Summary of fold-change in nPo (NADH:ct) in patches from wild type, Kvβ1.1^{-/-}, and Kvβ2^{-/-} mice. *P<0.01 (Kruskal-Wallis test).

human coronary myocytes

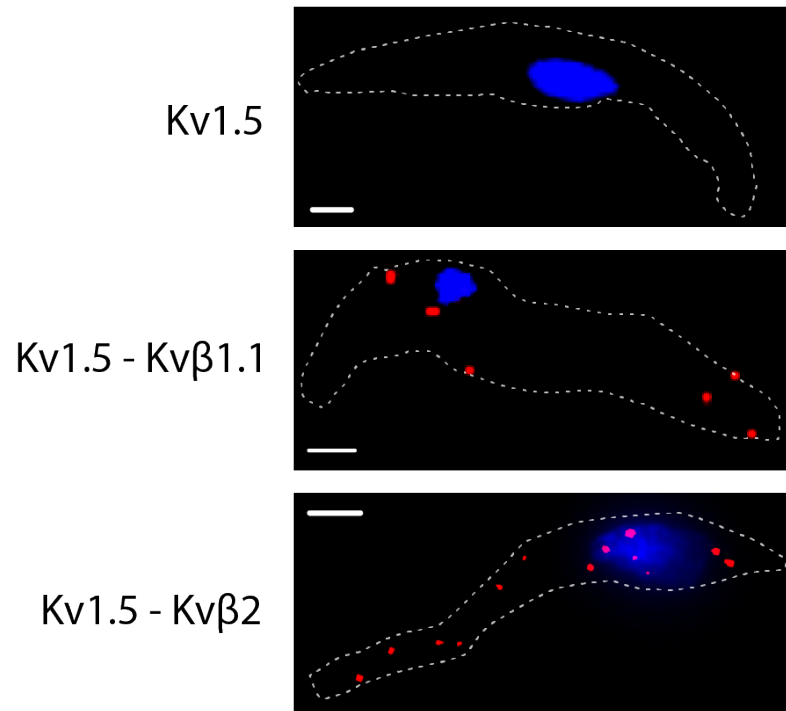


Figure 4.5: Native Kv1 channels in human coronary arterial myocytes associate with Kvβ proteins. Representative fluorescent images showing proximity ligation – positive punctate (red) in isolated human coronary arterial myocytes co-labelled for Kv1.5 and Kvβ1.1, and Kv1.5 and Kvβ2 proteins. As a control, cells were also labelled for Kv1.5 alone. Images are representative of 4, 10, and 14 cells for cells labelled for Kv1.5 alone, Kv1.5 – Kvβ1.1, and Kv1.5 – Kvβ2, respectively. These experiments were performed in collaboration with my colleague Xumei Hu.

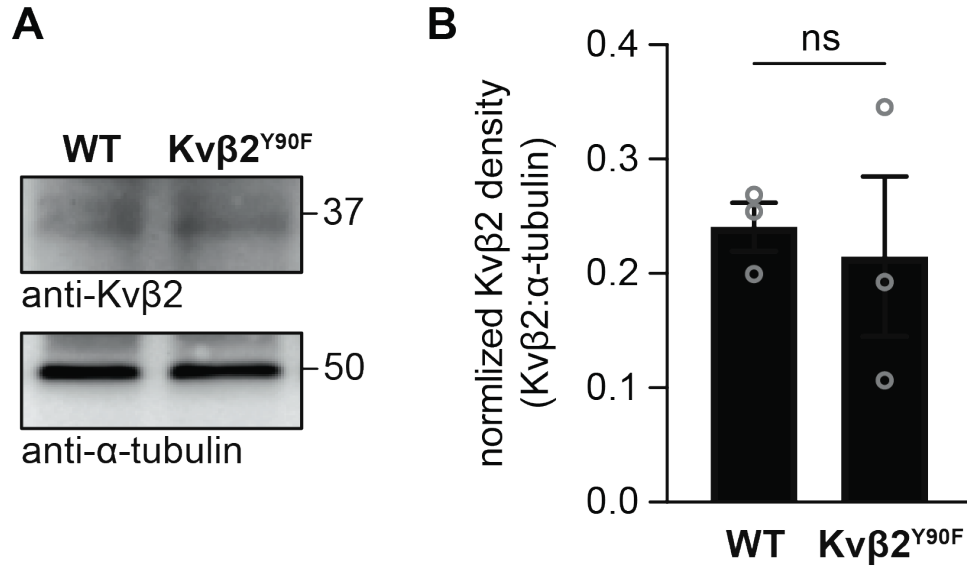


Figure 4.6: The Y90F mutation in Kvβ2 does not alter the abundance of vascular Kvβ2. (A-B) Representative blot images showing immunoreactive bands for Kvβ2 and α-tubulin (loading control) (A) and summary of Kvβ2-associated band densities normalized to α-tubulin (B) in mesenteric artery lysates from wild type and Kvβ2^{Y90F} mice. n = 3 each; ns: P>0.05 (Mann Whitney U test). These experiments were performed by my colleague Xumei Hu.

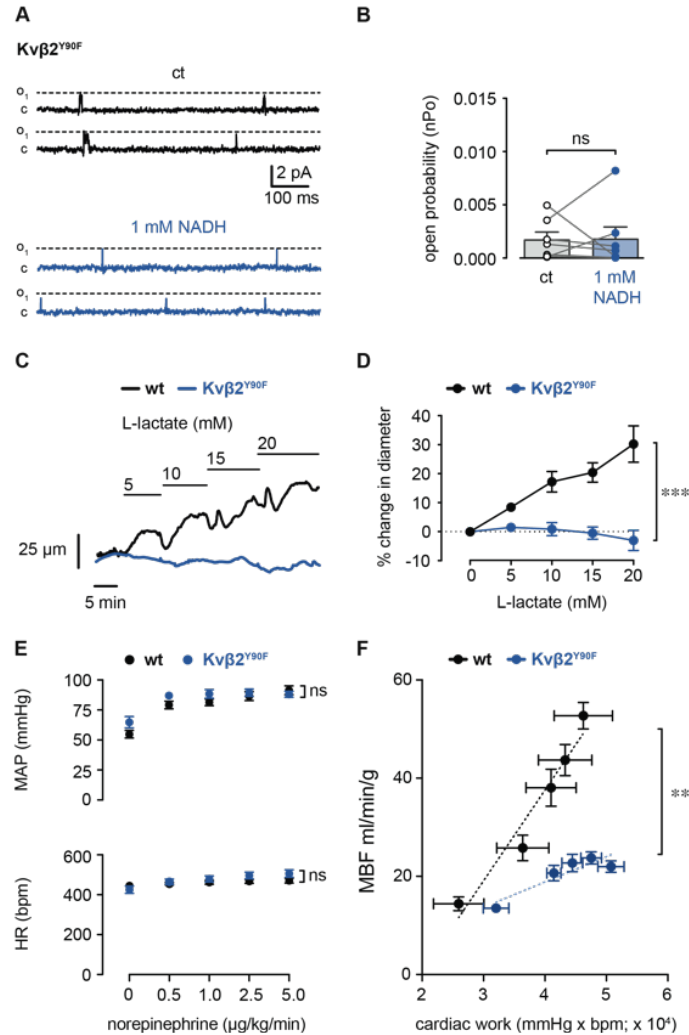


Figure 4.7: Loss of Kv β 2 catalytic function prevents redox-mediated increases in Kv1 activity and vasodilation, and suppresses MBF. (A) Inside-out recordings of Kv1 activity in membrane patches from Kv β 2^{Y90F} mice before and after application of 1 mM NADH. (B) Summary of Kv1 open probabilities (nPo) in membrane patches from Kv β 2^{Y90F} mice before and after application of 1 mM NADH. n = 6 cells from 3 mice; ns: P \geq 0.05 (Wilcoxon matched-pairs signed rank test). (C) Representative arterial diameter recordings in arteries from wild type (129SvEv) and Kv β 2^{Y90F} mice in the absence and presence of L-lactate (5-20 mM) in the perfusate. (D) Summary of percent change in diameter in response to L-lactate (5-20 mM) relative to baseline (0 mM L-lactate). ***P $<$ 0.001 (two-way repeated measures ANOVA). (E) Summary of mean arterial pressure (MAP) and heart rate (HR) in wild type and Kv β 2^{Y90F} mice during intravenous norepinephrine infusion (0-5 μ g/kg/min). n = 4 each, ns: P \geq 0.05 (two way repeated measures ANOVA). (F) Summary of relationships between MBF (ml/min/g) cardiac work (pressure rate product; PRP; bpm x mmHg) in wild type (wt; 129SvEv) versus Kv β 2^{Y90F} mice. **P $<$ 0.01, slope wt vs. Kv β 2^{Y90F}, n = 4-6 mice, (linear regression). Myography experiments were performed by my colleague Sean Raph. Echocardiography experiments were performed by Dr. Vahagn Ohanyan at Northeast Ohio Medical University.

CHAPTER V

SUMMARY & CONCLUSIONS

This dissertation work presented in this study provides a novel mechanism by which coronary vascular smooth muscle cells can regulate coronary blood flow in accordance with myocardial metabolic demand. Overall, we demonstrated that upon increased myocardial metabolic demand cytosolic NADH/NAD⁺ ratio increases in proximal arterial myocytes. This accumulation of reduced pyridine nucleotides is sensed by Kvβ2 proteins associated with Kv1 channels in the coronary vascular smooth muscle membrane. These Kvβ2 proteins utilize these abundant reduced pyridine nucleotides in redox reactions which promotes K⁺ efflux through the Kv1 channel pore. K⁺ efflux induces membrane potential hyperpolarization across the vascular smooth muscle membrane, leading to coronary vascular relaxation and enhanced coronary blood flow to sustain oxygen delivery to the myocardium during increased metabolic demand. Thus, this regulatory process provides a new mechanism by which coronary vascular smooth muscle cells can sense myocardial metabolic demand to appropriately adjust coronary blood flow. This overarching mechanism is depicted in Figure 5.1.

The foremost finding related to this study is that this mechanism significantly regulates coronary blood flow in the context of physiological myocardial demand. As outlined in the introduction of this study, while many of the identified regulators of coronary blood flow (e.g., nitric oxide, eicosanoids, adenosine) impact coronary blood flow, none of the previously identified mediators are absolutely essential to metabolic hyperemia. Many of these previously identified signaling pathways significantly influence other processes

related to coronary blood flow regulation. For example, many of these mediators act as tonic regulators (e.g., eicosanoids) or maintain coronary vascular tone under different physiological conditions such as shear stress or variable perfusion pressures (e.g., nitric oxide, EDHFs). In contrast, the signaling pathway identified in this study appears to be vital to metabolic hyperemia. This conclusion is evident due to the significant disruption in coronary blood flow in the context of increased myocardial demand that occurs upon mutation of the catalytic tyrosine residue in the Kv β 2 subunit (Figure 4.7 F). Furthermore, disruption in the pyridine nucleotide-sensing capacity could underlie the significant reduction in coronary blood flow in the context of increased myocardial metabolic demand observed in the Kv β 2^{Y90F} mice. This hypothesis is supported by the data demonstrating that isolated Kv β 2^{Y90F} vessels fail to dilate in response to extracellular lactate and isolated coronary vascular Kv1 channels from the Kv β 2^{Y90F} mice do not activate in response to NADH (Figure 4.7 A-D). Collectively, these data indicate the pyridine nucleotide sensing capacity and AKR enzymatic activity of Kv β 2 auxiliary subunits could be essential to metabolic hyperemia. While these data demonstrate a novel mechanism that controls coronary blood flow in the context of increased myocardial metabolic demand, further data is needed to clarify this mechanism and support that the pyridine nucleotide sensing capacity of Kv β 2 subunits is required for metabolic hyperemia.

The most obvious remaining question related to this study is the identification of metabolic mediators and carbonyl substrates that can act through this pathway to regulate blood flow in the context of metabolic hyperemia. Many of the metabolic mediators discussed in the background (e.g. extracellular K⁺, ATP, lactate) could potentially increase cytosolic NADH/NAD⁺ ratio in coronary vascular smooth muscle cells ²⁸⁹ (Figure 5.1). However, whether these mediators possess a functional role in signaling through this pathway during metabolic hyperemia remains unknown. Future work should focus on identifying specific myocardial-derived factors or circulating signaling molecules released

during metabolic hyperemia that could increase cytosolic NADH/NAD⁺ in proximal coronary arterial myocytes. The most apparent mediator to investigate is hydrogen peroxide as this molecule is released by the working myocardium and affects Kv1 channel activity¹⁷²⁻¹⁷⁵. However, whether hydrogen peroxide produced at concentrations by the myocardium can increase cytosolic NADH/NAD⁺ ratio in proximal arterial myocytes is uncertain. This mechanism also indicates that catalytic turnover at the Kvβ2 subunit is vital to metabolic hyperemia. This result suggests the presence of carbonyl substrates during metabolic hyperemia that induce Kvβ2-mediated turnover and increase Kv1 channel activity to promote enhanced coronary blood flow. While previous work has identified that Kvβ2 can act on several carbonyl substrates, whether any of these substrates influence metabolic hyperemia is unknown^{244, 247}. The possibility exists that hydrogen peroxide released by the myocardium during increased myocardial demand could oxidize phospholipids in the coronary vascular smooth muscle membrane to produce substrates for Kvβ2 subunits²⁴⁷. Furthermore, glycolytic byproducts could also potentially act upon Kvβ2 AKR enzymes during metabolic hyperemia, considering methylglyoxal is a potential substrate for these auxiliary complexes²⁴⁴.

Another remaining question to be investigated is whether pyridine nucleotide turnover occurs at the Kvβ2 subunit during metabolic hyperemia in vivo. We demonstrated in vitro that catalytic turnover at Kvβ2 subunits utilizing reduced pyridine nucleotides can modulate Kv1 channel activity and coronary vascular tone. These results support that the disruption of metabolic hyperemia observed in Kvβ2^{Y90F} mice could involve the pyridine nucleotide sensing capacity of the auxiliary complex, but the data does not directly show that the pyridine-nucleotide sensing capacity of Kvβ2 subunits is functional in vivo. For this reason, the identification of metabolic mediators and carbonyl substrates is essential to support this overarching mechanism shown in Figure 5.1. If these substrates and mediators are identified, these compounds could be infused into the circulation of both

wild-type and $Kv\beta 2^{Y90F}$ mice which could potentially provide further support for the involvement of the pyridine nucleotide sensing capacity of $Kv\beta 2$ subunits during metabolic hyperemia in vivo.

In conclusion, this dissertation work provides evidence for a novel mechanism that coronary vascular smooth muscle cells utilize to regulate blood flow in the context of enhanced myocardial demand. This mechanism is distinct from any of the previously identified signaling pathways discussed in the background of this dissertation. Furthermore, this mechanism is vital to metabolic hyperemia that occurs during physiological increases in metabolic demand, further enhancing this data's impact as other signaling pathways are more essential to other processes related to coronary vascular tone regulation. This body of work provides a new strategy to study the mechanism of metabolic hyperemia that could potentially contribute to the development of therapies for cardiovascular diseases that are characterized by a mismatch between MVO_2 and coronary blood flow. Furthermore, this mechanism could lead to a greater understanding of processes involving normal physiological changes in metabolic demand such as during exercise.

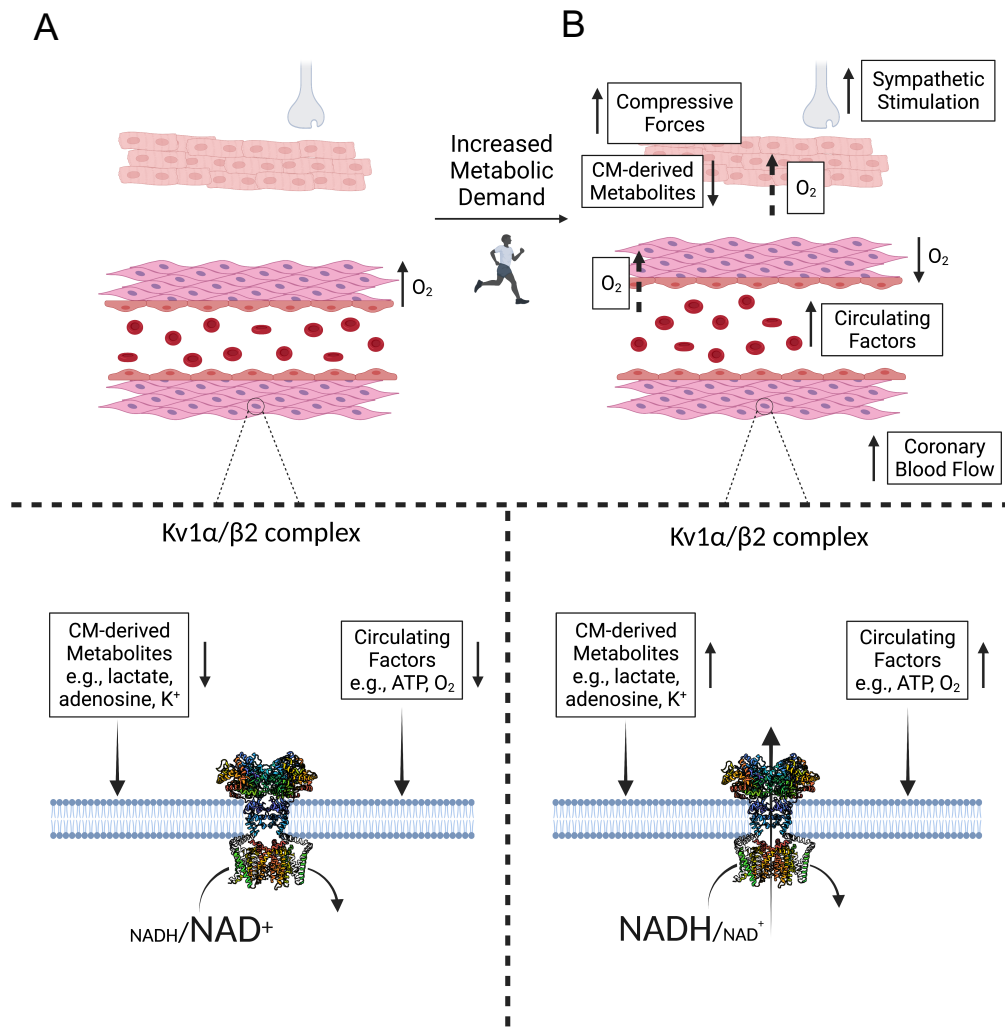


Figure 5.1: Hypothetical mechanism of metabolic hyperemia and the involvement of auxiliary Kv β 2 subunits. (A) Conditions at rest promote basal coronary vascular tone as oxygen demand by the myocardium is not enhanced. The release of cardiomyocyte-derived metabolites and circulating factors that could potentially promote a reduced pyridine nucleotide redox state in the cytosol of proximal arterial myocytes is decreased. NADH/NAD⁺ ratio remains low in coronary vascular smooth muscle cells. Turnover at the Kv β 2 catalytic site, due to a decreased NADH/NAD⁺, does not promote Kv1 channel-mediated K⁺ efflux, hyperpolarization, and coronary vascular relaxation. (B) Increased myocardial metabolic demand, such as during exercise, increases local demand for oxygen, possibly by siphoning of O₂ by the myocardium. This increases the release of myocardial-derived metabolites and circulating factors that could potentially increase cytosolic NADH/NAD⁺ ratio in proximal arterial myocytes. The increase in cytosolic NADH/NAD⁺ is sensed by Kv β 2 proteins and turnover at the Kv β 2 catalytic site promotes Kv1 channel-mediated K⁺ efflux, hyperpolarization, and coronary vascular relaxation. Oxygen delivery to the myocardium is maintained and myocardial blood flow is matched with MVO₂. Created with Biorender.com. Adapted from Long, S.B., Campbell, E.B., Mackinnon, R. (2005) Kv1.2- β 2 subunit complex. doi: 10.1126/pdb2A79/pdb, 10.1126/science.111629

REFERENCES

1. Tune JD, Gorman MW, Feigl EO. Matching coronary blood flow to myocardial oxygen consumption. *J Appl Physiol (1985)*. 2004;97:404-415
2. von Restorff W, Holtz J, Bassenge E. Exercise induced augmentation of myocardial oxygen extraction in spite of normal coronary dilatory capacity in dogs. *Pflugers Arch*. 1977;372:181-185
3. Duncker DJ, Bache RJ. Regulation of coronary blood flow during exercise. *Physiol Rev*. 2008;88:1009-1086
4. Goodwill AG, Noblet JN, Sassoon D, Fu L, Kassab GS, Schepers L, Herring BP, Rottgen TS, Tune JD, Dick GM. Critical contribution of kv1 channels to the regulation of coronary blood flow. *Basic Res Cardiol*. 2016;111:56
5. Ohanyan V, Yin L, Bardakjian R, Kolz C, Enrick M, Hakobyan T, Luli J, Graham K, Khayata M, Logan S, Kmetz J, Chilian WM. Kv1.3 channels facilitate the connection between metabolism and blood flow in the heart. *Microcirculation*. 2017;24
6. Ohanyan V, Yin L, Bardakjian R, Kolz C, Enrick M, Hakobyan T, Kmetz J, Bratz I, Luli J, Nagane M, Khan N, Hou H, Kuppusamy P, Graham J, Fu FK, Janota D, Oyewumi MO, Logan S, Lindner JR, Chilian WM. Requisite role of kv1.5 channels in coronary metabolic dilation. *Circ Res*. 2015;117:612-621
7. Liu SQ, Jin H, Zacarias A, Srivastava S, Bhatnagar A. Binding of pyridine nucleotide coenzymes to the beta-subunit of the voltage-sensitive k⁺ channel. *J Biol Chem*. 2001;276:11812-11820
8. Pan Y, Weng J, Levin EJ, Zhou M. Oxidation of nadph on kvbeta1 inhibits ball-and-chain type inactivation by restraining the chain. *Proc Natl Acad Sci U S A*. 2011;108:5885-5890
9. Tipparaju SM, Saxena N, Liu SQ, Kumar R, Bhatnagar A. Differential regulation of voltage-gated k⁺ channels by oxidized and reduced pyridine nucleotide coenzymes. *Am J Physiol Cell Physiol*. 2005;288:C366-376
10. Weng J, Cao Y, Moss N, Zhou M. Modulation of voltage-dependent shaker family potassium channels by an aldo-keto reductase. *J Biol Chem*. 2006;281:15194-15200
11. Müller B, Lang S, Dominietto M, Rudin M, Schulz G, Deyhle H, Germann M, Pfeiffer F, David C, Weitkamp T. High-resolution tomographic imaging of microvessels. *Proc SPIE*. 2008;7078:70780B

12. Rahman M, Siddik AB. Anatomy, arterioles. *Statpearls*. Treasure Island (FL); 2021.
13. Belt TH. The anatomy and physiology of the coronary circulation. *Can Med Assoc J*. 1933;29:19-21
14. Estes EH, Jr., Entman ML, Dixon HB, 2nd, Hackel DB. The vascular supply of the left ventricular wall. Anatomic observations, plus a hypothesis regarding acute events in coronary artery disease. *Am Heart J*. 1966;71:58-67
15. Wearn JT, Technical Assistance of Louise JZ. The extent of the capillary bed of the heart. *J Exp Med*. 1928;47:273-290
16. Xie Z, Gao M, Batra S, Koyama T. The capillarity of left ventricular tissue of rats subjected to coronary artery occlusion. *Cardiovasc Res*. 1997;33:671-676
17. Chilian WM, Eastham CL, Marcus ML. Microvascular distribution of coronary vascular resistance in beating left ventricle. *Am J Physiol*. 1986;251:H779-788
18. Morita K, Mori H, Tsujioka K, Kimura A, Ogasawara Y, Goto M, Hiramatsu O, Kajiya F, Feigl EO. Alpha-adrenergic vasoconstriction reduces systolic retrograde coronary blood flow. *Am J Physiol*. 1997;273:H2746-2755
19. Khouri EM, Gregg DE, Rayford CR. Effect of exercise on cardiac output, left coronary flow and myocardial metabolism in the unanesthetized dog. *Circ Res*. 1965;17:427-437
20. Downey JM, Kirk ES. Inhibition of coronary blood flow by a vascular waterfall mechanism. *Circ Res*. 1975;36:753-760
21. Bayliss WM. On the local reactions of the arterial wall to changes of internal pressure. *J Physiol*. 1902;28:220-231
22. Berwick ZC, Moberly SP, Kohr MC, Morrical EB, Kurian MM, Dick GM, Tune JD. Contribution of voltage-dependent k^+ and ca^{2+} channels to coronary pressure-flow autoregulation. *Basic Res Cardiol*. 2012;107:264
23. Mellander S, Johansson B. Control of resistance, exchange, and capacitance functions in the peripheral circulation. *Pharmacol Rev*. 1968;20:117-196
24. Brayden JE, Nelson MT. Regulation of arterial tone by activation of calcium-dependent potassium channels. *Science*. 1992;256:532-535
25. Knot HJ, Nelson MT. Regulation of arterial diameter and wall $[ca^{2+}]$ in cerebral arteries of rat by membrane potential and intravascular pressure. *J Physiol*. 1998;508 (Pt 1):199-209
26. Knot HJ, Standen NB, Nelson MT. Ryanodine receptors regulate arterial diameter and wall $[ca^{2+}]$ in cerebral arteries of rat via ca^{2+} -dependent k^+ channels. *J Physiol*. 1998;508 (Pt 1):211-221

27. Walsh MP. Vascular smooth muscle myosin light chain diphosphorylation: Mechanism, function, and pathological implications. *IUBMB Life*. 2011;63:987-1000
28. Gifford JL, Walsh MP, Vogel HJ. Structures and metal-ion-binding properties of the Ca^{2+} -binding helix-loop-helix ef-hand motifs. *Biochem J*. 2007;405:199-221
29. Kamisoyama H, Araki Y, Ikebe M. Mutagenesis of the phosphorylation site (serine 19) of smooth muscle myosin regulatory light chain and its effects on the properties of myosin. *Biochemistry*. 1994;33:840-847
30. Lincoln TM. Myosin phosphatase regulatory pathways: Different functions or redundant functions? *Circ Res*. 2007;100:10-12
31. Murphy RA. Myosin phosphorylation and crossbridge regulation in arterial smooth muscle. State-of-the-art review. *Hypertension*. 1982;4:3-7
32. Floyd R, Wray S. Calcium transporters and signalling in smooth muscles. *Cell Calcium*. 2007;42:467-476
33. Nelson MT, Quayle JM. Physiological roles and properties of potassium channels in arterial smooth muscle. *Am J Physiol*. 1995;268:C799-822
34. Barrett JN, Magleby KL, Pallotta BS. Properties of single calcium-activated potassium channels in cultured rat muscle. *J Physiol*. 1982;331:211-230
35. Nelson MT, Cheng H, Rubart M, Santana LF, Bonev AD, Knot HJ, Lederer WJ. Relaxation of arterial smooth muscle by calcium sparks. *Science*. 1995;270:633-637
36. Horrigan FT, Cui J, Aldrich RW. Allosteric voltage gating of potassium channels i. $Mslo$ ionic currents in the absence of Ca^{2+} . *J Gen Physiol*. 1999;114:277-304
37. Meera P, Wallner M, Song M, Toro L. Large conductance voltage- and calcium-dependent K^{+} channel, a distinct member of voltage-dependent ion channels with seven n-terminal transmembrane segments (s0-s6), an extracellular n terminus, and an intracellular (s9-s10) c terminus. *Proc Natl Acad Sci U S A*. 1997;94:14066-14071
38. Shen KZ, Lagrutta A, Davies NW, Standen NB, Adelman JP, North RA. Tetraethylammonium block of slowpoke calcium-activated potassium channels expressed in xenopus oocytes: Evidence for tetrameric channel formation. *Pflugers Arch*. 1994;426:440-445
39. Wallner M, Meera P, Toro L. Determinant for beta-subunit regulation in high-conductance voltage-activated and Ca^{2+} -sensitive K^{+} channels: An additional transmembrane region at the n terminus. *Proc Natl Acad Sci U S A*. 1996;93:14922-14927
40. Ma Z, Lou XJ, Horrigan FT. Role of charged residues in the s1-s4 voltage sensor of BK channels. *J Gen Physiol*. 2006;127:309-328
41. Yusifov T, Javaherian AD, Pantazis A, Gandhi CS, Olcese R. The rck1 domain of the human $BKCa$ channel transduces Ca^{2+} binding into structural rearrangements. *J Gen Physiol*. 2010;136:189-202

42. Yusifov T, Savalli N, Gandhi CS, Ottolia M, Olcese R. The rck2 domain of the human bkca channel is a calcium sensor. *Proc Natl Acad Sci U S A*. 2008;105:376-381
43. Ge ZD, Zhang XH, Fung PC, He GW. Endothelium-dependent hyperpolarization and relaxation resistance to n(g)-nitro-l-arginine and indomethacin in coronary circulation. *Cardiovasc Res*. 2000;46:547-556
44. Wu X, Davis MJ. Characterization of stretch-activated cation current in coronary smooth muscle cells. *Am J Physiol Heart Circ Physiol*. 2001;280:H1751-1761
45. Furstenau M, Lohn M, Ried C, Luft FC, Haller H, Gollasch M. Calcium sparks in human coronary artery smooth muscle cells resolved by confocal imaging. *J Hypertens*. 2000;18:1215-1222
46. Perez GJ, Bonev AD, Patlak JB, Nelson MT. Functional coupling of ryanodine receptors to kca channels in smooth muscle cells from rat cerebral arteries. *J Gen Physiol*. 1999;113:229-238
47. Hagiwara S, Miyazaki S, Rosenthal NP. Potassium current and the effect of cesium on this current during anomalous rectification of the egg cell membrane of a starfish. *J Gen Physiol*. 1976;67:621-638
48. Fakler B, Brandle U, Glowatzki E, Weidemann S, Zenner HP, Ruppersberg JP. Strong voltage-dependent inward rectification of inward rectifier k⁺ channels is caused by intracellular spermine. *Cell*. 1995;80:149-154
49. Ho K, Nichols CG, Lederer WJ, Lytton J, Vassilev PM, Kanazirska MV, Hebert SC. Cloning and expression of an inwardly rectifying atp-regulated potassium channel. *Nature*. 1993;362:31-38
50. Kubo Y, Baldwin TJ, Jan YN, Jan LY. Primary structure and functional expression of a mouse inward rectifier potassium channel. *Nature*. 1993;362:127-133
51. Kuo A, Gulbis JM, Antcliff JF, Rahman T, Lowe ED, Zimmer J, Cuthbertson J, Ashcroft FM, Ezaki T, Doyle DA. Crystal structure of the potassium channel kirbac1.1 in the closed state. *Science*. 2003;300:1922-1926
52. Lopatin AN, Nichols CG. [k⁺] dependence of polyamine-induced rectification in inward rectifier potassium channels (irk1, kir2.1). *J Gen Physiol*. 1996;108:105-113
53. Chang HK, Lee JR, Liu TA, Suen CS, Arreola J, Shieh RC. The extracellular k⁺ concentration dependence of outward currents through kir2.1 channels is regulated by extracellular na⁺ and ca²⁺. *J Biol Chem*. 2010;285:23115-23125
54. Ishihara K. External k⁽⁺⁾ dependence of strong inward rectifier k⁽⁺⁾ channel conductance is caused not by k⁽⁺⁾ but by competitive pore blockade by external na^(.). *J Gen Physiol*. 2018;150:977-989
55. Knot HJ, Zimmermann PA, Nelson MT. Extracellular k⁽⁺⁾-induced hyperpolarizations and dilatations of rat coronary and cerebral arteries involve inward rectifier k⁽⁺⁾ channels. *J Physiol*. 1996;492 (Pt 2):419-430

56. Murray PA, Belloni FL, Sparks HV. The role of potassium in the metabolic control of coronary vascular resistance of the dog. *Circ Res.* 1979;44:767-780
57. Zhao G, Joca HC, Nelson MT, Lederer WJ. Atp- and voltage-dependent electro-metabolic signaling regulates blood flow in heart. *Proc Natl Acad Sci U S A.* 2020;117:7461-7470
58. Standen NB, Quayle JM, Davies NW, Brayden JE, Huang Y, Nelson MT. Hyperpolarizing vasodilators activate atp-sensitive k⁺ channels in arterial smooth muscle. *Science.* 1989;245:177-180
59. Inagaki N, Gono T, Clement JPt, Namba N, Inazawa J, Gonzalez G, Aguilar-Bryan L, Seino S, Bryan J. Reconstitution of ikatp: An inward rectifier subunit plus the sulfonylurea receptor. *Science.* 1995;270:1166-1170
60. Aguilar-Bryan L, Nichols CG, Rajan AS, Parker C, Bryan J. Co-expression of sulfonylurea receptors and katp channels in hamster insulinoma tumor (hit) cells. Evidence for direct association of the receptor with the channel. *J Biol Chem.* 1992;267:14934-14940
61. Aguilar-Bryan L, Nichols CG, Wechsler SW, Clement JPt, Boyd AE, 3rd, Gonzalez G, Herrera-Sosa H, Nguy K, Bryan J, Nelson DA. Cloning of the beta cell high-affinity sulfonylurea receptor: A regulator of insulin secretion. *Science.* 1995;268:423-426
62. Sturgess NC, Ashford ML, Cook DL, Hales CN. The sulphonylurea receptor may be an atp-sensitive potassium channel. *Lancet.* 1985;2:474-475
63. Inagaki N, Gono T, Clement JP, Wang CZ, Aguilar-Bryan L, Bryan J, Seino S. A family of sulfonylurea receptors determines the pharmacological properties of atp-sensitive k⁺ channels. *Neuron.* 1996;16:1011-1017
64. Isomoto S, Kondo C, Yamada M, Matsumoto S, Higashiguchi O, Horio Y, Matsuzawa Y, Kurachi Y. A novel sulfonylurea receptor forms with bir (kir6.2) a smooth muscle type atp-sensitive k⁺ channel. *J Biol Chem.* 1996;271:24321-24324
65. Yamada M, Isomoto S, Matsumoto S, Kondo C, Shindo T, Horio Y, Kurachi Y. Sulphonylurea receptor 2b and kir6.1 form a sulphonylurea-sensitive but atp-insensitive k⁺ channel. *J Physiol.* 1997;499 (Pt 3):715-720
66. Conti LR, Radeke CM, Shyng SL, Vandenberg CA. Transmembrane topology of the sulfonylurea receptor sur1. *J Biol Chem.* 2001;276:41270-41278
67. Shyng S, Nichols CG. Octameric stoichiometry of the katp channel complex. *J Gen Physiol.* 1997;110:655-664
68. Merkus D, Haitzma DB, Fung TY, Assen YJ, Verdouw PD, Duncker DJ. Coronary blood flow regulation in exercising swine involves parallel rather than redundant vasodilator pathways. *Am J Physiol Heart Circ Physiol.* 2003;285:H424-433
69. Richmond KN, Tune JD, Gorman MW, Feigl EO. Role of k⁺atp channels in local metabolic coronary vasodilation. *Am J Physiol.* 1999;277:H2115-2123

70. Sharifi-Sanjani M, Zhou X, Asano S, Tilley S, Ledent C, Teng B, Dick GM, Mustafa SJ. Interactions between $\alpha(2a)$ adenosine receptors, hydrogen peroxide, and k_{ATP} channels in coronary reactive hyperemia. *Am J Physiol Heart Circ Physiol*. 2013;304:H1294-1301
71. Jackson WF, Konig A, Dambacher T, Busse R. Prostacyclin-induced vasodilation in rabbit heart is mediated by atp-sensitive potassium channels. *Am J Physiol*. 1993;264:H238-243
72. Yang M, Dart C, Kamishima T, Quayle JM. Hypoxia and metabolic inhibitors alter the intracellular atp:Adp ratio and membrane potential in human coronary artery smooth muscle cells. *PeerJ*. 2020;8:e10344
73. Berwick ZC, Payne GA, Lynch B, Dick GM, Sturek M, Tune JD. Contribution of adenosine $\alpha(2a)$ and $\alpha(2b)$ receptors to ischemic coronary dilation: Role of $k(v)$ and $k(atp)$ channels. *Microcirculation*. 2010;17:600-607
74. Farouque HM, Worthley SG, Meredith IT, Skyrme-Jones RA, Zhang MJ. Effect of atp-sensitive potassium channel inhibition on resting coronary vascular responses in humans. *Circ Res*. 2002;90:231-236
75. Samaha FF, Heineman FW, Ince C, Fleming J, Balaban RS. Atp-sensitive potassium channel is essential to maintain basal coronary vascular tone in vivo. *Am J Physiol*. 1992;262:C1220-1227
76. Stepp DW, Kroll K, Feigl EO. K^{+} atp channels and adenosine are not necessary for coronary autoregulation. *Am J Physiol*. 1997;273:H1299-1308
77. Dwenger MM, Ohanyan V, Navedo MF, Nystoriak MA. Coronary microvascular k_v1 channels as regulatory sensors of intracellular pyridine nucleotide redox potential. *Microcirculation*. 2018;25
78. Kalia J, Swartz KJ. Common principles of voltage-dependent gating for h_v and k_v channels. *Neuron*. 2013;77:214-216
79. Long SB, Campbell EB, Mackinnon R. Crystal structure of a mammalian voltage-dependent shaker family k^{+} channel. *Science*. 2005;309:897-903
80. Pongs O, Schwarz JR. Ancillary subunits associated with voltage-dependent k^{+} channels. *Physiol Rev*. 2010;90:755-796
81. Campomanes CR, Carroll KI, Manganas LN, Hershberger ME, Gong B, Antonucci DE, Rhodes KJ, Trimmer JS. K_v beta subunit oxidoreductase activity and k_v1 potassium channel trafficking. *J Biol Chem*. 2002;277:8298-8305
82. Tune JD, Richmond KN, Gorman MW, Feigl EO. $K(atp)(+)$ channels, nitric oxide, and adenosine are not required for local metabolic coronary vasodilation. *Am J Physiol Heart Circ Physiol*. 2001;280:H868-875
83. Borbouse L, Dick GM, Payne GA, Payne BD, Svendsen MC, Neeb ZP, Alloosh M, Bratz IN, Sturek M, Tune JD. Contribution of $bk(ca)$ channels to local metabolic coronary

- vasodilation: Effects of metabolic syndrome. *Am J Physiol Heart Circ Physiol*. 2010;298:H966-973
84. Crecelius AR, Luckasen GJ, Larson DG, Dinunno FA. Kir channel activation contributes to onset and steady-state exercise hyperemia in humans. *Am J Physiol Heart Circ Physiol*. 2014;307:H782-791
85. Crecelius AR, Richards JC, Luckasen GJ, Larson DG, Dinunno FA. Reactive hyperemia occurs via activation of inwardly rectifying potassium channels and na⁺/k⁺-atpase in humans. *Circ Res*. 2013;113:1023-1032
86. Woollard HH. The innervation of the heart. *J Anat*. 1926;60:345-373
87. Lever JD, Ahmed M, Irvine G. Neuromuscular and intercellular relationships in the coronary arterioles. A morphological and quantitative study by light and electron microscopy. *J Anat*. 1965;99:829-840
88. Cowan CL, McKenzie JE. Cholinergic regulation of resting coronary blood flow in domestic swine. *Am J Physiol*. 1990;259:H109-115
89. Duncker DJ, Stubenitsky R, Verdouw PD. Autonomic control of vasomotion in the porcine coronary circulation during treadmill exercise: Evidence for feed-forward beta-adrenergic control. *Circ Res*. 1998;82:1312-1322
90. Lamping KG, Chilian WM, Eastham CL, Marcus ML. Coronary microvascular response to exogenously administered and endogenously released acetylcholine. *Microvasc Res*. 1992;43:294-307
91. Van Winkle DM, Feigl EO. Acetylcholine causes coronary vasodilation in dogs and baboons. *Circ Res*. 1989;65:1580-1593
92. Feigl EO. Parasympathetic control of coronary blood flow in dogs. *Circ Res*. 1969;25:509-519
93. Gross GJ, Buck JD, Warltier DC. Transmural distribution of blood flow during activation of coronary muscarinic receptors. *Am J Physiol*. 1981;240:H941-946
94. Murphree SS, Saffitz JE. Delineation of the distribution of beta-adrenergic receptor subtypes in canine myocardium. *Circ Res*. 1988;63:117-125
95. Chilian WM. Functional distribution of alpha 1- and alpha 2-adrenergic receptors in the coronary microcirculation. *Circulation*. 1991;84:2108-2122
96. Klocke FJ, Kaiser GA, Ross J, Jr., Braunwald E. An intrinsic adrenergic vasodilator mechanism in the coronary vascular bed of the dog. *Circ Res*. 1965;16:376-382
97. Trivella MG, Broten TP, Feigl EO. Beta-receptor subtypes in the canine coronary circulation. *Am J Physiol*. 1990;259:H1575-1585

98. Baumgart D, Haude M, Gorge G, Liu F, Ge J, Grosse-Eggebrecht C, Erbel R, Heusch G. Augmented alpha-adrenergic constriction of atherosclerotic human coronary arteries. *Circulation*. 1999;99:2090-2097
99. Feigl EO. Sympathetic control of coronary circulation. *Circ Res*. 1967;20:262-271
100. Hein TW, Zhang C, Wang W, Kuo L. Heterogeneous beta2-adrenoceptor expression and dilation in coronary arterioles across the left ventricular wall. *Circulation*. 2004;110:2708-2712
101. Scornik FS, Codina J, Birnbaumer L, Toro L. Modulation of coronary smooth muscle kca channels by gs alpha independent of phosphorylation by protein kinase a. *Am J Physiol*. 1993;265:H1460-1465
102. Miyashiro JK, Feigl EO. Feedforward control of coronary blood flow via coronary beta-receptor stimulation. *Circ Res*. 1993;73:252-263
103. Feigl EO. Neural control of coronary blood flow. *J Vasc Res*. 1998;35:85-92
104. Gorman MW, Tune JD, Richmond KN, Feigl EO. Feedforward sympathetic coronary vasodilation in exercising dogs. *J Appl Physiol (1985)*. 2000;89:1892-1902
105. Gorman MW, Tune JD, Richmond KN, Feigl EO. Quantitative analysis of feedforward sympathetic coronary vasodilation in exercising dogs. *J Appl Physiol (1985)*. 2000;89:1903-1911
106. Furchgott RF, Zawadzki JV. The obligatory role of endothelial cells in the relaxation of arterial smooth muscle by acetylcholine. *Nature*. 1980;288:373-376
107. Ignarro LJ, Buga GM, Byrns RE, Wood KS, Chaudhuri G. Endothelium-derived relaxing factor and nitric oxide possess identical pharmacologic properties as relaxants of bovine arterial and venous smooth muscle. *J Pharmacol Exp Ther*. 1988;246:218-226
108. Ignarro LJ, Buga GM, Wood KS, Byrns RE, Chaudhuri G. Endothelium-derived relaxing factor produced and released from artery and vein is nitric oxide. *Proc Natl Acad Sci U S A*. 1987;84:9265-9269
109. Palmer RM, Ferrige AG, Moncada S. Nitric oxide release accounts for the biological activity of endothelium-derived relaxing factor. *Nature*. 1987;327:524-526
110. Durand MJ, Gutterman DD. Diversity in mechanisms of endothelium-dependent vasodilation in health and disease. *Microcirculation*. 2013;20:239-247
111. Michel JB, Feron O, Sacks D, Michel T. Reciprocal regulation of endothelial nitric-oxide synthase by ca2+-calmodulin and caveolin. *J Biol Chem*. 1997;272:15583-15586
112. Maniatis NA, Brovkovich V, Allen SE, John TA, Shajahan AN, Tiruppathi C, Vogel SM, Skidgel RA, Malik AB, Minshall RD. Novel mechanism of endothelial nitric oxide synthase activation mediated by caveolae internalization in endothelial cells. *Circ Res*. 2006;99:870-877

113. Darkow DJ, Lu L, White RE. Estrogen relaxation of coronary artery smooth muscle is mediated by nitric oxide and cgmp. *Am J Physiol.* 1997;272:H2765-2773
114. Forstermann U, Sessa WC. Nitric oxide synthases: Regulation and function. *Eur Heart J.* 2012;33:829-837, 837a-837d
115. Moncada S, Palmer RM, Higgs EA. Nitric oxide: Physiology, pathophysiology, and pharmacology. *Pharmacol Rev.* 1991;43:109-142
116. Li PL, Jin MW, Campbell WB. Effect of selective inhibition of soluble guanylyl cyclase on the k(ca) channel activity in coronary artery smooth muscle. *Hypertension.* 1998;31:303-308
117. Bychkov R, Gollasch M, Steinke T, Ried C, Luft FC, Haller H. Calcium-activated potassium channels and nitrate-induced vasodilation in human coronary arteries. *J Pharmacol Exp Ther.* 1998;285:293-298
118. Hein TW, Kuo L. Camp-independent dilation of coronary arterioles to adenosine : Role of nitric oxide, g proteins, and k(atp) channels. *Circ Res.* 1999;85:634-642
119. Tune JD, Richmond KN, Gorman MW, Feigl EO. Role of nitric oxide and adenosine in control of coronary blood flow in exercising dogs. *Circulation.* 2000;101:2942-2948
120. Stepp DW, Nishikawa Y, Chilian WM. Regulation of shear stress in the canine coronary microcirculation. *Circulation.* 1999;100:1555-1561
121. Goldblatt MW. Properties of human seminal plasma. *J Physiol.* 1935;84:208-218
122. von Euler US. On the specific vaso-dilating and plain muscle stimulating substances from accessory genital glands in man and certain animals (prostaglandin and vesiglandin). *The Journal of Physiology.* 1936;88:213-234
123. Bergstrom S, Samuelsson B. Isolation of prostaglandin e1 from human seminal plasma. Prostaglandins and related factors. 11. *J Biol Chem.* 1962;237:3005-3006
124. Bogatcheva NV, Sergeeva MG, Dudek SM, Verin AD. Arachidonic acid cascade in endothelial pathobiology. *Microvasc Res.* 2005;69:107-127
125. Cohen RA, Vanhoutte PM. Endothelium-dependent hyperpolarization. Beyond nitric oxide and cyclic gmp. *Circulation.* 1995;92:3337-3349
126. Earley S, Heppner TJ, Nelson MT, Brayden JE. Trpv4 forms a novel ca2+ signaling complex with ryanodine receptors and bkca channels. *Circ Res.* 2005;97:1270-1279
127. Li PL, Campbell WB. Epoxyeicosatrienoic acids activate k+ channels in coronary smooth muscle through a guanine nucleotide binding protein. *Circ Res.* 1997;80:877-884
128. Park SK, Herrnreiter A, Pfister SL, Gauthier KM, Falck BA, Falck JR, Campbell WB. Gpr40 is a low-affinity epoxyeicosatrienoic acid receptor in vascular cells. *J Biol Chem.* 2018;293:10675-10691

129. Dai XZ, Bache RJ. Effect of indomethacin on coronary blood flow during graded treadmill exercise in the dog. *Am J Physiol*. 1984;247:H452-458
130. Edlund A, Sollevi A, Wennmalm A. The role of adenosine and prostacyclin in coronary flow regulation in healthy man. *Acta Physiol Scand*. 1989;135:39-46
131. Merkus D, Houweling B, Zarbanoui A, Duncker DJ. Interaction between prostanoids and nitric oxide in regulation of systemic, pulmonary, and coronary vascular tone in exercising swine. *Am J Physiol Heart Circ Physiol*. 2004;286:H1114-1123
132. Hillig T, Krstrup P, Fleming I, Osada T, Saltin B, Hellsten Y. Cytochrome p450 2c9 plays an important role in the regulation of exercise-induced skeletal muscle blood flow and oxygen uptake in humans. *J Physiol*. 2003;546:307-314
133. Zhou Z, Hemradj V, de Beer VJ, Gao F, Hoekstra M, Merkus D, Duncker DJ. Cytochrome p-450 2c9 exerts a vasoconstrictor influence on coronary resistance vessels in swine at rest and during exercise. *Am J Physiol Heart Circ Physiol*. 2012;302:H1747-1755
134. De Mey JG, Claeys M, Vanhoutte PM. Endothelium-dependent inhibitory effects of acetylcholine, adenosine triphosphate, thrombin and arachidonic acid in the canine femoral artery. *J Pharmacol Exp Ther*. 1982;222:166-173
135. Vanhoutte PM. Endothelium-dependent hyperpolarizations: The history. *Pharmacol Res*. 2004;49:503-508
136. Nishikawa Y, Stepp DW, Chilian WM. In vivo location and mechanism of edhf-mediated vasodilation in canine coronary microcirculation. *Am J Physiol*. 1999;277:H1252-1259
137. Batenburg WW, Popp R, Fleming I, de Vries R, Garrelds IM, Saxena PR, Danser AH. Bradykinin-induced relaxation of coronary microarteries: S-nitrosothiols as edhf? *Br J Pharmacol*. 2004;142:125-135
138. Edwards G, Dora KA, Gardener MJ, Garland CJ, Weston AH. K⁺ is an endothelium-derived hyperpolarizing factor in rat arteries. *Nature*. 1998;396:269-272
139. Matoba T, Shimokawa H, Nakashima M, Hirakawa Y, Mukai Y, Hirano K, Kanaide H, Takeshita A. Hydrogen peroxide is an endothelium-derived hyperpolarizing factor in mice. *J Clin Invest*. 2000;106:1521-1530
140. Griffith TM, Chaytor AT, Taylor HJ, Giddings BD, Edwards DH. Camp facilitates edhf-type relaxations in conduit arteries by enhancing electrotonic conduction via gap junctions. *Proc Natl Acad Sci U S A*. 2002;99:6392-6397
141. Kurian MM, Berwick ZC, Tune JD. Contribution of ikca channels to the control of coronary blood flow. *Exp Biol Med (Maywood)*. 2011;236:621-627
142. Gremels H, Starling EH. On the influence of hydrogen ion concentration and of anaemia upon the heart volume. *J Physiol*. 1926;61:297-304

143. Hilton R, Eichholtz F. The influence of chemical factors on the coronary circulation. *J Physiol.* 1925;59:413-425
144. Jimenez AH, Tanner MA, Caldwell WM, Myers PR. Effects of oxygen tension on flow-induced vasodilation in porcine coronary resistance arterioles. *Microvasc Res.* 1996;51:365-377
145. Miura H, Wachtel RE, Loberiza FR, Jr., Saito T, Miura M, Nicolosi AC, Gutterman DD. Diabetes mellitus impairs vasodilation to hypoxia in human coronary arterioles: Reduced activity of atp-sensitive potassium channels. *Circ Res.* 2003;92:151-158
146. Afonso S, Bandow GT, Rowe GG. Indomethacin and the prostaglandin hypothesis of coronary blood flow regulation. *J Physiol.* 1974;241:299-308
147. Liu Q, Flavahan NA. Hypoxic dilatation of porcine small coronary arteries: Role of endothelium and katp-channels. *Br J Pharmacol.* 1997;120:728-734
148. Dart C, Standen NB. Activation of atp-dependent k⁺ channels by hypoxia in smooth muscle cells isolated from the pig coronary artery. *J Physiol.* 1995;483 (Pt 1):29-39
149. Park WS, Han J, Kim N, Ko JH, Kim SJ, Earm YE. Activation of inward rectifier k⁺ channels by hypoxia in rabbit coronary arterial smooth muscle cells. *Am J Physiol Heart Circ Physiol.* 2005;289:H2461-2467
150. Hedegaard ER, Nielsen BD, Kun A, Hughes AD, Kroigaard C, Mogensen S, Matchkov VV, Frobert O, Simonsen U. Kv 7 channels are involved in hypoxia-induced vasodilatation of porcine coronary arteries. *Br J Pharmacol.* 2014;171:69-82
151. Duncker DJ, Stubenitsky R, Verdouw PD. Role of adenosine in the regulation of coronary blood flow in swine at rest and during treadmill exercise. *Am J Physiol.* 1998;275:H1663-1672
152. Herrmann SC, Feigl EO. Adrenergic blockade blunts adenosine concentration and coronary vasodilation during hypoxia. *Circ Res.* 1992;70:1203-1216
153. Berne RM. Cardiac nucleotides in hypoxia: Possible role in regulation of coronary blood flow. *Am J Physiol.* 1963;204:317-322
154. Hein TW, Belardinelli L, Kuo L. Adenosine a(2a) receptors mediate coronary microvascular dilation to adenosine: Role of nitric oxide and atp-sensitive potassium channels. *J Pharmacol Exp Ther.* 1999;291:655-664
155. Dick GM, Bratz IN, Borbouse L, Payne GA, Dincer UD, Knudson JD, Rogers PA, Tune JD. Voltage-dependent k⁺ channels regulate the duration of reactive hyperemia in the canine coronary circulation. *Am J Physiol Heart Circ Physiol.* 2008;294:H2371-2381
156. Bender SB, Tune JD, Borbouse L, Long X, Sturek M, Laughlin MH. Altered mechanism of adenosine-induced coronary arteriolar dilation in early-stage metabolic syndrome. *Exp Biol Med (Maywood).* 2009;234:683-692

157. Borbouse L, Dick GM, Asano S, Bender SB, Dincer UD, Payne GA, Neeb ZP, Bratz IN, Sturek M, Tune JD. Impaired function of coronary bk(ca) channels in metabolic syndrome. *Am J Physiol Heart Circ Physiol*. 2009;297:H1629-1637
158. Cabell F, Weiss DS, Price JM. Inhibition of adenosine-induced coronary vasodilation by block of large-conductance ca(2+)-activated k+ channels. *Am J Physiol*. 1994;267:H1455-1460
159. Son YK, Park WS, Ko JH, Han J, Kim N, Earm YE. Protein kinase a-dependent activation of inward rectifier potassium channels by adenosine in rabbit coronary smooth muscle cells. *Biochem Biophys Res Commun*. 2005;337:1145-1152
160. Bacchus AN, Ely SW, Knabb RM, Rubio R, Berne RM. Adenosine and coronary blood flow in conscious dogs during normal physiological stimuli. *Am J Physiol*. 1982;243:H628-633
161. Ely SW, Knabb RM, Bacchus AN, Rubio R, Berne RM. Measurements of coronary plasma and pericardial infusate adenosine concentrations during exercise in conscious dog: Relationship to myocardial oxygen consumption and coronary blood flow. *J Mol Cell Cardiol*. 1983;15:673-683
162. Bache RJ, Dai XZ, Schwartz JS, Homans DC. Role of adenosine in coronary vasodilation during exercise. *Circ Res*. 1988;62:846-853
163. Ellsworth ML, Forrester T, Ellis CG, Dietrich HH. The erythrocyte as a regulator of vascular tone. *Am J Physiol*. 1995;269:H2155-2161
164. Sprague RS, Ellsworth ML. Erythrocyte-derived atp and perfusion distribution: Role of intracellular and intercellular communication. *Microcirculation*. 2012;19:430-439
165. Gorman MW, Rooke GA, Savage MV, Jayasekara MP, Jacobson KA, Feigl EO. Adenine nucleotide control of coronary blood flow during exercise. *Am J Physiol Heart Circ Physiol*. 2010;299:H1981-1989
166. Farias M, 3rd, Gorman MW, Savage MV, Feigl EO. Plasma atp during exercise: Possible role in regulation of coronary blood flow. *Am J Physiol Heart Circ Physiol*. 2005;288:H1586-1590
167. Bender SB, Berwick ZC, Laughlin MH, Tune JD. Functional contribution of p2y1 receptors to the control of coronary blood flow. *J Appl Physiol (1985)*. 2011;111:1744-1750
168. Ohta M, Toyama K, Gutterman DD, Campbell WB, Lemaître V, Teraoka R, Miura H. Ecto-5'-nucleotidase, cd73, is an endothelium-derived hyperpolarizing factor synthase. *Arterioscler Thromb Vasc Biol*. 2013;33:629-636
169. Strobaek D, Christophersen P, Dissing S, Olesen SP. Atp activates k and cl channels via purinoceptor-mediated release of ca2+ in human coronary artery smooth muscle. *Am J Physiol*. 1996;271:C1463-1471

170. Liu GX, Vepa S, Artman M, Coetzee WA. Modulation of human cardiovascular outward rectifying chloride channel by intra- and extracellular atp. *Am J Physiol Heart Circ Physiol*. 2007;293:H3471-3479
171. Rivers RJ, Hein TW, Zhang C, Kuo L. Activation of barium-sensitive inward rectifier potassium channels mediates remote dilation of coronary arterioles. *Circulation*. 2001;104:1749-1753
172. Saitoh S, Zhang C, Tune JD, Potter B, Kiyooka T, Rogers PA, Knudson JD, Dick GM, Swafford A, Chilian WM. Hydrogen peroxide: A feed-forward dilator that couples myocardial metabolism to coronary blood flow. *Arterioscler Thromb Vasc Biol*. 2006;26:2614-2621
173. Yada T, Shimokawa H, Hiramatsu O, Shinozaki Y, Mori H, Goto M, Ogasawara Y, Kajiya F. Important role of endogenous hydrogen peroxide in pacing-induced metabolic coronary vasodilation in dogs in vivo. *J Am Coll Cardiol*. 2007;50:1272-1278
174. Rogers PA, Chilian WM, Bratz IN, Bryan RM, Jr., Dick GM. H₂O₂ activates redox- and 4-aminopyridine-sensitive kv channels in coronary vascular smooth muscle. *Am J Physiol Heart Circ Physiol*. 2007;292:H1404-1411
175. Rogers PA, Dick GM, Knudson JD, Focardi M, Bratz IN, Swafford AN, Jr., Saitoh S, Tune JD, Chilian WM. H₂O₂-induced redox-sensitive coronary vasodilation is mediated by 4-aminopyridine-sensitive k⁺ channels. *Am J Physiol Heart Circ Physiol*. 2006;291:H2473-2482
176. Saitoh S, Kiyooka T, Rocic P, Rogers PA, Zhang C, Swafford A, Dick GM, Viswanathan C, Park Y, Chilian WM. Redox-dependent coronary metabolic dilation. *Am J Physiol Heart Circ Physiol*. 2007;293:H3720-3725
177. Barlow RS, El-Mowafy AM, White RE. H₂O₂ opens bk(ca) channels via the pla(2)-arachidonic acid signaling cascade in coronary artery smooth muscle. *Am J Physiol Heart Circ Physiol*. 2000;279:H475-483
178. Thengchaisri N, Kuo L. Hydrogen peroxide induces endothelium-dependent and -independent coronary arteriolar dilation: Role of cyclooxygenase and potassium channels. *Am J Physiol Heart Circ Physiol*. 2003;285:H2255-2263
179. Zhang DX, Borbouse L, Gebremedhin D, Mendoza SA, Zinkevich NS, Li R, Gutterman DD. H₂O₂-induced dilation in human coronary arterioles: Role of protein kinase g dimerization and large-conductance ca²⁺-activated k⁺ channel activation. *Circ Res*. 2012;110:471-480
180. Sun F, Dai C, Xie J, Hu X. Biochemical issues in estimation of cytosolic free nad/nadh ratio. *PLoS One*. 2012;7:e34525
181. Williamson DH, Lund P, Krebs HA. The redox state of free nicotinamide-adenine dinucleotide in the cytoplasm and mitochondria of rat liver. *Biochem J*. 1967;103:514-527
182. Ido Y, Chang K, Williamson JR. Nadh augments blood flow in physiologically activated retina and visual cortex. *Proc Natl Acad Sci U S A*. 2004;101:653-658

183. Ido Y, Chang K, Woolsey TA, Williamson JR. NADH: Sensor of blood flow need in brain, muscle, and other tissues. *FASEB J.* 2001;15:1419-1421
184. Mintun MA, Vlassenko AG, Rundle MM, Raichle ME. Increased lactate/pyruvate ratio augments blood flow in physiologically activated human brain. *Proc Natl Acad Sci U S A.* 2004;101:659-664
185. Rasmussen P, Madsen CA, Nielsen HB, Zaar M, Gjedde A, Secher NH, Quistorff B. Coupling between the blood lactate-to-pyruvate ratio and mca vmean at the onset of exercise in humans. *J Appl Physiol (1985).* 2009;107:1799-1805
186. Brooks GA. Role of the heart in lactate shuttling. *Front Nutr.* 2021;8:663560
187. Messonnier LA, Emhoff CA, Fattor JA, Horning MA, Carlson TJ, Brooks GA. Lactate kinetics at the lactate threshold in trained and untrained men. *J Appl Physiol (1985).* 2013;114:1593-1602
188. Laughlin MR, Heineman FW. The relationship between phosphorylation potential and redox state in the isolated working rabbit heart. *J Mol Cell Cardiol.* 1994;26:1525-1536
189. Bergman BC, Tsvetkova T, Lowes B, Wolfel EE. Myocardial glucose and lactate metabolism during rest and atrial pacing in humans. *J Physiol.* 2009;587:2087-2099
190. Wengrowski AM, Kuzmiak-Glancy S, Jaimes R, 3rd, Kay MW. NADH changes during hypoxia, ischemia, and increased work differ between isolated heart preparations. *Am J Physiol Heart Circ Physiol.* 2014;306:H529-537
191. Barron JT, Gu L, Parrillo JE. Relation of NADH/NAD to contraction in vascular smooth muscle. *Mol Cell Biochem.* 1999;194:283-290
192. Barron JT, Gu L, Parrillo JE. Cytoplasmic redox potential affects energetics and contractile reactivity of vascular smooth muscle. *J Mol Cell Cardiol.* 1997;29:2225-2232
193. Barron JT, Gu L, Parrillo JE. NADH/NAD redox state of cytoplasmic glycolytic compartments in vascular smooth muscle. *Am J Physiol Heart Circ Physiol.* 2000;279:H2872-2878
194. Barron JT, Gu L, Parrillo JE. Malate-aspartate shuttle, cytoplasmic NADH redox potential, and energetics in vascular smooth muscle. *J Mol Cell Cardiol.* 1998;30:1571-1579
195. Tipparaju SM, Li XP, Kilfoil PJ, Xue B, Uversky VN, Bhatnagar A, Barski OA. Interactions between the c-terminus of Kv1.5 and Kvbeta regulate pyridine nucleotide-dependent changes in channel gating. *Pflugers Arch.* 2012;463:799-818
196. Kilfoil PJ, Chapalamadugu KC, Hu X, Zhang D, Raucci FJ, Jr., Tur J, Brittan KR, Jones SP, Bhatnagar A, Tipparaju SM, Nystoriak MA. Metabolic regulation of Kv channels and cardiac repolarization by Kvbeta2 subunits. *J Mol Cell Cardiol.* 2019;137:93-106

197. Tiong SYX, Oka Y, Sasaki T, Taniguchi M, Doi M, Akiyama H, Sato M. Kcnab1 is expressed in subplate neurons with unilateral long-range inter-areal projections. *Front Neuroanat.* 2019;13:39
198. Tur J, Chapalamadugu KC, Padawer T, Badole SL, Kilfoil PJ, 2nd, Bhatnagar A, Tipparaju SM. Deletion of kvbeta1.1 subunit leads to electrical and haemodynamic changes causing cardiac hypertrophy in female murine hearts. *Exp Physiol.* 2016;101:494-508
199. Jan YN, Jan LY, Dennis MJ. Two mutations of synaptic transmission in drosophila. *Proc R Soc Lond B Biol Sci.* 1977;198:87-108
200. Tanouye MA, Ferrus A, Fujita SC. Abnormal action potentials associated with the shaker complex locus of drosophila. *Proc Natl Acad Sci U S A.* 1981;78:6548-6552
201. Kaplan WD, Trout WE, 3rd. The behavior of four neurological mutants of drosophila. *Genetics.* 1969;61:399-409
202. Salkoff L. Genetic and voltage-clamp analysis of a drosophila potassium channel. *Cold Spring Harb Symp Quant Biol.* 1983;48 Pt 1:221-231
203. Salkoff L, Wyman R. Genetic modification of potassium channels in drosophila shaker mutants. *Nature.* 1981;293:228-230
204. Iverson LE, Tanouye MA, Lester HA, Davidson N, Rudy B. A-type potassium channels expressed from shaker locus cDNA. *Proc Natl Acad Sci U S A.* 1988;85:5723-5727
205. Timpe LC, Jan YN, Jan LY. Four cDNA clones from the shaker locus of drosophila induce kinetically distinct a-type potassium currents in xenopus oocytes. *Neuron.* 1988;1:659-667
206. Stocker M, Stuhmer W, Wittka R, Wang X, Muller R, Ferrus A, Pongs O. Alternative shaker transcripts express either rapidly inactivating or noninactivating k⁺ channels. *Proc Natl Acad Sci U S A.* 1990;87:8903-8907
207. Timpe LC, Schwarz TL, Tempel BL, Papazian DM, Jan YN, Jan LY. Expression of functional potassium channels from shaker cDNA in xenopus oocytes. *Nature.* 1988;331:143-145
208. Butler A, Wei A, Salkoff L. Shal, shab, and shaw: Three genes encoding potassium channels in drosophila. *Nucleic Acids Res.* 1990;18:2173-2174
209. Butler A, Wei AG, Baker K, Salkoff L. A family of putative potassium channel genes in drosophila. *Science.* 1989;243:943-947
210. Covarrubias M, Wei AA, Salkoff L. Shaker, shal, shab, and shaw express independent k⁺ current systems. *Neuron.* 1991;7:763-773

211. Grupe A, Schroter KH, Ruppertsberg JP, Stocker M, Drewes T, Beckh S, Pongs O. Cloning and expression of a human voltage-gated potassium channel. A novel member of the rck potassium channel family. *EMBO J.* 1990;9:1749-1756
212. Swanson R, Marshall J, Smith JS, Williams JB, Boyle MB, Folander K, Luneau CJ, Antanavage J, Oliva C, Buhrow SA, et al. Cloning and expression of cDNA and genomic clones encoding three delayed rectifier potassium channels in rat brain. *Neuron.* 1990;4:929-939
213. Tempel BL, Jan YN, Jan LY. Cloning of a probable potassium channel gene from mouse brain. *Nature.* 1988;332:837-839
214. Wei A, Covarrubias M, Butler A, Baker K, Pak M, Salkoff L. K⁺ current diversity is produced by an extended gene family conserved in drosophila and mouse. *Science.* 1990;248:599-603
215. Chandy KG. Simplified gene nomenclature. *Nature.* 1991;352:26
216. Mehraban F, Breeze AL, Dolly JO. Identification by cross-linking of a neuronal acceptor protein for dendrotoxin, a convulsant polypeptide. *FEBS Lett.* 1984;174:116-122
217. Parcej DN, Dolly JO. Dendrotoxin acceptor from bovine synaptic plasma membranes. Binding properties, purification and subunit composition of a putative constituent of certain voltage-activated k⁺ channels. *Biochem J.* 1989;257:899-903
218. MacKinnon R. Determination of the subunit stoichiometry of a voltage-activated potassium channel. *Nature.* 1991;350:232-235
219. Parcej DN, Scott VE, Dolly JO. Oligomeric properties of alpha-dendrotoxin-sensitive potassium ion channels purified from bovine brain. *Biochemistry.* 1992;31:11084-11088
220. Long SB, Campbell EB, Mackinnon R. Voltage sensor of kv1.2: Structural basis of electromechanical coupling. *Science.* 2005;309:903-908
221. Doyle DA, Morais Cabral J, Pfuetzner RA, Kuo A, Gulbis JM, Cohen SL, Chait BT, MacKinnon R. The structure of the potassium channel: Molecular basis of k⁺ conduction and selectivity. *Science.* 1998;280:69-77
222. Choi KL, Aldrich RW, Yellen G. Tetraethylammonium blockade distinguishes two inactivation mechanisms in voltage-activated k⁺ channels. *Proc Natl Acad Sci U S A.* 1991;88:5092-5095
223. Pau V, Zhou Y, Ramu Y, Xu Y, Lu Z. Crystal structure of an inactivated mutant mammalian voltage-gated k(+) channel. *Nat Struct Mol Biol.* 2017;24:857-865
224. Hoshi T, Zagotta WN, Aldrich RW. Biophysical and molecular mechanisms of shaker potassium channel inactivation. *Science.* 1990;250:533-538

225. Rettig J, Heinemann SH, Wunder F, Lorra C, Parcej DN, Dolly JO, Pongs O. Inactivation properties of voltage-gated k⁺ channels altered by presence of beta-subunit. *Nature*. 1994;369:289-294
226. Gulbis JM, Zhou M, Mann S, MacKinnon R. Structure of the cytoplasmic beta subunit-t1 assembly of voltage-dependent k⁺ channels. *Science*. 2000;289:123-127
227. Kobertz WR, Williams C, Miller C. Hanging gondola structure of the t1 domain in a voltage-gated k(+) channel. *Biochemistry*. 2000;39:10347-10352
228. Pfaffinger PJ, DeRubeis D. Shaker k⁺ channel t1 domain self-tetramerizes to a stable structure. *J Biol Chem*. 1995;270:28595-28600
229. Gulbis JM, Mann S, MacKinnon R. Structure of a voltage-dependent k⁺ channel beta subunit. *Cell*. 1999;97:943-952
230. Leicher T, Bähring R, Isbrandt D, Pongs O. Coexpression of the kcna3b gene product with kv1.5 leads to a novel a-type potassium channel. *J Biol Chem*. 1998;273:35095-35101
231. McCormack K, McCormack T, Tanouye M, Rudy B, Stuhmer W. Alternative splicing of the human shaker k⁺ channel beta 1 gene and functional expression of the beta 2 gene product. *FEBS Lett*. 1995;370:32-36
232. Kues WA, Wunder F. Heterogeneous expression patterns of mammalian potassium channel genes in developing and adult rat brain. *Eur J Neurosci*. 1992;4:1296-1308
233. Nakahira K, Shi G, Rhodes KJ, Trimmer JS. Selective interaction of voltage-gated k⁺ channel beta-subunits with alpha-subunits. *J Biol Chem*. 1996;271:7084-7089
234. Rhodes KJ, Keilbaugh SA, Barrezueta NX, Lopez KL, Trimmer JS. Association and colocalization of k⁺ channel alpha- and beta-subunit polypeptides in rat brain. *J Neurosci*. 1995;15:5360-5371
235. Xu J, Yu W, Jan YN, Jan LY, Li M. Assembly of voltage-gated potassium channels. Conserved hydrophilic motifs determine subfamily-specific interactions between the alpha-subunits. *J Biol Chem*. 1995;270:24761-24768
236. Bocksteins E. Kv5, kv6, kv8, and kv9 subunits: No simple silent bystanders. *J Gen Physiol*. 2016;147:105-125
237. Hopkins WF, Demas V, Tempel BL. Both n- and c-terminal regions contribute to the assembly and functional expression of homo- and heteromultimeric voltage-gated k⁺ channels. *J Neurosci*. 1994;14:1385-1393
238. Lee TE, Philipson LH, Kuznetsov A, Nelson DJ. Structural determinant for assembly of mammalian k⁺ channels. *Biophys J*. 1994;66:667-673
239. Li M, Jan YN, Jan LY. Specification of subunit assembly by the hydrophilic amino-terminal domain of the shaker potassium channel. *Science*. 1992;257:1225-1230

240. Shen NV, Pfaffinger PJ. Molecular recognition and assembly sequences involved in the subfamily-specific assembly of voltage-gated k⁺ channel subunit proteins. *Neuron*. 1995;14:625-633
241. Zerangue N, Jan YN, Jan LY. An artificial tetramerization domain restores efficient assembly of functional shaker channels lacking t1. *Proc Natl Acad Sci U S A*. 2000;97:3591-3595
242. McCormack T, McCormack K. Shaker k⁺ channel beta subunits belong to an nad(p)h-dependent oxidoreductase superfamily. *Cell*. 1994;79:1133-1135
243. Mindnich RD, Penning TM. Aldo-keto reductase (akr) superfamily: Genomics and annotation. *Hum Genomics*. 2009;3:362-370
244. Tipparaju SM, Barski OA, Srivastava S, Bhatnagar A. Catalytic mechanism and substrate specificity of the beta-subunit of the voltage-gated potassium channel. *Biochemistry*. 2008;47:8840-8854
245. Barski OA, Tipparaju SM, Bhatnagar A. Kinetics of nucleotide binding to the beta-subunit (akr6a2) of the voltage-gated potassium (kv) channel. *Chem Biol Interact*. 2009;178:165-170
246. Pollak N, Dolle C, Ziegler M. The power to reduce: Pyridine nucleotides--small molecules with a multitude of functions. *Biochem J*. 2007;402:205-218
247. Xie Z, Barski OA, Cai J, Bhatnagar A, Tipparaju SM. Catalytic reduction of carbonyl groups in oxidized papc by kvbeta2 (akr6). *Chem Biol Interact*. 2011;191:255-260
248. Pan Y, Weng J, Cao Y, Bhosle RC, Zhou M. Functional coupling between the kv1.1 channel and aldoketoreductase kvbeta1. *J Biol Chem*. 2008;283:8634-8642
249. Bahring R, Milligan CJ, Vardanyan V, Engeland B, Young BA, Dannenberg J, Waldschutz R, Edwards JP, Wray D, Pongs O. Coupling of voltage-dependent potassium channel inactivation and oxidoreductase active site of kvbeta subunits. *J Biol Chem*. 2001;276:22923-22929
250. Tipparaju SM, Liu SQ, Barski OA, Bhatnagar A. Nadph binding to beta-subunit regulates inactivation of voltage-gated k(+) channels. *Biochem Biophys Res Commun*. 2007;359:269-276
251. Peri R, Wible BA, Brown AM. Mutations in the kv beta 2 binding site for nadph and their effects on kv1.4. *J Biol Chem*. 2001;276:738-741
252. Tur J, Chapalamadugu KC, Katnik C, Cuevas J, Bhatnagar A, Tipparaju SM. Kvbeta1.1 (akr6a8) senses pyridine nucleotide changes in the mouse heart and modulates cardiac electrical activity. *Am J Physiol Heart Circ Physiol*. 2017;312:H571-H583
253. Berwick ZC, Dick GM, Moberly SP, Kohr MC, Sturek M, Tune JD. Contribution of voltage-dependent k(+) channels to metabolic control of coronary blood flow. *J Mol Cell Cardiol*. 2012;52:912-919

254. Giese KP, Storm JF, Reuter D, Fedorov NB, Shao LR, Leicher T, Pongs O, Silva AJ. Reduced k⁺ channel inactivation, spike broadening, and after-hyperpolarization in kvbeta1.1-deficient mice with impaired learning. *Learn Mem.* 1998;5:257-273
255. McCormack K, Connor JX, Zhou L, Ho LL, Ganetzky B, Chiu SY, Messing A. Genetic analysis of the mammalian k⁺ channel beta subunit kvbeta 2 (kcnab2). *The Journal of biological chemistry.* 2002;277:13219-13228
256. Dick GM, Sanders KM. (xeno)estrogen sensitivity of smooth muscle bk channels conferred by the regulatory beta1 subunit: A study of beta1 knockout mice. *The Journal of biological chemistry.* 2001;276:44835-44840
257. El Gebeily G, El Khoury N, Mathieu S, Brouillette J, Fiset C. Estrogen regulation of the transient outward k(+) current involves estrogen receptor alpha in mouse heart. *Journal of molecular and cellular cardiology.* 2015;86:85-94
258. Wellman GC, Bonev AD, Nelson MT, Brayden JE. Gender differences in coronary artery diameter involve estrogen, nitric oxide, and ca²⁺-dependent k⁺ channels. *Circulation research.* 1996;79:1024-1030.
259. Nystoriak MA, Zhang D, Jagatheesan G, Bhatnagar A. Heteromeric complexes of aldo-keto reductase auxiliary kvbeta subunits (akr6a) regulate sarcolemmal localization of kv1.5 in coronary arterial myocytes. *Chem Biol Interact.* 2017
260. Syed AU, Reddy GR, Ghosh D, Prada MP, Nystoriak MA, Morotti S, Grandi E, Sirish P, Chiamvimonvat N, Hell JW, Santana LF, Xiang YK, Nieves-Cintrón M, Navedo MF. Adenylyl cyclase 5-generated camp controls cerebral vascular reactivity during diabetic hyperglycemia. *The Journal of clinical investigation.* 2019;129:3140-3152
261. Hung YP, Yellen G. Live-cell imaging of cytosolic nadh-nad⁺ redox state using a genetically encoded fluorescent biosensor. *Methods Mol Biol.* 2014;1071:83-95
262. Ohanyan V, Raph SM, Dwenger MM, Hu X, Pucci T, Mack G, Moore JBt, Chilian WM, Bhatnagar A, Nystoriak MA. Myocardial blood flow control by oxygen sensing vascular kvbeta proteins. *Circ Res.* 2021;128:738-751
263. Belcik JT, Davidson BP, Foster T, Qi Y, Zhao Y, Peters D, Lindner JR. Contrast-enhanced ultrasound assessment of impaired adipose tissue and muscle perfusion in insulin-resistant mice. *Circ Cardiovasc Imaging.* 2015;8
264. Wei K, Skyba DM, Firschke C, Jayaweera AR, Lindner JR, Kaul S. Interactions between microbubbles and ultrasound: In vitro and in vivo observations. *Journal of the American College of Cardiology.* 1997;29:1081-1088
265. Nystoriak MA, O'Connor KP, Sonkusare SK, Brayden JE, Nelson MT, Wellman GC. Fundamental increase in pressure-dependent constriction of brain parenchymal arterioles from subarachnoid hemorrhage model rats due to membrane depolarization. *Am J Physiol Heart Circ Physiol.* 2011;300:H803-812
266. Nystoriak MA, Nieves-Cintrón M, Patriarchi T, Buonarati OR, Prada MP, Morotti S, Grandi E, Fernandes JD, Forbush K, Hofmann F, Sasse KC, Scott JD, Ward SM, Hell JW,

- Navedo MF. Ser1928 phosphorylation by pka stimulates the l-type ca²⁺ channel cav1.2 and vasoconstriction during acute hyperglycemia and diabetes. *Sci Signal*. 2017;10
267. Sugiura Y, Katsumata Y, Sano M, Honda K, Kajimura M, Fukuda K, Suematsu M. Visualization of in vivo metabolic flows reveals accelerated utilization of glucose and lactate in penumbra of ischemic heart. *Sci Rep*. 2016;6:32361
268. Hung YP, Albeck JG, Tantama M, Yellen G. Imaging cytosolic nadh-nad(+) redox state with a genetically encoded fluorescent biosensor. *Cell Metab*. 2011;14:545-554
269. Frobert O, Mikkelsen EO, Bagger JP, Gravholt CH. Measurement of interstitial lactate during hypoxia-induced dilatation in isolated pressurised porcine coronary arteries. *J Physiol*. 2002;539:277-284
270. Hu D, Linders A, Yamak A, Correia C, Kijlstra JD, Garakani A, Xiao L, Milan DJ, van der Meer P, Serra M, Alves PM, Domian IJ. Metabolic maturation of human pluripotent stem cell-derived cardiomyocytes by inhibition of hif1alpha and Idha. *Circ Res*. 2018;123:1066-1079
271. Diaz-Garcia CM, Mongeon R, Lahmann C, Koveal D, Zucker H, Yellen G. Neuronal stimulation triggers neuronal glycolysis and not lactate uptake. *Cell Metab*. 2017;26:361-374 e364
272. Kim JS, Saengsirisuwan V, Sloniger JA, Teachey MK, Henriksen EJ. Oxidant stress and skeletal muscle glucose transport: Roles of insulin signaling and p38 mapk. *Free Radic Biol Med*. 2006;41:818-824
273. Liu Y, Kabakov AY, Xie A, Shi G, Singh AK, Sodha NR, Ehsan A, Usheva A, Agbortoko V, Koren G, Dudley SC, Jr., Sellke FW, Feng J. Metabolic regulation of endothelial sk channels and human coronary microvascular function. *Int J Cardiol*. 2020;312:1-9
274. Rehm H, Lazdunski M. Purification and subunit structure of a putative k⁺-channel protein identified by its binding properties for dendrotoxin i. *Proc Natl Acad Sci U S A*. 1988;85:4919-4923
275. McGahon MK, Dawicki JM, Arora A, Simpson DA, Gardiner TA, Stitt AW, Scholfield CN, McGeown JG, Curtis TM. Kv1.5 is a major component underlying the a-type potassium current in retinal arteriolar smooth muscle. *Am J Physiol Heart Circ Physiol*. 2007;292:H1001-1008
276. Heinemann SH, Rettig J, Graack HR, Pongs O. Functional characterization of kv channel beta-subunits from rat brain. *J Physiol*. 1996;493 (Pt 3):625-633
277. Raph SM, Bhatnagar A, Nystoriak MA. Biochemical and physiological properties of k(+) channel-associated akr6a (kvbeta) proteins. *Chem Biol Interact*. 2019;305:21-27
278. Bessho M, Tajima T, Hori S, Satoh T, Fukuda K, Kyotani S, Ohnishi Y, Nakamura Y. Nad and nadh values in rapidly sampled dog heart tissues by two different extraction methods. *Anal Biochem*. 1989;182:304-308

279. Glock GE, McLean P. Levels of oxidized and reduced diphosphopyridine nucleotide and triphosphopyridine nucleotide in animal tissues. *Biochem J.* 1955;61:388-390
280. Nystoriak MA, Zhang D, Jagatheesan G, Bhatnagar A. Heteromeric complexes of aldo-keto reductase auxiliary kvbeta subunits (akr6a) regulate sarcolemmal localization of kv1.5 in coronary arterial myocytes. *Chem Biol Interact.* 2017;276:210-217
281. Xu J, Li M. Kvbeta2 inhibits the kvbeta1-mediated inactivation of k⁺ channels in transfected mammalian cells. *J Biol Chem.* 1997;272:11728-11735
282. Xu J, Yu W, Wright JM, Raab RW, Li M. Distinct functional stoichiometry of potassium channel beta subunits. *Proc Natl Acad Sci U S A.* 1998;95:1846-1851
283. Decher N, Gonzalez T, Streit AK, Sachse FB, Renigunta V, Soom M, Heinemann SH, Daut J, Sanguinetti MC. Structural determinants of kvbeta1.3-induced channel inactivation: A hairpin modulated by pip2. *EMBO J.* 2008;27:3164-3174
284. Kwak YG, Hu N, Wei J, George AL, Jr., Grobaski TD, Tamkun MM, Murray KT. Protein kinase a phosphorylation alters kvbeta1.3 subunit-mediated inactivation of the kv1.5 potassium channel. *J Biol Chem.* 1999;274:13928-13932
285. Kwak YG, Navarro-Polanco RA, Grobaski T, Gallagher DJ, Tamkun MM. Phosphorylation is required for alteration of kv1.5 k(+) channel function by the kvbeta1.3 subunit. *J Biol Chem.* 1999;274:25355-25361
286. Jow F, Zhang ZH, Kopsco DC, Carroll KC, Wang K. Functional coupling of intracellular calcium and inactivation of voltage-gated kv1.1/kvbeta1.1 a-type k⁺ channels. *Proc Natl Acad Sci U S A.* 2004;101:15535-15540
287. Swain SM, Sahoo N, Dennhardt S, Schonherr R, Heinemann SH. Ca(2+)/calmodulin regulates kvbeta1.1-mediated inactivation of voltage-gated k(+) channels. *Sci Rep.* 2015;5:15509
288. Siddique YH, Ara G, Afzal M. Estimation of lipid peroxidation induced by hydrogen peroxide in cultured human lymphocytes. *Dose Response.* 2012;10:1-10
289. Kohler S, Winkler U, Sicker M, Hirrlinger J. Nbce1 mediates the regulation of the nadh/nad(+) redox state in cortical astrocytes by neuronal signals. *Glia.* 2018;66:2233-2245
290. Virani SS, Alonso A, Benjamin EJ, Bittencourt MS, Callaway CW, Carson AP, Chamberlain AM, Chang AR, Cheng S, Delling FN, Djousse L, Elkind MSV, Ferguson JF, Fornage M, Khan SS, Kissela BM, Knutson KL, Kwan TW, Lackland DT, Lewis TT, Lichtman JH, Longenecker CT, Loop MS, Lutsey PL, Martin SS, Matsushita K, Moran AE, Mussolino ME, Perak AM, Rosamond WD, Roth GA, Sampson UKA, Satou GM, Schroeder EB, Shah SH, Shay CM, Spartano NL, Stokes A, Tirschwell DL, VanWagner LB, Tsao CW, American Heart Association Council on E, Prevention Statistics C, Stroke Statistics S. Heart disease and stroke statistics-2020 update: A report from the american heart association. *Circulation.* 2020:CIR0000000000000757

291. Tsagalou EP, Anastasiou-Nana M, Agapitos E, Gika A, Drakos SG, Terrovitis JV, Ntalianis A, Nanas JN. Depressed coronary flow reserve is associated with decreased myocardial capillary density in patients with heart failure due to idiopathic dilated cardiomyopathy. *Journal of the American College of Cardiology*. 2008;52:1391-1398
292. Brush JE, Jr., Cannon RO, 3rd, Schenke WH, Bonow RO, Leon MB, Maron BJ, Epstein SE. Angina due to coronary microvascular disease in hypertensive patients without left ventricular hypertrophy. *The New England journal of medicine*. 1988;319:1302-1307
293. Di Carli MF, Charytan D, McMahon GT, Ganz P, Dorbala S, Schelbert HR. Coronary circulatory function in patients with the metabolic syndrome. *J Nucl Med*. 2011;52:1369-1377
294. Fukuda D, Yoshiyama M, Shimada K, Yamashita H, Ehara S, Nakamura Y, Kamimori K, Tanaka A, Kawarabayashi T, Yoshikawa J. Relation between aortic stiffness and coronary flow reserve in patients with coronary artery disease. *Heart*. 2006;92:759-762
295. Pepine CJ, Anderson RD, Sharaf BL, Reis SE, Smith KM, Handberg EM, Johnson BD, Sopko G, Bairey Merz CN. Coronary microvascular reactivity to adenosine predicts adverse outcome in women evaluated for suspected ischemia results from the national heart, lung and blood institute wise (women's ischemia syndrome evaluation) study. *Journal of the American College of Cardiology*. 2010;55:2825-2832
296. Merz CN, Kelsey SF, Pepine CJ, Reichek N, Reis SE, Rogers WJ, Sharaf BL, Sopko G. The women's ischemia syndrome evaluation (wise) study: Protocol design, methodology and feasibility report. *Journal of the American College of Cardiology*. 1999;33:1453-1461
297. Feigl EO. Coronary physiology. *Physiol Rev*. 1983;63:1-205
298. Goodwill AG, Dick GM, Kiel AM, Tune JD. Regulation of coronary blood flow. *Compr Physiol*. 2017;7:321-382
299. Binak K, Harmanci N, Sirmaci N, Ataman N, Ogan H. Oxygen extraction rate of the myocardium at rest and on exercise in various conditions. *Br Heart J*. 1967;29:422-427
300. Kilfoil PJ, Tipparaju SM, Barski OA, Bhatnagar A. Regulation of ion channels by pyridine nucleotides. *Circulation research*. 2013;112:721-741
301. Nishijima Y, Korishettar A, Chabowski DS, Cao S, Zheng X, Gutterman DD, Zhang DX. Shaker-related voltage-gated k(+) channel expression and vasomotor function in human coronary resistance arteries. *Microcirculation*. 2018;25
302. West J, Fagan K, Steudel W, Fouty B, Lane K, Harral J, Hoedt-Miller M, Tada Y, Ozimek J, Tuder R, Rodman DM. Pulmonary hypertension in transgenic mice expressing a dominant-negative bmprii gene in smooth muscle. *Circulation research*. 2004;94:1109-1114

303. Tsang SY, Yao X, Wong CM, Chan FL, Chen ZY, Huang Y. Differential regulation of K^+ and Ca^{2+} channel gene expression by chronic treatment with estrogen and tamoxifen in rat aorta. *Eur J Pharmacol.* 2004;483:155-162
304. Kaufmann PA, Gneccchi-Ruscione T, Schafers KP, Luscher TF, Camici PG. Low density lipoprotein cholesterol and coronary microvascular dysfunction in hypercholesterolemia. *Journal of the American College of Cardiology.* 2000;36:103-109
305. Wei K, Jayaweera AR, Firoozan S, Linka A, Skyba DM, Kaul S. Quantification of myocardial blood flow with ultrasound-induced destruction of microbubbles administered as a constant venous infusion. *Circulation.* 1998;97:473-483.
306. Vogel R, Indermuhle A, Reinhardt J, Meier P, Siegrist PT, Namdar M, Kaufmann PA, Seiler C. The quantification of absolute myocardial perfusion in humans by contrast echocardiography: Algorithm and validation. *Journal of the American College of Cardiology.* 2005;45:754-762
307. Coggins MP, Sklenar J, Le DE, Wei K, Lindner JR, Kaul S. Noninvasive prediction of ultimate infarct size at the time of acute coronary occlusion based on the extent and magnitude of collateral-derived myocardial blood flow. *Circulation.* 2001;104:2471-2477
308. Raheer MJ, Thibault H, Poh KK, Liu R, Halpern EF, Derumeaux G, Ichinose F, Zapol WM, Bloch KD, Picard MH, Scherrer-Crosbie M. In vivo characterization of murine myocardial perfusion with myocardial contrast echocardiography: Validation and application in nitric oxide synthase 3 deficient mice. *Circulation.* 2007;116:1250-1257
309. Teichholz LE, Kreulen T, Herman MV, Gorlin R. Problems in echocardiographic volume determinations: Echocardiographic-angiographic correlations in the presence of absence of asynergy. *The American journal of cardiology.* 1976;37:7-11
310. van de Weijer T, van Ewijk PA, Zandbergen HR, Slenter JM, Kessels AG, Wildberger JE, Hesselink MK, Schrauwen P, Schrauwen-Hinderling VB, Kooi ME. Geometrical models for cardiac mri in rodents: Comparison of quantification of left ventricular volumes and function by various geometrical models with a full-volume mri data set in rodents. *American journal of physiology. Heart and circulatory physiology.* 2012;302:H709-715
311. Soderberg O, Gullberg M, Jarvius M, Ridderstrale K, Leuchowius KJ, Jarvius J, Wester K, Hydbring P, Bahram F, Larsson LG, Landegren U. Direct observation of individual endogenous protein complexes in situ by proximity ligation. *Nat Methods.* 2006;3:995-1000
312. Berger MG, Vandier C, Bonnet P, Jackson WF, Rusch NJ. Intracellular acidosis differentially regulates K_v channels in coronary and pulmonary vascular muscle. *The American journal of physiology.* 1998;275:H1351-1359
313. Clements RT, Sodha NR, Feng J, Boodhwani M, Liu Y, Mieno S, Khabbaz KR, Bianchi C, Sellke FW. Impaired coronary microvascular dilation correlates with enhanced vascular smooth muscle mlc phosphorylation in diabetes. *Microcirculation.* 2009;16:193-206

314. Otter D, Austin C. Mechanisms of hypoxic vasodilatation of isolated rat mesenteric arteries: A comparison with metabolic inhibition. *The Journal of physiology*. 1999;516 (Pt 1):249-259
315. Otter D, Austin C. Hypoxia, metabolic inhibition, and isolated rat mesenteric tone: Influence of arterial diameter. *Microvasc Res*. 2000;59:107-114
316. Dunn RB, Griggs DM, Jr. Transmural gradients in ventricular tissue metabolites produced by stopping coronary blood flow in the dog. *Circulation research*. 1975;37:438-445
317. Hester RK, Weiss GB, Willerson JT. Basis of ph-independent inhibitory effects of lactate on 45ca movements and responses to kcl and pgf2 alpha in canine coronary arteries. *Circulation research*. 1980;46:771-779
318. Archer SL, Weir EK, Reeve HL, Michelakis E. Molecular identification of o2 sensors and o2-sensitive potassium channels in the pulmonary circulation. *Adv Exp Med Biol*. 2000;475:219-240
319. Chen YL, Wolin MS, Messina EJ. Evidence for cgmp mediation of skeletal muscle arteriolar dilation to lactate. *J Appl Physiol (1985)*. 1996;81:349-354
320. Jackson WF. Kv channels and the regulation of vascular smooth muscle tone. *Microcirculation*. 2018;25
321. Cox RH, Fromme S. Functional expression profile of voltage-gated k(+) channel subunits in rat small mesenteric arteries. *Cell Biochem Biophys*. 2016;74:263-276
322. Knot HJ, Nelson MT. Regulation of membrane potential and diameter by voltage-dependent k⁺ channels in rabbit myogenic cerebral arteries. *The American journal of physiology*. 1995;269:H348-355.
323. Nelson MT, Patlak JB, Worley JF, Standen NB. Calcium channels, potassium channels, and voltage dependence of arterial smooth muscle tone. *The American journal of physiology*. 1990;259:C3-18.
324. Aaronson PI, Bolton TB, Lang RJ, MacKenzie I. Calcium currents in single isolated smooth muscle cells from the rabbit ear artery in normal-calcium and high-barium solutions. *The Journal of physiology*. 1988;405:57-75
325. Aiello EA, Malcolm AT, Walsh MP, Cole WC. Beta-adrenoceptor activation and pka regulate delayed rectifier k⁺ channels of vascular smooth muscle cells. *The American journal of physiology*. 1998;275:H448-459
326. Andersen MN, Skibsbye L, Tang C, Petersen F, MacAulay N, Rasmussen HB, Jespersen T. Pkc and ampk regulation of kv1.5 potassium channels. *Channels (Austin)*. 2015;9:121-128
327. Cheang WS, Wong WT, Shen B, Lau CW, Tian XY, Tsang SY, Yao X, Chen ZY, Huang Y. 4-aminopyridine-sensitive k⁺ channels contributes to nahs-induced membrane

hyperpolarization and relaxation in the rat coronary artery. *Vascul Pharmacol.* 2010;53:94-98

328. Christie MJ, North RA, Osborne PB, Douglass J, Adelman JP. Heteropolymeric potassium channels expressed in xenopus oocytes from cloned subunits. *Neuron.* 1990;4:405-411

329. Ruppertsberg JP, Schroter KH, Sakmann B, Stocker M, Sewing S, Pongs O. Heteromultimeric channels formed by rat brain potassium-channel proteins. *Nature.* 1990;345:535-537

330. McCormack K, Lin JW, Iverson LE, Rudy B. Shaker k⁺ channel subunits from heteromultimeric channels with novel functional properties. *Biochemical and biophysical research communications.* 1990;171:1361-1371

331. Zhu J, Watanabe I, Gomez B, Thornhill WB. Heteromeric kv1 potassium channel expression: Amino acid determinants involved in processing and trafficking to the cell surface. *The Journal of biological chemistry.* 2003;278:25558-25567

332. Accili EA, Kiehn J, Yang Q, Wang Z, Brown AM, Wible BA. Separable kvbeta subunit domains alter expression and gating of potassium channels. *The Journal of biological chemistry.* 1997;272:25824-25831

333. McGahon MK, Dawicki JM, Scholfield CN, McGeown JG, Curtis TM. A-type potassium current in retinal arteriolar smooth muscle cells. *Invest Ophthalmol Vis Sci.* 2005;46:3281-3287

334. Liu SQ, Yin J, Bhatnagar A. Protein kinase c-dependent phosphorylation of the beta-subunit of the voltage-sensitive potassium channels (kvbeta2). *Chem Biol Interact.* 2003;143-144:597-604

335. Hasan R, Jaggar JH. Kv channel trafficking and control of vascular tone. *Microcirculation.* 2018;25

336. Tune JD, Goodwill AG, Kiel AM, Baker HE, Bender SB, Merkus D, Duncker DJ. Disentangling the gordian knot of local metabolic control of coronary blood flow. *American journal of physiology. Heart and circulatory physiology.* 2020;318:H11-H24

337. Moran Y, Barzilai MG, Liebeskind BJ, Zakon HH. Evolution of voltage-gated ion channels at the emergence of metazoa. *J Exp Biol.* 2015;218:515-525

338. Strauer BE, Motz W, Vogt M, Schwartzkopff B. Impaired coronary flow reserve in niddm: A possible role for diabetic cardiopathy in humans. *Diabetes.* 1997;46 Suppl 2:S119-124

339. Dayanikli F, Grambow D, Muzik O, Mosca L, Rubenfire M, Schwaiger M. Early detection of abnormal coronary flow reserve in asymptomatic men at high risk for coronary artery disease using positron emission tomography. *Circulation.* 1994;90:808-817

340. Lynch FM, Austin C, Heagerty AM, Izzard AS. Adenosine- and hypoxia-induced dilation of human coronary resistance arteries: Evidence against the involvement of k(atp) channels. *Br J Pharmacol*. 2006;147:455-458
341. Lynch FM, Austin C, Heagerty AM, Izzard AS. Adenosine and hypoxic dilation of rat coronary small arteries: Roles of the atp-sensitive potassium channel, endothelium, and nitric oxide. *Am J Physiol Heart Circ Physiol*. 2006;290:H1145-1150
342. Tune JD, Richmond KN, Gorman MW, Olsson RA, Feigl EO. Adenosine is not responsible for local metabolic control of coronary blood flow in dogs during exercise. *Am J Physiol Heart Circ Physiol*. 2000;278:H74-84
343. Nishijima Y, Cao S, Chabowski DS, Korishettar A, Ge A, Zheng X, Sparapani R, Gutterman DD, Zhang DX. Contribution of kv1.5 channel to hydrogen peroxide-induced human arteriolar dilation and its modulation by coronary artery disease. *Circulation research*. 2017;120:658-669
344. Aggarwal SK, MacKinnon R. Contribution of the s4 segment to gating charge in the shaker k⁺ channel. *Neuron*. 1996;16:1169-1177
345. Coetzee WA, Amarillo Y, Chiu J, Chow A, Lau D, McCormack T, Moreno H, Nadal MS, Ozaita A, Pountney D, Saganich M, Vega-Saenz de Miera E, Rudy B. Molecular diversity of k⁺ channels. *Ann N Y Acad Sci*. 1999;868:233-285
346. Scott VE, Rettig J, Parcej DN, Keen JN, Findlay JB, Pongs O, Dolly JO. Primary structure of a beta subunit of alpha-dendrotoxin-sensitive k⁺ channels from bovine brain. *Proceedings of the National Academy of Sciences of the United States of America*. 1994;91:1637-1641
347. Darman RB, Ivy AA, Ketty V, Blaustein RO. Constraints on voltage sensor movement in the shaker k⁺ channel. *The Journal of general physiology*. 2006;128:687-699
348. Kratzer R, Kavanagh KL, Wilson DK, Nidetzky B. Studies of the enzymic mechanism of candida tenuis xylose reductase (akr 2b5): X-ray structure and catalytic reaction profile for the h113a mutant. *Biochemistry*. 2004;43:4944-4954
349. Archer SL, London B, Hampl V, Wu X, Nsair A, Puttagunta L, Hashimoto K, Waite RE, Michelakis ED. Impairment of hypoxic pulmonary vasoconstriction in mice lacking the voltage-gated potassium channel kv1.5. *FASEB journal : official publication of the Federation of American Societies for Experimental Biology*. 2001;15:1801-1803
350. Coppock EA, Tamkun MM. Differential expression of k(v) channel alpha- and beta-subunits in the bovine pulmonary arterial circulation. *Am J Physiol Lung Cell Mol Physiol*. 2001;281:L1350-1360
351. Yuan XJ, Wang J, Juhaszova M, Golovina VA, Rubin LJ. Molecular basis and function of voltage-gated k⁺ channels in pulmonary arterial smooth muscle cells. *The American journal of physiology*. 1998;274:L621-635

352. Xu C, Lu Y, Tang G, Wang R. Expression of voltage-dependent k(+) channel genes in mesenteric artery smooth muscle cells. *The American journal of physiology*. 1999;277:G1055-1063
353. Thorneloe KS, Chen TT, Kerr PM, Grier EF, Horowitz B, Cole WC, Walsh MP. Molecular composition of 4-aminopyridine-sensitive voltage-gated k(+) channels of vascular smooth muscle. *Circulation research*. 2001;89:1030-1037
354. Lassegue B, Griendling KK. NADPH oxidases: Functions and pathologies in the vasculature. *Arterioscler Thromb Vasc Biol*. 2010;30:653-661
355. Lotscher HR, Winterhalter KH, Carafoli E, Richter C. Hydroperoxides can modulate the redox state of pyridine nucleotides and the calcium balance in rat liver mitochondria. *Proc Natl Acad Sci U S A*. 1979;76:4340-4344
356. Oka S, Hsu CP, Sadoshima J. Regulation of cell survival and death by pyridine nucleotides. *Circ Res*. 2012;111:611-627
357. Sistare FD, Haynes RC, Jr. The interaction between the cytosolic pyridine nucleotide redox potential and gluconeogenesis from lactate/pyruvate in isolated rat hepatocytes. Implications for investigations of hormone action. *J Biol Chem*. 1985;260:12748-12753
358. Weiner MW, Lardy HA. Reduction of pyridine nucleotides induced by adenosine diphosphate in kidney mitochondria. The influence of sodium, magnesium, and inhibitors of oxidative phosphorylation. *J Biol Chem*. 1973;248:7682-7687
359. Wolin MS, Ahmad M, Gupte SA. Oxidant and redox signaling in vascular oxygen sensing mechanisms: Basic concepts, current controversies, and potential importance of cytosolic NADPH. *Am J Physiol Lung Cell Mol Physiol*. 2005;289:L159-173
360. Liu Y, Bubolz AH, Mendoza S, Zhang DX, Gutterman DD. H₂O₂ is the transferrable factor mediating flow-induced dilation in human coronary arterioles. *Circ Res*. 2011;108:566-573
361. Sahoo N, Hoshi T, Heinemann SH. Oxidative modulation of voltage-gated potassium channels. *Antioxid Redox Signal*. 2014;21:933-952
362. Ruppertsberg JP, Stocker M, Pongs O, Heinemann SH, Frank R, Koenen M. Regulation of fast inactivation of cloned mammalian I_{K(A)} channels by cysteine oxidation. *Nature*. 1991;352:711-714
363. Caouette D, Dongmo C, Berube J, Fournier D, Daleau P. Hydrogen peroxide modulates the Kv1.5 channel expressed in a mammalian cell line. *Naunyn-Schmiedeberg's Arch Pharmacol*. 2003;368:479-486
364. Park SW, Noh HJ, Sung DJ, Kim JG, Kim JM, Ryu SY, Kang K, Kim B, Bae YM, Cho H. Hydrogen peroxide induces vasorelaxation by enhancing 4-aminopyridine-sensitive Kv currents through S-glutathionylation. *Pflügers Arch*. 2015;467:285-297

365. Tang H, Viola HM, Filipovska A, Hool LC. Ca(v)1.2 calcium channel is glutathionylated during oxidative stress in guinea pig and ischemic human heart. *Free Radic Biol Med.* 2011;51:1501-1511
366. Kelm M. Nitric oxide metabolism and breakdown. *Biochim Biophys Acta.* 1999;1411:273-289
367. Liu Y, Terata K, Chai Q, Li H, Kleinman LH, Gutterman DD. Peroxynitrite inhibits ca²⁺-activated k⁺ channel activity in smooth muscle of human coronary arterioles. *Circulation research.* 2002;91:1070-1076
368. Nunez L, Vaquero M, Gomez R, Caballero R, Mateos-Caceres P, Macaya C, Iriepa I, Galvez E, Lopez-Farre A, Tamargo J, Delpon E. Nitric oxide blocks hkv1.5 channels by s-nitrosylation and by a cyclic gmp-dependent mechanism. *Cardiovasc Res.* 2006;72:80-89
369. Favaloro JL, Kemp-Harper BK. Redox variants of no (no{middle dot}) and hno) elicit vasorelaxation of resistance arteries via distinct mechanisms. *Am J Physiol Heart Circ Physiol.* 2009;296:H1274-1280
370. Yang Q, Chen SR, Li DP, Pan HL. Kv1.1/1.2 channels are downstream effectors of nitric oxide on synaptic gaba release to preautonomic neurons in the paraventricular nucleus. *Neuroscience.* 2007;149:315-327
371. Tanaka Y, Tang G, Takizawa K, Otsuka K, Eghbali M, Song M, Nishimaru K, Shigenobu K, Koike K, Stefani E, Toro L. Kv channels contribute to nitric oxide- and atrial natriuretic peptide-induced relaxation of a rat conduit artery. *J Pharmacol Exp Ther.* 2006;317:341-354
372. Li H, Gutterman DD, Rusch NJ, Bubolz A, Liu Y. Nitration and functional loss of voltage-gated k⁺ channels in rat coronary microvessels exposed to high glucose. *Diabetes.* 2004;53:2436-2442
373. Hu H, Chiamvimonvat N, Yamagishi T, Marban E. Direct inhibition of expressed cardiac l-type ca²⁺ channels by s-nitrosothiol nitric oxide donors. *Circ Res.* 1997;81:742-752
374. Gubitosi-Klug RA, Mancuso DJ, Gross RW. The human kv1.1 channel is palmitoylated, modulating voltage sensing: Identification of a palmitoylation consensus sequence. *Proc Natl Acad Sci U S A.* 2005;102:5964-5968
375. Watanabe I, Zhu J, Sutachan JJ, Gottschalk A, Recio-Pinto E, Thornhill WB. The glycosylation state of kv1.2 potassium channels affects trafficking, gating, and simulated action potentials. *Brain Res.* 2007;1144:1-18
376. Hogan-Cann A, Li W, Guo J, Yang T, Zhang S. Proteolytic cleavage in the s1-s2 linker of the kv1.5 channel does not affect channel function. *Biochim Biophys Acta.* 2016;1858:1082-1090
377. Syrbe S, Hedrich UBS, Riesch E, Djemie T, Muller S, Moller RS, Maher B, Hernandez-Hernandez L, Synofzik M, Caglayan HS, Arslan M, Serratosa JM, Nothnagel

M, May P, Krause R, Loffler H, Detert K, Dorn T, Vogt H, Kramer G, Schols L, Mullis PE, Linnankivi T, Lehesjoki AE, Sterbova K, Craiu DC, Hoffman-Zacharska D, Korff CM, Weber YG, Steinlin M, Gallati S, Bertsche A, Bernhard MK, Merckenschlager A, Kiess W, Euro ERES, Gonzalez M, Zuchner S, Palotie A, Suls A, De Jonghe P, Helbig I, Biskup S, Wolff M, Maljevic S, Schule R, Sisodiya SM, Weckhuysen S, Lerche H, Lemke JR. De novo loss- or gain-of-function mutations in *kcna2* cause epileptic encephalopathy. *Nat Genet.* 2015;47:393-399

378. Yang Y, Li J, Lin X, Yang Y, Hong K, Wang L, Liu J, Li L, Yan D, Liang D, Xiao J, Jin H, Wu J, Zhang Y, Chen YH. Novel *kcna5* loss-of-function mutations responsible for atrial fibrillation. *J Hum Genet.* 2009;54:277-283

379. Christophersen IE, Olesen MS, Liang B, Andersen MN, Larsen AP, Nielsen JB, Haunso S, Olesen SP, Tveit A, Svendsen JH, Schmitt N. Genetic variation in *kcna5*: Impact on the atrial-specific potassium current *ikur* in patients with lone atrial fibrillation. *Eur Heart J.* 2013;34:1517-1525

380. Portero V, Le Scouarnec S, Es-Salah-Lamoureux Z, Burel S, Gourraud JB, Bonnaud S, Lindenbaum P, Simonet F, Violleau J, Baron E, Moreau E, Scott C, Chatel S, Loussouarn G, O'Hara T, Mabo P, Dina C, Le Marec H, Schott JJ, Probst V, Baro I, Marionneau C, Charpentier F, Redon R. Dysfunction of the voltage-gated k^+ channel beta2 subunit in a familial case of brugada syndrome. *J Am Heart Assoc.* 2016;5

APPENDIX A

Myocardial Blood Flow Control by Oxygen Sensing Vascular Kv β Proteins¹

Introduction

An imbalance between myocardial oxygen supply and demand is a salient feature of heart disease, which remains the leading cause of death worldwide²⁹⁰. Impaired cardiac function associated with inadequate myocardial perfusion is commonly observed in patients with heart failure, hypertension, diabetes, and coronary artery disease²⁹¹⁻²⁹⁴. Even in the absence of stenoses in large diameter conduit arteries, suppressed vasodilator capacity of small diameter coronary arteries and arterioles can lead to ischemia^{295, 296}. Despite the vital importance of oxygen delivery to the preservation of cardiac structure and function, the fundamental mechanisms by which the coronary vasculature responds to fluctuations in myocardial metabolic demand remain poorly understood.

In the healthy heart, the coronary arteries and arterioles remain partially constricted, and they dilate or constrict further according to myocardial requirements for oxygen and nutrient delivery^{297, 298}. As myocardial oxygen consumption increases (e.g., due to an increase in heart rate, myocardial contractility, or afterload), there is a corresponding demand for an increase in oxygen supply to sustain oxidative energy production. However, with little reserve for increased oxygen extraction, sustained cardiac

¹ This is a non-final version of an article published in final form in Ohanyan V, Raph SM, Dwenger MM, Hu X, Pucci T, Mack G, Moore JBt, Chilian WM, Bhatnagar A, Nystoriak MA. Myocardial blood flow control by oxygen sensing vascular kvbeta proteins. *Circ Res.* 2021;128:738-751, <https://www.ahajournals.org/doi/10.1161/CIRCRESAHA.120.317715>

function relies on the intimate link between local and regional metabolic activity and vasodilation of the coronary vascular bed to deliver adequate blood flow to the myocardium (i.e., metabolic hyperemia)²⁹⁹. In searching for molecular entities that couple vascular function to myocardial oxygen demand, recent studies from our group^{5, 6} and others⁴ have found that increased cardiac work promotes coronary vasodilation and hyperemia via the activation of Kv1 channels in smooth muscle cells. Nonetheless, how vascular Kv1 channels sense changes in oxygen demand to regulate blood flow to the heart is unclear.

In this study, we tested the hypothesis that regulation of myocardial blood flow (MBF) by Kv1 channels depends upon their auxiliary Kv β subunits. The Kv β proteins are functional aldo-keto reductases that bind NAD(P)(H) and differentially regulate channel gating in response to changes in cellular redox status^{7,9}. Hence, these proteins represent a plausible molecular link between metabolic activity, oxygen availability, and Kv activity that could regulate vasoreactivity³⁰⁰. The mammalian genome encodes three Kv β proteins, which have been shown to control the voltage sensitivity, surface localization, and subcellular distribution of Kv1 channels in excitable cells of the cardiovascular and nervous systems⁸⁰. Consistent with this, in our previous work, we reported that Kv β proteins support the functional expression of Kv channels in cardiomyocytes and contribute to the metabolic regulation of cardiac repolarization¹⁹⁶. The Kv β proteins are expressed throughout the coronary vasculature of humans³⁰¹ and rodents,²⁵⁹ and we have recently reported that native Kv1 channels of coronary arterial myocytes are heteromeric assemblies of Kv β 1.1 and Kv β 2 proteins²⁵⁹. Using a combination of genetically engineered mice with *ex vivo* and *in vivo* approaches, we now report that Kv β 1.1 and Kv β 2 have contrasting roles in regulating MBF and cardiac function under stress, and that they impart oxygen sensitivity to vascular tone.

Methods

Animals: All animal procedures were conducted as approved by the Institutional Animal Care and Use Committees at the University of Louisville and Northeast Ohio Medical University. $Kv\beta 1.1^{-/-}$ and $Kv\beta 2^{-/-}$ mice^{254, 255} and strain-matched wild type (C57Bl/6N and 129/SvEv, respectively) mice (25-30 g body mass) were bred in house and fed normal rodent chow. Transgenic animals were generated (Cyagen) with mouse *Kcnab1* (NM_01059734) at the control of the tetracycline responsive element (TRE, 2nd generation) promoter (TRE-*Kcnab1.1*). Hemizygous TRE-*Kcnab1.1* mice were bred with transgenic mice with the reverse tetracycline transactivator under the control of the murine SM22-alpha (SM22 α) promoter (SM22 α -rtTA; Jackson Laboratories, stock no. 006875, FVB/N-Tg(TagIn-rtTA)E1Jwst/J)³⁰² to yield double hemizygous SM22 α -rtTA:TRE-*Kcnab1.1* and littermate single transgenic SM22 α -rtTA controls. To avoid confounding results due to the effects of estrogen on vascular Kv channel expression,³⁰³ only male mice (aged 3-6 months) were used for this study. All animals were housed in a temperature-controlled room on a 12:12 light:dark cycle with *ad libitum* access to food and water. Summarized body weight and cardiac structural parameters from echocardiographic studies (see below) are shown in Table 3. Mice were euthanized by intraperitoneal injection of sodium pentobarbital (150 mg·kg⁻¹) and thoracotomy, and tissues were excised immediately for ex vivo functional and biochemical assessments.

In vivo measurements of cardiac function and myocardial blood flow: Mice were anesthetized with 3% isoflurane and supplemental O₂, administered (1 L·min⁻¹) in a small induction chamber. After induction, the mice were placed on a controlled heating table in a supine position. Anesthesia was maintained throughout the procedure by delivery of 1-2% isoflurane and supplemental O₂ (0.5 L·min⁻¹). The extremities were secured to the surgical table by tape and a lubricated probe was inserted rectally to monitor body

temperature. The chest, neck, and hind limb hair were then removed using a depilatory agent, the skin was rinsed with warm water, and the neck area was disinfected with 70% ethanol/betadine and an incision (10-15 mm) was made at the right side of the neck. For infusion of contrast agent and drugs, the jugular vein was isolated using blunt forceps and catheterized with sterilized PE-50 polyethylene tubing (pre-filled with heparinized saline; 50 U·ml⁻¹). The jugular vein catheter was then secured in place with two sutures. For continuous measurement of arterial blood pressure, a small incision was made on the hind limb and the femoral artery was isolated and cannulated with a 1.2 F pressure catheter (SciSense, Transonic Systems, Inc., Ithaca, NY, USA) connected to a PowerLab data acquisition system (ADInstruments, Colorado Springs, CO, USA) through a SP200 pressure interface unit designed to measure arterial blood pressure and heart rate. After cannulation, the pressure catheter was advanced ~10 mm into the abdominal aorta.

Ultrasound gel was centrifuged in a 60 mL syringe (1500xg, 10 min) to remove air bubbles, warmed to 37°C, and applied to the chest. Cardiac function was measured by M-mode transthoracic echocardiographic imaging of the parasternal short axis view, mid-papillary level using a Vevo 2100 high resolution echocardiography imaging system (FujiFilm VisualSonics, Toronto, ON, Canada). Contrast echocardiography was performed by using Siemens ultrasound imaging system (Sequoia Acuson C512; Siemens Medical Systems USA Inc., Mountain View, CA) with a high-frequency linear-array probe (15L8) held in place by a 3D railing system. For myocardial contrast echocardiography (MCE), we administered lipid-shelled microbubbles, which were freshly prepared by sonication of a decafluorobutane gas-saturated aqueous suspension of distearoylphosphatidylcholine (2 mg/mL) and polyoxyethylene-40-stearate (1 mg/mL)^{6, 264, 304}. The contrast agent was intravenously infused via the jugular vein catheter at a rate of ~5 x 10⁵ microbubbles·min⁻¹ (20 µl·min⁻¹) and MCE was performed by administering a multi-pulse contrast-specific pulse sequence to detect non-linear microbubble contrast signal at low mechanical index

(MI = 0.18 – 0.25). Data were acquired during and after a 1.9 MI pulse sequence to destruct microbubbles within the acoustic field, followed by imaging of replenished contrast signal.

Long axis images were obtained for perfusion imaging. All settings for processing were adapted and optimized for each animal: penetration depth was ~2–2.5 cm, near field was focused on the middle of the left ventricle (long axis view), and gains were adjusted to obtain images with no signal from the myocardium and then held constant. Regions of interest (ROI) were positioned within the anterolateral region in the short axis view. A curve of signal intensity over time was obtained in the ROI and fitted to an exponential function: $y = A(1 - e^{-\beta t})$, where y is the signal intensity at any given time, A is the signal intensity corresponding to the microvascular cross sectional volume, and β is the initial slope of the curve, which corresponds to the blood volume exchange frequency^{305, 306}. Relative blood volume (RBV) was calculated as the ratio of myocardial to cavity signal intensity ($RBV=A/A_{LV}$). A_{LV} corresponds to the signal intensity for the LV cavity. Color coded parametric images were used to outline a region of interest (region of the left ventricle). Myocardial blood flow (MBF) was estimated as the product of $RBV \times \beta$ ³⁰⁷. The analysis of nearby regions within the myocardium and the left ventricle is proposed to compensate for regional beam inhomogeneities and contrast shadowing³⁰⁸. MBF was calculated from the blood volume pool relative to the surrounding myocardial tissue, the exchange frequency (initial slope of curve), and tissue density ρ ($\rho_T=1.05$)³⁰⁶. MBF was measured in 3-5 different images obtained from the same condition (baseline and treatments). To compare the relationships between MBF and cardiac workload, a simple linear regression equation was fit to the data (Graphpad Prism 8). **MCE analyses were performed by readers blinded to genotype and treatment.**

Measurements of cardiac function, myocardial perfusion, and arterial blood pressure were performed at baseline, after administration of hexamethonium (5 mg·kg⁻¹, i.v.), and following successive doses of norepinephrine (0.5, 1.0, 2.5, and 5.0 µg·kg⁻¹·min⁻¹; ~3 min duration each dose, followed by 3-5 min washout). Animals that did not complete the entire procedure of norepinephrine infusions (1-3 mice per group) were excluded from analysis. All data analyses and calculations of cardiac workload (double product of mean arterial pressure and heart rate), cardiac function, myocardial blood flow, and mean arterial pressure were performed offline. For pressure measurements, we used Lab Chart 8 software (ADInstruments, Colorado Springs, CO, USA). Left ventricular volume at end diastole (LVEDV) and end systole (LVESV), as well left ventricular internal diameter at end diastole (LVID,d) and end systole (LVID,s) were measured at steady state after drug infusions. Left ventricular volume was calculated by a modified Teichholz formula: $LVV = ((7.0 / (2.4 + LVID)) * LVID^3)^{309, 310}$. Left ventricular ejection fraction (LVEF %) was calculated by: $(LVEDV - LVESV) / LVEDV$. All echocardiographic calculations and measurements were carried out offline using VevoLab 3.1 software (FujiFilm VisualSonics, Toronto, ON, Canada). All measurements were averaged over 3-5 cardiac cycles.

Arterial diameter measurements: Primary and secondary branches of the left anterior descending coronary arteries and third and fourth order branches of mesenteric arteries and were dissected and kept in ice-cold isolation buffer consisting of (in mM): 134 NaCl, 6 KCl, 1 MgCl₂, 2 CaCl₂, 10 HEPES, 7 D-glucose, pH 7.4. Isolated arteries were used for arterial diameter measurements within 8 h after dissection. Isolated arteries were cleaned of connective tissue and cannulated on glass micropipettes mounted in a linear alignment single vessel myograph chamber (Living Systems Instrumentation, St. Albans, VT, USA). For some experiments, the vascular endothelium was functionally ablated by passage of

air through the lumen (~30 s) during the cannulation procedure. After cannulation, the chamber was placed on an inverted microscope and arteries were equilibrated at 37°C and intravascular pressure of 20 mmHg, maintained with a pressure servo control unit (Living Systems Instrumentation, St. Albans, VT, USA) under continuous perfusion (3-5 ml·min⁻¹) of physiological saline solution (PSS) consisting of (in mM): 119 NaCl, 4.7 KCl, 1.2 KH₂PO₄, 1.2 MgCl₂, 7 D-glucose, 24 NaHCO₃, 2 CaCl₂, maintained at pH 7.35-7.45 via aeration with gas mixture containing 5% CO₂ and 20% O₂ (balanced with N₂).

Following an equilibration period (45-60 min), luminal diameter was continuously monitored and recorded with a charge coupled device (CCD) camera and edge detection software (IonOptix, Milton, MA, USA). Experiments were performed to examine effects of step-wise increases in intravascular pressure (20-100 mmHg), elevated [K⁺]_o (via isosmotic replacement of KCl for NaCl), the synthetic thromboxane A₂ analogue U46619 (Tocris Bioscience, Minneapolis, MN, USA), adenosine (Sigma Aldrich, St. Louis, MO, USA), or L-lactate (Sigma Aldrich, St. Louis, MO, USA). For some experiments, hypoxic bath conditions were generated by perfusion of 1 mM Na₂S₂O₄-containing PSS aerated with 5% CO₂ (balance N₂; 0% O₂). Bath O₂ levels were measured using a dissolved oxygen meter (World Precision Instruments, Sarasota, FL, USA). At the end of each experiment, the maximum passive diameter was measured in the presence of Ca²⁺-free PSS containing the L-type Ca²⁺ channel inhibitor nifedipine (1 μM) and adenylyl cyclase activator forskolin (0.5 μM), as described previously^{265, 266}. Vasoconstriction is expressed as a decrease in arterial diameter relative to the maximum passive diameter at a given intravascular pressure. Changes in diameter (e.g., vasodilation) are normalized to differences from baseline and maximum passive diameters for each experiment.

Western blotting: Whole tissue lysates were obtained from mesenteric arteries and brain, as described previously²⁵⁹. Briefly, tissues were homogenized in lysis buffer containing

150 mM NaCl, 50 mM Tris-HCl, 0.25% deoxycholic acid, 1% NP-40, 1 EDTA, with protease inhibitors (Complete Mini protease inhibitor cocktail, Roche) and phosphatase inhibitors (Phosphatase Inhibitor Cocktail, Thermo), pH 7.4. Homogenates were sonicated and centrifuged at 10,000 xg (10 min, 4°C), and supernatants were boiled in Laemmli sample buffer for 10 min and run on a 4-20% Mini-PROTEAN TGX precast Protein gel (Bio-Rad) and subjected to SDS-PAGE. Following transfer to a polyvinylidene fluoride (PVDF) membrane, total protein was assessed for each lane by staining with Ponceau S. Non-specific binding was blocked with 5% dry milk in Tris-buffered saline (TBS) and membranes were then incubated overnight (at 4°C) in primary antibodies against Kv β 1.1 (Neuromab, 75-018, 1:500) in TBS containing 0.1% Tween-20 (TBS-t). After washing (5x with TBS-t at room temperature), the membranes were incubated in TBS-t containing 5% dry milk and horseradish peroxidase (HRP)-conjugated secondary antibodies (anti-mouse IgG; Cell Signaling, 7076S, 1:3000). HRP was detected with Pierce ECL Plus Western Blotting Substrate (Thermo) and a myECL imaging system (Thermo). Densitometry was performed for immunoreactive bands using FIJI software (National Institutes of Health).

In situ proximity ligation: Arterial myocytes were isolated from coronary and mesenteric arteries using enzymatic digestion procedures, similar to those described previously²⁶⁶. Briefly, arteries were incubated in digestion buffer containing (in mM): 140 NaCl, 5 KCl, 2 MgCl₂, 10 HEPES, 10 glucose, pH 7.4 at 37°C for 1 min. The buffer was exchanged for digestion buffer containing papain (1 mg/mL; Worthington) and dithiothreitol (1 mg/mL; Sigma Aldrich) and incubated at 37°C for 5 min with gentle agitation; the papain/dithiothreitol buffer was then exchanged for digestion buffer containing collagenase type H (1.25 mg/mL; Sigma Aldrich) and trypsin inhibitor (1 mg/mL; Sigma Aldrich) and incubated at 37°C for 5 min with gentle agitation. The digested tissue was

then washed three times with ice-cold enzyme-free digestion buffer and triturated with a flame-polished Pasteur pipette to liberate individual arterial myocytes.

Isolated arterial myocytes were transferred in suspension to glass microscope slides and allowed to adhere (~20 min; room temperature). After adherence, the cells were washed with phosphate-buffered saline (PBS) and fixed in paraformaldehyde (4% in PBS) (for 10 min at room temperature). Following fixation, cells were permeabilized in PBS containing 0.1% Triton X-100 (for 10 min at room temperature). To detect protein-protein proximity (≤ 40 nm),³¹¹ an *in situ* proximity ligation assay (PLA) kit (Duolink; Sigma Aldrich) was used per manufacturer's instructions. Cells were blocked with Duolink blocking solution and incubated in primary antibodies against Kv1.5 (Neuromab, 75-011, 1:50), Kv β 1 (Abcam, AB174508, 1:100), and Kv β 2 (Aviva system biology, ARP37678_T100, 1:100).¹⁹⁶ Antibody-labelled Kv subunits were detected with oligonucleotide-conjugated PLA probe secondary antibodies (anti-rabbit PLUS and anti-mouse MINUS) followed by a solution with PLA probe-specific oligonucleotides and ligase to generate circular nucleotide products at sites of probe-probe proximity. Cells were then incubated (100 min, 37°C) in a solution consisting of polymerase and fluorophore-tagged oligonucleotides for rolling circle amplification, concatemeric product generation, and fluorescent labelling. After washing, the slides were mounted with Duolink mounting media containing DAPI nuclear stain and coverslips were sealed with nail polish. Fluorescent images were captured using a Keyence BZ-X800 All-in-One fluorescence microscopy imaging system. Images were analyzed to obtain counts of total fluorescent PLA punctae in each cell using FIJI software (National Institutes of Health). Images from complete z-series (1 μ m step) for each cell were flattened using the z-project function and PLA-associated punctate particles for each cell were counted and normalized to the area of the cell footprint, obtained from transmitted light images.

Patch clamp electrophysiology: Arterial myocytes were isolated from coronary arteries as described above. Isolated arterial myocytes were allowed to adhere (5 min) to a glass coverslip in a recording chamber. Total outward K^+ currents (I_K) were recorded from coronary arterial myocytes using the perforated whole cell configuration of the patch clamp technique in voltage clamp mode using an Axopatch 200B patch clamp amplifier (Axon Instruments). Borosilicate glass pipettes were pulled to a resistance of 5-7 M Ω and filled with a solution containing (in mM) 87 K^+ -aspartate, 20 KCl, 1 MgCl₂, 5 Mg²⁺ ATP, 10 EGTA, and 10 HEPES with 36 μ g/mL amphotericin B (pH 7.2 with KOH). Cells were bathed in external solution containing (in mM) 134 NaCl, 6 KCl, 1 MgCl₂, 0.1 CaCl₂, 10 glucose, and 10 HEPES (pH 7.4 with NaOH). K^+ currents were recorded from each cell in the absence and presence of L-lactate (10 mM) in bath solution with and without psora-4 (500 nM). To obtain the I-V relationships, cells were sequentially depolarized for 500 ms from a holding potential of -70 mV to +50 mV in 10 mV increments. All patch clamp experiments were performed at ambient room temperature (21-23°C). Patch clamp data were analyzed using Clampfit 9 software (Axon Instruments). I_K is expressed as peak currents reached during the period of depolarization normalized by cell capacitance and expressed as pA/pF.

Statistics: Data are mean \pm SEM. All data were analyzed using GraphPad Prism software using paired or unpaired Student's t-tests, and Mann Whitney U and Wilcoxon signed rank non-parametric tests for comparisons of two experimental groups as appropriate. One-way and two-way analysis of variance or non-parametric tests with Tukey post-hoc tests were used for comparing multiple groups and repeated measures datasets, as indicated in Figure Legends. $P < 0.05$ was considered statistically significant.

Results

Kv β 2 is required for sustained cardiac pump function during stress.

Under conditions of heightened cardiac workload, sustained pump function is critically dependent on Kv1-mediated coronary vasodilation for sufficient oxygen delivery to meet the metabolic demands of the myocardium^{5, 6, 77}. Thus, we first tested whether loss of Kv β proteins affects cardiac performance under stress. Figure 1 shows representative M mode echocardiographic images from wild type (WT) and Kv β 2^{-/-} animals during intravenous infusion of norepinephrine (5 μ g/kg·min⁻¹). Norepinephrine infusion enhanced cardiac function, as indicated by an increase in ejection fraction. However, steady-state ejection fraction during infusion of 2.5 and 5 μ g/kg·min⁻¹ norepinephrine was significantly lower in Kv β 2^{-/-} animals than in WT animals (Figure 1 A, B). Specifically, ejection fraction after ~1 min of 5 μ g/kg·min⁻¹ norepinephrine infusion was 71 \pm 1.7% in Kv β 2^{-/-} mice versus 84 \pm 2.2% in WT animals. Ejection fraction in Kv β 1.1^{-/-} mice did not differ significantly from that in WT mice at any dose of norepinephrine (P = 0.093).

Figure 1 C shows the effects of norepinephrine infusion on arterial blood pressure in WT and Kv β 2^{-/-} mice. Infusion of norepinephrine increased steady state blood pressure in both groups. Consistent with our previous report,⁶ infusion of norepinephrine led to an increase in arterial blood pressure in WT animals that was sustained for the duration of drug administration. However, in Kv β 2^{-/-} mice, norepinephrine-induced elevation of pressure was not sustained, but declined after ~40 s of infusion. This inability to maintain elevated blood pressure upon norepinephrine infusion is reminiscent of the effects of norepinephrine in Kv1.5-null mice⁶. Therefore, as is the case with Kv1.5, Kv β 2 appears to play an essential role in supporting cardiac contractile performance under conditions of catecholamine stress and enhanced cardiac workload.

Relationship between myocardial blood flow and cardiac workload is disrupted in Kv β 2-null mice.

The inability of $Kv\beta 2^{-/-}$ mice to sustain elevated cardiac performance may reflect insufficient oxygen delivery during stress. Thus, we postulated that $Kv\beta$ proteins may be integral to the relationship between myocardial blood flow (MBF) and cardiac workload. To test this, we used myocardial contrast echocardiography (MCE)^{5, 6} to compare MBF in WT and $Kv\beta$ -null mice. MCE uses high-power ultrasound to destruct lipid shelled echogenic microbubbles in circulation. The subsequent replenishment of signal intensity in a region of interest following disruption is used to calculate the perfusion rate of the tissue (Figure 2 A, see Methods). Because MBF responds to changes in ventricular workload and myocardial metabolic activity, we used MCE to evaluate MBF as a function of cardiac workload (i.e., double product of mean arterial blood pressure x heart rate),⁶ which was monitored at baseline and during intermittent intravenous infusions of norepinephrine (0.5 – 5 $\mu\text{g}/\text{kg}\cdot\text{min}^{-1}$). Figure 2 B shows representative contrast signal intensities plotted over a period of ~10 s after microbubble destruction and fit with a one-phase exponential function (see *inset*) in WT (129SvEv), $Kv\beta 1.1^{-/-}$, and $Kv\beta 2^{-/-}$ mice (5 $\mu\text{g}/\text{kg}\cdot\text{min}^{-1}$ norepinephrine). The relationship between MBF and double product shows a modest elevation of MBF, albeit across a lower workload range in $Kv\beta 1.1^{-/-}$ mice compared with WT mice (Figure 2 C, $P = 0.051$). However, consistent with impaired cardiac function under the stress conditions described above (see Figure 1 C), levels of MBF recorded in $Kv\beta 2^{-/-}$ mice were markedly reduced. Specifically, linear regression analysis showed a significant reduction in the slope of the MBF-work relationship in $Kv\beta 2^{-/-}$ mice (Figure 2 D). MAP, HR, and echocardiographic data at baseline and after acute norepinephrine infusion for each group are summarized in Figure 7 and Table 4. Note that cardiac workload in $Kv\beta 1.1^{-/-}$ mice was reduced due to lower MAP relative to corresponding wild type mice in the presence of 1-5 $\mu\text{g}/\text{kg}\cdot\text{min}^{-1}$ norepinephrine (see Figures 2 C and 7 A). However, MAP, HR, and double product were not significantly different between WT and $Kv\beta 2^{-/-}$ mice over the range of norepinephrine doses tested. Taken together, these data reflect differential

roles for Kv β 1.1 and Kv β 2 proteins in regulating MBF, whereby loss of Kv β 2 suppresses MBF and impairs cardiac function as the heart is subjected to increased workloads.

Sensitivity of coronary arterial diameter to oxygen is modified by Kv β 2.

Impaired Kv1-mediated coronary vasodilation results in a markedly reduced myocardial oxygen tension during increased metabolic demand⁶. We therefore posited that coronary vasodilation in response to metabolic stress may be impaired by the loss of Kv β 2. Arteries of the systemic circulation exhibit robust dilation in response to metabolic stressors such as hypoxia and intracellular acidosis via a number of purported mechanisms, including activation of Kv channels^{150, 312}. Hence, we examined the *ex vivo* vasoreactivity of coronary arteries isolated from WT and Kv β 2^{-/-} mice in response to an acute reduction in oxygen. When subjected to physiological intravascular pressures, isolated coronary arteries developed myogenic tone (i.e., 8 \pm 2% and 11 \pm 2% at 60 and 80 mmHg, respectively). To evaluate vasodilatory capacity, arteries were pressurized (60 mmHg), pre-constricted with 100 nM U46619, and subjected to hypoxic bath conditions (physiological saline solution aerated with 95% N₂/5% CO₂ and containing 1 mM hydrosulfite as an O₂ scavenger)³¹³⁻³¹⁵. Direct measurement of bath O₂ levels confirmed a significant reduction in O₂ from control levels during application of hypoxic bath conditions (Figure 3 A). As shown in Figures 3 B (*top*) and 8, coronary arteries isolated from WT mice responded to hypoxic perfusate with robust and reversible dilation. Vasodilation was not observed when 1 mM hydrosulfite was applied in the presence of 20% O₂ (Figure 8). Consistent with the involvement of Kv1 channels in this response, the selective Kv1 inhibitor psora-4 (500 nM) significantly attenuated (~58%) hypoxia-induced vasodilation (Figure 8). Likewise, hypoxia-induced dilation was reduced (2.9-fold) in arteries from Kv β 2^{-/-} animals (19.6 \pm 6.4%; n = 5 arteries from 3 mice) when compared with arteries from WT mice (56.9 \pm 6.2%; n = 6 arteries from 5 mice) (Figure 3 B-D). Taken

together, these data suggest that Kv β 2 proteins facilitate the vasodilatory response to reduced PO₂ and support the notion that Kv β proteins link tissue perfusion to local oxygen consumption.

Elevation of L-lactate augments I_{Kv} in coronary arterial myocytes and induces coronary vasodilation via Kv β 2.

We tested next whether Kv1 activity in coronary arterial myocytes is sensitive to acute changes in oxygen due to alterations in cellular redox potential via elevation of L-lactate. Our reasoning for examining the effects of L-lactate was two-fold: first, myocardial underperfusion leads to a rapid decline in tissue PO₂, increased anaerobic metabolism, and net accumulation of L-lactate that can promote feedback coronary vasodilation to increase MBF^{77, 175, 316-318}. Second, it is plausible that Kv1 channels, via association with Kv β proteins, may be acutely responsive to changes in lactate secondary to modification of cellular NADH:NAD⁺ ratio after uptake and interconversion to pyruvate via the lactate dehydrogenase reaction^{9, 80, 180, 181, 195, 225}. Consistent with this expectation, using the perforated whole cell configuration of the patch clamp technique, we observed a significant increase in outward K⁺ current density (pA/pF) in isolated coronary arterial myocytes immediately following (1-3 min) application of 10 mM L-lactate in the bath (Figure 4 A, C). However, this effect was abolished when L-lactate was applied in the presence of the Kv1 blocker psora-4 (500 nM, Figure 4 B, D). The change in I_K induced by application of 10 mM L-lactate in coronary arterial myocytes in the absence and presence of psora-4 is shown in Figure 4 E. These data indicate that L-lactate acutely potentiates I_{Kv} in coronary arterial myocytes.

We next examined the vasodilatory response of precontracted coronary arteries to increasing concentrations of extracellular L-lactate. As shown in Figure 4 F and consistent with previous studies,^{269, 319} isolated coronary arteries that were pre-constricted

with 100 nM U46619 exhibited step-wise vasodilation in response to elevation of external L-lactate (5-20 mM). This effect was abolished when L-lactate was applied in the presence of 500 nM psora-4 (Figure 4 G, I), consistent with involvement of I_{K_V} described above. Furthermore, L-lactate-induced vasodilation was also abolished in arteries isolated from $Kv\beta 2^{-/-}$ mice, indicating a key role for this subunit in L-lactate-induced vasodilation (Figure 4 H, I). These data are consistent with the notion that the regulation of $Kv\beta 2$ via vascular intermediary metabolism controls coronary vasodilatory function upon acute changes in myocardial oxygen tension.

Functional role for $Kv\beta 2$ in L-lactate-induced vasodilation of resistance mesenteric arteries.

We next asked whether the role for $Kv\beta$ in redox-dependent vasoreactivity is confined to the coronary vasculature or is generally observed in peripheral resistance arterial beds where $Kv1$ prominently controls vascular tone. For this, we first compared $Kv\beta$ protein-protein interactions in arterial myocytes of coronary versus mesenteric (3rd and 4th order) arteries using *in situ* proximity ligation (PLA), as previously described^{196, 259, 266}. The PLA method is based on dual labelling of proteins that are located within close proximity (<40 nm), and thus, is an approach used to identify protein-protein interactions in complexes with molecular resolution. We observed robust PLA-associated fluorescent signals in coronary arterial myocytes that were co-labelled with $Kv1.5$ and $Kv1.2$, $Kv1.5$ and $Kv\beta 1$, $Kv1.5$ and $Kv\beta 2$, or $Kv\beta 1$ and $Kv\beta 2$ (Figure 5 A), consistent with heteromeric oligomerization of Shaker channels^{219, 259}. The number of fluorescent sites assigned to these - α/α , α/β , and β/β interactions were similar between coronary and mesenteric arterial myocytes (Figure 5 A, B). PLA-associated fluorescence in cells labeled for $Kv1.5$ alone was negligible for arterial myocytes of both beds. These data suggest that $Kv \alpha/\beta$

subunit expression patterns and interactions are similar in arterial myocytes of these two distinct vascular beds.

Next, we tested whether knockout of Kv β 1.1 or Kv β 2 alters the regulation of mesenteric arterial diameter. Note that ablation of either of these Kv β proteins had no significant effect on the active (i.e., myogenic tone) or passive responses to increases in intravascular pressure, nor did it impact vasoconstriction responses to direct membrane potential depolarization with 60 mM K⁺ or the stable thromboxane A₂ receptor agonist U46619 (100 nM; Figure 9). Similar to observations in isolated coronary arteries (see Figure 4 F), application of L-lactate (5-20 mM) resulted in robust and reversible dilation of isolated mesenteric arteries (Figure 5 C). L-lactate-mediated vasodilation was insensitive to endothelial denudation, but was abolished when arteries were constricted with elevated external K⁺, rather than U46619 (Figure 10). Consistent with observations in isolated coronary arteries, vasodilation in response to L-lactate was eliminated by the Kv1-selective inhibitor psora-4 and loss of Kv β 2 (Figure 5 C-E). The dilatory response to L-lactate was not significantly different between arteries from Kv β 1.1^{-/-} mice when compared with arteries from corresponding WT animals (Figure 11). Moreover, in contrast to the disparate effects of L-lactate, vasodilation induced by adenosine (1 - 100 μ M) was not significantly different between Kv β 1.1^{-/-} or Kv β 2^{-/-} arteries, when compared with corresponding WT arterial preparations (Figure 12). Together with results shown in Figures 2-4, these data identify Kv β 2 as a functional regulatory constituent of Kv1 channels that imparts stimulus-dependent redox control of vascular tone.

Increasing the Kv β 1.1: Kv β 2 ratio suppresses redox-dependent vasodilation and MBF.

Native Kv1 channels are comprised of pore-forming subunits associated with more than one Kv β subtype. This combinatorial variability may contribute to the diversity and

cell-specific adaptability of channel function to a wide range of physiological and pathological stimuli. In coronary arterial myocytes, both Kv β 1.1 and Kv β 2 proteins are present in native Kv1 auxiliary subunit complexes;²⁵⁹ however, our data suggest that these proteins may have divergent roles in the regulation of arterial diameter and myocardial perfusion. That is, in contrast to our observations made in Kv β 2^{-/-} mice, deletion of Kv β 1.1 did not impede MBF. Structural comparison of the two subunits shows a clear difference in the N-termini of Kv β 1 and Kv β 2 subunits. The N-termini of Kv β 1 proteins form a ball-and-chain-like inactivation domain, a feature that is lacking in Kv β 2⁸⁰. Thus, we hypothesized that the association of Kv β 1.1 with Kv1 channels may serve to counter the regulatory function imparted by Kv β 2. A testable prediction based on this hypothesis is that increasing the ratio of Kv β 1.1:Kv β 2 subunits in arterial myocytes would recapitulate the effects of Kv β 2 deletion. To examine this possibility, we generated transgenic mice with conditional doxycycline-inducible overexpression of Kv β 1.1 in smooth muscle cells (Figure 6 A, see Methods). Briefly, this model consists of transgenic mice with a reverse tetracycline trans-activator driven by the SM22 α promoter (SM22 α -rtTA)³⁰² crossed to novel transgenic mice with Kcnab1 downstream of the tetracycline responsive element (TRE-Kv β 1) to yield double transgenic (SM22 α -rtTA:TRE-Kv β 1) and single transgenic littermate control (SM22 α -rtTA) mice. Western blot revealed elevated Kv β 1 protein abundance in arteries of SM22 α -rtTA:TRE-Kv β 1 mice after doxycycline treatment, compared with arteries from doxycycline-treated SM22 α -rtTA mice (Figure 6 B,C). Consistent with a lack of doxycycline effects on Kv β 1 protein in peripheral tissues, no differences were observed in Kv β 1-associated band intensities in brain lysates of SM22 α -rtTA:TRE-Kv β 1 versus SM22 α -rtTA mice.

We next measured the relative levels of Kv1 α :Kv β protein interactions in coronary arterial myocytes via PLA. We observed PLA-associated fluorescent punctae in coronary arterial myocytes from SM22 α -rtTA that were either co-labelled with Kv1.5 and Kv β 1, or

with Kv1.5 and Kv β 2. Consistent with results of Western blot experiments described above, we observed a significant increase in Kv1.5:Kv β 1-associated PLA signal in coronary arterial myocytes from SM22 α -rtTA:TRE-Kv β 1 when compared with myocytes from SM22 α -rtTA mice (Figure 6 D, E). Notably, Kv1.5-Kv β 2-associated PLA signal was reduced in myocytes from SM22 α -rtTA:TRE-Kv β 1 when compared with myocytes from SM22 α -rtTA mice, suggesting that double transgenic mice express vascular Kv1 complexes with increased ratios of Kv β 1.1:Kv β 2 subunits. Functionally, enhanced Kv β 1.1:Kv β 2 subunit composition in arterial myocytes from SM22 α -rtTA:TRE-Kv β 1 was associated with significantly blunted vasodilation of isolated mesenteric arteries in response to extracellular L-lactate when compared with arteries from single transgenic control mice (Figure 6 F, G). Indeed, these observations in SM22 α -rtTA:TRE-Kv β 1 arteries were similar to those made in coronary and mesenteric arteries from Kv β 2^{-/-} mice, as well as arteries from WT mice pre-treated with the Kv1-selective inhibitor psora-4 (see Figure 4 F-I and and 5 C-E). *In vivo* evaluation of the relationship between MBF and cardiac workload revealed significantly suppressed MBF in SM22 α -rtTA:TRE-Kv β 1 mice when compared with SM22 α -rtTA mice (Figure 6 H). No differences in heart rate or MAP were observed between groups of mice (Figure 13). Together, these results indicate that Kv β 1.1 in arterial myocytes functions as an inhibitory regulator of vasodilation, and that the control of MBF is balanced on the juxtaposing functional influences of Kv β 1.1 and Kv β 2 proteins.

Discussion

In this study we identify vascular Kv β proteins as key regulators of myocardial blood flow. Our findings suggest that the auxiliary Kv β subunits impart oxygen sensitivity to Kv1 channel function, enabling them to trigger vasodilation in response to an increase in oxygen demand. A functional role of Kv β proteins in imparting oxygen-sensitivity to Kv1

channels and thereby regulating vasodilation is supported by the following key findings: 1) $Kv\beta 2^{-/-}$ mice exhibit acute cardiac failure during administration of norepinephrine; 2) MBF is significantly suppressed across the physiological range of cardiac workload in $Kv\beta 2^{-/-}$ mice, yet is moderately enhanced in $Kv\beta 1.1^{-/-}$ mice; 3) vasodilation of isolated coronary arteries in response to hypoxia and elevation of extracellular L-lactate is strongly attenuated by loss of $Kv\beta 2$; 4) whereas ablation of $Kv\beta$ proteins does not impact vasoconstriction of resistance caliber mesenteric arteries, vasodilation of these vessels in response to L-lactate is abolished by ablation of $Kv\beta 2$, comparable to effects of $Kv\beta 2$ deletion in coronary arteries; and 5) increasing the $Kv\beta 1.1:Kv\beta 2$ ratio in smooth muscle impairs L-lactate-induced vasodilation and suppresses MBF, similar to observations made in $Kv\beta 2^{-/-}$ arteries and mice. Collectively these results support the concept that $Kv\beta 1.1$ and $Kv\beta 2$ cooperatively control vascular function and regulate MBF upon changes in metabolic demand.

$Kv1$ channels belong to one of several Kv subfamilies that regulate membrane potential and $[Ca^{2+}]_i$ in arterial myocytes to control vessel diameter and blood flow³²⁰. Pharmacological blockade of $Kv1$ channels reduces whole-cell outward I_K by $\geq 50\%$,³²¹ whereas increased steady-state I_{Kv} results in membrane hyperpolarization and reduced Ca^{2+} influx via voltage-gated Ca^{2+} channels.³²² The resultant reduction in cytosolic $[Ca^{2+}]_i$ leading to myocyte relaxation, and vasodilation increases local tissue perfusion. Considering the relatively high resting input resistance (1-10 G Ω) of arterial smooth muscle cells, the opening or closure of few K^+ channels can generate substantial changes in membrane potential and vascular tone^{323, 324}. Consequently, the functional expression of native Kv channels of arterial myocytes is dynamically controlled by multiple molecular processes, which include post-transcriptional regulation (e.g., phosphorylation, glycosylation), subcellular trafficking and recycling, redox modifications, as well as association with accessory subunits and regulatory proteins^{77, 175, 325-327}. Adding to this

complexity, our observation that deletion of Kv β 2 disrupts Kv1-dependent vasodilation is consistent with a functional role of this subunit in regulating the vasodilatory response to metabolic stress.

Kv channels in excitable cells assemble as either homomeric or heteromeric structures with varied $\alpha_4\beta_4$ configurations of pore-forming and auxiliary subunits³²⁸⁻³³¹. This 'mix-and-match' capability of Kv channels contributes to the wide heterogeneity of K⁺ currents that enables diverse physiological roles across different cell types. In our previous work we found that Kv1 channels in murine coronary arterial myocytes interact with Kv β 1.1/Kv β 2 heteromers,²⁵⁹ and our present findings suggest a divergent functional regulation of vascular tone and blood flow by these proteins. These divergent roles are revealed by the observation that even though Kv β 2 ablation suppressed vasodilatory function and MBF, the loss of Kv β 1.1 had little impact on arterial diameter *ex vivo*, but elevated MBF *in vivo*. These findings suggest that Kv β 1 and β 2 have somewhat divergent and potentially antagonist roles, which may relate to differences in their structures. The Kv β 1 has a ball-and-chain inactivation domain at the N-terminus, a feature that is lacking in Kv β 2. Potentially as a result of these differences, individual subunits have differential effects on the gating of non- and slowly-inactivating Kv1 α channels³³². Specifically, Kv β 1 induces N-type inactivation in non-inactivating Kv1 α proteins whereas Kv β 2 increases current amplitude and shifts the voltage-dependence of activation towards more hyperpolarized potentials, with little impact on channel inactivation^{9, 195, 332}. These effects are consistent with a greater steady-state activity of non-inactivating Kv1 α channels (e.g., Kv1.5) when assembled with Kv β 2, as compared with those predominantly consisting of Kv β 1 proteins.

How the net competing influences of multiple Kv β subtypes impact the function of native Kv1 channels remains to be resolved; however, it has been reported that within the same auxiliary complex, the N-terminal inactivation function of Kv β 1 is inhibited by Kv β 2

subunits,²⁸¹ an effect which may be due to competition between Kv β subtypes for the intracellular domain of pore-forming Shaker subunits, or through modification of Kv β 1 function via β : β subunit interactions. We found that in arterial myocytes both Kv β 1.1 and Kv β 2 proteins are expressed in native Kv1 channels, therefore it seems plausible that the greater abundance of Kv β 2 relative to Kv β 1.1 in Kv1 channels of coronary arterial myocytes underlies its functional dominance under physiological conditions. Consistent with this are the apparent differences in inactivation kinetics between slowly inactivating outward K⁺ currents measured in coronary arterial myocytes in comparison with rapidly inactivating (i.e., A-type) currents recorded in retinal arteriolar myocytes, which predominantly express Kv1.5 + Kv β 1 proteins^{174, 275, 333}. Indeed, our current data obtained from novel double transgenic mice overexpressing Kv β 1.1 in smooth muscle suggest that increased abundance of Kv β 1 proteins effectively diminishes the vasodilatory function attributed to Kv β 2. Thus, based on these findings, we speculate that Kv β 1 and β 2 play antagonistic roles and that Kv channel remodeling which results in functional upregulation of Kv β 1.1 or downregulation of Kv β 2 (i.e., elevated Kv β 1.1:Kv β 2 ratio) could impair vasodilation and limit tissue perfusion.

The Kv β proteins were discovered as functional AKRs, a group of enzymes that catalyze the reduction of carbonyl compounds by NAD(P)H^{242, 244}. In our previous work, we found that the binding of oxidized and reduced pyridine nucleotides to Kv β proteins differentially modifies channel gating,^{8-10, 195, 196} thus, raising the possibility that the Kv β subunits provide a molecular link between the metabolic state of a cell and Kv channel activity. Given the high affinity of Kv β proteins for pyridine nucleotides,^{7, 250} it is plausible that rapid changes in intracellular redox potential of pyridine nucleotides in arterial myocytes may underlie Kv-mediated control of blood flow in the heart upon changes in metabolic demand. We recently reported that Kv β 2 subunits facilitate surface expression of Kv1 and Kv4 channels in cardiomyocytes and that they impart redox and metabolic

sensitivity to cardiac Kv channels, thus coupling cardiac repolarization with intracellular pyridine nucleotide redox status;¹⁹⁶ however, to the best of our knowledge, the current study is the first to suggest a fundamental role for these subunits in controlling resistance vascular tone and blood flow.

Although our data show that Kv β proteins regulate the diameter of resistance arteries subsequent to the modulation of NAD(H) redox via elevation of L-lactate, the precise identity of the factors responsible for coupling between myocardial oxygen consumption and coronary arterial tone remain unclear. Several myocardium-derived 'metabolites' (e.g., local O₂/CO₂ tensions, reactive oxygen species such as H₂O₂, lactate, endothelial-derived factors such as arachidonic acid metabolites)²⁹⁸ could conceivably alter intracellular pyridine nucleotide redox potential and further work is required to identify specific metabolic processes that link intracellular redox changes to Kv activity. The function of coronary Kv1 channels could also be affected by other long-term biochemical processes. For example, the Kv β protein could plausibly alter patterns of basal post-transcriptional regulatory pathways (e.g., PKC-mediated channel phosphorylation)³³⁴ or the surface density of functional channels. However, such differences would likely manifest as differences in myogenic tone development or differential responses to vasoconstrictor stimuli,³³⁵ which were not seen in our study, suggesting that the vasoregulatory effects of Kv β may reflect more dynamic modifications of channel function.

Even though our study has many strengths, some limitations should be considered. Our studies were performed in mice, which exhibit greater heart rates and MBF relative to larger mammals, including humans ³³⁶. Nonetheless, the positive correlation between myocardial oxygen consumption and MBF is highly conserved across species, and the parallel importance of Kv1 channels in the regulation of MBF is established in small rodents and larger mammals (i.e., swine) ⁴⁻⁶. Thus, it is likely that regulation of MBF by Kv β proteins, observed in our current study, extends to larger

species. Additionally, we cannot exclude the possibility that deletion of Kv β proteins in non-vascular cell types (e.g., cardiomyocytes, neurons) may contribute to effects on MBF in vivo. However, this is unlikely for several reasons. First, prior work from our group indicates that suppression of blood flow in animals lacking Kv1.5, a predominant Kv1 α binding partner of Kv β , is restored via its conditional reconstitution in smooth muscle.⁶ Second, data from novel transgenic mice generated for the current study (SM22 α -rtTA:TRE-Kv β 1) indicate that smooth muscle-selective overexpression of Kv β 1.1, which increases the ratio of Kv β 1.1:Kv β 2 subunits in native Kv1 channels in arterial myocytes, leads to robust suppression of vasodilation and MBF, similar to observations in global Kv β 2 knockout mice. Additional evidence from *ex vivo* arterial diameter measurements further supports the role for vascular Kv β proteins in the regulation of vasoreactivity and is consistent with the notion that Kv β subunits of native arterial Kv1 channels facilitate the metabolic hyperemia response.

In summary, we report a novel role for intracellular Kv β subunits in the differential regulation of resistance artery diameter and control of myocardial blood flow. Our results indicate that proper coupling between coronary arterial diameter and myocardial oxygen consumption relies on the molecular composition of Kv1 accessory subunit complexes such that the functional expression of Kv β 2 is essential for Kv1-mediated vasodilation. Moreover, the current study suggests that perturbations in Kv β function or expression profile (i.e., Kv β 1.1:Kv β 2) may underlie the dysregulation of blood flow in disease states characterized by impaired microvascular function and ischemia-related cardiac dysfunction.

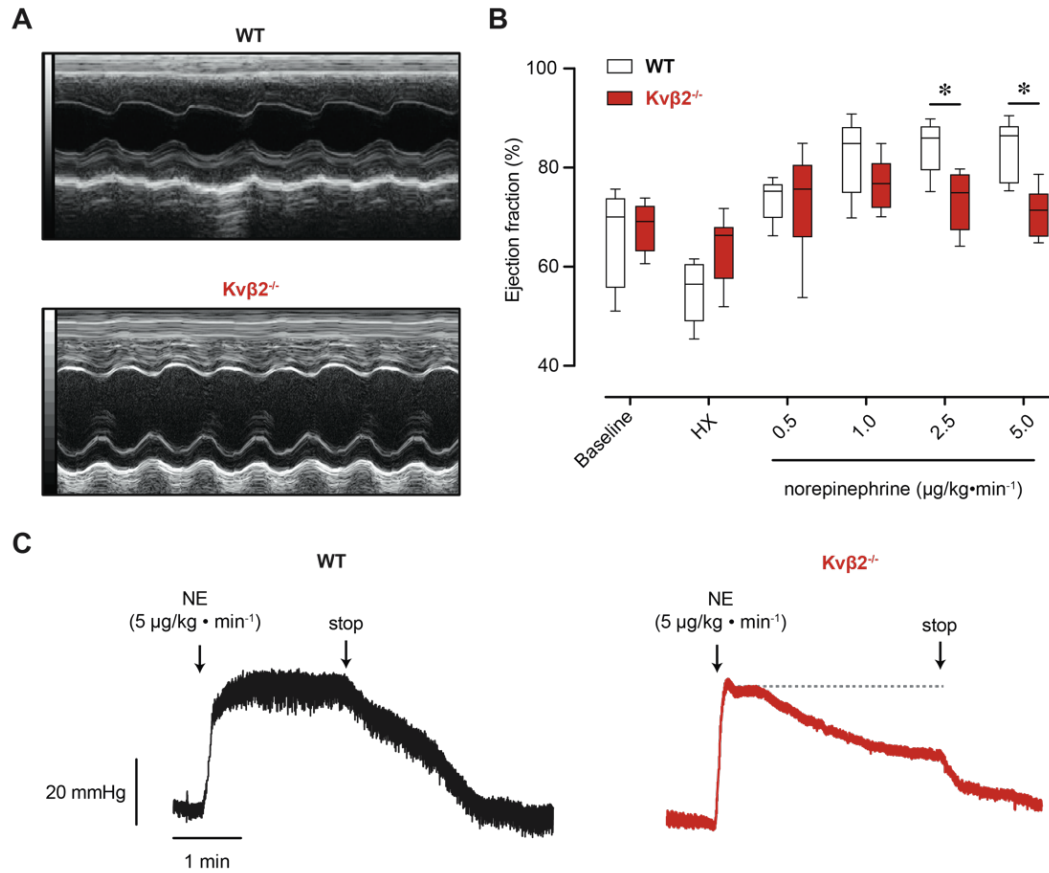


Figure 1: Loss of Kvβ2 impairs cardiac pump function during stress. (A) Representative M-mode echocardiographic images obtained from wild type (WT; 129SvEv), and Kvβ2^{-/-} mice during infusion of 5 μg/kg·min⁻¹ norepinephrine. (B) Summary ejection fraction data for WT and Kvβ2^{-/-} mice at baseline, after administration of hexamethonium (HX; 5 mg·kg⁻¹, i.v.), and during norepinephrine infusions (0.5 – 5 μg/kg·min⁻¹; 2-3 min duration). n = 8 each, *P = 0.009 at 2.5 μg/kg·min⁻¹, P = 0.003 at 5.0 μg/kg·min⁻¹ (two-way ANOVA). (C) Arterial blood pressure recordings obtained via femoral artery catheter in WT and Kvβ2^{-/-} mice, before and after treatment with norepinephrine (NE, 5 μg/kg·min⁻¹), as indicated by arrows.

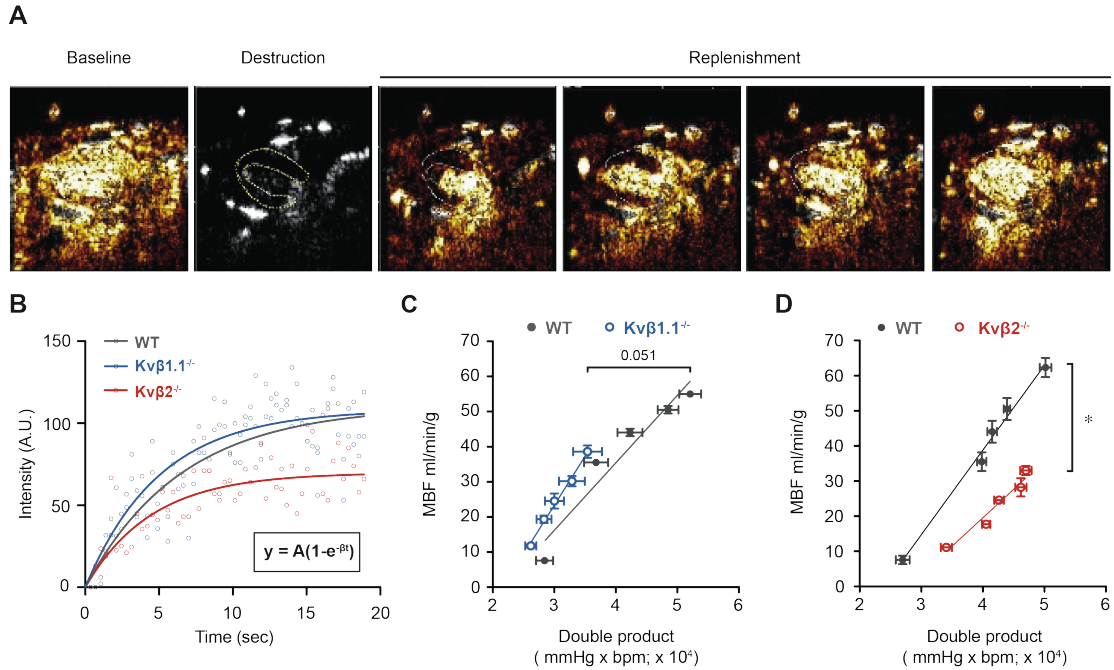


Figure 2: Relationship between myocardial blood flow and cardiac workload in Kvβ-null mice. (A) Long axis echocardiographic images showing signal intensity from myocardial tissue and cavity before high power destruction frame and during signal replenishment phase (~10 sec). In destruction frame, the left ventricular wall is outlined with a yellow dashed line. (B) Signal intensity plotted versus time following destruction in region of interest in the anterior left ventricular myocardial wall of WT (129SvEv), Kvβ1.1^{-/-}, and Kvβ2^{-/-} mice, as indicated. Data were fit with exponential function (equation in *inset*). (C,D) Summary of myocardial blood flow (MBF) as a function of cardiac workload (double product; heart rate x mean arterial pressure) in Kvβ1.1^{-/-} (C) and Kvβ2^{-/-} (D) versus strain-matched wild type (WT) control mice. Data were fit with a simple linear regression model with slopes: WT (0.00192 ± 0.00031), Kvβ1.1^{-/-} (0.00279 ± 0.00016); n = 6-8 mice; WT (0.00241 ± 0.00014), Kvβ2^{-/-} (0.00162 ± 0.00022); n = 4-8 mice, *P = 0.025, Kvβ2^{-/-} vs. WT (linear regression).

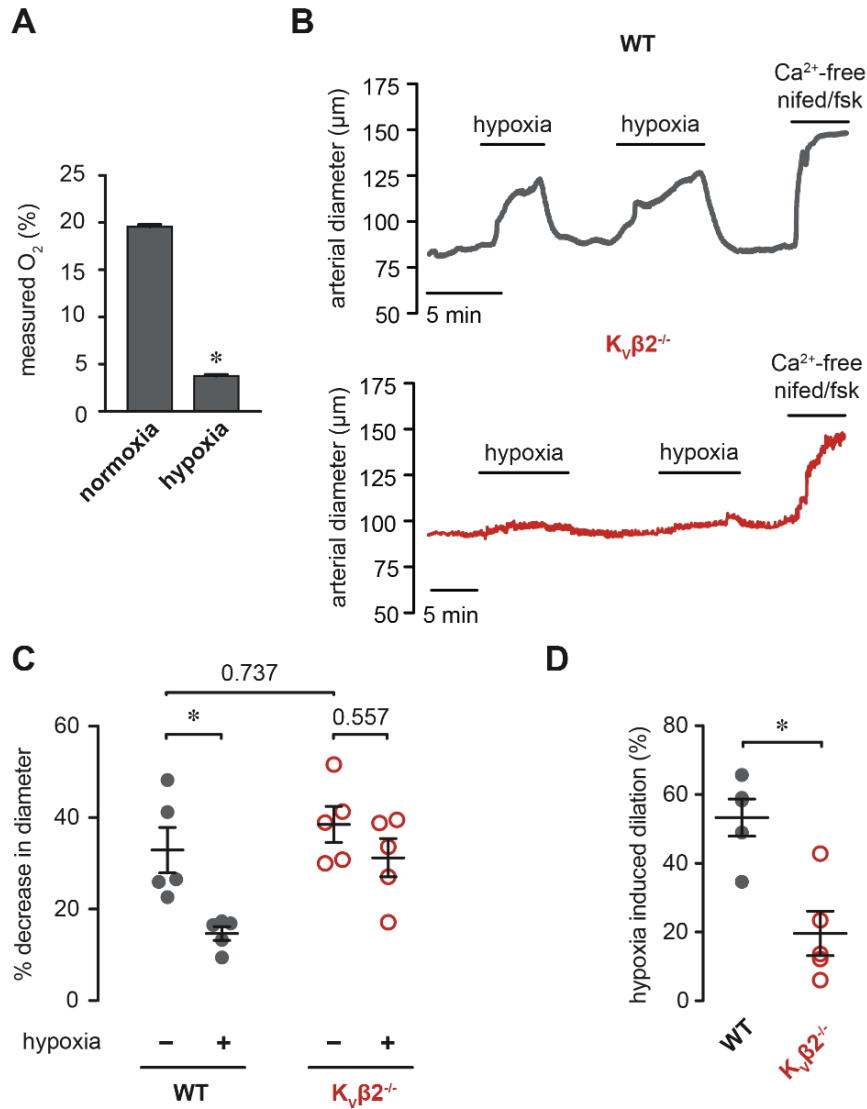


Figure 3: Ablation of Kvβ2 attenuates coronary vasodilation in response to hypoxia.

(A) Summary of bath O₂ (%) measured in normoxic and hypoxic conditions (bath solution aerated with 5% CO₂, balance N₂, and containing 1 mM Na₂S₂O₄); data are pooled from measurements obtained with wild type (129SvEv) and Kvβ2^{-/-} coronary arteries. n = 7-9, *P<0.001 (Mann Whitney U test). (B) Representative arterial diameter recordings in isolated coronary arteries from wild type (WT; 129SvEv) and Kvβ2^{-/-} mice in normoxic conditions and hypoxic conditions. Arteries were precontracted with 100 nM U46619. Ca²⁺-free perfusate containing nifedipine (nifed; 1 μM) and forskolin (fsk; 0.5 μM) was introduced at the end of the experiment to induce maximum passive dilation. (C) Scatter-plot and mean ± SEM showing percent decrease in diameter recorded under normoxic (- hypoxia) and hypoxic (+ hypoxia) conditions for coronary arteries from WT and Kvβ2^{-/-} mice (n = 5 arteries from 3-4 mice per group). Normoxic and hypoxic conditions were both applied in the continuous presence of 100 nM U46619, as described above (B). *P = 0.020 (one-way ANOVA with Tukey post-hoc test). (D) Scatter-plot and mean ± SEM showing hypoxia-induced dilation (%) for arteries from WT and Kvβ2^{-/-} mice. *P = 0.009 (Mann-Whitney U test).

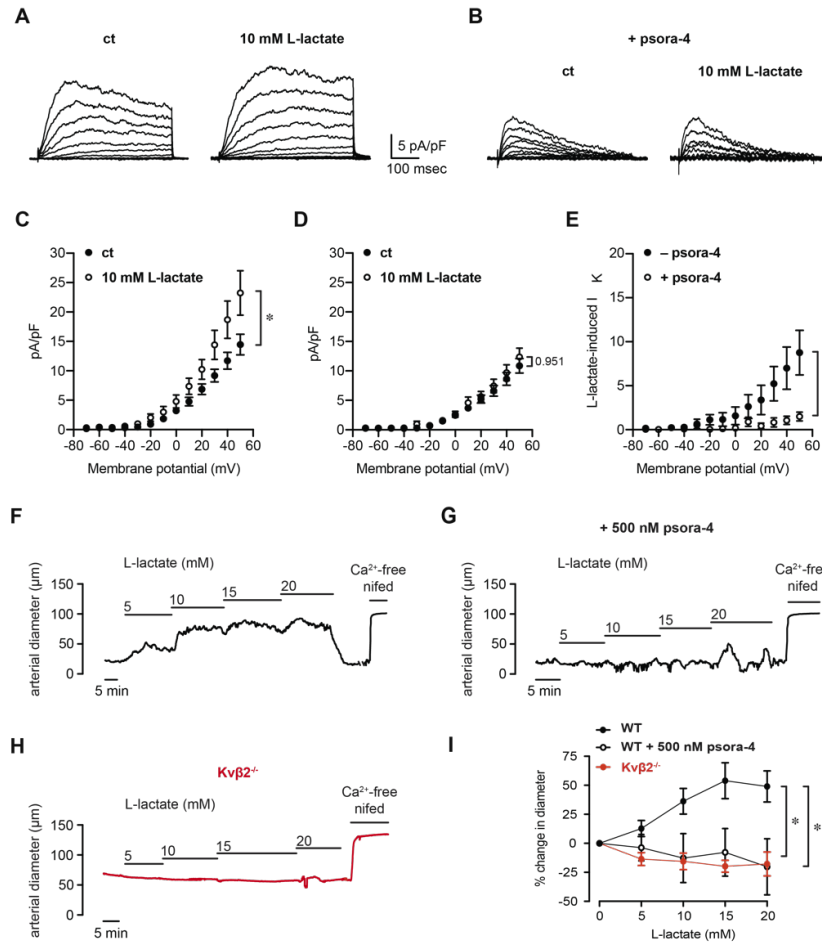


Figure 4: L-lactate enhances I_{Kv} in coronary arterial myocytes and promotes coronary vasodilation via $Kv\beta 2$. (A, B) Representative outward K^+ current recordings normalized to cell capacitance (pA/pF) in response to step-wise (10 mV) depolarization to +50 mV from a holding potential of -70 mV in isolated coronary arterial myocytes. Currents were recorded before and after application of 10 mM L-lactate in bath solution lacking (A) or containing (B) 500 nM psora-4. (C, D) Summary current-voltage relationships obtained in coronary arterial myocytes before and after application of 10 mM L-lactate in bath solution lacking (C) or containing (D) 500 nM psora-4. n = 5-7 cells from 4-7 mice. *P < 0.001 (two-way ANOVA). (E) Summary of L-lactate-induced currents recorded in the absence and presence of 500 nM psora-4. n = 5-7 cells from 4-7 mice. *P < 0.001 (two-way ANOVA). (F-H) Arterial diameter traces obtained from pressurized (80 mmHg) coronary arteries isolated from wild type (F,G; 129SvEv) and $Kv\beta 2^{-/-}$ (H) mice in the absence and presence of L-lactate (5-20 mM, as indicated). Arteries were preconstricted with 100 nM U46619; for WT arteries, L-lactate was applied in the absence (top) and presence (bottom) of psora-4 (500 nM). Maximum passive diameter was recorded at the end of each experiment in Ca^{2+} -free saline solution with nifedipine (nifed; 1 μ M) and forskolin (fsk; 0.5 μ M). (I) Summary plot showing L-lactate-induced dilation, expressed as a percent change from baseline diameter relative to maximum passive diameter, for arteries isolated from WT (129SvEv; \pm 500 nM psora-4) and $Kv\beta 2^{-/-}$ mice. n = 4 arteries from 4 mice for each. *P = 0.001, WT vs. WT + psora-4; *P < 0.001, WT vs. $Kv\beta 2^{-/-}$ (two-way ANOVA with Tukey post hoc test).

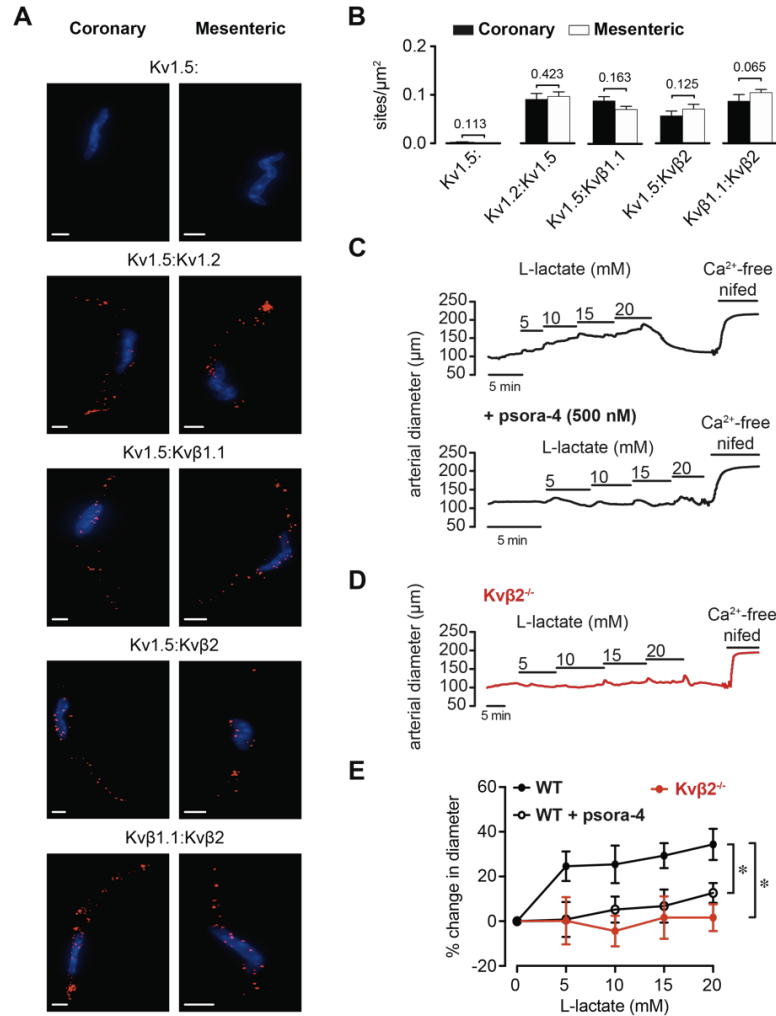


Figure 5: K β 2 controls redox-dependent vasoreactivity in resistance mesenteric arteries. (A) Representative fluorescence images showing PLA-associated fluorescent punctae (red) in wild type coronary and mesenteric arterial myocytes. Cells were labelled for Kv1.5 alone, or co-labelled for Kv1.5 and Kv1.2, Kv1.5 and Kv β 1.1, Kv1.5 and Kv β 2, or Kv β 1.1 and Kv β 2 proteins. DAPI nuclear stain is shown for each condition (blue). Scale bars represent 5 μm . (B) Summary of PLA-associated punctate sites normalized to total cell footprint area for conditions and groups as in D. P values are shown for coronary versus mesenteric arteries (Mann Whitney U). (C,D) Arterial diameter traces obtained from pressurized (80 mmHg) mesenteric arteries isolated from wild type (C; 129SvEv) and Kv β 2^{-/-} (D) mice in the absence and presence of L-lactate (5-20 mM, as indicated). Arteries were precontracted with 100 nM U46619 and L-lactate was applied in the absence (*top*) and presence (*bottom*) of the selective Kv1 channel inhibitor psora-4 (500 nM). Maximum passive diameters were recorded at the end of each experiment in Ca²⁺-free saline solution with nifedipine (nifed; 1 μM) and forskolin (fsk; 0.5 μM). (E) Summary plot of L-lactate-induced dilation, expressed as the percent change from baseline diameter relative to maximum passive diameter, for arteries isolated from WT (129SvEv; \pm psora-4) and Kv β 2^{-/-} mice. WT: n = 6 arteries from 6 mice; WT + psora-4: 6 arteries from 6 mice; Kv β 2^{-/-}: 5 arteries from 5 mice. *P < 0.001 for each (mixed effects two-way ANOVA with Tukey post hoc test).

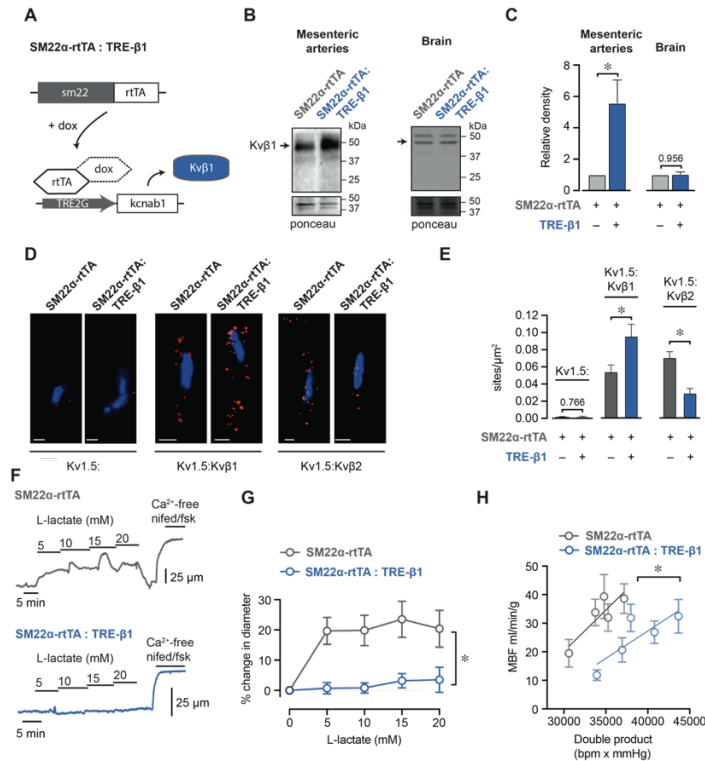


Figure 6: Increasing the ratio of Kv β 1.1:Kv β 2 subunits in smooth muscle inhibits L-lactate-induced vasodilation and suppresses myocardial blood flow. (A) Schematic diagram describing the SM22 α -rtTA: TRE- β 1 model. Double transgenic animals (+dox) results in activation of the reverse tetracycline trans-activator (rtTA) in smooth muscle cells, and drives expression of Kv β 1.1. **(B)** Western blots showing immunoreactive bands for Kv β 1 in whole mesenteric artery and brain lysates from SM22 α -rtTA (single transgenic control) and SM22 α -rtTA: TRE- β 1 (double transgenic) mice after doxycycline treatment. Ponceau-stained membrane (mol. Wt.: ~30-55 kDa) is shown as an internal control for total loaded protein. **(C)** Summarized relative densities of Kv β 1.1-associated immunoreactive bands in mesenteric arteries and brains of SM22 α -rtTA: TRE- β 1 relative to SM22 α -rtTA. n = 3 each. *P<0.05 (One sample t test). **(D)** Representative fluorescence images showing PLA-associated fluorescent punctae (red) in coronary arterial myocytes isolated from SM22 α -rtTA and SM22 α -rtTA: TRE- β 1 mice. Cells were labelled for Kv1.5 alone, or co-labelled for Kv1.5 and Kv β 1, or Kv1.5 and Kv β 2 proteins. DAPI nuclear stain is shown for each condition (blue). Scale bars represent 5 μ m. **(E)** Summary of PLA-associated punctate sites normalized to total cell footprint area for conditions and groups as in D. *P<0.05, **P<0.01 (Mann Whitney U). **(F)** Representative arterial diameter recordings from 100 nM U46619-precontracted mesenteric arteries isolated from SM22 α -rtTA and SM22 α -rtTA: TRE- β 1 mice in the absence and presence of L-lactate (5-20 mM), as in Figure 5 C,D. Passive dilation in the presence of Ca²⁺-free solution + nifedipine (1 μ M) and forskolin (fsk; 0.5 μ M) is shown for each recording. **(G)** Summary plot of L-lactate-induced dilation for arteries isolated from SM22 α -rtTA and SM22 α -rtTA: TRE- β 1 mice. SM22 α -rtTA: n = 6 arteries from 5 mice; SM22 α -rtTA: TRE- β 1: n = 10 arteries from 6 mice; *P<0.05 (two-way ANOVA). **(H)** Summary relationships between myocardial blood flow (MBF) and cardiac workload (double product; heart rate x mean arterial pressure) in SM22 α -rtTA: TRE- β 1 vs. SM22 α -rtTA control mice. n = 5 each; **P<0.01 (linear regression).

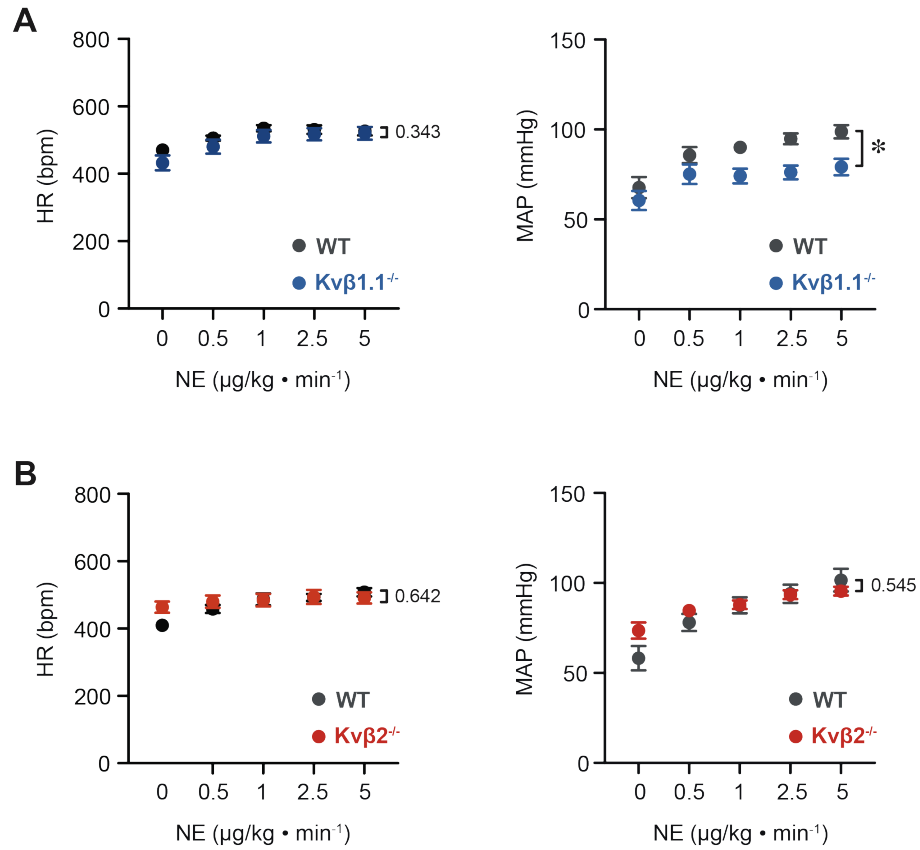


Figure 7: Heart rate and mean arterial pressure in wild type and Kvβ-null mice during catecholamine-induced stress. (A, B) Summary graphs showing heart rate (HR; *left*) and mean arterial pressure (MAP; *right*) in Kvβ1.1^{-/-} (A) and Kvβ2^{-/-} (B) and strain-matched wild type (WT) mice at baseline (0 μg/kg·min⁻¹ NE) and during intravenous infusion of norepinephrine (0.5-5 μg/kg·min⁻¹). WT, Kvβ1.1^{-/-}: n = 6-8 mice; WT, Kvβ2^{-/-}: n = 4-8 mice *P = 0.019 (two-way ANOVA).

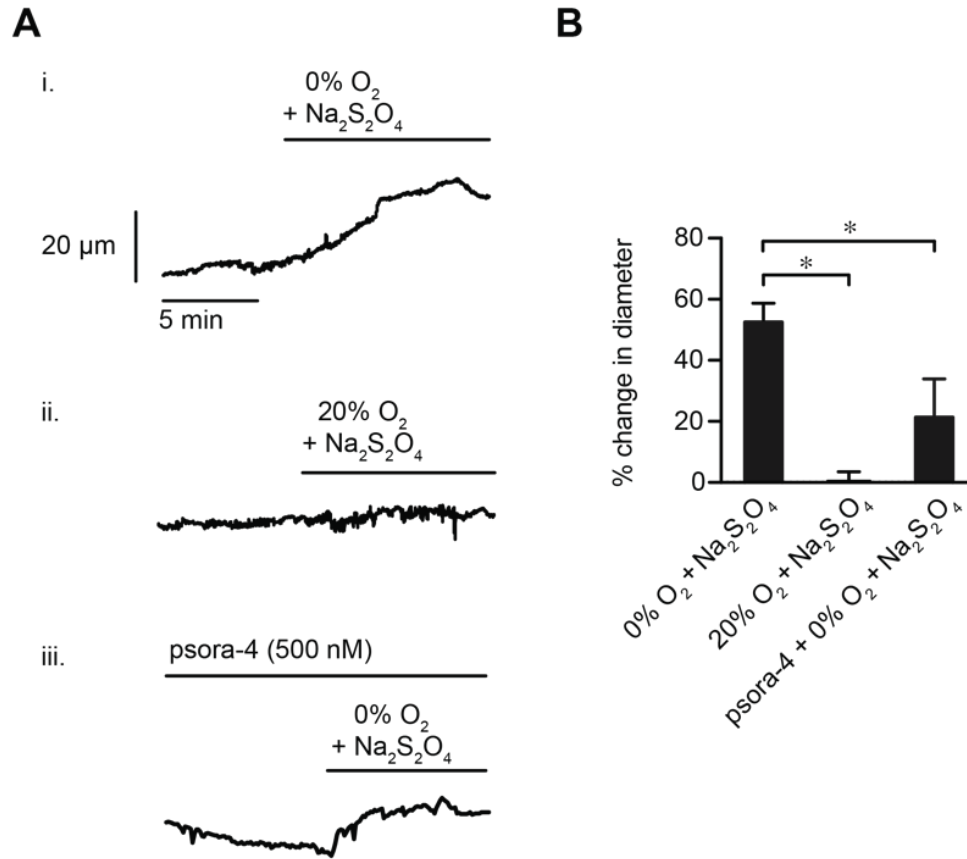


Figure 8: Hypoxia-induced vasodilation of isolated coronary arteries is attenuated in the presence of psora-4. (A) Representative coronary arterial diameter recordings obtained in the absence and presence of either 1 mM sodium hydrosulfite aerated with 95% N₂/0% O₂ (0% O₂ + Na₂S₂O₄; i.), 1 mM sodium hydrosulfite aerated with 20% O₂ (20% O₂ + Na₂S₂O₄; ii.), or 1 mM sodium hydrosulfite aerated with 95% N₂/0% O₂ applied in the presence of 500 nM psora-4 (iii.). (B) Summary of normalized % change in arterial diameter for conditions as indicated in A. n = 4-5 arteries from 4-5 mice, *P = 0.001, 0% O₂ + Na₂S₂O₄ vs. 20% O₂ + Na₂S₂O₄; *P = 0.023, 0% O₂ + Na₂S₂O₄ vs. psora-4 + 0% O₂ + Na₂S₂O₄ (one-way ANOVA with Tukey post hoc test).

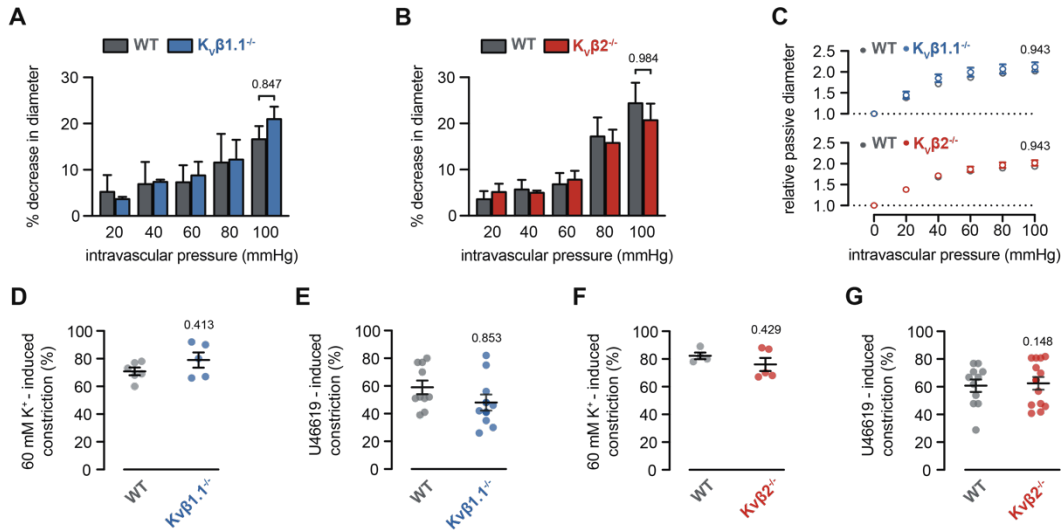


Figure 9: Loss of Kv β subunits does not impact vasoconstriction in response to increases in intravascular pressure, membrane depolarization, or thromboxane A₂ receptor activation. (A,B) Bar plots showing summarized % decrease in diameter at intravascular pressures of 20, 40, 60, 80, and 100 mmHg for mesenteric arteries from WT (C57Bl6N; n = 4 arteries from 4 mice) and Kv β 1.1^{-/-} (n = 5 arteries from 5 mice) mice (A), and WT (129SvEV; n = 6 arteries from 5 mice) and Kv β 2^{-/-} (n = 6 arteries from 5 mice) mice (B). P values are shown for Kv β 1.1 vs WT, and Kv β 2^{-/-} vs. WT at 100 mmHg (one-way ANOVA with Tukey post hoc test). (C) Symbol plots showing summarized passive diameters, obtained in Ca²⁺-free bath solution containing 0.5 μ M forskolin and 1 μ M nifedipine, relative to diameters at 0 mmHg across the range of intravascular pressures tested for arteries from Kv β 1.1^{-/-} (n = 5 arteries from 5 mice), Kv β 2^{-/-} (n = 6 arteries from 5 mice), and corresponding WT mice (n = 4 arteries from 4 mice; n = 6 arteries from 5 mice, respectively). P values are shown for Kv β 1.1^{-/-} vs. WT, and Kv β 2^{-/-} vs. WT at 100 mmHg (two-way ANOVA with Tukey post hoc test). (D-G) Scatter plots summarizing % decrease in diameter obtained from mesenteric arteries before and after application of 60 mM [K⁺]_o (E, G) and 100 nM U46619 (F, H) (indicated by arrows in traces) in Kv β 1.1^{-/-}, Kv β 2^{-/-}, and corresponding WT mice. P values for Kv β -null vs. WT are provided (Mann Whitney U test); [K⁺]_o (D), WT: n = 4 arteries from 4 mice, Kv β 1.1^{-/-}: n = 5 arteries from 5 mice; (F), WT: n = 6 arteries from 5 mice, Kv β 2^{-/-}: n = 5 arteries from 4 mice; U46619 (E), WT: n = 11 arteries from 10 mice, Kv β 1.1^{-/-}: n = 11 arteries from 11 mice; U46619 (G), WT: n = 10 arteries from 9 mice, Kv β 2^{-/-}: n = 10 arteries from 10 mice.

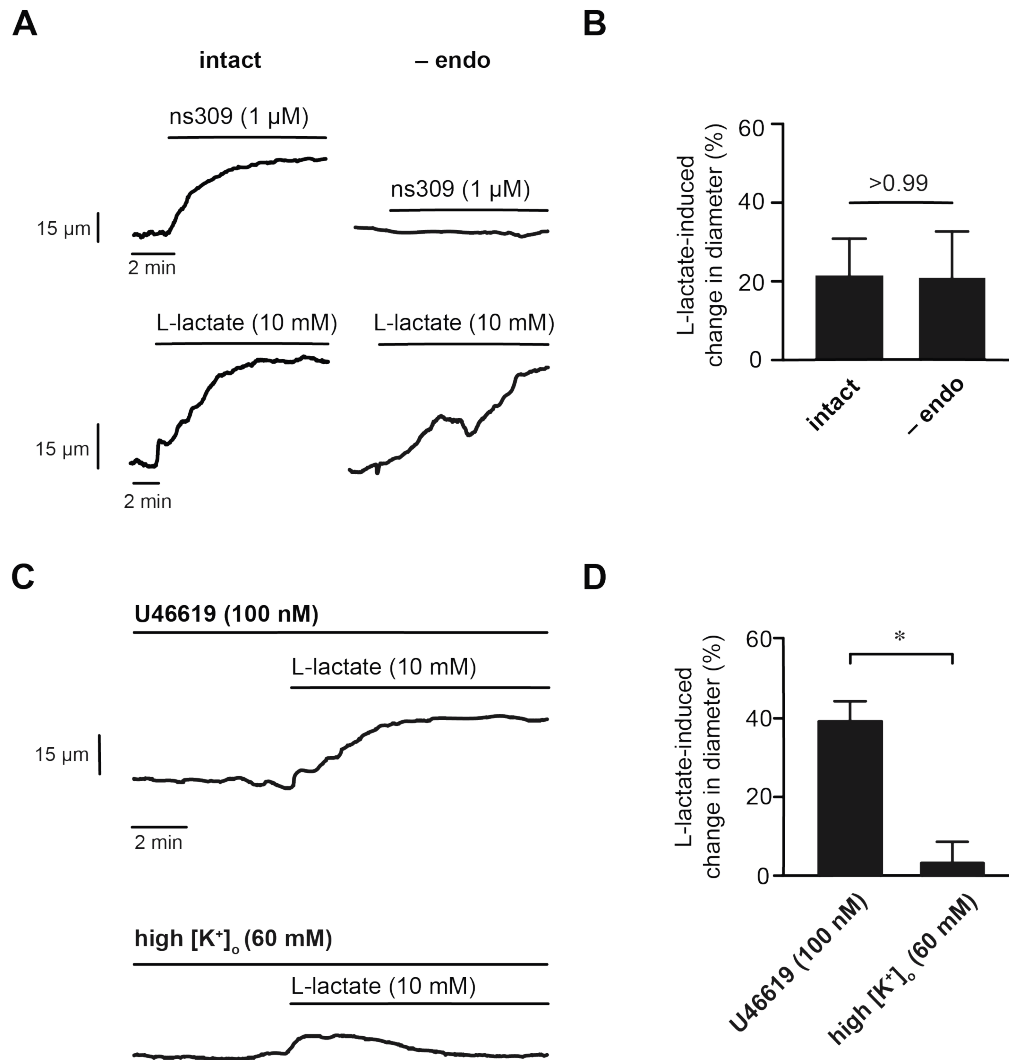


Figure 10: Vasodilation in response to L-lactate is independent of endothelial function and requires changes in membrane potential. (A) Arterial diameter recordings from precontracted (100 nM U46619) intact and endothelium-denuded (-endo) arteries in the absence and presence of the SK_{Ca}/IK_{Ca} opener NS309 (1 μ M; *top*) and absence and presence of 10 mM L-lactate (*bottom*). (B) Bar graph summarizing percent change in diameter in response to 10 mM L-lactate in intact and -endo arteries. Intact: n = 4 arteries from 4 mice; -endo: n = 6 arteries from 3 mice (Mann-Whitney U). (C) Arterial diameter traces from pressurized (80 mmHg) mesenteric arteries isolated from wild type mice precontracted with either U46619 (100 nM) or high $[K^+]_o$ (60 mM), before and after application of 10 mM L-lactate. (D) Bar graph summarizing 10 mM L-lactate-induced vasodilation (percent of maximal dilation) in arteries precontracted with either 100 nM U46619 or with high $[K^+]_o$. U46619: n= 6 arteries from 5 mice; high $[K^+]_o$: 4 arteries from 4 mice. *P = 0.010 (Mann-Whitney U).

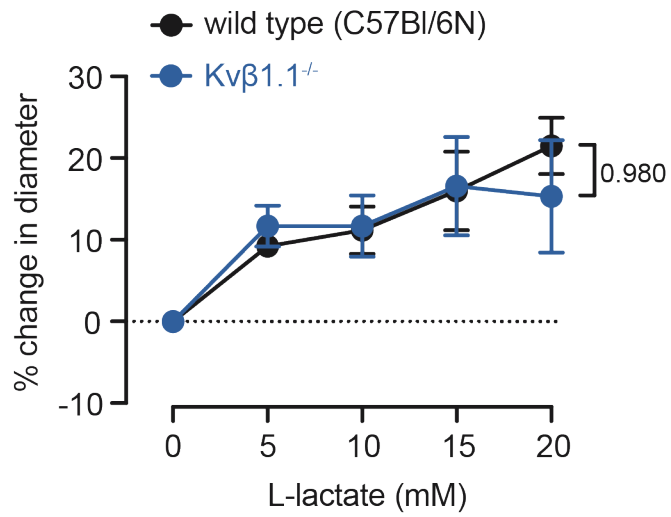


Figure 11: L-lactate-induced vasodilation is not altered in arteries from Kvβ1.1^{-/-} mice. Summary of L-lactate-induced dilation for arteries from Kvβ1.1^{-/-} and WT mice. WT: n = 6 arteries from 6 mice, Kvβ1.1^{-/-}: 7 arteries from 7 mice. (two-way ANOVA).

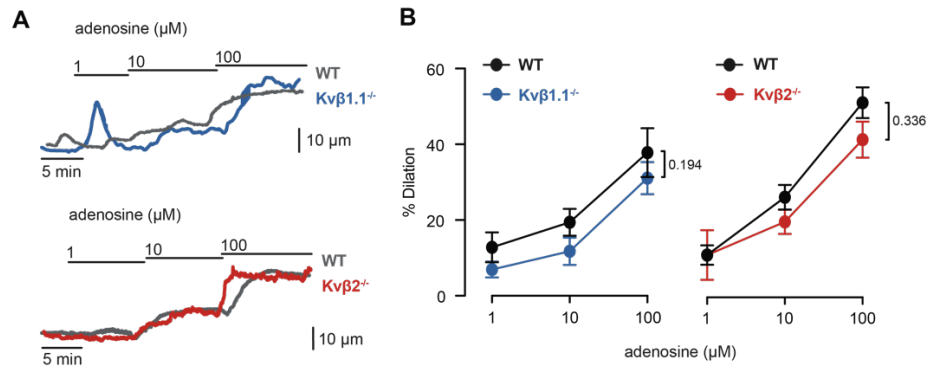


Figure 12: Ablation of Kv β proteins does not impact vasodilation in response to adenosine. (A) Representative diameter measurements obtained from mesenteric arteries (80 mmHg) from Kv β 1.1^{-/-} and Kv β 2^{-/-} mice and respective wild type (WT) control mice in the absence and presence of 1-100 μM adenosine. (B) Summary of adenosine-induced dilation in arteries from Kv β 1.1^{-/-} (left) and Kv β 2^{-/-} (right) versus respective WT mice. (two-way ANOVA).

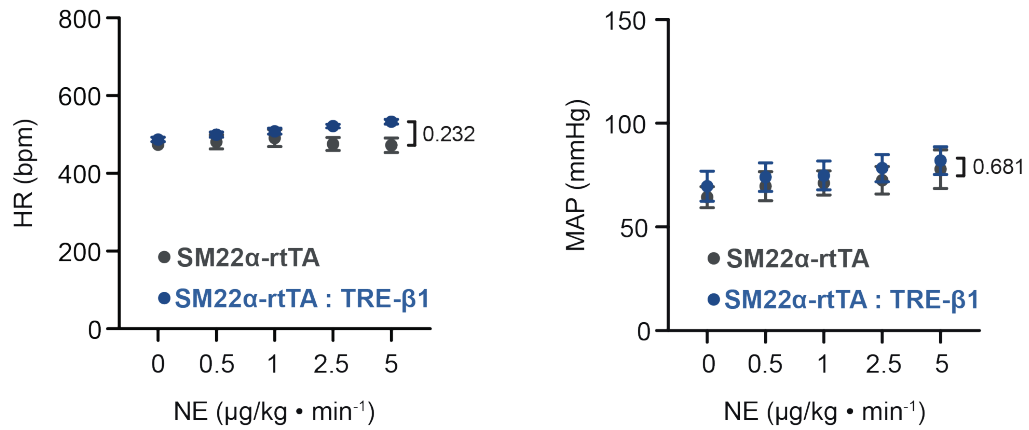


Figure 13: Heart rate and mean arterial pressure in double transgenic SM22 α -rtTA:TRE- β 1 and single transgenic control SM22 α -rtTA mice in the absence and presence of catecholamine-induced stress. Summary graphs showing heart rate (HR; *left*) and mean arterial pressure (MAP; *right*) in SM22 α -rtTA:TRE- β 1 and SM22 α -rtTA mice before and after intravenous infusion of norepinephrine (0-5 $\mu\text{g}/\text{kg} \cdot \text{min}^{-1}$). n = 5 each (two-way ANOVA).

Table 3: Body weight and cardiac structural parameters for wild type and Kv β -null mice.

Measurement	Wild type (C57Bl6N)	Kvβ1.1^{-/-}	Wild type (129SvEv)	Kvβ2^{-/-}	SM22α-rtTA	SM22α-rtTA:TRE-Kvβ1
Body Weight (g)	26.7 \pm 1.2	25.2 \pm 2.0	25.8 \pm 2.6	25.0 \pm 0.7	27.6 \pm 0.3	25.6 \pm 0.8
Wall Thickness						
LVPWd (mm)	1.06 \pm 0.07	1.03 \pm 0.05	1.29 \pm 0.11	1.01 \pm 0.06*	1.15 \pm 0.11	1.14 \pm 0.15
LVPWs (mm)	1.57 \pm 0.12	1.41 \pm 0.04	1.62 \pm 0.11	1.33 \pm 0.07	1.61 \pm 0.11	1.48 \pm 0.16
LVAWd (mm)	0.97 \pm 0.03	1.25 \pm 0.02*	1.23 \pm 0.06	1.10 \pm 0.04	1.15 \pm 0.06	1.05 \pm 0.10
LVAWs (mm)	1.43 \pm 0.05	1.71 \pm 0.03*	1.67 \pm 0.07	1.52 \pm 0.04	1.77 \pm 0.08	1.53 \pm 0.15
RWT	0.59 \pm 0.03	0.61 \pm 0.06	0.75 \pm 0.06	0.63 \pm 0.04	0.69 \pm 0.05	0.66 \pm 0.06
LV Mass (mg)	106.7 \pm 6.4	120.6 \pm 4.5	142.0 \pm 16.5	103.9 \pm 6.1*	120.2 \pm 12.5	111.6 \pm 12.7

Data are mean \pm SEM. *P<0.05 vs. respective wild type/single transgenic control (unpaired t test). Abbreviations: LVPWd, left ventricular posterior wall at diastole; LVPWs, left ventricular posterior wall at systole; LVAWd, left ventricular anterior wall at diastole; LVAWs, left ventricular anterior wall at systole; RWT, relative wall thickness.

Table 4: Echocardiographic parameters in wild type and Kvβ-null mice.

Endocardial values		Wild type (C57Bl6N)	Kvβ1.1^{-/-}	Wild type (129SvEv)	Kvβ2^{-/-}	SM22α-rtTA	SM22α-rtTA:TRE-Kvβ1
EDV (μl)							
NE (μg/kg·min ⁻¹)	0	61.7 ± 2.9	53.8 ± 8.1	53.9 ± 4.5	50.8 ± 2.3	44.6 ± 3.3	52.2 ± 1.5
	0.5	57.8 ± 2.3	53.5 ± 4.9	50.5 ± 7.8	48.3 ± 2.7	43.6 ± 2.9	45.9 ± 3.8
	1	61.6 ± 3.2	47.6 ± 8.1	46.7 ± 7.4	48.7 ± 4.6	49.4 ± 2.9	46.9 ± 4.9
	2.5	62.8 ± 3.7	41.5 ± 8.8	48.8 ± 6.0	52.8 ± 3.5	51.5 ± 2.8	47.5 ± 5.5
	5.0	66.1 ± 4.4	45.7 ± 11.9	56.4 ± 5.0	54.6 ± 4.5	56.9 ± 3.9	49.3 ± 5.7
ESV (μl)							
NE (μg/kg·min ⁻¹)	0	26.14 ± 2.5	23.1 ± 4.6	26.3 ± 4.7	19.3 ± 2.5	13.7 ± 2.4	30.2 ± 3.5*
	0.5	16.37 ± 1.4	21.3 ± 3.9	19.4 ± 3.7	13.6 ± 1.6	8.1 ± 2.0	17.7 ± 3.6
	1	17.12 ± 1.3	14.1 ± 3.4	14.7 ± 4.3	13.3 ± 1.8	10.0 ± 2.6	12.7 ± 3.2
	2.5	17.22 ± 1.7	9.4 ± 2.7	16.0 ± 2.7	15.7 ± 1.6	12.2 ± 3.1	13.2 ± 4.3
	5.0	17.85 ± 2.3	10.4 ± 3.4	17.3 ± 1.6	18.5 ± 3.1	13.4 ± 3.9	15.6 ± 3.9
SV (μl)							
NE (μg/kg·min ⁻¹)	0	35.56 ± 2.4	30.7 ± 3.5	27.6 ± 0.9	31.5 ± 2.0	30.9 ± 1.9	22.0 ± 3.3
	0.5	41.46 ± 2.3	32.2 ± 1.8	31.2 ± 4.2	34.7 ± 2.4	35.4 ± 1.6	28.2 ± 2.7
	1	44.52 ± 2.3	33.5 ± 5.2	32.0 ± 3.7	42.7 ± 8.2	39.4 ± 1.8	34.2 ± 2.0
	2.5	45.63 ± 2.6	32.1 ± 6.1	32.8 ± 3.6	37.1 ± 2.8	39.3 ± 2.1	34.3 ± 1.4
	5.0	48.26 ± 2.7	35.3 ± 8.5	39.1 ± 4.1	36.1 ± 2.3	43.5 ± 3.1	33.7 ± 2.6
EF (%)							
NE (μg/kg·min ⁻¹)	0	57.84 ± 3.2	57.8 ± 2.6	52.1 ± 4.6	62.4 ± 3.8	70.0 ± 3.8	42.3 ± 6.6
	0.5	71.64 ± 2.2	61.4 ± 4.2	63.5 ± 2.5	71.9 ± 3.3	82.3 ± 3.3	62.7 ± 6.0
	1	72.40 ± 1.2	70.9 ± 3.1	70.7 ± 5.3	73.1 ± 1.8	80.6 ± 4.2	74.2 ± 3.9
	2.5	72.88 ± 1.8	78.2 ± 2.0	67.9 ± 2.7	70.1 ± 2.6	77.4 ± 5.1	74.2 ± 5.7
	5.0	73.65 ± 2.4	79.1 ± 2.7	69.1 ± 2.4	67.5 ± 3.8	77.7 ± 5.8	69.9 ± 5.0
FS (%)							
NE (μg/kg·min ⁻¹)	0	30.17 ± 2.1	29.8 ± 1.6	26.1 ± 2.8	33.7 ± 2.7	39.0 ± 3.2	20.5 ± 3.6*
	0.5	40.48 ± 2.0	32.5 ± 2.8	34.2 ± 1.9	40.7 ± 2.8	50.9 ± 3.6	33.9 ± 4.1
	1	40.97 ± 1.0	40.1 ± 2.4	40.1 ± 4.6	41.4 ± 1.6	49.6 ± 4.3	42.7 ± 3.3
	2.5	41.47 ± 1.5	46.0 ± 1.8	37.4 ± 2.1	39.0 ± 2.2	46.8 ± 4.8	43.1 ± 4.8
	5.0	42.39 ± 2.1	47.1 ± 2.4	38.3 ± 1.9	37.3 ± 3.0	48.1 ± 6.0	39.3 ± 4.2

Data are mean ± SEM. *P<0.05; (mixed effects with Tukey post hoc test). Abbreviations: EDV, left ventricular end diastolic volume; ESV, left ventricular end systolic volume; SV, stroke volume; EF, ejection fraction; FS, fractional shortening.

APPENDIX B

Coronary microvascular Kv1 channels as regulatory sensors of intracellular pyridine nucleotide redox potential²

1. Introduction

Excitable cells utilize ionic gradients across biological membranes to enable numerous life processes. In this respect, the intracellular environment is rich in potassium ions, and transmembrane voltage-dependent potassium (Kv) channels are widely expressed to control the electrical properties of both eukaryotic and prokaryotic cells. Kv channels, due to their broad phyletic distribution and genetic diversity, are thought to be the oldest of voltage-gated ion channels. Mammalian excitable cells express a number of Kv channel subtypes that work in concert to regulate membrane potential³³⁷. Through their ability to sense changes in membrane voltage, these channels rapidly respond to depolarization by altering the conformation of their gating apparatus to allow potassium efflux, reducing intracellular positive charge and thus changing the membrane potential to a more hyperpolarized state. In this manner, the activity of Kv channels contributes to the regulation of neuronal action potential firing, muscle contraction, and hormonal secretion. In excitable cells of the cardiovascular system, the coordinated K⁺ efflux by numerous Kv channel subtypes promotes physiological processes such as cardiac action potential repolarization and vascular smooth muscle (VSM) relaxation.

² This is a non-final version of an article published in final form in Dwenger MM, Ohanyan V, Navedo MF, Nystoriak MA. Coronary microvascular kv1 channels as regulatory sensors of intracellular pyridine nucleotide redox potential. *Microcirculation*. 2018;25, <https://onlinelibrary.wiley.com/doi/10.1111/micc.12426>

Smooth muscle cells of the vasculature have been reported to express channel subtypes belonging to the Kv1, Kv2, Kv3, Kv4, Kv6, Kv7, Kv9 and Kv11 families (see reference ³²⁰, in this issue). In addition to their regulation by membrane voltage, Kv channels are sensitive to functional modulation by a wide variety of intracellular signaling pathways. In small arteries and arterioles of the microcirculation, these pathways tune local and regional blood flow in response to endogenous vasoconstrictor and vasodilator stimuli. In the coronary microcirculation, recent evidence has revealed the importance of redox-mediated Kv1 functional upregulation for physiological enhancement of blood flow (i.e., 'functional' or "metabolic" hyperemia), that occurs during periods of increased cardiac oxygen consumption (e.g., during increased heart rate and ventricular contractility) ⁴⁻⁶. While the underlying cellular and molecular mechanisms connecting the level of oxygen demand of cardiomyocytes in an active heart to the redox regulation of Kv1 function in coronary arterial myocytes are not clear, this process likely involves the complex coordination of multiple contributing pathways. Indeed, a thorough understanding of these mechanisms could aid the rational development of novel strategies to improve the coupling between oxygen supply and demand in the heart, which is impaired in a number of conditions such as hypertension, diabetes mellitus, heart failure, and coronary artery disease ^{291-294, 338, 339}.

Here, we discuss the known role for Kv1 in linking cellular metabolism to regulation of coronary blood flow. A brief discussion of redox-dependent mechanisms of Kv1 channel regulation with respect to the control of coronary blood flow is followed by a review of Kv1 structural features and the potential role for modulation of channel activity via sensing of changes in cellular pyridine nucleotide status by the regulatory auxiliary Kv β subunits. This is followed by a condensed review of direct influence of reactive oxygen species and reactive nitrogen species on Kv1 channel function. We emphasize cellular redox changes following altered myocardial workload and how these may be sensed by Kv1 channels in

the coronary vasculature to promote VSM hyperpolarization and vasodilation to match blood flow with metabolic demand in the heart.

2. Physiological role of Kv1 channels in coronary functional hyperemia.

Unlike other organs, the heart extracts most of the oxygen delivered to it by the arterial blood supply at rest ¹⁶⁰. With little reserve for further oxygen extraction, enhancement of pump activity (e.g., during exercise) and greater demand for oxygen by the myocardium must be coupled with dilation of the coronary arteries and arterioles to instantaneously increase blood flow. This hyperemic response is crucial for maintenance of proper pump function via prevention of myocardial ischemia during periods of increased workloads. While extensive research efforts have aimed to reveal the signaling pathways responsible for metabolic hyperemia in the heart, the mechanisms underlying this process remain poorly understood. In the search for a molecular link between vascular function and myocardial metabolism, decades of pharmacological studies employing receptor and ion channel blockade have yielded controversial conclusions ^{69, 76, 82, 151, 160, 162, 340-342}. The vasoactive metabolite adenosine, which is released from active cardiomyocytes, was long postulated as a primary mediator of coronary artery dilation in response to increase cardiac workload ¹⁶⁰. Yet, studies have shown that administration of adenosine receptor blockers fails to disrupt the normal relationship between myocardial oxygen consumption, coronary vasodilation and blood flow during exercise ^{151, 162, 342}. Intriguing results of a study by Tune et al. demonstrated that simultaneous blockade of adenosine receptors, K_{ATP} channels, and nitric oxide synthesis, failed to lower coronary blood flow in exercising dogs ⁸², suggesting a critical role for an alternative mediator of hyperemia.

A growing body of evidence now supports the concept that coronary hyperemia requires activation of smooth muscle Kv1 channels via a redox-dependent mechanism. For example, a study by Dick et al. reported that the Kv channel blocker 4-aminopyridine

decreases coronary blood flow at rest and reduces normalized debt repayment ratio during reactive hyperemia ¹⁵⁵. Moreover, mice in which Kv1.5 is genetically ablated have significantly blunted hyperemic responses to increases in cardiac work via administration of norepinephrine, yet the normal relationship between cardiac work and myocardial blood flow is restored when Kv1.5 is selectively reconstituted in smooth muscle on an otherwise Kv1.5-null background ⁶, strongly suggesting that loss of hyperemia in the Kv1.5-null animals occurs due to the absence of these channels from the coronary arterial myocytes. These results were corroborated in a separate investigation in which in vivo administration of correolide, a selective Kv1 channel blocker, decreased blood flow in response to dobutamine challenge and inhibited blood flow repayment during reactive hyperemia ⁴. Interestingly, mice lacking Kv1.3 subunits also exhibit decreased myocardial blood flow in response to increases in cardiac work, ⁵, suggesting a potential role of heteromeric Kv1 channels in mediating metabolism-dependent vasodilation. In vitro work has also indicated that vasodilation of coronary arteries to H₂O₂, a purported metabolic vasodilator of coronary arteries, is sensitive to the thiol reductant dithioerithritol and 4-aminopyridine, but not the BK_{Ca} channel inhibitor iberiotoxin ^{174, 175}. These results suggest that Kv channels in VSM may respond to redox-modulating myocardial derived metabolites to induce coronary vasodilation.

While Kv1 channel activity has been implicated as an important regulator of human vascular tone, suppression of Kv1 function may contribute to vascular pathologies. Consistent with this, a recent study found that inhibition of H₂O₂-induced dilation by DPO-1, a selective Kv1.5 channel blocker, was attenuated in arterioles from patients with coronary artery disease, suggesting a reduced capacity for Kv1-dependent vasodilator function ³⁴³. Thus, an improved understanding of mechanisms linking cellular metabolism and vascular Kv1 channel function is essential, as this process likely becomes compromised during pathology. In the following sections, we discuss redox regulation of

Kv1 channels with respect to intracellular pyridine nucleotides and reactive oxygen and nitrogen species and how channel function may be altered to influence coronary vascular tone and myocardial blood flow via these mediators.

3. Mechanisms of Kv1 regulation by cellular pyridine nucleotide redox.

Structurally, channels of the Kv1 family share a similar pore complex consisting of four individual α subunits. Each subunit consists of six transmembrane segments (S1-S6) with S1-S4 forming the voltage sensor complex while S5 and S6 form the pore region, together with the S4-S5 linker comprising the gating apparatus⁷⁹. Voltage-sensitivity is conferred by a group of highly conserved positive residues within each S4 segment³⁴⁴, which render the channel responsive to depolarization. Members of one Kv subfamily can co-assemble with each other to form heterotetrameric pore complexes, an attribute thought to contribute to greater functional diversity of Kv membrane potential regulation³⁴⁵. Pore-forming Kv subunits are known to assemble with a variety of intracellular ancillary subunits such as the Kv β s⁸⁰. Like the α pore subunits, the Kv β proteins can also assemble as heterotetramers^{225, 346}, and extend the structure of the channel by approximately 30 Å into the cytosolic compartment⁷⁹. Each β protein binds an α subunit at a T1 docking domain (Figure 1), which interacts with the voltage sensor and may constrain its conformation^{220, 347}, thus providing a plausible means of regulating the voltage sensitivity of the channel.

A primary mode of regulation of Kv1 in the coronary arteries and arterioles could conceivably arise via specific α/β interactions. The Kv β proteins were found in an early study to share significant identity with proteins belonging to the aldo-keto reductase (AKR) superfamily²⁴². The AKR enzymes catalyze the reduction of carbonyl substrates to primary and secondary alcohols in a manner requiring hydride transfer from a nicotinamide adenine dinucleotide (i.e., NAD(P)H) cofactor. Structurally, the Kv β s share key features with other AKR proteins, including an α_8/β_8 barrel and key amino acid residues that are

required for catalysis and NAD(P)(H) binding. Consistent with other AKRs, the model three-dimensional structure of the Kv β 2 homotetramer revealed high affinity binding of NADP⁺ within a deep cleft of the active site^{226, 229}. The reasons for the pairing between a reductase and a voltage-gated potassium channel persisting in a number of excitable cell types are not known. However, interactions between the active site of Kv β with the α subunit voltage sensor support the notion that there may be functional coupling between Kv channels and β -subunits such that either (1) the catalytic activity of Kv β could be controlled by voltage-dependent channel gating via conformational changes in the active site, or perhaps more likely (2) that Kv activity could be differentially affected by catalysis or cofactor oxidation at the active site of Kv β via conformational changes in the voltage sensor affecting the Kv β protein.

Numerous reports support the concept that Kv β proteins strongly influence Kv1 channel function (see reviews⁸⁰ and³⁰⁰). Studies in heterologous expression systems demonstrate that co-expression of Kv β with Kv α subunits confers rapid inactivation to otherwise non-inactivating K⁺ currents and shifts the voltage-dependence of channel activation towards more negative membrane potentials⁸⁰. Several lines of evidence now suggest the potential importance of Kv β as a functional sensor of cellular metabolic status such that biochemical modification upon binding pyridine nucleotide cofactors modifies channel gating^{8, 10, 300}. Purified Kv β proteins have been demonstrated to exhibit catalytic function with a wide range of aldehyde and ketone substrates, albeit their in vitro catalytic efficiency is remarkably low relative to other known AKRs^{244, 348}. Nonetheless, all Kv β proteins bind to both oxidized (i.e. NAD(P)⁺) and reduced (NAD(P)H) pyridine nucleotide cofactors with affinities in the low micromolar range, which is well below normal intracellular levels. Moreover, the activation and inactivation properties of Kv1 α/β channels are sensitive to the redox state of NAD(P)(H) that interacts with the Kv β subunits. For

example, Tipparaju et al. demonstrated that although non-inactivating currents mediated by Kv1.5 expressed alone in COS-7 cells are insensitive to pyridine nucleotides applied via the patch pipette solution, application of NAD(P)H increased total inactivation and shifted the voltage-dependence of inactivation and activation towards more negative membrane potentials relative to when NAD(P)⁺ was applied in cells co-expressing both Kv1.5 and Kvβ1.3⁹. A reduction in Kvβ1-mediated channel inactivation upon application of NADP⁺ was also observed for Kv1.1 channels²⁴⁸. Similar results were shown for Kv1.5 channels co-expressed with Kvβ3 subunits¹⁹⁵, which similar to Kvβ1, also contain an N-terminal inactivation domain⁸⁰. Redox modulation of channel inactivation by pyridine nucleotides appears to require both the C-terminal region of the Kv1α protein and electrostatic interactions between the N-terminal region and AKR enzymatic core of the β protein^{8, 195}. In contrast to effects of pyridine nucleotides on cells expressing Kv1/Kvβ1 and Kv1/Kvβ3 couples, channel inactivation is unchanged by coexpression of Kv1/Kvβ2, which likely reflects the lack of an N-terminal inactivation domain on the Kvβ2 subunit (Figure 1)⁸⁰. Nonetheless, a robust negative shift in the voltage-dependence of activation of Kv1 channels interacting with Kvβ2 is observed in the presence of reduced pyridine nucleotides¹⁹⁵. Despite the availability of data demonstrating differential regulation of Kv1 activity by oxidized versus reduced redox couples, the *in vivo* relevance of these phenomena has not been demonstrated.

The functional role for Kvβ proteins in modulating vascular Kv1 channel activity *in vivo* and tone regulation are currently lacking, yet several studies have reported the expression profiles of Kv1/Kvβ proteins in various vascular beds. Acute inhibition of Kv1 channel activity is considered a primary contributor to hypoxic pulmonary vasoconstriction (HPV)³⁴⁹ and Kvβ subunits have been proposed as determinants of redox sensing capacity of Kv1 channels for oxygen tension in the lung parenchyma³⁵⁰. Primary cultures of rat arterial myocytes derived from branches and left and right main pulmonary arteries

express transcripts for several Kv1 α members as well as Kv β 1.1, Kv β 2, and Kv β 3 subunits³⁵¹, yet the specific contribution of these subunits to the HPV response remains unclear. In small mesenteric arterial smooth muscle of rats, mRNA encoding Kv β 1, Kv β 2 and Kv β 3 is present³⁵². Whereas, in rabbit portal vein, mRNAs for Kv β 1.1, β 1.2, and β 2, but not β 3.1, are detectable³⁵³. A recent study examining Kv1 expression in human adipose arterioles revealed mRNA expression of three splice variants of Kv β 1 (i.e., β 1.1, β 1.2 and β 1.3) in these vessels³⁴³. Note that while many early studies investigating the molecular identity of delayed rectifier 4-aminopyridine-sensitive K⁺ currents in VSM have mostly examined gross mRNA and protein levels in crude ex vivo artery preparations, further characterization of regional variations in subunit stoichiometry of heteromeric channel structures in the vasculature at the molecular level have remained largely unexplored. Considering the marked differences in channel regulation imparted by the diverse repertoire of channel subunits, distinct bed-specific expression patterns of Kv α and β subunits may indeed reflect differences in the demand for redox regulation for control of organ perfusion and should be revisited with newly available advanced technologies and experimental approaches. Furthermore, altered channel composition following more sustained changes in metabolic demand could represent an important microvascular adaptation in vivo that may become compromised to varying degrees in disease states, and adversely affect vascular resistance and tissue oxygenation.

To begin to examine the aforementioned issues, we recently examined the molecular identity of Kv β proteins that are expressed in the murine coronary circulation²⁵⁹. In first and second order left anterior descending coronary arteries, we found mRNA transcripts for Kv β 1, Kv β 2 and Kv β 3. At the protein level, Kv β 1 and Kv β 2 were detected by Western blot, whereas in situ proximity ligation analyses suggested that both of these Kv β isoforms interact with Kv1.5 subunits in native coronary Kv channels²⁵⁹. Additionally, our results suggest that Kv β 1 and Kv β 2 may assemble as heterotetramers in a

subpopulation of Kv1 channels in coronary arterial myocytes. These findings may have important implications for arterial function in regards to redox regulation of smooth muscle contractility and blood flow. For example, as mentioned above, Kv β 2 is structurally and functionally unique among the Kv β proteins in that it lacks the N-terminal inactivating domain found in Kv β 1 and Kv β 3, which occludes the channel pore to confer rapid inactivation to otherwise non-inactivating Kv currents. Thus, the functional influences of these ancillary subunits on Kv1 activity in response to changes in NAD(P)H:NAD(P)⁺ could oppose each other. Experiments performed in COS cells suggest that Kv β 2 subunits can indeed mask the inactivation function of Kv β 1²⁸¹, yet the net effect of Kv β complexes consisting of more than one Kv β isoform on the gating properties of native vascular Kv1 channels remains unknown. Nonetheless, given that smooth muscle contractility is strongly influenced by relatively small changes in membrane potential^{33, 323}, Kv β may couple vascular function to cellular metabolism by modulating the Kv1 window current (Figure 2). Considering that a subpopulation of Kv β subunits induces time-dependent inactivation of Kv1 channels, only a fraction of channels in association with these subunits may be available at steady state membrane potentials in coronary arterial myocytes. With the remainder of channels lacking the dominant inactivation function, the Kv β -induced negative shift in voltage-dependence of activation may represent a key contributor to greater macroscopic current upon changes in cellular metabolic status. While the functional relevance of this balance is currently unclear, divergent functional regulation of Kv1 by distinct auxiliary subunits in association with the channel pore complex may also contribute to fine tuning of Kv1 function with respect to coupling of local blood flow with metabolic demands of the local tissue environment.

Importantly, a number of factors could participate in transient or sustained modulation of intracellular pyridine nucleotide redox ratio in VSM upon increases in heart rate and ventricular contractility. These include systemic circulating factors (e.g., bFGF,

IL-1 β , TNF α , lactate) as well as diffusible factors released into the interstitium by the active myocardium (e.g, H₂O₂, adenosine) and a set of myocyte or endothelial-derived growth factors³⁵⁴⁻³⁵⁸. Additionally, while the heart does not itself undergo sustained hypoxia under physiological conditions, myocardial oxygen consumption is markedly increased during moderate to intense exercise and augmented demand for oxygen by cardiomyocytes could siphon oxygen from the vascular wall, thereby producing a local modest oxygen-deprived microenvironment to promote accumulation of reduced pyridine nucleotides in VSM³⁵⁹. However, it remains possible that discrepancies may exist in the regulation of pyridine nucleotide redox between vascular beds. Thus, a detailed assessment of the relationship between vascular smooth muscle pyridine nucleotide redox and cardiac oxygen demand would be valuable to future studies addressing the role of Kv β :NAD(P)(H) interactions in the control of blood flow to the heart. Moreover, future studies employing knock-in strategies to target key residues in the Kv β subunits (e.g., Tyr⁹⁰ of Kv β 2)^{244, 255} are needed to evaluate the specific in vivo roles for oxido-reductase catalytic function versus cofactor binding, in Kv1-mediated vasodilation.

4. Direct influence of reactive oxygen and nitrogen species on vascular Kv1 function:

Elevated levels of reactive oxygen species (ROS) likely contribute to the control of coronary Kv channel function. Experiments examining human, rodent and large animal coronary arterioles have demonstrated that hydrogen peroxide (i.e., H₂O₂), a product of superoxide dismutation, functions as a cardiomyocyte- and endothelium-derived physiological vasoactive agent that can freely diffuse across the plasma membrane and hyperpolarize VSM membrane potential via direct and indirect modulation of K⁺ channel activity^{174-176, 179, 360}. Direct functional regulation of Kv channels by oxidative agents may occur via modification of specific cysteine, methionine, histidine and tyrosine residues within the channel complex³⁶¹. In particular, early studies using expression of cloned

mammalian Kv subunits in *Xenopus* oocytes have suggested that oxidation of N-terminal cysteine residues within both the $Kv\alpha$ and β subunits inhibits channel inactivation, possibly due to rapid and reversible disulphide bridge formation between the inactivation gate and a neighboring site within the channel complex^{225, 362}. Application of H_2O_2 was also shown to augment peak Kv current, shift the voltage-dependence of channel activation toward more negative membrane potentials, and accelerate channel activation in CHO cells expressing Kv1.5, in the absence of $Kv\beta$ co-expression³⁶³. A recent study in mesenteric arterial myocytes suggests that H_2O_2 -mediated Kv potentiation may also occur via incorporation of glutathione in the channel protein at cysteine residues³⁶⁴, which has also been suggested to promote activation of Cav1.2 voltage-dependent calcium channels³⁶⁵. However, in the presence of heightened oxidative stress, H_2O_2 fails to further activate Kv channels and may even lead to channel inhibition, thus supporting a bidirectional functional influence of oxidative modification, depending on the redox state of the cell.

Superoxide production by the mitochondria can also lead to the formation of peroxynitrite ($ONOO^-$) via reaction with nitric oxide³⁶⁶. $ONOO^-$ is known to be highly reactive with tyrosine residues and can alter the function of cellular proteins, including voltage-gated ion channels³⁶⁷. In addition to numerous pathways by which nitric oxide and reactive nitrogen species could influence Kv-mediated vasodilation³⁶⁸⁻³⁷¹, channel activity could be directly altered by reaction of $ONOO^-$ with channel proteins. In coronary arteries of rats, increased production of $ONOO^-$ may impair Kv-mediated vasodilation via nitration of tyrosine residues in Kv1.2 subunits³⁷². In addition to nitration of tyrosine residues, S-nitrosothiols, like S-nitroso-N-actylpenicillamine (SNAP), have been shown to modify cysteines in the L-type Ca^{2+} channel through multiple mechanisms including transnitrosation, mixed disulfide bonds, and disulfide bond formation between cysteines³⁷³. A biotin-switch assay revealed the presence of S-nitrosylated cysteine residues in SNAP-treated Itk^{-/-} cells stably expressing human Kv1.5. Through molecular modeling, two

cysteines in the S2 segment (i.e., C331 and C346) were identified as a potential site of S-nitrosylation, as S-nitrosothiol groups at these cysteines could be stabilized by hydrogen bridge bonds with I262, located in S1, and R342, located in S2. Interestingly, this modification correlated with a reduction in Kv1.5 current density. Although direct modification identified thus far at cysteine and tyrosine residues generally appears to be associated with channel inhibition, it is unclear whether direct modification of Kv channels by NO-derived factors impacts the regulation of coronary vasomotor tone and myocardial blood flow. Nonetheless, nitration of Kv channels may impair vasodilatory function in the presence of pathological conditions in which superoxide production is elevated, such as hyperglycemia and diabetes. Future work is needed to address the precise functional consequences of specific tyrosine and cysteine modifications within the Kv channel complex and the differential effects conferred by α/β subunit compositions in the context of physiological and pathological regulation of coronary vasodilation.

6. Summary

Kv1 channels in the microcirculation are capable of sensing cellular redox state by a variety of mechanisms which ultimately act in concert to control VSM membrane potential to adapt blood flow to constantly changing metabolic conditions (Figure 3). In addition to their regulation by pyridine nucleotide redox and reactive oxygen/nitrogen species discussed here, Kv1 channel subunits can be functionally modulated by a number of other modifications including phosphorylation, palmitoylation, and glycosylation³⁷⁴⁻³⁷⁶. Future work using in silico modeling could help shape a better understanding of how this complex network of pathways works in an integrated fashion to influence vascular function in a variety of physiological and pathological states. Advanced gene editing technology now offers an exceptional tool to determine precise sites of redox sensing within the channel structure in the setting of native channels of the vasculature. Importantly, a

number of both gain-of function and loss-of-function mutations have been identified in Kv1 channel subunits ³⁷⁷⁻³⁸⁰. In addition to the impact that these mutations likely have on cardiac and neuronal repolarization, it is plausible that altered coupling between myocardial metabolism and coronary blood flow may also contribute to cardiovascular disease in patients harboring these mutations. Thus, future advances in our understanding of redox regulation of coronary Kv channels during disease states could ultimately lead to improved strategies to enhance coupling between metabolic demand and myocardial blood flow for therapeutic benefit.

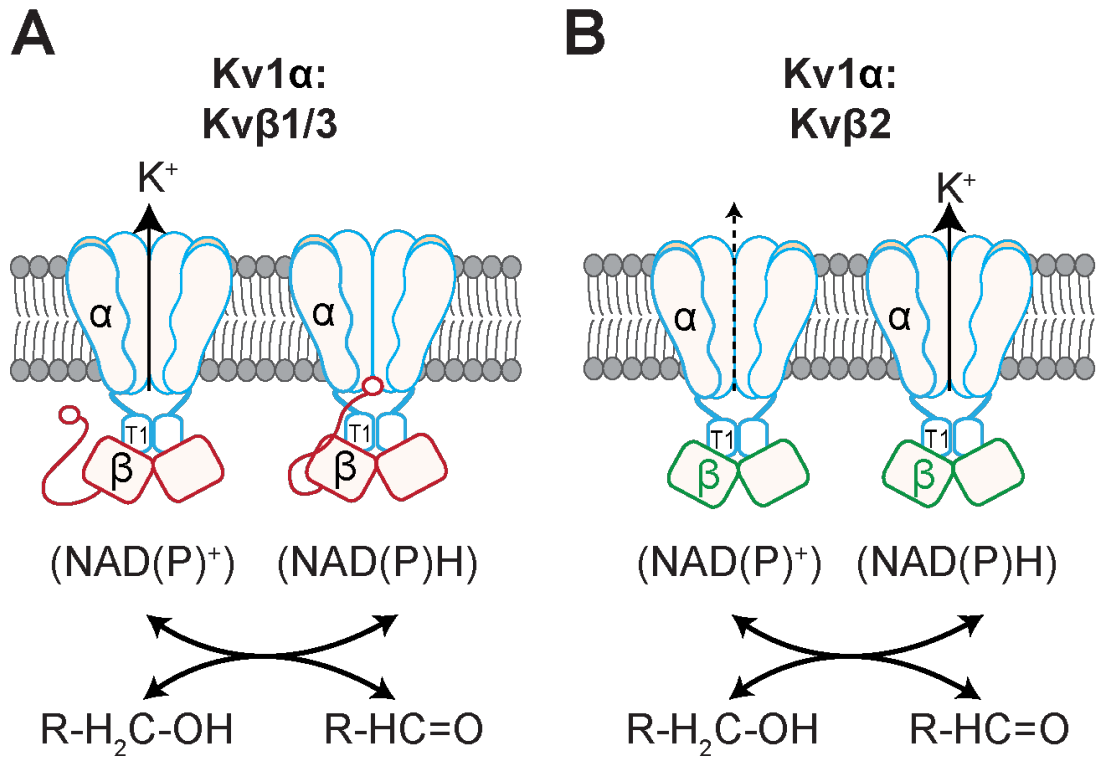


Figure 1: Kvβ-dependent regulation of Kv1 activity by pyridine nucleotide cofactors. (A) Regulation of Kv1 function by Kvβ1 and Kvβ3 subunits, which possess NH₂-terminal ball-and-chain-like inactivation. Inactivation is enhanced by bound pyridine nucleotides in their reduced form (i.e., NAD(P)H). (B) Regulation of Kv1 function by Kvβ2 subunits. Kvβ2 proteins lack the NH₂-terminal inactivation domain. Voltage-dependence of activation is shifted towards more negative membrane potentials in the presence of reduced pyridine nucleotide cofactors. Transition between states can occur by exchange of pyridine nucleotides or by catalytic activity to oxidize bound pyridine nucleotide cofactors.

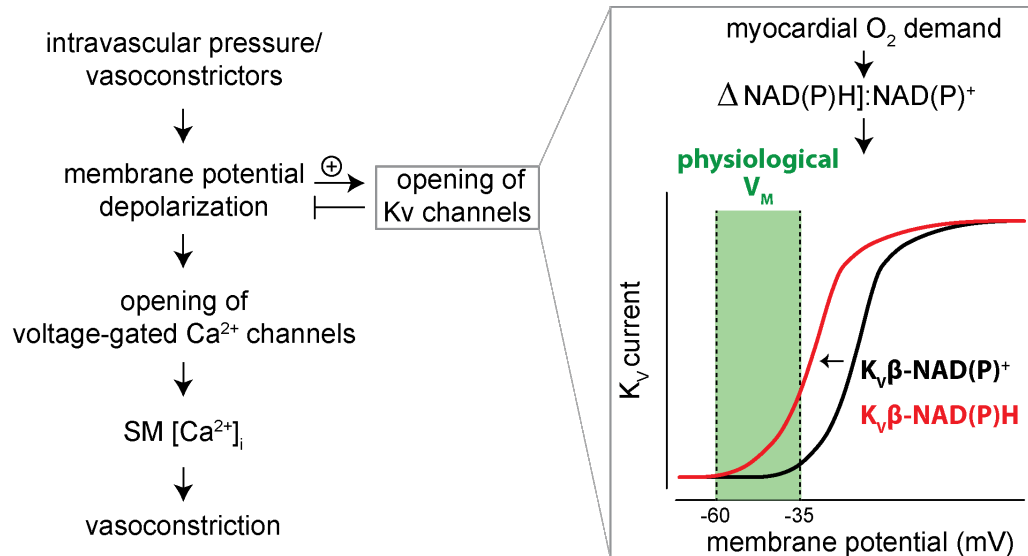


Figure 2: Hypothetical model of coronary blood flow regulation by pyridine nucleotide-mediated activation of Kv1 channels. Flow diagram on the left shows role of smooth muscle Kv channels in opposing membrane potential depolarization and vasoconstriction. Expanded window shows proposed model of Kv1 activation during periods of elevated cardiac workload. In this scheme, increases in myocardial oxygen demand leads to changes in pyridine nucleotide redox status in coronary arterial myocytes. Accumulation of reduced pyridine nucleotides could shift the threshold and voltage-dependence of activation of available Kv1 channels further into the narrow window of physiological steady-state membrane potential in arterial myocytes of pressurized arteries and arterioles (-60 to -35 mV), thereby significantly increasing Kv1 activity leading to membrane hyperpolarization, vasodilation, and enhanced blood flow.

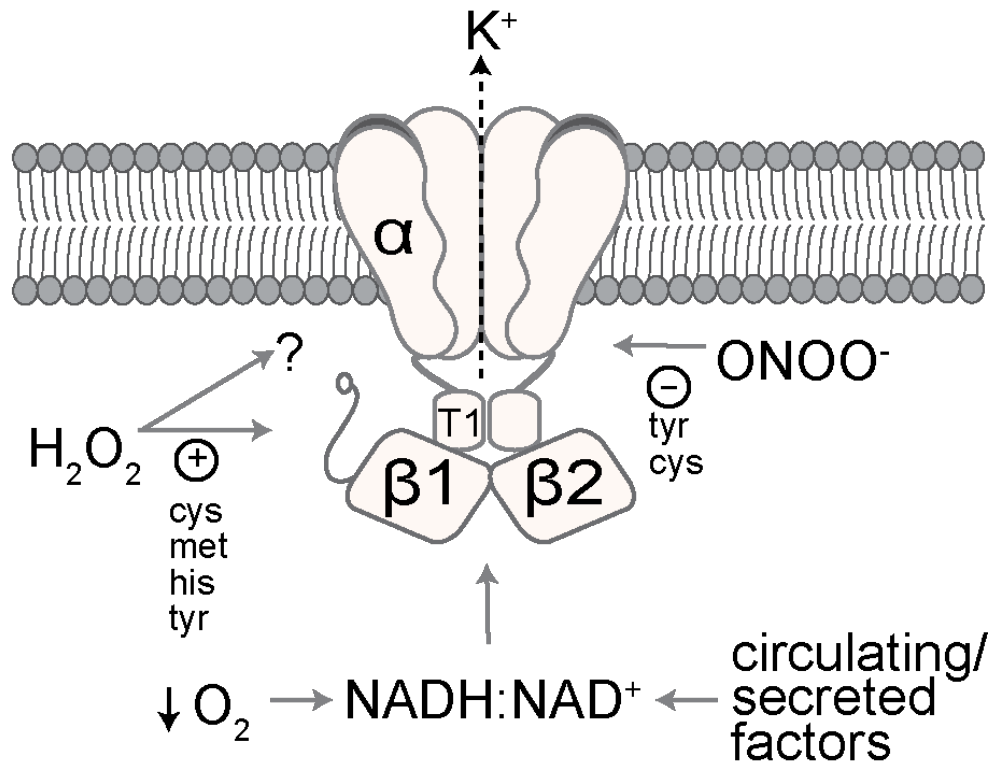


Figure 3: Coronary smooth muscle Kv1 channel modulation by cellular redox. Shown are the major discussed pathways which could contribute to functional alteration of Kv1 activity upon changes in myocardial oxygen demand.

CURRICULUM VITAE

Marc Dwenger, M.S.
580 S Preston St.
Louisville, KY,
40202
(502) 528-0928

marc.dwenger@louisville.edu

EDUCATION

- 05/2013 B.A. in Biology, Minor in Chemistry, (Summa cum laude) GPA 3.9
Simpson College, Indianola, IA
- 05/2018 M.S. in Pharmacology & Toxicology, GPA 3.9
University of Louisville, Louisville, KY
- 08/2021 Ph.D. in Pharmacology & Toxicology
Advisor: Dr. Matthew Nystoriak
Dissertation: PYRIDINE NUCLEOTIDE REDOX POTENTIAL IN
CORONARY SMOOTH MUSCLE COUPLES MYOCARDIAL
BLOOD FLOW TO CARDIAC METABOLISM

POSITIONS AND EMPLOYMENT

- 09/2014 Graduate Research Assistant, University of Louisville School of Medicine,
Dr. Bradley Keller's Lab
- 06/2017 Graduate Research Assistant, University of Louisville School of
Medicine, Dr. Matthew Nystoriak's Lab

LABORATORY SKILLS/TECHNIQUES

- 09/2014 Construction of engineered cardiac tissues from hiPSC-CMs
- 06/2015 Construction of a novel optogenetic pacing device
- 06/2015 Optogenetic training of engineered cardiac tissues
- 06/2017 Murine dissection of the coronary vasculature vascular cell biology
- 06/2017 Isolation of coronary vascular smooth muscle cells
- 06/2017 Patch clamp electrophysiology (e.g., whole cell, inside-out patch clamp)
- 06/2017 Cell culture, variety of cell types
- 06/2017 Data management (e.g., Excel, GraphPad Prism)
- 03/2018 Isolation of aortic vascular smooth muscle cells
- 08/2018 Plasmid purification
- 08/2018 Heterologous expression (e.g., transfection, electroporation)

08/2018 Grant writing
06/2019 Live-cell imaging with aortic vascular smooth muscle cells

PROFESSIONAL MEMBERSHIPS AND ACTIVITIES

07/2018 AHA/ASA Professional Member

ORAL PRESENTATIONS

1. **Dwenger MM**, Tinney JP, Keller BB. Evidence for iKr potassium channel maturation in chick ECT by E4031 block. University of Louisville Seminar in Pharmacology and Toxicology, Louisville, KY, April 2015.
2. **Dwenger MM**, Kowalski WJ, Ye F, Yuan F, Tinney JP, Setozaki S, Nakane T, Masumoto H, Campbell P, Guido W, Keller BB. Maturation of human induced pluripotent stem cell derived engineered cardiac tissues using ChIEF transfection and chronic optical pacing. University of Louisville Master's Thesis Seminar for Pharmacology and Toxicology Department, Louisville, KY, May 2017.
3. **Dwenger MM.**, Wohl Z.B., Bhatnagar A and Nystoriak M.A. Functional regulation of native coronary arterial voltage-gated K⁺ channels by cytosolic NAD(H). University of Louisville Annual Departmental Seminar for Pharmacology and Toxicology Department, Louisville, KY, September 2019.
4. **Dwenger MM**, Wohl Z.B., Bhatnagar A and Nystoriak M.A. Functional regulation of native coronary arterial voltage-gated K⁺ channels by cytosolic NAD(H). University of Louisville Annual Departmental Seminar for Pharmacology and Toxicology Department, Louisville, KY, September 2020.

POSTERS

1. **Dwenger MM**, Barve A, Nakane, T, Tinney JP, Beverly B, Keller BB. Design and Fabrication of an Optically Activated Engineered Cardiac Tissue. 2015 Research! Louisville, University of Louisville School of Medicine, Louisville, KY, October 2015.
2. **Dwenger MM**, Kowalski WJ, Ye F, Setozaki S, Nakane T, Yuan F, Tinney JP, Campbell P, Guido W, Keller BB. Chronic Optogenetic Pacing of human iPSC-derived Engineered Cardiac Tissues. 2016 Research! Louisville, University of Louisville School of Medicine, Louisville, KY, October 2016.
3. **Dwenger MM**, Kowalski WJ, Ye F, Yuan F, Tinney JP, Setozaki S, Nakane T, Campbell P, Guido W, Keller BB. Chronic Optogenetic Pacing of human iPSC-derived Engineered Cardiac Tissues. 2017 Research! Louisville, University of Louisville School of Medicine, Louisville, KY, October 2017.
4. **Dwenger MM**, Wohl Z.B., Bhatnagar A and Nystoriak M.A. Pyridine nucleotides manipulate the gating properties of native coronary vascular Kv1 channels. 2018 Research! Louisville, University of Louisville School of Medicine, Louisville, KY, October 2018.

5. **Dwenger MM**, Wohl Z.B., Bhatnagar A and Nystoriak M.A. Functional Regulation of Native Coronary Kv1 Channels by Pyridine Nucleotides. AHA Scientific Sessions, Chicago Illinois, November, 2018. Published in Circulation November, 2018.
6. **Dwenger MM** and Nystoriak M.A. Functional regulation of native coronary arterial voltage-gated K⁺ channels by cytosolic NAD(H). 2019 Research! Louisville, University of Louisville School of Medicine, Louisville, KY, September 2019.
7. Nystoriak, M.A., Ohanyan, V., **Dwenger, MM**, Chilian, W.M. and Bhatnagar, A. Role for NADH-sensitive Kv channels in the myocardial-vascular signaling axis. April, 2020. Published FASEB Journal April, 2020.
8. **Dwenger, MM**, Moore, J.B IV, Nystoriak, M. Influence of Cardiac Workload on Vascular Pyridine Nucleotide Redox State. AHA Scientific Sessions, Online, November 2020. Published in Circulation November, 2020.

PUBLICATIONS

PEER-REVIEWED ORIGINAL RESEARCH MANUSCRIPTS

1. **Dwenger MM**, Kowalski WJ, Ye F, Yuan F, Tinney JP, Setozaki S, Nakane T, Masumoto H, Campbell P, Guido W, Keller BB. Chronic optical pacing conditioning of h-iPSC engineered cardiac tissues. J Tissue Eng. 2019 Apr 17;10:2041731419841748. doi: 10.1177/2041731419841748. PMID: 31024681; PMCID: PMC6472158.
2. Ohanyan V, Raph SM, **Dwenger MM**, Hu X, Pucci T, Mack GD, Moore Iv JB, Chilian WM, Bhatnagar A, Nystoriak MA. Myocardial Blood Flow Control by Oxygen Sensing Vascular Kv β Proteins. Circ Res. 2021 Jan 27. doi: 10.1161/CIRCRESAHA.120.317715. Epub ahead of print. PMID: 33499656.

OTHER PUBLICATIONS

1. Kowalski WJ, Yuan F, Nakane T, Masumoto H, **Dwenger MM**, Ye F, Tinney JP, Keller BB. Quantification of Cardiomyocyte Alignment from Three-Dimensional (3D) Confocal Microscopy of Engineered Tissue. Microsc Microanal. 2017 Aug;23(4):826-842. doi: 10.1017/S1431927617000666. Epub 2017 Jun 19. PMID: 28625174.
2. **Dwenger MM**, Ohanyan V, Navedo MF, Nystoriak MA. Coronary microvascular Kv1 channels as regulatory sensors of intracellular pyridine nucleotide redox potential. Microcirculation. 2018 Jan;25(1):10.1111/micc.12426. doi: 10.1111/micc.12426. PMID: 29110409; PMCID: PMC5760281.
3. **Dwenger MM**, Kowalski WJ, Masumoto H, Nakane T, Keller BB. Chronic Optogenetic Pacing of Human-Induced Pluripotent Stem Cell-Derived Engineered Cardiac Tissues. Methods Mol Biol. 2021;2191:151-169. doi: 10.1007/978-1-0716-0830-2_10. PMID: 32865744.